BULGARIAN CHEMICAL COMMUNICATIONS

2021 Volume 53 / Number 3

Journal of the Chemical Institutes
of the Bulgarian Academy of Sciences
and of the Union of Chemists in Bulgaria

Bulgarian Chemical Communications, Volume 53, Issue 3 (pp. 265 - 268) 2021 *DOI: 10.34049/bcc.53.3.0195*

Processing of rice husk and straw into activated carbon

N. Appazov[1,2*], B. Diyarova[3], R. Turmanov[1], R. Zhapparbergenov[1], O. Lygina[4], A. Tapalova[1], K.Saduakaskyzy[1], B. Dzhiembaev[3]

[1]*Korkyt Ata Kyzylorda University, Kyzylorda, Kazakhstan*
[2]*I. Zhakhaev Kazakh Scientific Research Institute of Rice Growing, Kazakhstan*
[3]*Kazakh National Women's Teacher Training University, Almaty, Kazakhstan*
[4]*Universidade Nova de Lisboa, Lisbon, Portugal*

Received: February 10, 2020, Revised: April 26, 2021

A method of processing rice waste (husk, straw) into activated carbon is proposed in the study. The thermolysis of the raw material and the activation of the carbonizate were carried out at 500ºC and 800ºC, respectively. The properties of the obtained activated carbon were determined by standard methods. The porous structure of the activated carbon was studied using scanning electron microscopy. According to the results of the experimental studies, activated charcoal obtained from rice husk corresponds to the WAC brand, whereas activated charcoal obtained from rice straw corresponds to BAU-A grade. This research proposes a rational method of using agricultural waste to obtain useful secondary adsorbent products for adsorption in liquid media.

Keywords: carbonization, rice husk and straw, activation of carbonizate, sorbent, activated carbon.

INTRODUCTION

Rice is one of the most important agricultural food products in the world. Nowadays, the estimated world production of rice is more than 485 million tons per year. According to Kazagromarketing JSC, rice-growing regions of Kazakhstan are Kyzylorda, Almaty and Turkestan. Kyzylorda is the leading rice-growing region of the country, which produces more than 85% of the local crop.

During harvesting and industrial rice processing, a waste in the form of husk (up to 20% of mass) and straw (up to 50% of mass) is formed in large numbers. The utilization of straw and husk, in fact, remains the main problem for rice producers. The majority of rice husk and straw are incinerated which leads to a deterioration of the ecological situation. A joint solution for ecological and technological problems is the utilization of rice husk and straw, as well as the production of demanded solid products.

There are some works in the literature on the thermal processing of rice husk and the production of phenol-containing products from it [1, 2].

In this research, using rice husk and straw to obtain the widely applicable adsorbent activated carbon is suggested. Activated carbon is produced from various carbon-containing materials of organic origin: charcoal (BAU, DAK, etc.) [3], coal coke (activated carbon brand AG, AR, etc.) [4], petroleum coke, coconut shells, fruit pits, agricultural waste, paper production waste, garbage, sewage sludge, worn rubber tires, synthetic polymer waste and so on [5-13].

The use of agricultural waste to produce activated carbon is environmentally friendly because the use of wood as a raw material is excluded, which in turn, minimizes deforestation and promotes the rational use of agricultural waste. Method of producing activated carbon from barley waste by pre-drying in hot air and performing one-step carbonization in a cylindrical reactor at 290-320°C for 7-15 minutes was discovered [14], another method of activated carbon production is using rapeseed straw and carrying out carbonization in an inert nitrogen atmosphere at a temperature of 450-500°C and activation by steam at a temperature of 820-850°C [15].

There are some works on obtaining highly porous activated carbon from rice husk, where the product has a selective sorption activity of lead ions [16-17]. In another research [18] it is reported that the co-processing of rice husks and polytetrafluoroethylene gives a highly porous structured product.

EXPERIMENTAL

10 g of raw material was placed in a stainless steel tube furnace with a height of 250 mm and an internal diameter of 25 mm. The tube was sealed and carbonization was carried out. The temperature of carbonization was increased at a rate of 10°C per minute up to 500°C. This temperature was kept for 100 minutes. The yield of carbonizate obtained from husk and straw was 44 and 37%, respectively.

* To whom all correspondence should be sent:
E-mail:nurasar.82@mail.ru

© 2021Bulgarian Academy of Sciences, Union of Chemists in Bulgaria

Afterwards, a vessel was connected to the bottom of the tube furnace to supply the system with steam, keeping a ratio of water:carbonizate 2:1 by weight. The activation was carried out at a temperature of 800°C, the yield of activated carbon was 27% and 29%, depending on the weight of the husk and straw used.

The surface of the obtained activated carbon was analyzed with a scanning electron microscope JSM-6510 LV from JEOL Company(Japan).

The properties of the obtained activated carbon: iodine adsorption activity, water total pore volume, mass fraction of moisture and bulk density were determined by the known methods [3,19-21].

RESULTS AND DISCUSSION

Microphotographs of activated carbon (500-fold magnification) are shown in Figures 1 and 2, where developed porous structure of the obtained sorbents can be observed.

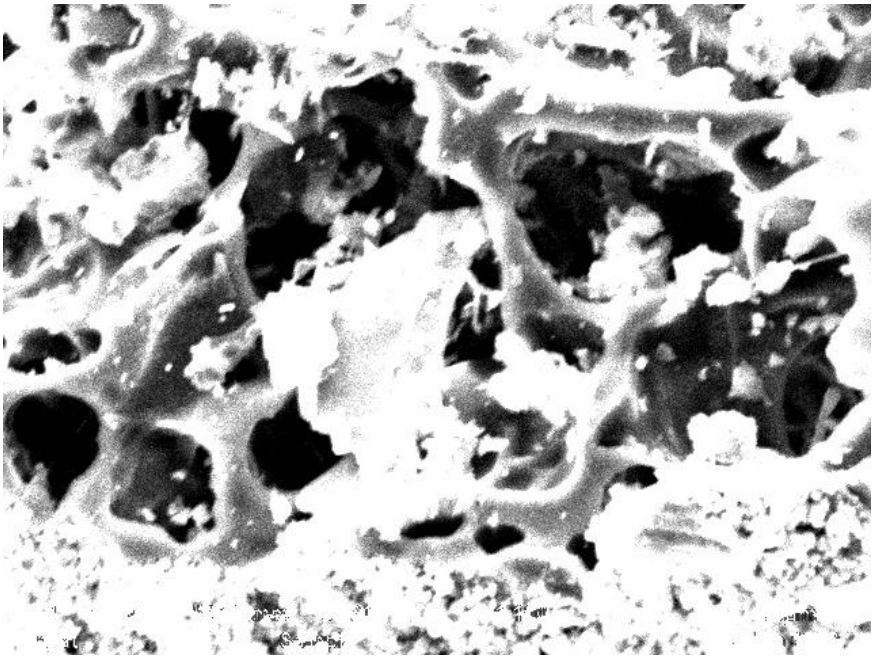

Figure 1. Photomicrograph of activated carbon obtained from rice husk

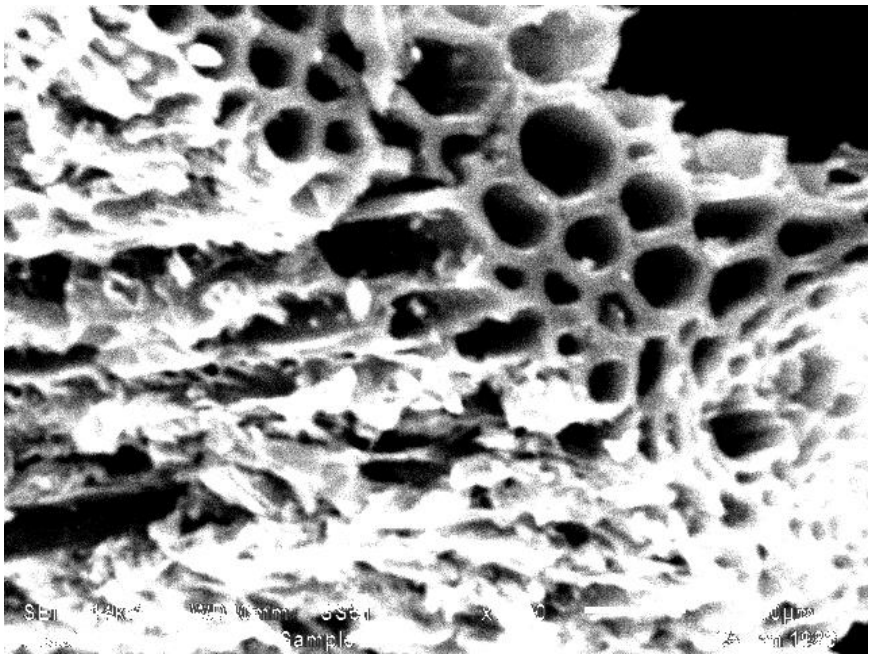

Figure 2. Photomicrograph of activated carbon obtained from rice straw

Table 1. Properties of activated carbons obtained from rice husk and straw

Activated carbon	Iodine absorption activity, %	Water total pore volume, cm^3/g	Mass fraction of moisture, %	Bulk density, g/dm^3
Activated carbon obtained from rice husk	51	1.57	3.6	236.1
Activated carbon obtained from rice straw	64	1.63	3.6	181.3
BAU-A grade	More than 60	1.60	Less than 10.0	Less than 240.0
WAC brand	More than 30	1.40	Less than 10.0	Less than 220.0-250.0

The properties of the obtained activated carbon were determined by the following methods: iodine adsorption activity by a titrimetric method, water total pore volume by filling pores with water and removing excess water from the surface of the sample by suction, mass fraction of moisture by drying the sample to constant weight, bulk density by a weighing method. The data are given in Table 1.

According to the results, activated charcoal obtained from rice husk corresponds to WAC activated charcoal, whereas activated charcoal obtained from rice straw corresponds to BAU-A grade, which are used for adsorption in liquid media [3].

CONCLUSIONS

Activated carbon was obtained from rice husk and straw. The properties of the products obtained were determined. According to certain properties, the obtained sorbents can replace wood activated charcoal, which makes possible the rational dispose of agricultural waste, reduces deforestation, and helps to produce value-added products.

Funding: *This work was carried out with the financial support of the Committee of Science of the Ministry of Education and Science of the Republic of Kazakhstan, project no. AP05134356.*

REFERENCES

1. B. Biswas, R. Singh, J. Kumar, R. Singh, P. Gupta, B. B. Krishna, T. Bhaskar, *Renewable Energy*, **129**, 686 (2018).
2. J. Wu, S. R. A. Collins, A. Elliston, N. Wellner, J. Dicks, I. N. Roberts, K. W. Waldron, *Biotechnology for Biofuels*, **11**, DOI: 10.1186/s13068-018-1157-1 (2018).
3. GOST 6217, Ugol' aktivnyj drevesnyj droblenyj. Tehnicheskie uslovija, M., IPK Izdatel'stvo standartov, 2003 (in Russian).
4. GOST R 56357-2015, Ugol' aktivirovannyj AG-3. Tehnicheskie uslovija, M., Standartinform., 2016 (in Russian).
5. H. Kinle, Je. Bader, Aktivnye ugli i ih promyshlennoe primenenie, L., Himija, 1984, p. 216 (in Russian).
6. Himicheskij jenciklopedicheskij slovar', M., Sovetskaja Jenciklopedija, **19,** 1983 (in Russian).
7. N. Arezou, N. Bahram, *Biomass and Bioenergy*, **106**, 43 (2017).
8. L. Yeru, Y. Chen, D. Hanwu, L. Wenqi, H. Hang, X. Yong, Z. Mingtao, L. Yingliang, *ACS Sustainable Chem. Eng.*, DOI: 10.1021/acssuschemeng.7b01315 (2017).
9. Z. Wenli, L. Nan, L. Debo, X. Jinhui, S. Jinxin, Y. Jian, T. Xiaobo, Y. Huiping, L. Haiyan, L. Haibo, *Energy*, **128**, 618 (2017).
10. Z. A. Mansurov, R. M. Mansurova, A. F. Nikolaeva, D. G. Vasil'ev, *KZ Patent* 15933 (2005).
11. S. Lyubchyk, O. Shapovalova, O. Lygina, M. C. Oliveira, N. Appazov, A. Lyubchyk, A. J. Charmier, S. Lyubchik, A. J. L. Pombeiro, *Scientific Reports*, https://doi.org/10.1038/s41598-019-53817-8 (2019).
12. N. O. Appazov, B. M. Bazarbayev, T. Assylbekkyzy, B. M. Diyarova, S. A. Kanzhar, S. Magauiya, R. U. Zhapparbergenov, N. I. Akylbekov, B. A. Duisembekov, *News of NAS RK, Series of Chemistry and Technology*, https://doi.org/10.32014/2021.2518-1491.8 (2021).
13. N. O. Appazov, B. M. Diyarova, B. M. Bazarbayev, T. Assylbekkyzy, S. A. Kanzhar, B. Zh. Dzhiembaev, *News of NAS RK, Series of Chemistry and Technology*, https://doi.org/10.32014/2021.2518-1491.28 (2021).
14. K. B. Hoang, V. S. Timofeev, O. N. Tjomkin, I. G. Gafarov, A. V. Timoshenko, T. V. Artamonova, O. V. Gorbacheva, I. P. Kol'vah, G. M. Mishulin, M. B. Shhepakin, E. A. Kozhura, R. M. Haziev, A. K. Vatolin, RU Patent 2315712 (2008).
15. V. M. Muhin, N. L. Voropaeva, V. V. Karpachev, S. A. Harlamov, Ju. Ja. Spiridonov, V. V. Gur'janov, E. E. Dmitrjakova, RU Patent (2014).
16. F. Hanum, O. Bani, L. I. Wirani, in: IOP Conf. Series: Materials Science and Engineering, **180**, doi:10.1088/1757-899X/180/1/012151(2017).

17. F. Hanum, O. Bani, A. M. Izdiharo, in: IOP Conf. Series: Materials Science and Engineering, **180**, doi:10.1088/1757-899X/180/1/012149 (2017).
18. L. Yeru, Y. Chen, D. Hanwu, L. Wenqi, H. Hang, X. Yong, Z. Mingtao, L. Yingliang, *ACS Sustainable Chem. Eng.*, DOI: 10.1021/ acssuschemeng.7b01315.
19. GOST 17219. Ugli aktivnye. Metod opredelenija summarnogo ob'ema por po vode, M., Izdatel'stvo standartov, 1988 (in Russian).
20. GOST 12597. Sorbenty. Metod opredelenija massovoj doli vody v aktivnyh ugljah i katalizatorakh na ih osnove, M., Izdatel'stvo standartov, 1989 (in Russian).
21. GOST 16190. Sorbenty, Metod opredelenija nasypnoj plotnosti, M., Izdatel'stvo standartov, 1970 (in Russian).

Bulgarian Chemical Communications, Volume 53, Issue 3 (pp. 269 - 274) 2021 *DOI: 10.34049/bcc.53.3.5202*

Solid-phase extraction of trace gallium(III) and indium(III) prior to their determination by diffuse reflectance spectroscopy

A. Chebotarev[1*], E. Rachlitskaya[1], E. Guzenko[1], K. Bevziuk[2], D. Snigur[1]

[1]*Department of Analytical and Toxicological Chemistry, Odessa I. I. Mechnikov National University, Dvoryanskaya 2, UA-65082 Odessa, Ukraine*

[2]*Department of Medical Chemistry, Odessa National Medical University, Valikhovskiy lane 2, UA-65082 Odessa, Ukraine*

Received: November 15, 2020, Revised: February 07, 2021

A sensitive and selective method for the solid-phase extraction preconcentration and diffuse reflectance determination of Ga(III) and In(III) was developed. A new adsorbent based on dimethylchlorosilane aerosil impregnated with acetone or ethanol as a pseudomembrane for solid phase extraction of gallium(III) and indium(III) was proposed. The optimal pH value for Ga(III) and In(III) adsorption is 2.7 and 4.0, respectively. Xylenol orange forms (1:1) complexes with the ions of these metals on the surface. The calibration graphs for determining Ga(III) and In(III) by diffuse reflectance spectroscopy are linear in the concentration range 0.020 ÷ 5.5 and 0.018 ÷ 5.2 mg L^{-1}, respectively. The proposed method was successfully tested in determining Ga(III) and In(III) in water samples with RSD of not more than 3.7%.

Keywords: diffuse reflectance spectroscopy, gallium, indium, solid-phase extraction.

INTODUCTION

Gallium and indium are economically significant elements due to their widespread use in various industries. Gallium and its compounds are used to create components of electronics, optoelectronic materials, fusible alloys, as well as in medicine as anti-cancer and tumor-scanning agents [1, 2]. High-purity indium and its compounds are used to create semiconductor materials, liquid crystal displays and infrared photodetectors [1]. At the same time, the content of gallium and indium in the Earth's crust is low, and these elements are found in trace amounts in bauxite and some zinc ores [1]. It should also be noted that these elements can have a negative impact on human health and the environment. The compounds of Ga(III) and In(III) produce pulmonary toxicity, and In(III) compounds also induce nephrotoxicity and hepatotoxicity [3]. Thus, the determination of these elements is an important task from the standpoint of health and economy.

Various methods for determining gallium(III) and indium(III) have been proposed. For example, there are spectrophotometry and derivate spectrophotometry [4, 5], voltammetry [6], flame atomic absorption spectrometry (FAAS) [7-9], graphite furnace atomic absorption spectrometry (GFAAS) [10, 11] and inductively coupled plasma optical emission spectrometry (ICP-OES) [12]. Regardless of the method used to detect the analytical signal, preconcentration of the trace quantities of gallium(III) and indium(III) should precede their determination. For preconcentration of these elements are offered liquid-liquid extraction [13, 14], cloud-point extraction [7, 15] and ion exchange [16] techniques. A special place among preconcentration techniques takes solid phase extraction [9, 17, 18]. The most interesting adsorbents are functionalized silicas because they allow to effectively combine solid phase extraction, complexation with chromogenic reagents such as Xylenol orange [19-21], 4-(2-pyridylazo)-resorcinol or 1-(2-pyridylazo)-2-naphtol [22] and detection *via* diffuse reflectance spectroscopy.

In continuation of our previous studies [23-25] on the solid-phase extraction preconcentration of trace amounts of analytes on modified and unmodified silica and similar adsorbents, this manuscript is devoted to the development of a method for aluminium(III), gallium(III) and indium(III) separation. The current study is aimed at developing a solid-phase extraction procedure for separation and preconcentration of gallium(III) and indium(III) as neutral monomeric hydroxoforms using dimethylchlorosilane aerosil (DMClSA) impregnated with acetone or ethanol as a pseudomembrane prior to their determination by diffuse reflectance spectroscopy with Xylenol orange.

* To whom all correspondence should be sent:
E-mail alexch@ukr.net

© 2021 Bulgarian Academy of Sciences, Union of Chemists in Bulgaria

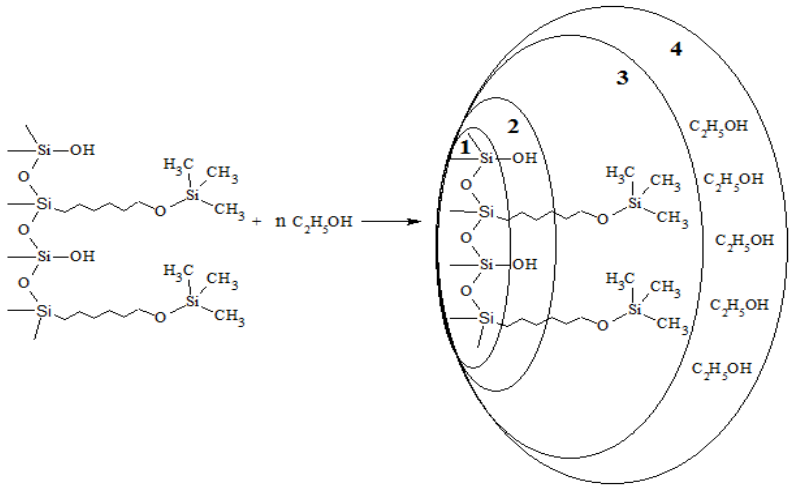

Fig. 1. The DMClSA-Solv surface: 1 - silica matrix; 2 - residual silanol groups; 3 - bonded fragments of dimethylchlorosilane; 4 - organic solvent (ethanol or acetone) impregnated due to hydrophobic interactions.

EXPERIMENTAL

Reagents. As an adsorbent, the dimethylchlorosilane aerosil (Ukraine) impregnated with acetone or ethanol as a pseudomembrane (DMClSA-Solv) was used. Based on our previous works [25], the surface of this sorbent is depicted in Fig. 1.

All solutions were prepared with double distilled water. A stock $1 \cdot 10^{-3}$ mol L^{-1} solution of Xylenol orange was prepared by dissolving an appropriate weight of the chromogenic reagent in water. A solution of Ga(III) and In(III) $1 \cdot 10^{-2}$ mol dm^{-3} was prepared by dissolving a sample of gallium(III) oxide and indium(III) oxide in concentrated nitric acid and dilution up to 100 mL with water. In standard solutions, the concentration of nitric acid is 1 mol dm^{-3}. Solutions with lower concentrations were prepared by appropriate dilutions. The reagents used in the work were not lower than analytical reagent grade.

Apparatus. Electronic absorption spectra and diffuse reflectance spectra were recorded on a spectrophotometer SF-56 (OKB "LOMO-Spectrum", Russia) in the wavelength range 380 ÷ 780 nm. The medium acidity was monitored by means of a glass electrode ESL-63-07 paired with a silver chloride reference electrode EVL-1M3 on an ionometer I-160 (ZIP, Belarus). Solid-phase extraction was studied in a static mode and mixing was performed with a shaker Elpan type 357 (Elpin+, Poland) with a frequency of 150 cycles min^{-1}. The Optima 2100 DV spectrometer (Perkin Elmer, USA) was used for ICP-OES determination of Ga(III) and In(III).

General procedure. Weights of 0.5 g of DMClSA were placed in 100 mL conical flasks and 6 mL of acetone (DMClSA-Ac) or 6 mL of ethanol (DMClSA-EtOH) was added to hydrophilize the surface of the silica matrix (to obtain a pseudomembrane on the surface). It should be noted that without solvent impregnation, the adsorbent is not wetted with water and is not suitable for the extraction of Ga(III) and In(III). 25 mL of the test solution containing Al(III), Ga(III), In(III) was added to 50-mL beakers, and pH was adjusted to 2.7 with 0.1 mol dm^{-3} sulfuric acid and 0.1 mol dm^{-3} sodium hydroxide solutions. The obtained solutions were quantitatively transferred to flasks with DMClSA-Ac and stirred for 60 min. The concentrate containing Ga(III) was separated from the solution by filtration through a blue ribbon filter. In the remaining solution containing Al(III) and In(III) the pH was adjusted to 4.0 and adsorption was carried out in static mode for 60 min by using DMClSA-EtOH as a sorbent. Concentrates were processed by 2 mL of 0.1% solution of Xylenol orange with pH 2.7 and 4.0, respectively, were air-dried, then diffuse reflection spectra were registered and the values of the Gurevich-Kubelka-Munk function (ΔF(R)) were determined:

$$\Delta F(R) = \frac{(1-R)^2}{2R} = \frac{\varepsilon_\lambda C}{S}$$

where, R – diffuse reflectance; S – scattering coefficient; C – concentration; ε_λ – molar absorptivity.

The diffuse reflectance coefficient of the concentrates does not change at least during the day.

The proposed procedure was applied to the analysis of model solutions and water samples without any special treatment.

RESULTS AND DISCUSSION

To clarify the nature of the interactions of Ga(III) and In(III) with Xylenol orange on the surface of DMClSA-Solv a comparative analysis was made of the absorption spectra of aqueous Xylenol Orange solutions and of its Ga(III) and In(III) complexes with the diffuse reflection spectra of DMClSA-Solv impregnated by Xylenol orange and its complexes with the investigated elements (Fig. 2).

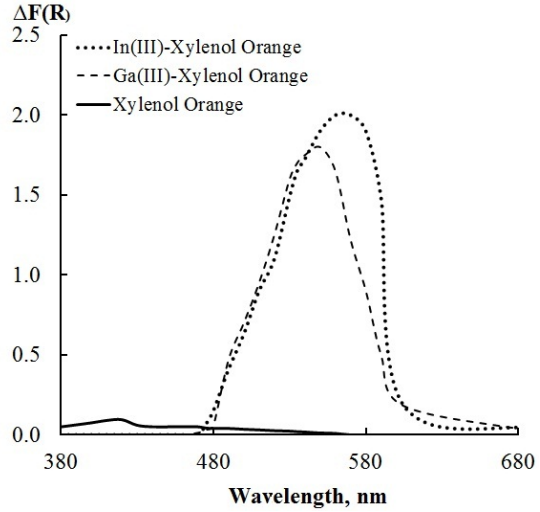

Fig. 2. Diffuse reflectance spectra of Xylenol orange and its complexes with Ga(III) and In(III) on the DMClSA-Solv surface.

As you can see on Fig. 2, the reflection maximum of Xylenol orange on the DMClSA-Solv surface is observed at 430 nm. It should be noted that Xylenol orange isn't practically sorbed by DMClSA-Solv because the reagent, unlike its Ga(III) and In(III) complexes, is not soluble in acetone and ethanol which form a pseudo-membrane on the surface of the sorbent. The formation of complexes of Xylenol orange with Ga(III) and In(III) on the silica surface is accompanied by a bathochromic shift of the main absorption band to 550 and 560 nm, respectively.

To optimize the conditions of Ga(III) and In(III) interaction with Xylenol orange on the surface of DMClSA-Solv the dependence of ΔF(R) on the solution pH, the volume and concentration of reagent was studied (Fig. 3a, b).

Fig. 3a shows that the pH of the medium in the range of pH 1-8 does not practically affect the value of the function of Gurevich-Kubelka-Munk sorbates of Xylenol orange, and the optimal acidity interval for interaction with Ga(III) is 2-4 and with In(III) 4-6. The obtained data on the complex formation of Xylenol orange with Ga(III) and In(III) in the solid phase are consistent with the data on the flow of these reactions in solutions. In [29] it is generalized that in aqueous solutions at pH ≈ 3 for Ga(III) and at pH ≈ 4 for In(III) red complexes are formed with Xylenol orange with a molar ratio M:R = 1:1 with maximal absorption at λ 550 and 560 nm, accordingly. The study of the influence of volume and concentration of reagent applied to concentrates Ga(III) and In(III), showed that for quantitative formation of a complex a two-fold excess of reagent is necessary (Fig. 3b). Therefore, in the further the concentrates were processed with 2.0 ml of 0.1% Xylenol orange solution with pH 2.7 and 4.0, respectively, for Ga(III) and In(III) because in these conditions the maximum values of the Gurevich-Kubelka-Munk function of the corresponding complexes on a surface of a solid phase were achieved (Fig. 3a, b).

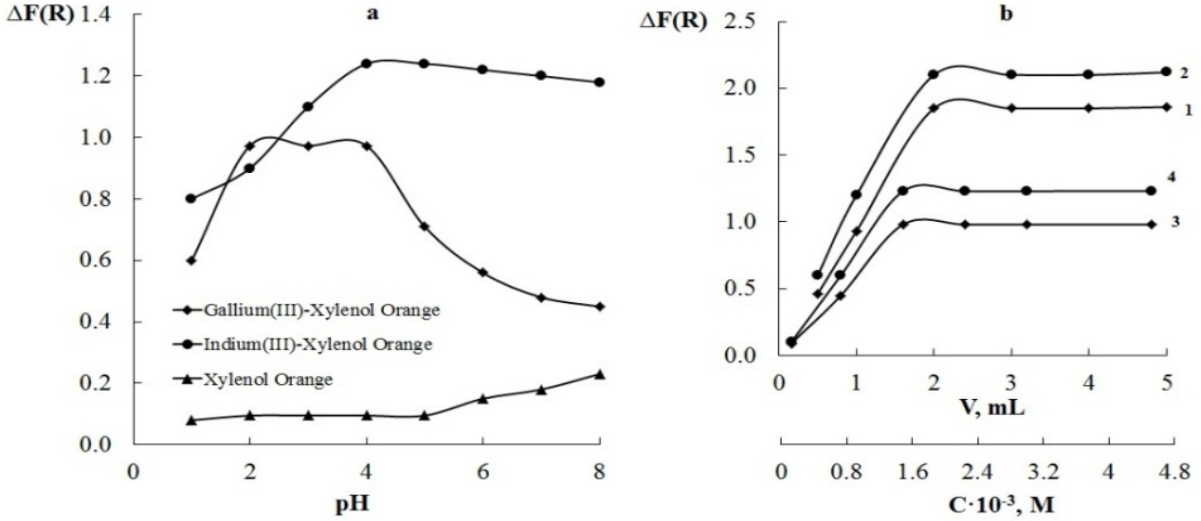

Fig. 3. Dependence of the Gurevich-Kubelka-Munk function on: **a** – acidity for Xylenol orange (λ = 430 nm) and its Ga(III) (560 nm) and In(III) complexes (λ = 550 nm) on the DMClSA-Solv surface; **b** – volume of 0.1% solution of chromogenic reagent (1, 2) and its concentration (3.4) for the complexes of Ga(III) (1, 3) and In(III) (2, 4), respectively.

Complex formation proceeds instantaneously and further increase of contact time of the concentrates with reagent does not noticeably change optical characteristics. The colored solid samples were air dried and diffuse reflection spectra were recorded using DMClSA-Solv passed through the entire course of analysis as a blank.

The composition of the complexes was established by the method of molar relations (Fig. 4).

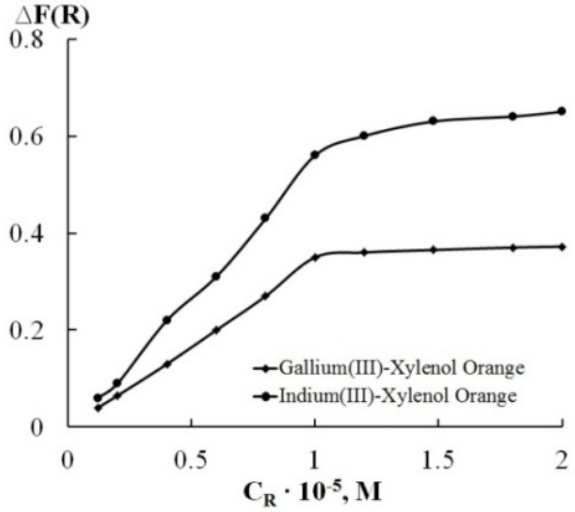

Fig. 4. Xylenol orange saturation curve for concentrates on the surface of DMClSA-Solv (Cm = $1 \cdot 10^{-5}$ mol L).

From Fig. 4 it is visible that on the DMClSA-Solv surface Xylenol orange forms complexes with Ga(III) and In(III) with a molar ratio of 1:1. Taking into account the condition of the chromogenic reagent and metal ions, it is possible to assume that the complex formation in the solid-phase system, as well as in the solution, is carried out due to substitution of hydrogen ions of carboxyl groups and coordination with nitrogen to formation of two cycles. The values of the molar absorptivity (ε_λ) of the Xylenol orange complexes with Ga(III) and In(III), which are equal to 34900 and 36400 L mol^{-1} cm^{-1}, respectively, and their stability constants ($6.0 \cdot 10^8$ and $1.0 \cdot 10^9$) were calculated by processing the saturation curve (Fig. 4) by the equilibrium shift method. It should be noted that the stability of the complexes on the surface of DMClSA-Solv increases in comparison with aqueous solutions ($2.0 \cdot 10^8$ and $1.7 \cdot 10^8$). The similar effect is observed for Xylenol orange complexes with Ga(III) and In(III) in aqueous-organic solutions [19].

Analytical figures of merit and interference study

The analytical signal dependence from Ga(III) and In(III) concentration was studied in the concentration range of 0.01÷10 mg L^{-1}. The maximum in the diffuse reflection spectra of fixed complexes does not depend on the metals concentration, and the F(R) function linearly increases with the increase of the initial Ga(III) and In(III) concentration of the investigated solutions. Calibration graphs $\Delta F(R) = f(C_0)$ are linear in a wide range of concentrations and are described by the equations given in Table. 1. It was established that the signals of Ga(III) and In(III) are not affected by a 100-fold excess of Pb^{2+}, Zn^{2+}, Co^{2+}, Ni^{2+}, Cd^{2+}, Sn (IV), Cu^{2+}, Mn^{2+}.

Table 1. Analytical figures of merit (n = 5; P = 0.95).

Analyte	Linear regression equation	pH	λ_{max}, nm	Linearity, mg L^{-1}
Ga(III)	y = 0.358x + 0.007 R^2 = 0.997	2.7	550	0.020÷5.5
In(III)	y = 0.395x + 0.017 R^2 =0.996	4.0	560	0.018÷5.2

Table 2. Intra-day and inter-day accuracy and precision data for the proposed procedure for determination of Ga(III) and In(III) after solid-phase extraction preconcentration (n=5, P=0.95)

Spiked (μg L^{-1})	Intra-day					
	Found (μg L^{-1})		RSD(%)		R(%)	
	Ga(III)	In(III)	Ga(III)	In(III)	Ga(III)	In(III)
25	24.2±0.7	25.4±0.8	2.3	2.5	96.8	101.6
75	76.1±2.5	76.5±2.6	2.6	2.7	101.5	102.0
Spiked (μg L^{-1})	Inter-day					
	Found (μg L^{-1})		RSD(%)		R(%)	
	Ga(III)	In(III)	Ga(III)	In(III)	Ga(III)	In(III)
25	25.4±0.9	25.8±1.1	2.8	3.4	101.6	103.2
75	76.7±3.3	76.3±3.5	3.5	3.7	102.3	101.7

The influence of Bi^{3+} and Ti(IV), which are also adsorbed by DMClSA-Solv, can possibly be eliminated with the introduction of an additional stage of their adsorption removal from the solutions at pH = 1.0. The interfering effect of Fe^{3+} is eliminated by masking it with 1 cm^3 of 5% solution of NaF or with 1 cm^3 of freshly prepared 1% solutions of ascorbic or tartaric acid. The limits of detection (LOD), defined as $3s_a/b$, were 6.0 and 5.4 μg L^{-1} for Ga(III) and In(III), respectively. The limits of quantification (LOQ, $10s_a/b$) for Ga(III) and In(III) were 20 μg L^{-1} and 18 μg L^{-1}, respectively. The precision of the proposed method for the solid-phase extraction and diffuse reflectance spectroscopic determination technique were checked by performing 5 measurements at two concentration levels (25 and 75.0 μg L^{-1}) of Ga(III) and In(III) over two consecutive days and are summarized in Table 2.

Analytical application of the proposed technique

The proposed method was successfully applied to the determination of Ga(III) and In(III) in binary model solutions and water samples (Table 3).

Table 3. Determination of Ga(III) and In(III) trace quantities after their preconcentration by solid-phase extraction on DMClSA-Solv (n=5; P=0.95)

Sample		Spiked, mg L^{-1}	Found, mg L^{-1}	RSD, %	R, %	Found*, mg L^{-1}	RSD, %	R, %
Binary model solutions	Ga(III)	0.5 5.0	0.489±0.015 4.906±0.073	2.4 1.2	97.8 98.1	0.511±0.02 4.956±0.23	3.6 3.7	102.2 99.1
	In(III)	0.5 5.0	0.483±0.019 4.864±0.181	3.1 3.0	96.6 97.3	0.498±0.02 5.016±0.24	3.5 3.9	99.6 100.3
Water sample**	Ga(III)	- 0.5	0.852±0.024 1.353±0.045	2.3 2.7	- 100.2	0.891±0.04 1.375±0.06	3.4 3.7	- 96.8
	In(III)	- 0.5	0.231±0.009 0.728±0.032	3.3 3.5	- 99.4	0.254±0.01 0.749±0.04	3.6 3.8	- 99.0

RSD – relative standard deviation, %; R – recovery, %. * determined by ICP-OES according to ISO 11885:2007. ** circulating water in Bayer process which contains the following ions: Bi^{3+}, Ti^{4+}, Fe^{3+}, Pb^{2+}, Zn^{2+}, Co^{2+}, Ni^{2+}, Cd^{2+}, Sn^{4+}, Cu^{2+}, Mn^{2+}

Table 4. Comparison with some literature studies

Analyte	Separation method	Detection technique	LOD, μg L^{-1}	Ref.
Ga	Amberlite XAD-4/5-phenylazo-8-quinolinol	XRF	81.0	26
	Polyurethane foam	FAAS	6.00	27
	Amberlite XAD-2/1-(2-pyridylazo)-2-naphthol	GFAAS	2.1	28
	Amberlite XAD-4/HMPN	FAAS	3.42	29
	Amberlite XAD-4/BTAHN	SF	3.1	30
In	Naphthalene/1-(2-pyridylazo)-2-naphtol	Differential pulse polarography	200	31
	Naphthalene/morpholine-4-dithiocarbamate	Differential pulse polarography	100	32
Ga; In	CPE using Gallic acid as chelating agent and Triton X-144 as surfactant	FAAS	3.50; 1.25	7
	Sorption on amino silica gel modified by gallic acid	FAAS	5.80; 1.82	9
	Solid phase extraction using DAPCH loaded on Duolite C20 as a sorbent	FAAS	30; 13	33
	Amino silica modified with HBAAS	FAAS	4.10; 1.55	17
Ga	Dimethylchlorosilane aerosil impregnated with acetone or ethanol / Xylenol orange	Diffuse reflectance spectroscopy	6.0	This work
In	Dimethylchlorosilane aerosil impregnated with acetone or ethanol / Xylenol orange	Diffuse reflectance spectroscopy	5.4	This work

XRF – X-ray fluorescence spectroscopy; FAAS – flame atomic absorption spectroscopy; GFAAS – graphite furnace atomic absorption spectroscopy; SF – spectrophotometry; HMPN – 1{[(6-{[(E)-1-(2-hydroxy-1-naphthyl)methylidene]amino}-2-pyridyl)imino]methyl}-2-naphthol; BTAHN – 1-(2-benzothiazolylazo)-2-hydroxy-3-naphthoic acid; DAPCH – 1-(3,4-dihydroxybenzaldehyde)-2-acetylpyridiniumchloride hydrazone; HBAAS – 2-hydroxy-5-(2-hydroxybenzylideneamino)benzoic acid.

High recoveries (96.6-100.2 %) indicated that the proposed method was accurate, reliable and can be used for the preconcentration and determination of Ga(III) and In(III) traces *via* diffuse reflectance spectroscopy. The similarity of the results obtained by an alternative method also indicates the correctness of the proposed technique for Ga(III) and In(III) preconcentration and quantification.

Comparison of the present method with some other reported methods

A comparison of the proposed method with some analytical procedures for Ga(III) and In(III) determination, reported in the literature, is shown in Table 4. By comparing the data in Table 4, it is obvious that the sensitivity of the proposed technique is comparable with that of other spectrophotometric methods for the determination of Ga(III) and In(III).

CONCLUSION

This study presents a new adsorbent based on dimethylchlorosilane aerosil impregnated with acetone or ethanol as a pseudomembrane for solid phase extraction of gallium(III) and indium(III) and their determination by diffuse reflectance spectroscopy with Xylenol orange. The proposed method is simple, precise and accurate. The detection and quantification limits were 6.0 and 5.4 μg L^{-1}; 20 and 18 μg L^{-1} for Ga(III) and In(III), respectively. The developed method was successfully applied to the trace level determination of gallium(III) and indium(III) in water samples.

REFERENCES

1. S. Aldridge, A. J. Downs, The group 13 metals aluminium, gallium, indium and thallium: chemical patterns and peculiarities, New York, Wiley, 2011.
2. C. R. Chitambar, *Int. J. Environ. Res. Public Health.,* **7**, 2337 (2010).
3. G. Repetto, A. del Peso, Gallium, Indium, and Thallium, in: Patty's Toxicology, New York, Wiley, 2001.
4. V. K. Singh, N. K. Agnihotri, H. B. Singh, and R. L. Sharma, *Talanta,* **55**, 799 (2001).
5. H. Filik, M. Dogutan, E. Tütem, R. Apak, *Anal. Sci.,* **18**, 955 (2002).
6. J. Zhang, Y. Shan, J. Ma, L. Xie, X. Du, *Sens. Lett.,* **7**, 605 (2009).
7. W. I. Mortada, I. M. Kenawy, M. M. Hassanien, *Anal. Methods,* **7**, 2114 (2015).
8. K. Saberyan, E. Zolfonoun, M. Shamsipur, M. Salavati-Niasari, *Sep. Sci. Technol.,* **44**, 1851 (2009).
9. M. M. Hassanien, I. M. Kenawy, M. R. Mostafa, H. El-Dellay, *Microchim. Acta,* **172**, 137 (2011).
10. C.-C. Wu, H.-M. Liu, *J. Hazard. Mater.,* **163**, 1239 (2009).
11. M. Langødegård, G. Wibetoe, *Anal. Bioanal. Chem.,* **373**, 820 (2002).
12. H.-M. Liu, J.-K. Jiang, Y.-H. Lin, *Anal. Lett.,* **45**, 2096 (2012).
13. J. N. Iyer, P. M. Dhadke, *Sep. Sci. Technol.,* **36**, 2773 (2001).
14. S. Fan, Q. Jia, N. Song, R. Su, W. Liao, *Sep. Purif. Technol.,* **75**, 76 (2010).
15. C. B. Ojeda, F. S. Rojas, *Microchim. Acta,* **177**, 1 (2012).
16. C. R. M. Rao. *Anal. Chim. Acta.*, **318**,113 (1995).
17. M. M. Hassanien, W. I. Mortada, I. M. Kenawy, H. El-Daly, *Applied Spectroscopy*, **71**, 288 (2017).
18. M. Tuzen, M. Soylak, *J. Hazard. Mater.,* **129**, 179 (2006).
19. S. V. Mahamuni, P. P. Wadgaonkar, M. A. Anuse, *J. Serb. Chem. Soc.,* **75**, 1099 (2010).
20. K. P. P. R. M. Reddy, V. K. Reddy, P. R. Reddy, *Anal. Lett.*, **40**, 2374 (2007).
21. Y. Zhu, F. Jin, S. Yang, J. Li, D. Hu, L. Liao, *Exp. Ther. Med.,* **5**, 1001 (2013).
22. M. Krawczyk-Coda, *New J. Chem.*, **42**, 15444 (2018).
23. A. N. Chebotarev, V. P. Dubovyiy, D. V. Snigur, *Mosc. Univ. Chem. Bull.,* **73**, 116 (2018).
24. K. Bevziuk, A. Chebotarev, A. Koicheva, D. Snigur, *Monatsh. Chem.*, **149**, 2153 (2018).
25. A. N. Chebotarev, E. M. Rahlickaja, *Izv. Vuzov, Himija i Him. Tehnologija*, **45**, 108 (2002), (in Russian).
26. A. N. Masi, R. A. Olsina, *J. Trace Microprobe Tech.*, **17**, 315 (1999).
27. A. N. Anthemidis, G. A. Zachariadis, J. A. Stratis, *Talanta*, **60**, 929 (2003).
28. P. Bermejo-Barrera, N. Martinez-Alsonso, A. Bermejo-Barrera, *Fresenius J. Anal. Chem.*, 2001, **369**, 191 (2001).
29. K. Saberyan, E. Zolfonoun, M. Shamsipur, M. Salavati-Niasari, *Acta Chim. Slov.*, **57**, 222 (2010).
30. A. S. Amin, S. M. N. Moalla, *RSC Adv.*, **6**, 1938 (2016).
31. M. A. Taher, *Talanta*, **52**, 301 (2000).
32. R. K. Dubey, S. Puri, M. K. Gupta, B. K. Puri, *Anal. Lett.*, **31**, 2729 (1998).
33. M. M. Hassanien, I. M. Kenawy, A. M. El-Menshawy, A. A. El-Asmy, *Anal. Sci.*, **27**, 1403 (2007).

Bulgarian Chemical Communications, Volume 53, Issue 3 (pp. 275 - 278) 2021 *DOI: 10.34049/bcc.53.3.5311*

Analysis of some chemical characteristics of pumpkins of the genus Cucurbita moschata and Cucurbita maxima and their dependence on soil indicators

S. I. Papanov[1*], E. G. Petkova[2], I. G. Ivanov[3]

[1]*Medical University Plovdiv, Department of Pharmacognosy and Pharmaceutical Chemistry, Faculty of Pharmacy, 15A, V. Aprilov Blvd., 4000 Plovdiv, Bulgaria*
[2]*Medical University Plovdiv, Medical College, 120, Br. Bakston Str., 4004 Plovdiv, Bulgaria*
[3]*University of Food Technologies, Technological Faculty, 26, Maritza Blvd., 4002 Plovdiv, Bulgaria*

Received: July 21, 2020; Revised: July 12, 2021

The homeland of the pumpkin is Central and South America. There are over 300 species of pumpkins in Bulgaria. The high nutritional and biological qualities combined with the valuable dietary, medicinal and taste properties of pumpkin fruits determine their importance in the nutritional balance. The fruits are rich in mineral salts and vitamins. The highest content is of provitamin A (carotene) - from 6 to 20 mg%. The dietary qualities of the fruit are related to the content of peptonizing enzymes which break down insoluble proteins into soluble peptones. The orange color of the pumpkin is due to the antioxidant beta-carotene. This study presents the relationships between some characteristics of pumpkins and the qualities of the soils on which they were grown. The mineral composition and pH of the soil determine the pH of the studied fruits. There is a directly proportional relationship between the total phenols and the antioxidant activity. A directly proportional relationship between pH and total phenols and antioxidant activity was also found.

Keywords: pumpkins, antioxidant ability, total polyphenols content

INTRODUCTION

The homeland of the pumpkin is Central and South America. As a cultivated plant, pumpkins were grown as early as 1000 BC in Mexico and Peru and successfully in all parts of the world with a warmer climate. They were brought to Europe in the 16th century. Pumpkins are used because their fruits can be stored for a longer time due to their hard skin and can be consumed in winter too. Their fruits and seeds are used for consumption, medicinal purposes, for fodder and decoration [1-4]. There are over 300 species of pumpkins in Bulgaria. In our geographical region, pumpkins have found favorable conditions and are grown today in all areas around the country. The most widely-spread species and those with the biggest economic importance are: Cucurbita maxima Duch. - white pumpkin, large-fruited, chestnut; Cucurbita moschata Duch. - nutmeg pumpkin, violin; Cucurbita pepo L. - plain pumpkin, pork pumpkin [2-5].

The high nutritional and biological qualities combined with the valuable dietary, medicinal and taste properties of pumpkin fruits determine their importance in the nutritional balance. The usable part of the pumpkin comprises up to 85% of the weight. The starch content is high - 2 to 7% of the raw mass. The fruits are rich in mineral salts and vitamins. The highest content is of provitamin A (carotene) - from 6 to 20 mg%.

The dietary qualities of the fruit are related to the content of peptonizing enzymes, which break down insoluble proteins into soluble peptones. The orange color of the pumpkin is due to the antioxidant beta-carotene. It is one of the most important ingredients in pumpkins. In the human body it becomes the vital vitamin A - reduces the risk of developing certain types of cancer, offers protection against heart disease, and improves eyesight [5-7]. In 100 grams of pumpkin there are more than 3 mg of this provitamin, which is approximately one third of the recommended daily amount. Also 100 grams contain 9 mg of vitamin C or about 11% of the recommended daily intake [8]. Pumpkin also contains some of the very rare vitamins found in plant foods - such as vitamin K which is responsible for proper blood clotting. Vitamin D is also found in pumpkins. The most unique one, however, is the little-known vitamin T which helps treat anemia and hemophilia [9].

The vitamins with the highest content in pumpkins are vitamin C, vitamin E and several representatives of the vitamin B group - riboflavin (B2), niacin (B3), pyridoxine (B6) and folic acid (B9). Moreover, an extraordinary trait of pumpkin is its low caloric value, since its flesh, depending on variety, contains merely 15-25 kcal in 100 g, and thanks to the presence of numerous easily digestible

*To whom all correspondence should be sent:
E-mail: stoyan.papanov@abv.bg

© 2021 Bulgarian Academy of Sciences, Union of Chemists in Bulgaria

nutrients it has become an advantageous component of slimming diets. It regulates metabolism, lowers glucose level in blood, possesses detoxicating, as well as slightly dehydrating properties. Another attributed function of pumpkin species is defense against cancer [23].

The micro elements that are contained in highest doses in pumpkins are potassium, copper, manganese, iron, magnesium and phosphorus. Alongside with their other roles, some of these elements are also cofactors in enzyme complexes with potent antioxidant activity [10].

Due to its low sodium and high potassium content, pumpkin is a good natural diuretic. Pumpkin contains 90 % water and has a diuretic effect. Phosphorus and magnesium improve memory and the nervous system's activity [9].

Pumpkins have significant soil requirements. They grow well on rich, structural, well-aerated soils with high humus content. They do not tolerate compacted cold soils with insufficient water permeability. Doikova *et al*. (1997) have found that soil types and fertilizers influence the yield of different pumpkin types [7]. Pumpkin brings joy to people and it is no coincidence that it has found a place in folk tales and legends. This study presents the relationships between some characteristics of pumpkins and the qualities of the soils on which they were grown.

Material and methods

For the period of time from 09.2019 to 01.2020, pumpkins of the varieties Muscat pearl pumpkin and Tahitian melon squash of the Cucurbita moschata family and Argentina and Danka Polka varieties from the Cucurbita maxima family were examined.

The antioxidant characteristics of pumpkin from different varieties cultivated in Bulgaria were the object of the study. The varieties from Bulgaria were grown in the following order - in the area of the village of Kavrakirovo, (97 m above sea level), Petrich municipality, Blagoevgrad region. All studied pumpkins were raised on alluvial meadow soils. According to the research of Shaban *et al*., the optimal pH for pumpkins cultivation is from 6.5 to 6.8 [11].

The studies were conducted in the Laboratory of the University of Food Technology Plovdiv and the Laboratory of Pharmaceutical Analysis of the Medical University of Plovdiv.

The following research methods were used in the study:

• Systematic approach and critical analysis of the accessible scientific periodicals;

• DPPH method for determination of antioxidant activity (radical detecting activity);

• Spectrophotometric method for determination of absorption and calibration curve in gallic acid.

Determination of pH, titratable acidity and juice extraction. Using a Philips food processor, the pumpkin fruits were liquefied to juice. The latter was then pre-filtered and centrifuged at 3000 rpm for 15 min. With the WTWinoLab pH 7110, Germany pH meter the pH was potentiometrically measured. The titratable acidity was expressed as a percentage of malic acid. It was determined by titrating 10 mL of pumpkin juice with 0.1 M NaOH to a pH value of 8.1. The resultant findings were expressed in g citric acid per 100 g juice.

Total polyphenolics content (TPC). Using a Folin-Ciocalteu assay the measurements of the total phenolic contents were done correctly. Folin-Ciocalteu reagent (Sigma) (1 mL) was mixed with 0.2 mL of sample and 0.8 mL of 7.5% Na_2CO_3. At room temperature for about 20 minutes in darkness the reaction was performed. The absorbance of the sample was measured at 765 nm against a blank sample obtained in the same way without extract. The results were expressed in mg equivalent of gallic acid (GAE) per 100 g juice, according to the calibration curve built in the range of 0.02 - 0.10 mg gallic acid (Sigma) used as a standard.

Antioxidant activity (DPPH assay). A mixture of each analyzed extract (0.15 mL) with 2.85 mL of freshly prepared 0.1 mmol solution of 1,1-diphenyl-2-picrylhydrazyl radical (DPPH, Sigma) in methanol (Merck) was prepared. This was done at 37° C in darkness and the absorption at 517 nm was recorded after 15 min against methanol. The antioxidant activity was expressed as mmol Trolox equivalents (TE) per 100 g juice by using a calibration curve built with 0.05, 0.1, 0.2, 0.3, 0.4 and 0.5 mmol 6-hydroxy-2,5,7,8-tetramethylchroman-2-carboxylic acid (Trolox®, Fluka) dissolved in methanol (Sigma).

RESULTS AND DISCUSSION

In the present study, we considered pumpkins of the Muscat pearl pumpkin and Tahitian melon squash varieties of the Cucurbita moschata family and pumpkins of the Argentina and Danka Polka varieties of the Cucurbita maxima family. The pumpkins have been grown in the area of the village of Kavrakirovo, Petrich municipality, Blagoevgrad region. All varieties of the pumpkins have been grown on alluvial-meadow soils. The altitude at which the pumpkins were grown is about 97 meters.

The pH is an important variable indicator of

soils, as it affects many chemical processes. It particularly affects the plant's nutrition by controlling the chemical forms of various nutrients and influences the ongoing chemical reactions. The pH of the typical alluvial-meadow soils in the region is in the range from 6.5 to 6.8. With the help of a pH meter (WTWinoLab pH 7110, Germany) we found that the pH of the soils is within the above range. Alluvial-meadow soils are fertile soils that are formed in different climates along large rivers on loose sandy gravel with alluvial deposits. They are spread on I and II floodplain terraces of the country's rivers. They have only one thin surface horizon - darker, up to 10 cm, after which there are only layers that differ in the type of grouping. The optimal soil reaction of the respective soil type is slightly acidic to neutral (pH 6.5 to 6.8) [12-15].

Antioxidants are a group of biochemicals, low-molecular compounds that enter the body through various foods. The main property of these substances is the destruction of free radicals in the body. They connect to the free radicals and stop their harmful effects. It is believed that there are hundreds and probably thousands of substances that can act as antioxidants [12, 14, 16].

Phenols are hydroxyl derivatives of benzene in which the hydroxyl group is directly attached to the aromatic nucleus. Depending on the number of hydroxyl groups, the phenols are monovalent, divalent, trivalent and polyvalent. The more complex phenols may contain more than one phenolic residue in their molecule and are therefore divided into monophenols, diphenols, triphenols and polyphenols [12, 17-19].

An idea of the relationship between the general phenols and the antioxidant activity of the considered pumpkins is given in Table 1. As it can be seen from the table, with the increase in total phenols the antioxidant activity also increases. Total phenols range from 54.00 ± 0.50 mg GAE / 100 g to 117.70 ± 1.40 mg GAE / 100 g. Antioxidant activity ranges from 98.60 ± 5.30 mmol TE / 100 g to 138.20 ± 1.80 mmol TE / 100 g. It is highest in the Danka Polka variety and lowest in the Pearl variety. The established rectilinear relationship between the antioxidant activity and total phenols in this case gives us a reason to determine only one indicator and have information about the other. According to the content of total phenols and antioxidant activity, the considered varieties can be arranged as follows: Danka Polka (highest), Tahitian melon, Argentina and Pearl [20, 21].

Titratable acidity, expressed as a percentage of malic acid, was determined by titrating 10 mL of pumpkin juice with 0.1 M NaOH to a pH value of 8.2. The results were expressed in g malic acid per 100 g juice. The results for the obtained values of the total phenols and the titratable acidity are presented in Figure 1.

Table 1. Relationship between total phenols and antioxidant activity.

Cultivar	Total phenols	Antioxidant activity (DPPH)
Muscat pearl pumpkin	54.00 ± 0.50 mg GAE/ 100 g	98.60 ± 5.30 m mol TE/ 100 g
Tahitian melon squash	60.28 ± 1.60 mg GAE/ 100 g	110.50 ± 3.60 m mol TE/ 100 g
Argentina	55.85 ± 1.20 mg GAE/ 100 g	99.23 ± 1.21 m mol TE/ 100 g
Danka Polka	17.70 ± 1.40 mg GAE/ 100 g	138.20 ± 1.80 m mol TE/ 100 g

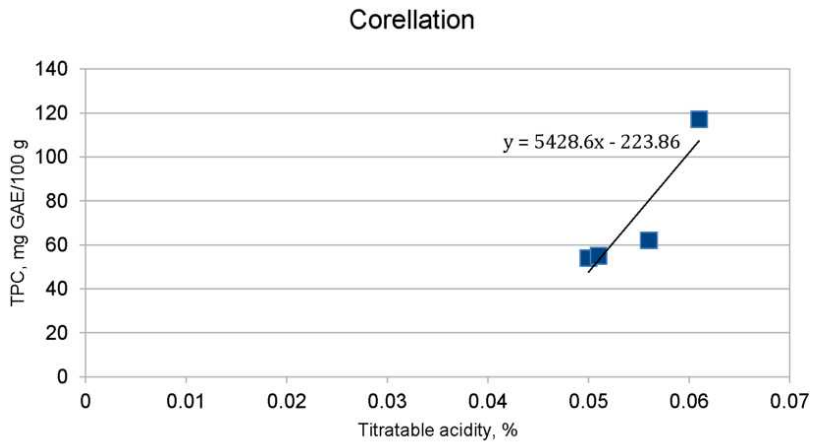

Figure 1. Correlation relationship between total polyphenols content (TPC) and titratable acidity in the investigated pumpkin fruits

The correlation between total polyphenols and titratable acidity is 0.9103. The examined pumpkin cultivars are characterized with the highest quantity of malic acid as compared to other organic acids, especially citric acid. Its content ranged from 2.27 g/kg FW to 4.54 g/kg FW. Changeable dominance of either malic or citric acid in pumpkin fruit was observed, depending on cultivar [22]. The obtained results regarding the indicators pH and titratable acidity are presented in Table 2.

Table 2. Relationship between pH and titratable acidity.

Cultivar	pH	Titratable acidity, %
Muscat pearl pumpkin	6.32	0.056
Tahitian melon squash	6.70	0.061
Argentina	6.48	0.050
Danka Polka	7.20	0.051

The obtained pH values are from 6.32 to 7.20. The highest pH value is in the Danka Polka variety, and the lowest in the Pearl variety. The titratable acidity has approximately the same value for the considered varieties - from 0.05% to 0.06%. The changes in the pH and titratable acidity are in a small range.

We determined the correlation between pH and titratable acidity for the considered fruits. Its value is 0.038677. The correlation between the total phenols and pH is 0.984078.

CONCLUSIONS

The mineral composition and the pH of the soil determine the pH of the studied fruits. There is a directly proportional relationship between the total phenols and the antioxidant activity. A directly proportional relationship between pH and total phenols and antioxidant activity was also found. No proportional relationship was found between total phenols and titratable acidity. The titratable acidity has approximately the same values for the different varieties of the same family.

REFERENCES

1. S. Genchev, Application of growth regulators in vegetable production, Plovdiv, Hr. G. Danov, 1981.
2. P. Gorbanov, *Fertilization of agricultural crops*, 351 (2010).
3. Hr. Daskalov, N. Kolev, T. Murtazov, G. Genkov, Vegetable Production, State Publishing House for Agricultural Literature, 1965.
4. MAFF. Quality control of fresh fruits and vegetables. Plant Growing and Quality Control Directorate for Fresh Fruits and Vegetables, 2002.
5. D. Cholakov, Vegetable production in the tropics and subtropics, Academic Publishing House Plovdiv, 2001.
6. http://www.adf.org.yu/Projects/KI/2-12-08-02.html
7. N. Shaban, S. Bistrichanov, Ts. Moskova, E. Kadum, I. Mitova, M. Tityanov, P. Bumov, Vegetable production, Sofia, 2014.
8. https://www.2befit.bg/bg/
9. https://www.hera.bg/s.php?n=280
10. https://www.puls.bg/khranene-c-21/
11. S. Papanov, Ek. Petkova, I. Ivanov, *Bulg. Chem. Commun*., **51**(1), 113 (2019).
12. https://sites.google.com/site/laboratoriacentral/za-nas/obsi-fizikohimicni- pokazateli/fenoli
13. M. Xanthopoulou, T. Nomikos, E. Fragopoulou, S. Antonopoulou, *Food Research International*, **42**(5-6), 641 (2009).
14. F. Que, L. Mao, X. Fang, T. Wu, *Food Science and Technology*, **43**, 1195 (2008).
15. H. Wu, J. Zhu, W. Diao, Ch. Wang, *Carbohydrate Polymer.,* **113**, 314 (2014).
16. I. Dini, G. C. Tenore, I. Dini, *LWT - Food Science and Technology*, **53**(1), 382 (2013).
17. Z. Vastag, L. Popovic, S. Popovic, V. Krimer, D. Pericin, *Food Chemistry*, **124**(4), 1316 (2011).
18. E. Nwanna, G. Oboh, *Pak. J. Biol. Sci*., **10**(16), 2682 (2007).
19. F. Oloyede, G. Agbaje, E. Obuotor, I. Obisesan, Food Chemistry, **135**(2), 460 (2012).
20. M. Kim, Ch. Hong, M. Nam, K. Lee, *Korean Journal of Food Science and Technology*, **43**(2), 195 (2011).
21. L. Chen, G. Huang, *International Journal of Biological Macromolecules*, **118**, Part A, 770 (2018).
22. A. Nawirska, 0. Iszanska, A. Biesiada, A. Sokottepwska, Z. Kucharska, *Food Chemistry*, **148**, 415 (2014).
23. P. Astorg, *Trends in Food Science and Technology*, **8**, 406 (1999).

Bulgarian Chemical Communications, Volume 53, Issue 3 (pp. 279 - 286) 2021 *DOI: 10.34049/bcc.53.3.5313*

Oil contents and fatty acid composition of walnut genotypes selected from Central Anatolia region and assessments through GT biplot analysis

A. Uzun[1*], M. Kaplan[2], H. Pinar[1], K. Paris[3]

[1]*Erciyes University, Department of Horticulture, Kayseri, Turkey*
[2]*Erciyes University, Department of Field Crops, Kayseri, Turkey*
[3]*Provincial Directorate of Ministry of Food Agriculture and Livestock, Kayseri, Turkey*

Received: July 28, 2020, Revised: January 30 2021

Walnuts with quite rich nutrient contents and several benefits on human health are among the significant nut fruits. Turkey is among the gene centers of walnut and thus has diverse walnut populations throughout the country. Therefore, it is highly significant to assess this rich source and to identify superior genotypes. Walnuts are rich in oil content and have several positive impacts on human health. In this study, 50 walnut genotypes having superior characteristics were selected from Kayseri province in Central Anatolia region of Turkey. Total oil (crude oil) and fatty acid composition of these genotypes were determined. The recorded data were subjected to variance analysis and assessed through a biplot method. Crude oil contents of walnut genotypes varied in the range of 61.22-74.00% and linoleic acid (32.52-65.47%) was identified as the major fatty acid. Unsaturated fatty acid contents of walnut genotypes varied between 88.20 and 96.16%. Genotype Trait (GT) biplot graph showed that the sum of the first two principal components explained about 59.5% of total variation. While the genotypes KW24, KW10, KW41, KW2, KW6, KW17, KW31 and KW25 were found to be prominent with their crude oil contents, the genotypes KW32 and KW34 were found to be prominent with unsaturated fatty acids. Present findings revealed that the GT biplot method could efficiently be used in selection of walnut genotypes prominent with their crude oil contents and fatty acid composition. It was also concluded that walnuts rich in unsaturated fatty acids could be used as functional food and the present superior genotypes could be used as parent materials in further walnut breeding studies.

Keywords: *Juglans regia*, nutritional characteristics, fatty acids

INTRODUCTION

The genus *Juglans* includes 20 species and *Juglans regia* L. has long been cultured worldwide [1]. This species with large, tasty and thin-shelled fruits is the most significant one cultured for fruits in different countries of the world including Turkey [2]. Gene center of *Juglans* species is believed to be Central Asia and surroundings [3], and Anatolia is also among these gene centers [4]. China, USA, Iran, Turkey and Ukraine are the leading walnut producers of the world. World annual production is around 3.75 million tons. Annual production of Turkey is 195 000 tons [5]. Walnuts have quite high oil contents (50-80%) and are rich in proteins (12-15%), minerals, vitamins. They have lower sugar contents (2.5-4%), thus they are consumed as an important dietary supplement [6]. Walnut oil is largely composed of oleic and linoleic acids [7]. Polyunsaturated fatty acids, like linoleic acid, reduce the risk of coronary hearth diseases. High natural antioxidant contents of walnuts also have preventive effects against some cancer types [8]. Walnuts green husks have also some antimicrobial activity [9].

The material used in walnut breeding should be true-to-name and its characteristics should be well-defined. Morphological and physiological descriptions either take long time because of youth sterility or are influenced by environmental conditions [10]. Identification of fatty acids of walnut populations in Turkey will put forth significant data for the identification of walnut genotypes with high oil contents. There are several seed-propagated walnut populations in Turkey with quite different genetic characteristics. So, there is huge genetic diversity in walnut populations. Yield and fruit characteristics of these genetic sources have been studied [11-19], and genetic diversity researches have been conducted [20-22]. However, there is a limited information available about fatty acid composition and variations in this attribute of the walnut genotypes.

Biplot analysis allows visual inspection of data and thus is commonly used in various sciences including economy, sociology, medicine, engineering, genetic and agriculture. Biplot is a two-way table design and presents graphically row and column factors. In this method of analysis, row and column factors can be assessed one by one

*To whom all correspondence should be sent:
E-mail: uzun38s@yahoo.com

© 2021 Bulgarian Academy of Sciences, Union of Chemists in Bulgaria

through the relationships between each pair of them and mutual interactions can also be presented visually [23]. Graphical presentation of more than one characteristic of the genotypes allows researchers to visually compare several genotypes and several attributes of these genotypes [24]. This study was conducted to determine oil contents and fatty acid compositions of walnut genotypes collected from Central Anatolia region of Turkey. The research results were assessed through biplot analysis. The prominent genotypes will be able to be used as a functional food and be also used in further breeding studies.

EXPERIMENTAL

Plant material

About 800 walnut genotypes, already known as seed-propagated from Kayseri province and surrounding town in Central Anatolia, were assessed in this study. With these assessments, 50 genotypes without any disease symptoms and prominent with yield and fruit quality attributes were selected and used as the plant material of the present experiments. Fruits were collected from the specified trees at harvest period. The shells of collected walnuts were removed and the walnuts were dried at shade.

Oil extraction and fatty acid composition

Deshelled walnut samples were cleaned from the foreign materials and ground in a hand-mill. Oil extraction was performed with hexane/isopropanol (2:1 v/v) [25]. Ten grams of ground walnut samples were weighed in a cellulosic cartridge and placed in a Soxhlet extractor for 5 h to provide oil extraction under continuously flowing solvent. At the end of the duration, the extracted oils were centrifuged at 10.000 *g* for 5 min to separate some possible strange material and the solvent was evaporated at 40 °C with a rotary evaporator. Finally, the crude oil content of the samples was calculated using the mass balance. The measurements were repeated two times with three replicates.

For quantification of fatty acids, methylation was initially performed. This process was carried out in accordance with AOAC (1990) (Official methods of analysis, method 969-33). About 100 mg of oil sample was weighed into centrifuge tubes and 3 ml of hexane was added to completely dissolve the oil. Then 100 µl of potassium hydroxide (2 N KOH in methanol) was added and the tubes were vortexed for one min. Finally, the samples were centrifuged at 5000 rpm for 5 min and the upper phase (1 ml) was taken in vials and analyzed by a gas chromatograph (Agilent GC, model 6890 N) equipped with a GC column (HP 88 capillary column - 100 m × 0.25 mm ID, 0.2 µm) and a flame ionization detector. Injection volume was 1 µl and injection temperature was set at 250 ºC. A temperature gradient was arranged for GC oven temperature (held at 130 ºC for 1 min, increased to 170 ºC with 6.5 ºC/min, increased to 215 ºC with 2.75 ºC/min, held at 215 ºC for 12 min, increased to 230 ºC with 4.0 ºC/min and held at 230 ºC for 5 min). Total analysis duration was recorded as 40.89 min. Detector temperature was 280 ºC, detector H_2 flow rate was 40 ml/min, dry air flow rate was 450 ml/min, column H_2 flow rate was 1.3 ml/min and split rate was 50/1 [26, 27]. Fatty acid components were identified according to the retention times of the compounds presented by peaks of the standards (FAME mix 37 components; Matreya, Sigma-Aldrich, Milan, Italy) containing C4-24 fatty acids. The analysis was repeated two times with two replicates.

Statistical analyses

Oil and fatty acid composition data of the genotypes were subjected to variance analysis (ANOVA) with SAS [28] software in accordance with randomized blocks experimental design and means were compared using the LSD multiple comparison test. GT biplot analysis was performed to group fatty acid substances and for visual assessment of the relationships between fatty acids. A polygon was formed through connecting the furthest genotypes from the origin of the graph. A graph can also be formed through the lines drawn from the origin perpendicular to polygon edges. Resultant data were analyzed visually with GT biplot analysis [29, 30]. Biplot was first proposed by Gabriel [31] as a graphical analysis method to present the results of principal component analysis (PCA). This chemometric method is a scatter plot graphically displaying a rank-2 matrix by both rows (entries) and columns (testers) [32]. Using the matrix, PCA-based genotype and feature-oriented Genotype-trait biplot analysis was performed to visually evaluate the data matrix, interpret the relationships between traits and group genotypes. The second module of the GGE-biplot program was used in the biplot analysis [33]. In this module, the figures obtained using the paired data based on the SVD values of the standardized data obtained using the standard deviations and standard errors of the numerical values of the genotype and traits were carried on the same plot (biplot). Information on the model used is given in the upper right corner of the biplot graphics. Visual evaluation was made

according to the location of the features and genotypes on the biplot [34].

RESULTS

Mean values of three replicates for oil contents and fatty acids of walnut genotypes are provided in Table 1. The differences in all investigated parameters of walnut genotypes were found to be highly significant ($P<0.01$). Crude oil levels of local walnut genotypes varied between 61.22 and 74.00% and the contents of palmitic acid between 2.04-7.83%, stearic acid between 0.62-6.66%, oleic acid between 13.14-47.28%, linoleic acid between 32.52-65.47%, α-linolenic acid between 7.08-17.28% and docosanoic acid between 0.00-0.34%. Docosanoic acid was not encountered in several genotypes. Unsaturated fatty acid contents of the walnut genotypes varied between 88.20 and 96.16%. The highest total unsaturated fatty acid content was obtained for KW32 genotype and the lowest total unsaturated fatty acid content was obtained for KW24 genotype.

Oil contents and fatty acids of the investigated walnut genotypes were used in GT biplot analysis to get chemical composition vectors and to determine the separation power of the relevant attributes. The attribute with a longer vector has a quite high capacity for the separation of the genotypes. While crude oil content and docosanoic acid had low separation capacity, other fatty acids had high separation capacity for the present genotypes (Fig 1). Image of biplot vectors provides information about the relationships between the investigated attributes. While there were positive correlations between linoleic acid and α-linolenic acid and between crude oil and oleic acid, the linoleic acid and α-linolenic acid negatively correlated with crude oil and oleic acid (Fig. 1).

In biplot analysis, there may be deviations in some attributes of the genotypes. In this sense, according to Table 2 in addition to Figure 1, there were significant positive correlations between palmitic acid and linoleic acid, between stearic acid and oleic acid and between linoleic acid and α-linolenic acid; while there were significant negative correlations between palmitic acid and oleic acid, between oleic acid and linoleic acid and between oleic acid and α-linolenic acid.

GT-biplot polygon also reveals which genotype is prominent with which attributes (GTI: genotype trait interaction) (Fig. 2). It was observed that the genotypes KW49, KW39 and KW4 were prominent with their oleic acid contents, KW22 and KW 24 were prominent with their total saturated fatty acid contents, KW47 with palmitic acid content, KW13, KW9, KW11 and KW36 with linoleic acid and α-linolenic acid content, KW32 and KW34 with total unsaturated fatty acid content.

In another study carried out in Moldova, oil contents of walnut genotypes were reported to be between 55 and 72% [37]. In Morocco, total oil contents of walnut genotypes were reported between 54.04 and 67.48% [38]. Previous studies carried out in different regions indicated variations in oil contents of walnut genotypes. Such differences were mostly resulted from genetic differences and ecological conditions.

Significant differences were observed in fatty acid components of the walnut genotypes. Linoleic acid had the highest quantity (32.52-65.47 %) followed by oleic acid (13.14-47.28 %), linolenic acid (7.08-17.28 %), palmitic acid (2.04-7.83 %) and stearic acid (0.62-6.66 %). Similar findings were also reported by previous studies carried out in different countries. In a study carried out in Turkey, fatty acids composition of walnuts was respectively reported as linoleic (55.3 %), oleic (13.4 %), linolenic (8.7 %) and palmitic acid (6.4 %) [39]. Linoleic acid (58%) was also reported as the major fatty acid in walnuts of Moldova [37]. In another study carried out in Serbia, linoleic acid (57.2–65.1%) was again identified as the major fatty acid followed by oleic acid (15.9–23.7%) [40]. Uzunova *et al.* [41] in a study carried out in Bulgaria reported the major fatty acids of walnut genotypes as linoleic acid (63.52-64.69%) and oleic acid (15.61-17.12%).

Biplot analysis allows researchers to test one or more characteristics under different environmental conditions. Through the use of two-way data like genotype-trait, the genotypes can be scanned for desired attributes [23, 29, 42]. In this study, local walnut genotypes selected from Central Anatolia were scanned and grouped for oil contents and fatty acids. GT-biplot analysis allows the researchers to identify the genotypes prominent with investigated traits (Fig. 2) [29]. It is also possible to identify ideal genotypes for entire traits (Fig. 3) [43]. Narrow angles between the vectors of any two traits indicate positive correlations between the traits (Fig. 1) and such a correlation can be visualized with biplot analysis [29]. Such characteristics of biplot analysis were also taken into consideration while finding out the correlations between the present traits (Fig. 1).

Table 1. Fatty acid composition and crude oil content of walnut genotypes (%).

Genotypes	*CO*	*PA*	*SA*	*OA*	*LA*	*a-LA*	*DA*	*TUSFA*	*TSFA*
KW1	64.11± 1.30r-t	5.40± 0.03o-q	3.82± 0.05d	24.35± 0.03m-o	54.97± 0.11mn	11.46± 0.15op	nd	90.78± 0.02su	9.22± 0.02c-e
KW2	71.5± 1.08a-e	5.18± 0.04qr	2.10± 0.05jk	31.43± 0.09e	51.10± 0.06u-w	10.19± 0.06q-s	nd	92.72± 0.09i-l	7.28l± 0.09-o
KW3	65.49± 1.91l-s	4.89± 0.06rs	2.29± 0.05ij	21.48± 0.26u	60.12± 0.19de	11.22± 0.07op	nd	92.82± 0.01h-l	7.18± 0.01l-p
KW4	65.05± 1.43o-s	4.63± 0.08st	4.81± 0.12c	41.53± 0.21c	40.76± 0.17b*	8.27± 0.42u	nd	90.56± 0.04tv	9.44± 0.04b-d
KW5	67.32± 0.94h-r	6.03±0.07 i-m	2.58± 0.05g-i	30.66± 0.29e-g	47.94± 0.11yz	12.79± 0.38k l	nd	91.39± 0.03np	8.61± 0.03h-j
KW6	72.02± 1.59a-d	5.66± 0.12m-o	0.97± 0.03o-t	20.06± 0.06wx	61.4± 0.08c	11.91± 0.01m-o	nd	93.37± 0.15dg	6.63± 0.15q-t
KW7	67.48± 0.42g-p	6.68± 0.23b-e	0.99± 0.07o-t	20.96± 0.16u-w	56.96± 0.62j-l	14.41± 0.62d-g	nd	92.33± 0.16k-m	7.67± 0.16k-m
KW8	67.60± 0.12g-p	6.65± 0.29b-e	1.03± 0.12o-s	30.37± 0.23fg	51.22± 0.96u-w	10.72± 0.79pq	nd	92.32± 0.41k-m	7.68± 0.41k-m
KW9	69.59± 1.23b-i	6.13± 0.18h-k	1.26± 0.14m-o	14.93± 0.20za*	61.76± 0.20c	15.670± 0.01b	0.24± 0.07b	92.61± 0.32j-l	7.39± 0.32l-n
KW10	70.66± 0.89b-f	6.06± 0.23i-l	1.08± 0.18o-r	29.27± 0.23hi	53.40± 0.61p-r	10.18± 0.43q-s	nd	92.86± 0.41g-k	7.14± 0.41n-q
KW11	68.11± 0.18g-n	6.76± 0.33b-d	0.87± 0.10p-t	17.55± 0.40y	60.66± 0.33cd	14.17± 0.30d-h	nd	92.37± 0.43k-m	7.63± 0.43k-m
KW12	67.54± 2.03g-p	6.17± 0.13g-k	0.67± 0.10t	32.68± 0.15d	51.3± 0.16u-w	9.18± 0.22t	nd	93.16± 0.23f-j	6.84± 0.23n-r
KW13	69.34± 0.35b-j	6.53± 0.19d-g	0.72± 0.10rt	15.30± 0.28z	65.47± 0.59a	11.8± 0.00no	0.19± 0.06c	92.75± 0.30h-l	7.25± 0.30l-p
KW14	69.57± 0.04b-i	5.98± 0.09i-m	2.36± 0.12h-j	21.24± 0.09uv	57.77± 0.32g-j	12.64± 0.38lm	nd	91.66± 0.03no	8.34± 0.03i-j
KW15	69.13± 0.14d-j	5.67± 0.17m-o	2.40± 0.13h-j	20.00± 0.18wx	58.56± 0.12f-h	13.36± 0.11h-l	nd	91.93± 0.05mn	8.07± 0.05jk
KW16	68.69± 1.11e-l	6.16± 0.24g-k	2.31± 0.25ij	25.79± 0.30kl	52.54± 0.54q-t	13.19± 0.35i-l	nd	91.53± 0.49np	8.47± 0.49h-j
KW17	72.29± 1.61a-c	5.59± 0.23n-p	0.78± 0.10q-t	29.3± 0.81hi	52.82± 0.53q-t	11.52± 0.05op	nd	93.63± 0.33c-f	6.37± 0.33r-u
KW18	64.82± 0.44o-s	6.69± 0.37b-e	1.03± 0.18o-s	28.79± 0.33i	53.48± 0.50p-r	10.00± 0.28q-t	nd	92.28± 0.55lm	7.72± 0.55kl
KW19	68.9± 1.03d-k	6.62± 0.22c-f	2.59± 0.36g-i	26.21± 0.27jk	50.71± 0.88vw	13.87± 0.58f-i	nd	90.79± 0.58ru	9.21± 0.58c-f
KW20	68.07± 1.04g-o	6.12± 0.23i-k	1.19± 0.25m-p	25.3± 0.53k-m	57.82± 1.79g-j	9.56± 0.78r-t	nd	92.69± 0.48i-l	7.31± 0.48l-o
KW21	69.33± 1.24b-j	6.12± 0.23i-k	0.69± 0.14t	25.93± 0.92kl	56.89± 0.76j-l	10.37± 0.25qr	nd	93.19± 0.08f-i	6.81± 0.08o-r
KW22	66.18± 1.40j-s	4.71± 0.27st	6.66± 0.46a	22.8± 0.43q-t	52.3± 0.38r-u	13.54± 0.63h-k	nd	88.63± 0.19w	11.37± 0.19a
KW23	64.15± 0.70q-t	5.37± 0.33o-q	0.68± 0.15t	22.93± 1.02p-s	53.74± 1.25o-q	17.28± 0.70a	nd	93.94± 0.47c	6.06± 0.47u
KW24	70.16± 1.24b-g	6.71± 0.37b-e	5.09± 0.90b	21.97± 1.03s-u	54.92± 1.06m-o	11.31± 0.82op	nd	88.20± 1.27w	11.80± 1.27a
KW25	74.00± 0.21a	5.89± 0.18j-m	2.82± 0.21e-g	31.31± 0.54ef	46.98± 1.14za*	13.00± 0.56j-l	nd	91.29± 0.03o-s	8.71± 0.03e-i
KW26	67.76± 0.33g-o	5.38± 0.22o-q	3.13± 0.37e	28.26± 0.28i	50.22± 0.47wx	13.01± 0.16j-l	nd	91.49± 0.59np	8.51± 0.59h-j
KW27	69.17± 0.06c-j	6.12± 0.35i-k	2.30± 0.26ij	25.94± 0.42kl	55.83± 0.50k-m	9.80± 0.82r-t	nd	91.57± 0.09np	8.43± 0.09h-j
KW28	68.55± 0.67e-m	5.22± 0.22p-r	1.15± 0.16n-q	24.00± 0.58no	54.36± 0.53n-p	15.28± 1.18bc	nd	93.63± 0.07c-f	6.37± 0.07r-u
KW29	65.44± 0.31m-s	7.01± 0.29b	1.56± 0.12lm	17.08± 0.84y	59.00± 0.43e-g	15.35± 0.86bc	nd	91.42± 0.42np	8.58± 0.42h-j

KW30	65.72± 1.21k-s	5.70± 0.27l-o	0.7± 0.11t	23.74± 0.91o-q	56.10± 1.63k-m	13.75± 0.34g-j	nd	93.60± 0.38cf	6.40± 0.38r-u
KW31	72.43± 1.06a	6.51± 0.20d-h	2.69± 0.26f-h	23.86± 0.16op	56.90± 0.45j-l	10.05± 0.16q-s	nd	90.80± 0.45qu	9.20± 0.45c-g
KW32	67.31± 0.95h-r	2.33± 0.26uv	1.51± 0.17l-n	20.26± 0.37v-x	61.08± 0.69cd	14.82± 0.41c-e	nd	96.16± 0.09a	3.84± 0.09w
KW33	67.4± 0.21h-q	6.51± 0.22d-h	2.39± 0.12h-j	23.59± 0.37o-r	53.11± 1.16q-s	14.4± 0.45d-g	nd	91.10± 0.34qt	8.90± 0.34d-h
KW34	67.68± 1.05g-p	2.04± 0.10v	2.82± 0.08e-g	30.49± 0.33e-g	51.89± 0.08s-v	12.76± 0.43kl	nd	95.14± 0.02b	4.86± 0.02v
KW35	69.44± 0.61b-i	5.33± 0.20o-q	2.98± 0.28ef	28.48± 0.46i	51.83± 0.26t-v	11.39± 0.24op	nd	91.69± 0.48no	8.31± 0.48i-j
KW36	61.22± 1.24t	5.79± 0.14l-n	0.91± 0.09o-t	13.14± 0.88b*	65.16± 1.41a	15.00± 0.76b-d	nd	93.30± 0.23e-h	6.70± 0.23ps
KW37	68.16± 1.57g-n	6.78± 0.09b-d	2.56± 0.16g-i	16.94± 0.64y	59.06± 0.43ef	14.66± 0.81c-f	nd	90.66± 0.26tu	9.34± 0.26cd
KW38	63.41± 6.94st	2.50± 0.23u	5.22± 0.04b	30.94± 0.44e-g	51.65± 1.32t-v	9.69± 0.69r-t	nd	92.28± 0.19lm	7.72± 0.19kl
KW39	68.61± 0.74e-m	4.5± 0.251t	4.14± 0.30d	47.28± 0.58a	32.52± 1.84d*	11.55± 0.71op	nd	91.35± 0.55oq	8.65± 0.55g-i
KW40	67.12± 2.62h-r	5.17± 0.13qr	0.95± 0.04o-t	33.45± 1.23d	46.25± 0.10a*	14.18± 1.24d-h	nd	93.88± 0.09cd	6.12± 0.09tu
KW41	70.96± 1.90a-f	6.25± 0.19f-j	0.62± 0.09t	25.01± 0.49l-n	55.53± 0.57mn	12.60± 0.97l-n	nd	93.13± 0.09f-i	6.87± 0.09n-r
KW42	69.72± 0.70b-i	6.08± 0.15i-l	2.59± 0.15g-i	21.01± 0.48u-w	57.71± 0.64h-j	12.62± 0.45l-n	nd	91.34± 0.29or	8.66± 0.29f-i
KW43	64.5± 1.36p-s	6.35± 0.25e-i	1.83± 0.20kl	21.81± 0.88u	57.05± 0.14i-k	12.98± 0.57j-l	nd	91.83± 0.45m-o	8.17± 0.45i-k
KW44	65.62± 4.81l-s	7.00± 0.18bc	2.92± 0.20e-g	24.96± 0.62l-n	53.26± 0.11p-r	11.86± 0.12m-o	nd	90.08± 0.38v	9.92± 0.38b
KW45	66.69± 1.19i-r	6.65± 0.27b-e	0.73± 0.05rt	27.01± 0.75j	55.79± 0.51lm	9.51± 0.09st	0.32± 0.11a	92.63± 0.22j-l	7.37± 0.22l-n
KW46	67.28±0. 06h-r	5.54± 0.18n-q	0.66± 0.05t	22.67± 0.17rt	58.25± 0.18f-i	12.54± 0.11l-n	0.34± 0.10a	93.79± 0.13c-e	6.21± 0.13s-u
KW47	66.64± 0.47i-s	7.83± 0.27a	1.69± 0.15l	14.14± 0.81ab*	63.35± 0.44b	12.99± 0.04j-l	nd	90.48± 0.41uv	9.52± 0.41bc
KW48	65.53± 0.67l-s	7.00± 0.26bc	0.72± 0.09rt	19.88± 0.29x	61.01± 0.30cd	11.40± 0.18op	nd	92.29± 0.16lm	7.71± 0.16kl
KW49	69.41± 1.11b-j	5.52± 0.24n-q	2.56± 0.19g-i	46.12± 0.20b	38.42± 0.11c*	7.08± 0.30v	0.30± 0.04a	91.92± 0.06mn	8.08± 0.06jk
KW50	67.23± 0.15h-r	2.19± 0.19uv	4.78± 0.26c	29.93± 0.52gh	49.00± 0.87xy	14.10± 0.27e-h	nd	93.03± 0.07g-j	6.97± 0.07n-q
Means	67.88	5.71	2.12	25.44	54.4	12.3	0.03	92.17	7.83
LSD	3.25	0.38	0.38	1.05	1.23	0.84	0.05	0.56	0.56
Sig. Dg.	**	**	**	**	**	**	**	**	**

[+]The small letters in each column show the significant difference among the genotypes. CO: crude oil; PA: palmitic acid; SA: stearic acid; OA: oleic acid; LA: linoleic acid; α-LA: α-linolenic acid; DA: docosanoic acid; TUSFA: total unsaturated fatty acids; TSFA: total saturated fatty acids; Sig. Dg.: significant degree; LSD: least significant difference; **: P≤0.01, *Since all the lettering between a-z was completed in the first set, the second set was started.

Table 2. Correlations among crude oil and fatty acids of walnut genotypes

	CO	PA	SA	OA	LA	*α*-LA	DA
CO	1						
PA	0.131	1					
SA	-0.081	**-0.425**	1				
OA	0.140	**-0.360**	**0.319**	1			
LA	-0.109	**0.315**	**-0.454**	**-0.947**	1		
aLA	-0.172	-0.025	-0.143	**-0.561**	**0.341**	1	
DA	0.053	0.084	-0.212	0.043	0.032	-0.185	1

In bold: significant values (except diagonal) at the level of significance alpha=0.050 (two-tailed test); CO: crude oil; PA: palmitic acid; SA: stearic acid; OA: oleic acid; LA: linoleic acid; α-LA: a-linolenic acid; DA: docosanoic acid.

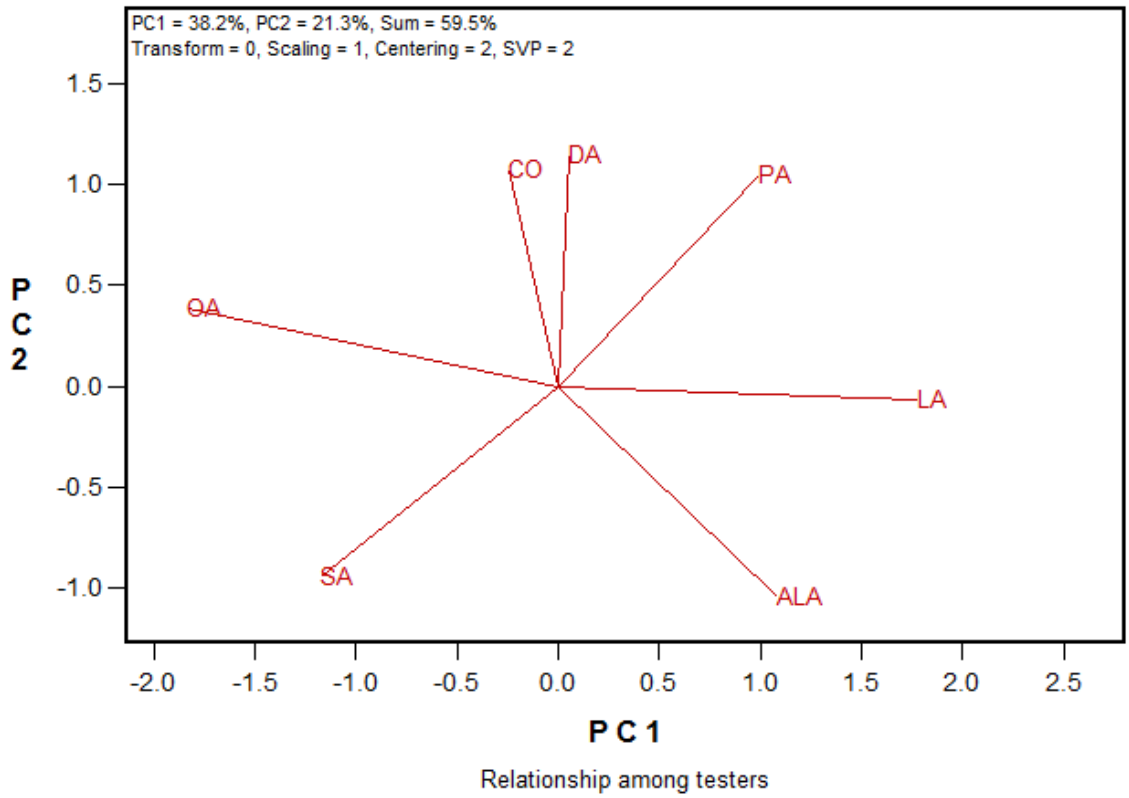

Fig. 1. GT-biplot based on oil content and fatty acid composition focus scaling.

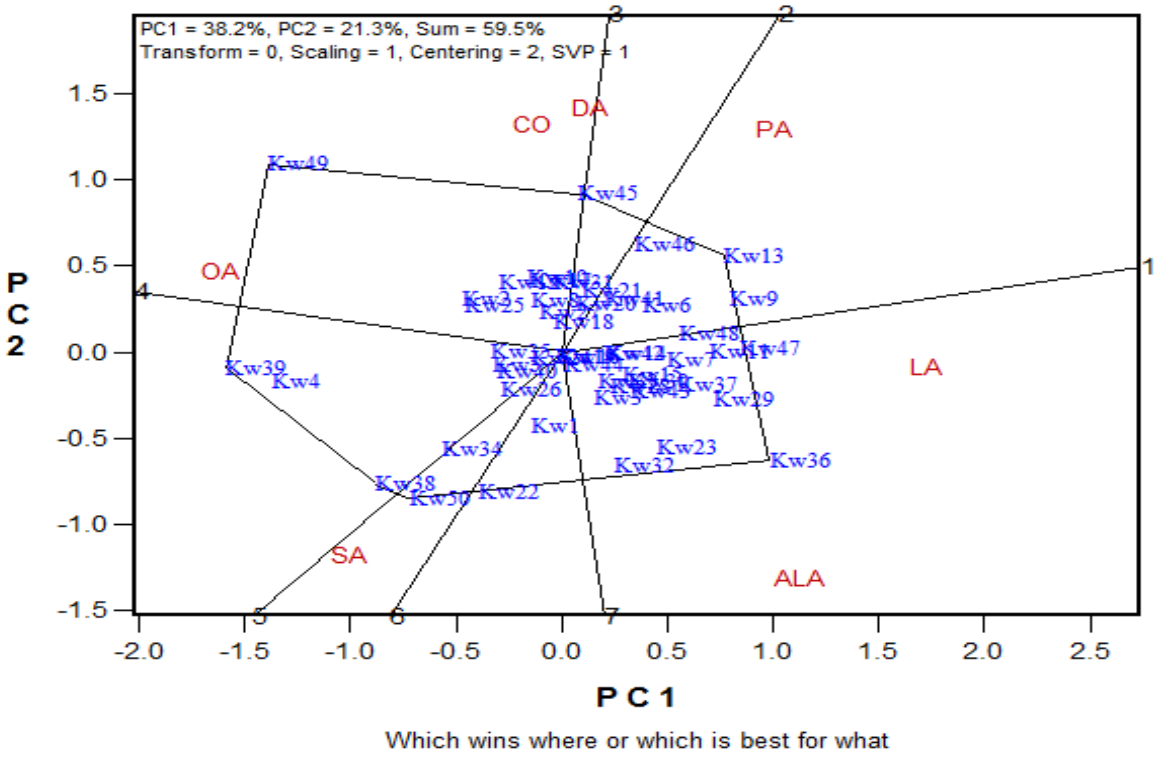

Fig. 2. Polygon views of the GT-biplot based on symmetrical scaling for the which-won-what pattern for genotypes and oil and fatty acids composition. Details of genotypes are presented in Table 1.

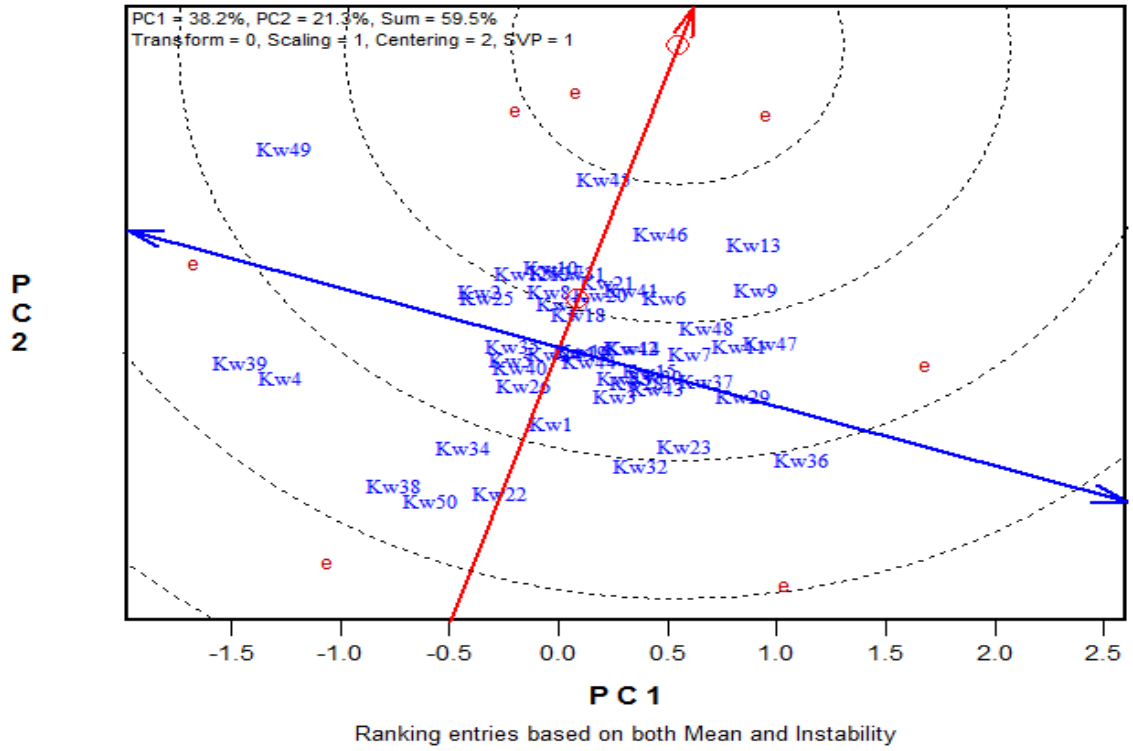

Fig. 3. GT-biplot based on genotype-focused scaling for comparison the genotypes with the ideal genotype

A polygon was created through connecting vector markers far from the origin of the biplot as to include all the genotypes within the polygon [42]. The genotypes with the greatest values for the investigated parameters were placed at the outermost section of the polygon.

Oil and fatty acid components of the selected 50 walnut genotypes were determined and prominent genotypes were identified. While the

genotypes KW24, KW10, KW41, KW2, KW6, KW17, KW31 and KW25 were found to be prominent with their crude oil contents, the genotypes KW32 and KW34 were found to be prominent with unsaturated fatty acids. Present findings revealed that GT biplot method could be used efficiently for selection of walnut genotypes prominent with oil content and fatty acid components.

CONCLUSIONS

Present findings revealed significant information about the selection of walnut genotypes with significant health benefits. It was observed that the fatty acid composition differed depending on the genotypes and it was concluded that the walnuts were quite rich in total unsaturated fatty acids. Because of richness in unsaturated fatty acid quantities and in linoleic acid which is an important fatty acid for the health, the walnuts have a highly significant potential to be a functional food. Present genotypes can also be used as parent materials in further walnut breeding studies.

Acknowledgement: *This study was supported by Scientific Research Projects Department of Erciyes University (with the project code: FHD-2017-7561).*

REFERENCES

1. G. H. McGranahan, C. A. Leslie, Walnut (*Juglans* L.), in: J. N. Moore, J. R. Ballington (eds.), Genetic resources of fruit and nut crops, 1990, p. 907.
2. E. Bakkalbasi, O. M. Yilmaz, N. Artik, *Akademik Gida*. **8** (1), 6 (2010) (in Turkish).
3. K. Browicz, *Juglandaceae*, in: Flora Iranica, vol. 121, K. H. Rechinger (ed.), Akademische Druck- u. Verlagsanstalt, 1976, p. 1.
4. Y. Akca, Ceviz Yetiştiriciliği, A. Matbaası, Ankara, 2009 (in Turkish).
5. FAO, Food and Agriculture data [online], available from: http://faostat.fao.org, accessed on 20.02.2018 (2016).
6. M. Mitrovic, M. Stanisavljevic, M. J. G. Danjanov, *Acta Hort*. **442**, 205 (1997).
7. P. Calvo, M. Lozano, A. Espinosa-Mansilla, D. Gonzalez-Gomez, *Food Res. Int*., **48**, 316 (2012).
8. M. Homayoonfal, F. Khodaiyan, M. Mousavi, *Food Chem*., **174**, 649 (2015).
9. I. Oliveira, A. Sousa, I. C. F. R. Ferreira, A. Bento, L. Estevinho, J. A. Pereira, *Food Chem. Toxicol*., doi: 10.1016/j.fct.2008.03.017 (2008).
10. A. Wunsch, J. I. Hormoza, *Euphytica*, **125**, 59 (2002).
11. S. M. Sen, Assoc. Prof. Thesis, Erzurum, 1980 (in Turkish).
12. Y. Akca, PhD Thesis, Van, 1993 (in Turkish).
13. Y. Ozkan, PhD Thesis, Van, 1993 (in Turkish).
14. A. Kuden, N. Kaska, N. Turemis, *Acta Hort*., **442**, 117 (1997)
15. M. Sutyemez, PhD Thesis, 1998, (in Turkish).
16. S. Bayazit, Master Thesis, Hatay, 2000, (in Turkish)
17. O. Kaymaz**,** Master Thesis, Tezi, Van, 2005 (in Turkish).
18. Z. Demir, Master Thesis, Tezi, Van, 2007 (in Turkish).
19. A. Uzun, K. Paris, *Bahce*, **46** (Ozel Sayı 2), 201 (2017) (in Turkish).
20. S. Kafkas, H. Ozkan, M. Sutyemez, *J. Am. Soc. Hortic. Sci*., **130**, 585 (2005).
21. S. Bayazit, K. Kazan, S. Gulbitti, V. Cevic, H. Ayanoglu, A. Ergul, *Sci. Hortic*., **111**, 394 (2007).
22. A. Uzun, O. F. Coskun, M. Yaman, H. Pinar, K. Paris, *Alatarim*. ,**16**(1), 26 (2017).
23. W. Yan, N. A. Tinker, *Canadian J. Plant Sci*., **86** (3), 623 (2006).
24. W. Yan, GGE biplot: *Agronomy J*. **93**, 1111 (2001).
25. A. Hara, N. S. Radin, *Anal. Biochem*., **90**, 420 (1978).
26. H. Yalcin, I. Ozturk, E. Tulukçu, O. Sagdic, *J. Cons. Prot. Food Saf.*, **6**, 197 (2011).
27. E. Tulukcu, H. Yalcin, I. Öztürk, O. Sagdic, *Ind. Crops Prod*., **39**, 69 (2012).
28. SAS User's Guide: Statistic. Statistical Analysis Systems Institute Inc., Cary, NC, 1999.
29. W. Yan, M. S. Kang, GGE Biplot Analysis: A Graphical Tool for Breeders, Geneticists, and Agronomists, Boca Raton, Fl., CRC Press, 2003.
30. W. Yan, Crop Variety Trials: Data Management and Analysis, John Wiley & Sons, 2014.
31. K. R. Gabriel, *Biometrika*, **58**, 453 (1971).
32. W. Yan, M. Kang, GGE Biplot Analysis: A Graphical Tool for Breeders, Geneticists, and Agronomists, CRC Press, 2002.
33. 33 W.Yan, Crop Variety Trials: Data Management and Analysis. Wiley Blackwell, 2014.
34. M. Akçura, *Turkish Journal of Agriculture and Forestry*, **35**(2), 115 (2011).
35. H. I. Oguz, PhD Thesis, Van, 1998 (in Turkish).
36. M. Simsek, *Bulgarian Chem. Comm*. **48**, 66 (2016)
37. A. Patras, P. Dorobantu, *Lucrări Ştiinţifice, seria Agronomie*, **53**, 57 (2010).
38. O. Kodad, G. Estopanan, T. Juan, R. Socias i Company, M. Sindic, *Grasas y Aceites*, **67**(1), e116 (2016).
39. M. M. Ozcan, *Iran. J. Chem. Chem. Eng*., **28,** 57 (2009).
40. B. Rabrenovic, E. Dimic, M. Maksimovic, S. Sobajic, L. Gajic-Krstajic, *Czech J. Food Sci*., **29**, 74 (2011).
41. G. Uzunova, M. Perifanova-Nemska, M. Stojanova, St. Gandev, *Bulgarian J. Agr. Sci*., **21**, 494 (2015).
42. M. Akcura, S. Taner, Y. Kaya, *Zemdirbyste-Agr*., **98**, 35 (2011).
43. Y. Kaya, M. Akcura, S. Taner, *Turkish J. Agric. For*. **30,** 325 (2006).

Bulgarian Chemical Communications, Volume 53, Issue 3 (pp. 287 - 293) 2021 *DOI: 10.34049/bcc.53.3.5333*

Application of waste-derived activated carbon as a sorbent for Re ions recovery from acidic aqueous solution

V. Toteva[1], T. Radoykova[1*], Ch. Tzvetkova[2], L. Raicheva[1], S. Nenkova[1], R. Nickolov[1]

[1]*University of Chemical Technology and Metallurgy, 8, Kl. Ohridski Blvd., Sofia 1756, Bulgaria*
[2]*Institute of General and Inorganic Chemistry, Bulgarian Academy of Sciences, 11, Acad. Georgi Bonchev Str., 1113 Sofia, Bulgaria*

Received: October 10, 2020; Revised: July 21, 2021

Activated carbons were prepared based on hydrolyzed lignocellulosic biomass, and were chemically activated with potassium hydroxide and phosphoric acid. The texture parameters of the adsorbents obtained were determined by low-temperature nitrogen adsorption; their thermal stability was studied by DTA/ TG and the surface functional groups - by FTIR spectroscopy. The adsorption properties of the obtained activated carbons toward perrhenate ions from an aqueous solution were investigated at three different pH values. The adsorbent obtained after activation of hydrolyzed lignin with KOH was found to have significantly better adsorption capacity than that obtained after activation with H_3PO_4. The maximum adsorption value of the perrhenate anion – 95.7% was obtained at a concentration of rhenium in the solution 5 mg l^{-1} and pH 2. Results from this study indicated that waste-derived activated carbon can act as an effective adsorbent for perrhenate ions from acidic wastewater.

Keywords: hydrolyzed lignocellulosic material; activated carbon; chemical activation; adsorption; rhenium

INTRODUCTION

Activated carbons are produced in great variety from carbonaceous materials including agricultural waste products [1, 2]. Various activation methods of the different species of wood biomass-derived carbonized materials have been described in the literature [3]. Two types of methods exist for activation in the production of activated carbons: physical and chemical. The properties of activated carbons largely depend on the quantity and nature of the pores at hand [4]. Due to the high carbon content and functionalized phenolic structure of lignin, it can be considered as one of the ideal precursors for activated carbons.

In case of physical activation, the lignocellulosic raw material or pre-carbonized materials can undergo gasification with water vapor, carbon dioxide or exhaust combustion gases. The chemical activation consists of impregnation of the lignocellulosic or other carbon-containing raw materials with chemical reagents such as alkali bases (KOH), $ZnCl_2$ or H_3PO_4, which are later subjected to carbonization or pyrolysis. The application of gaseous flow streams such as air or nitrogen is often met in the practice during the pyrolysis, which generates better development of the porosity of the material. Activated carbons are highly porous materials with large (500-2000 m^2g^{-1}) internal surface areas. These carbon materials have high thermal and chemical stability and they can be effectively used in a wide range of applications, such as energy storage, gas separation, catalyst supports and others [5].

The use of $ZnCl_2$ has been decreasing in recent years due to its influence upon the environment and the phosphoric acid has been increasingly preferred as an activating reagent [6]. The physical and the chemical properties of activated carbon prepared from Kraft lignin, commercial xylan and cellulose, have been studied upon activation with H_3PO_4. Diao *et al.* [7] reported that the results show higher reactivity of the precursor under acidic conditions, more developed porosity and particularly larger volume of the mesopores. This investigation also confirms the fact that the nature of the precursor, the ratio with respect to activating reagent, as well as the temperature of activation are substantial factors influencing the properties of the final products.

With regard to the porous structure of the activated carbon, Gonzalez-Serrano *et al*. [8] studied the influence of carbonization. It has been established that the maximal specific surface area is achieved at 600°C temperature of activation and upon using $ZnCl_2$ or H_3PO_4 as activating chemical reagents and the surface areas are as large as those of the trademarks of activated carbon. The use of a suitable activating reagent is aimed at increasing the rate of activation in order to improve the quality of the material, as well as to reduce the production expenses. In our previous investigations, carbonaceous material was obtained through the chemical activation of technical lignin hydrolyzed with H_3PO_4 [9] and KOH [10].

*To whom all correspondence should be sent:
E-mail: nusha_v@mail.edu

© 2021 Bulgarian Academy of Sciences, Union of Chemists in Bulgaria

The use of activated carbons is well known for cleaning dyes and many other organic and inorganic contaminants - ions and other compounds from aqueous or gaseous media. An important problem is the extraction of metal ions such as rhenium, molybdenum, gold, and more, from the environment.

Rhenium is one of the rarest elements, but it is widely used in high technology as an important component in super alloys for blades in turbine engines. It is a perfect metal for operation at very high temperatures, which makes it suitable for rocket engines. Rhenium is produced as by-product at pyro- and hydrometallurgical processing of molybdenum and copper concentrates. During the treatment processes, it passes into wash acidic solutions as perrhenic acid ($HReO_4$) in ppm concentrations [11]. Different methods are used for the selective separation and preconcentration of perrhenate ions ($ReO4^-$): ion exchange, solvent extraction, adsorption, electrolysis, etc. [12, 13]. Each of them has its advantages and drawbacks [14].

In this aspect, the aim of the present work is to investigate the adsorption capacity towards rhenium ions of activated carbons obtained from technical hydrolyzed lignin after chemical activation with KOH and H_3PO_4.

EXPERIMENTAL

Materials and methods

The experiments were carried out with technical hydrolyzed lignocellulosic biomass (THLB). Residual waste has been obtained in the course of wood hydrolysis from the forage yeast production. It is worth noting that it has been kept for more than 20 years in a depot.

The lignin first underwent a milling process and then sieve fractioning. Sieve fractions of 0.6-1 mm were used.

The initial material (THLB) was characterized with respect to its chemical composition (content of lignin, cellulose and mineral substances) and elemental composition, determined by automated analyzer EuroEA 3000. DTA analysis was also performed to determine its thermal stability.

The chemical activation was carried out with KOH and H_3PO_4. The appropriate conditions for activation of THL have been investigated in our previous studies [9].

The method of chemical activation as a typical thermochemical process was conducted in a controlled gaseous medium, by a modified version, under the conditions of continuous vacuum. It is considered that, by this modification, the mass transfer processes will be intensified as the gaseous products will be easily removed from the reaction zone during the activation process.

Chemical activation of hydrolyzed lignin

Activation with the activating reagent KOH. Technical hydrolyzed lignin contains residual polysaccharides in an amount of 15-35%. For the present study, the starting technical hydrolyzed lignin was further treated with 80% H_2SO_4 at room temperature in order to remove residual polysaccharides [14].

The preliminary pyrolysis of the hydrolyzed lignin was carried out in a standard retort. At 170 °C water was released, which could mean that the product contained a lot of O_2. At 414 °C, gaseous products were released. The final product obtained at a temperature of 520 °C, was the starting material for the production of activated carbon. The carbonized material thus obtained was mixed with KOH at a ratio of 1: 1.2 (precursor: KOH). The activation was carried out in a tube furnace at 600 °C under vacuum for 1 hour after which the product thus obtained was washed with deionized water until neutral reaction.

Activation with the activating reagent H_3PO_4. The starting sample (THLB) was activated with phosphoric acid at a ratio of 1:3 (precursor: H_3PO_4). After homogenizing, the samples were treated for 2 hours at 180°C. The actual activation was carried out in the tube furnace under vacuum, at 600°C for 1.5 hours. After cooling, the sample was washed with deionized water until neutral reaction. The reactivation of the sample was carried out at 300°C under vacuum according to Vladov *et al.* [9].

The carbonized samples obtained were labeled as follows:

- sample of activated lignin L_{H3PO4}, prepared by mixing of THL: H_3PO_4 at a ratio of 1:3;
- sample of activated lignin L_{KOH}, waste hydrolyzed lignin sample, further hydrolyzed to remove polysaccharides prior to pyrolysis in standard retort;
- initial THL denoted as L_0.

Characterization of activated carbons

The characterization of the specific surface area and the parameters of the porous texture of the samples prepared was carried out using a sorption apparatus - High-Speed Surface & Pore Size Analyzer System, model NOVA 1200, manufactured by QUANTACHROME Instruments (USA), by applying low-temperature adsorption of nitrogen (77 K).

The following textural parameters of the activated carbons were calculated: specific surface

areas (S_{BET}). based on the equation of Brunauer-Emmet-Teller (BET), for the interval p/po = 0.05 ÷ 0.35; volumes of the micropores (VMI), determined by means of the simplified equation; total pore volume (Vt) according t the rule of Gurvich at p/po = 0.95; volumes of the mesopores (V_{MES}) as the difference between the total pore volume and the volumes of micropores (V_{MI}) of the respective samples; size distribution of the mesopores, on the basis of the adsorption branch of the nitrogen isotherm assuming cylindrical model of the mesopores, by the method of Piers, within the interval $3 \leq D_{AV}$, nm ≤ 10; average pore diameter (D_{AV}), as a ratio between Vt (multiplied by four) and S_{BET}; size distribution of the micropores by means of the simplified equation, assuming flat-parallel model of the micropores; specific surface area of the micropores S_{MI} m^2/g.

FTIR spectra of the activated carbons were obtained on a Nicolet Avatar 360 FTIR Thermo Scientific spectrometer.

The thermal stability of the composites obtained was examined by differential thermal analysis (DTA/TG) with a Setaram Labsys Evo 1600 instrument in the temperature range 25-800 ºC at a heating rate of 10 ºC /min in air atmosphere.

The adsorption properties of the obtained activated carbons - L_{H3PO4} and L_{KOH} toward perrhenate ions (ReO_4^-) from an aqueous medium were investigated. The experiments were carried out in the batch mode in plugged polypropylene test tubes containing 10 ml of Re (VII) aqueous solution and 50 mg of sorbent at 20 ± 1^0 C. The effect of the following parameters on the adsorption was studied: i) pH of the solution (2-7), ii) initial rhenium concentration (5-100 mg l^{-1}), iii) contact time between solution and sorbent (5-180 min). Working solutions with different Re concentrations were obtained by diluting the stock solution of $KReO_4$ with C_{Re} = 1000 mg l^{-1} with distilled water. The pH of the starting solutions was adjusted by dropwise adding 0.1 N HNO_3 and 0.1 N NaOH. The samples were shaken on a rotary shaker at 150 rpm until equilibrium was reached, then filtered through a blue-ribbon filter. The content of Re in the filtrate was determined spectrophotometrically (UV-vis Thermo Evolution 160) by the highly selective catalytic method with N, N-dimethyldithioxamide [15]. The adsorption was calculated as follows:

$$A\ (\%) = \frac{(C_o - C_e)100}{C_0},$$

where C_0 and C_e are the initial and equilibrium concentration of rhenium (mg l^{-1}) in the solution.

RESULTS AND DISCUSSION

Physicochemical characteristics

The initial THLB (Lo) contains 78 % lignin, 12.8 % cellulose and 9.1 % mineral substances. Actually, THL contains a quantity of hardly hydrolysable polysaccharides, determined as cellulose, within the admissible limits. The content of mineral substances is high, probably due to contamination of the lignin when stored in the open air space. Table 1 presents the data from the elemental analysis of the activated samples.

Table 1. Elemental analysis of the initial THL and the THL activated with H_3PO_4 and KOH using the automated analyzer EuroEA 3000

Sample	Element, %			
	N	C	H	S
L_0	-	50.21	5.00	0.60
L_{KOH}	0.40	78.90	4.78	<0.01
L_{H3PO4}	0.33	58.50	4.60	<0.01

The above data show that the activated carbon obtained after activation of hydrolyzed lignin with KOH has a higher carbon content - 78.90% compared to that treated with H_3PO_4 - 58.50%, which shows that the treatment process hydrolyzed most of the residual polysaccharides.

Table 2 shows data on the specific surface areas and the main parameters of the porous texture of the initial THL material and the samples obtained from it [9, 10].

Table 2. Basic adsorption-textural parameters of the initial THL and the samples of activated carbons

Sample	S_{BET}, m^2/g	V_t, cm^3/g	V_{MI}, cm^3/g	V_{MES}, cm^3/g	D_{AV}, nm	S_{MI}, m^2/g	S_{EXT}, m^2/g
L_0	4	0.020	-	0.020	20.0	-	-
L_{KOH}	1428	0.700	0.515	0.185	2.0	1259	169
L_{H3PO4}	1497	0.790	0.320	0.471	2.1	741	756

The activated carbons obtained by both methods have almost the same surface area, S_{BET} - 1428 - 1497 m^2g^{-1}, but the activated carbon obtained after activation of hydrolyzed lignin with KOH, has a larger surface area and micropore volume - 1259 m^2g^{-1} and 0.515 m^3g^{-1}, respectively, compared to that treated with H_3PO_4 - 741 $m^2g^{-1}$and 0.32 m^3g^{-1}, indicating that the activated carbon obtained by activation with KOH is characterized by a much more developed microporous texture (more than 1.6 times in terms of micropore volume and almost twice in terms of specific micropore surface) compared to activated carbon obtained by phosphoric acid activation.

FTIR analysis

To identify the functional groups present on the surface of the initial sample, L_{KOH} and L_{H3PO4}, FTIR spectra were recorded, shown in Figs. 1 and 2.

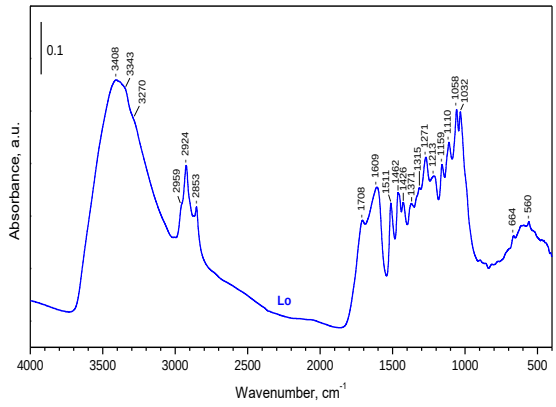

Fig.1. FTIR spectra of initial THL

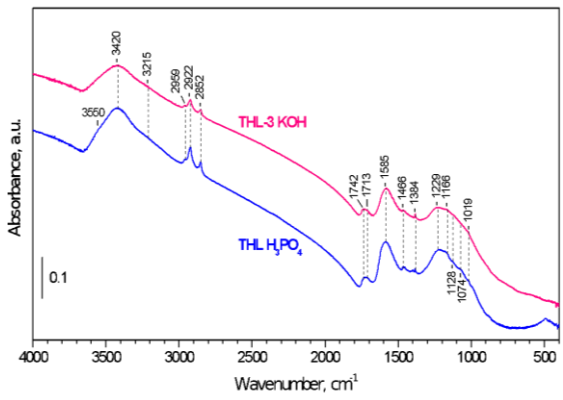

Fig. 2. FTIR spectra of activated carbons L_{KOH} and L_{H3PO4}

An intense broad band in the 3300-3500 cm^{-1} region is observed in the feedstock spectrum (Fig. 1) due to the valence vibrations of the alcohol and phenolic hydroxyl groups in lignin [16]. In the spectra of activated carbons, the bands in this region exist but are with lower intensity. The peak of activated carbon obtained by activation with phosphoric acid is more intense than that of L_{H3PO4} due to the greater amount of hardly hydrolysable polysaccharides (which have not been previously separated by THP).

The signals at 2924 and 2852 cm^{-1} are ascribed to the aliphatic -CH_3 and -CH_2 stretching vibrations. The bands in the range 1700 - 1600 cm^{-1} indicate the C=O group from the carboxyl groups. The signals at 1585 cm^{-1} (Fig. 2) are attributed to the C=C vibration in aromatic rings and the bands at 1229 cm^{-1} are due to the C-O stretching vibration of the phenol group. After activation, in the FTIR spectra (Fig. 2) of activated carbons, some of the peaks have disappeared or weakened [17].

Phenolic and carboxylic functional groups could transform into $–COOH^{2+}$, $–OH^{2+}$ or $=C=OH^{+}$ by reaction with H^+ in the solution. The more of these cations existed on the sorbent surface, the better was the recovery of perrhenate anion *via* adsorption from aqueous solution. In accordance with the conclusions of Hu *et al.* [18], the phenolic and carboxylic groups contributed to the Re (VII) adsorption on the examined sample.

Thermal analysis

The thermal characteristics of THL and activated carbon samples were determined using DTA/TG, and the thermogravimetric curves are shown in Figures 3-6.

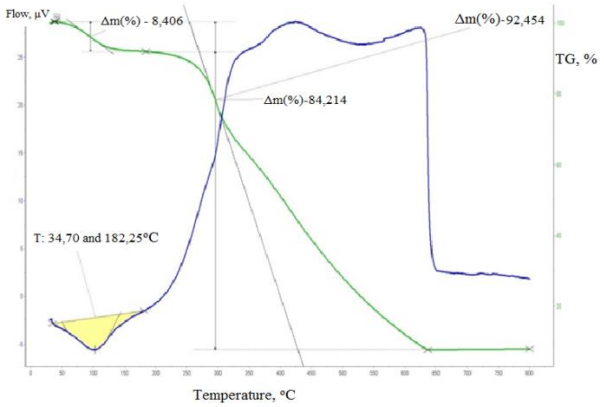

Fig. 3. DTA/TG curves of THL

As can be seen from Fig. 3, between 50 and 140°C, endothermic reactions occur that result from the separation of the adsorbed water on the surface of the lignin and the water bound in its structure. The wide exothermic effect in the 230-650 °C range may be due to the destruction of both weak and stable bonds in the lignin molecules, resulting in the destruction of lignin [19, 20]. Weight loss was about

84%. Total weight loss was 92.5% at the end of the process.

Fig. 4 shows the thermal stability of activated carbon from THL obtained after activation of lignin with KOH. In the range 25-210 ºC, 8.38% of the carbon weight is lost, which may be due to the separation of water and low-molecular weight fractions of residual polysaccharides in the lignin composition. In the interval from 411ºC to the end of the process at 810 °C, the total weight loss was 49.35%.

Fig. 5 shows the thermal stability of activated carbon obtained after activation of lignin with phosphoric acid.

In the temperature range 50 – 244 ºC, 14.3% of water was released and some of the lower-molecular weight residual polysaccharide components in lignin were destroyed. Mass weight loss from the sample was observed in the temperature range 500-740 ºC, 51.2%, respectively. The ultimate weight loss was 84.7%. Compared to DTA/TG, the analysis of Fig. 3 of the initial THL shows that after treatment with H_3PO_4, it becomes more resistant to thermal treatment.

Investigation of ReO_4^- adsorption

A quite important single parameter affecting the adsorption process, is pH of the solution [14]. The adsorption properties of the samples L_{H3PO4} and L_{KOH} were tested at four different pH values: 2, 3, 5 and 7 at an initial Re concentration C_{Re}= 5 mg l^{-1}. Experiments were performed at a contact time of 3 hours. The results are shown in Fig. 6.

It can be seen that, at all tested pH values, the adsorption capacity of the carbon activated with KOH is significantly better than that of the H_3PO_4-activated sorbent. Data show that ReO_4^- adsorption on the two obtained activated carbons is affected by the acidity of the initial solution. In both sorbents, the adsorption efficiency for rhenium is higher at lower pH values of the solution. The optimum pH value was found to be at pH 2.

The effect of initial Re concentration on the adsorption of ReO_4^- by the two sorbents was tested at pH 2. Fig. 7 shows that the maximum adsorption of 95.7% is achieved at C_{Re}=5 mg l^{-1} using KOH-activated carbon. The adsorption capacity of the H_3PO_4- activated sorbent under the same conditions is about two times lower. This tendency is also observed at higher concentrations of rhenium in the solution.

In order to optimize the contact time for the ReO_4^- adsorption, kinetic experiments were performed in the interval of 5 min - 3 hours. Solutions with initial Re concentrations of 50 mg l^{-1} were used for this aim.

As can be seen from Fig. 8, maximum adsorption of rhenium on both activated carbons was achieved within the first 15 min of contact between the solution and the sorbent. The rapid adsorption process indicates a good interaction between the adsorbent and the perrhenate ions.

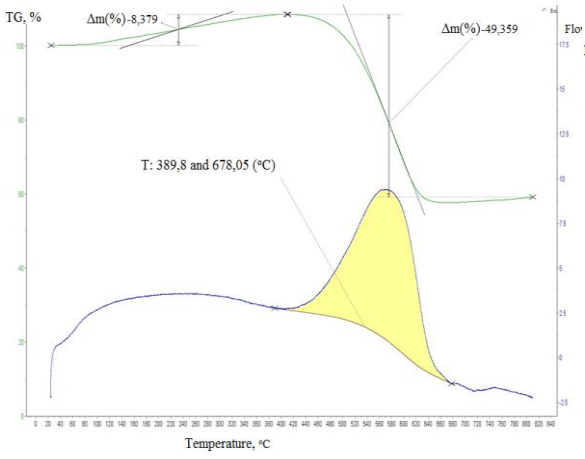

Fig. 4. DTA/TG curves of L_{KOH}

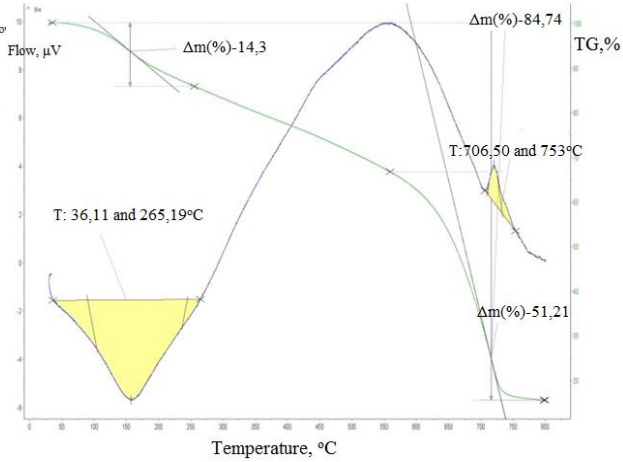

Fig. 5. DTA/TG curves of L_{H3PO4}

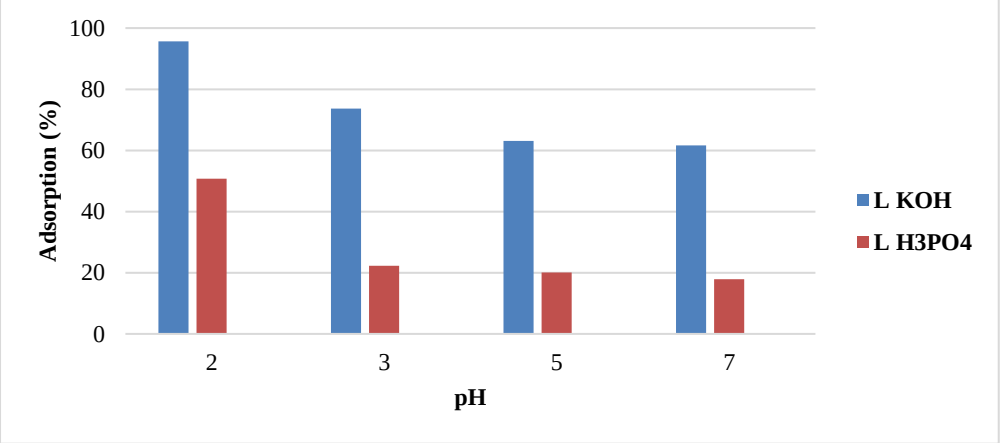

Fig. 6. Effect of pH of the solution with initial C_{Re}= 5 mg l^{-1} on adsorption of ReO_4^- by activated carbons L_{H3PO4} and L_{KOH}

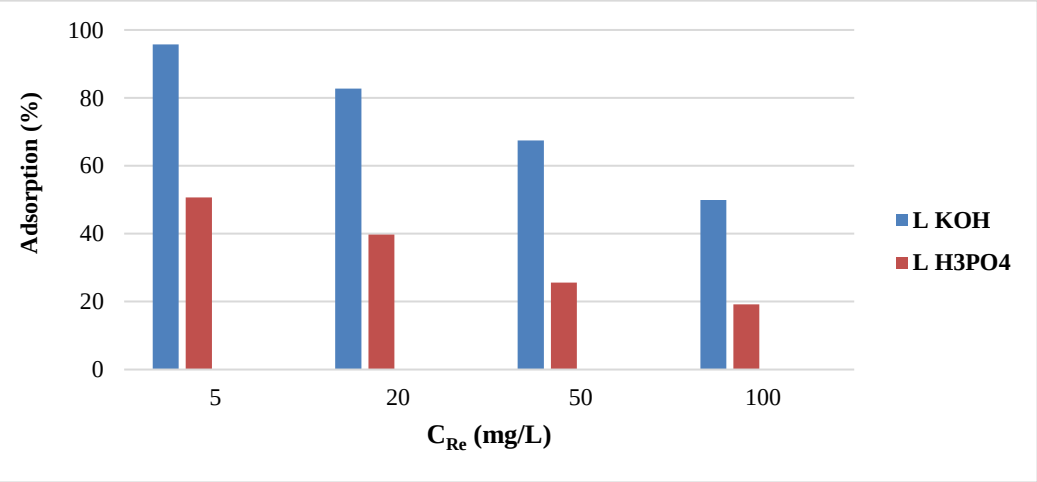

Fig. 7. Effect of initial Re concentration on ReO_4^- adsorption by activated carbons L_{H3PO4} and L_{KOH} at pH 2.

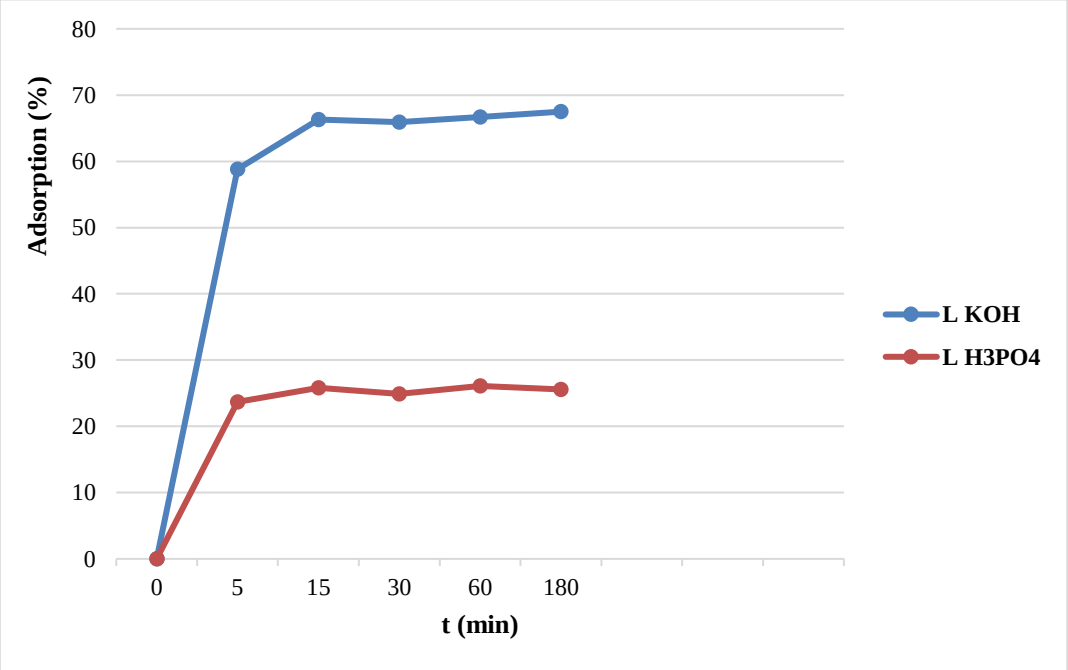

Fig. 8. Effect of contact time on ReO_4^- adsorption on L_{H3PO4} and L_{KOH} sorbents at C_{Re}=50 mg l^{-1} and pH 2

CONCLUSIONS

Activated carbons were obtained after activation of technical hydrolyzed lignocellulosic material with KOH and H_3PO_4. The sample obtained after treatment with KOH has a higher carbon content - 78.90% compared to that activated with H_3PO_4 - 58.5%, indicating that, in the first case, after lignin pretreatment with H_2SO_4, most of the residual polysaccharides were hydrolyzed.

- The activated carbons obtained by both methods have almost the same surface area, S_{BET} 1420 - 1497 $m^2 g^{-1}$, but the activated carbon obtained after activation of the hydrolytic lignin with KOH has a larger surface area and volume of micropores - 1259 m^2g^{-1} and 0.515 m^3g^{-1}, respectively, compared to that treated with H_3PO_4 - 741 m^2g^{-1} and 0.32 m^3g^{-1}, indicating that the first type of activated carbon has a more developed internal surface on the micropore level.
- DTA analysis showed that activated carbon obtained after treating THL with KOH, is more thermally resistant than that obtained after treating THL with phosphoric acid, which is probably due to the higher carbon content of the former sample. At a final temperature of 810 ^oC, the degradation of the starting lignin was 92.5%, of KOH-activated - 49.3% and of H_3PO_4-activated - 84.7%
- The activated carbon obtained after activation of hydrolyzed lignocellulosic material with KOH, has a better adsorption capacity for rhenium than that obtained after activation with H_3PO_4. At initial Re concentration C_{Re}=5 mg l^{-1} and pH 2 of the tested solution, 95.7 % of ReO_4^- are adsorbed. The adsorption process is fast and equilibrium is reached within 15 min, which is promising for the practical application of the sorbent.

REFERENCES

1. N. Supanchaiyamat, K. Jetsrisuparb, J. T. N. Knijnenburg, D. C W. Tsang, A. J. Hunt, *Current Trend, Perspectives and Opportunities. Bioresour. Technol.*, **272**, 570 (2019).
2. T. Vernersson, P. R. Bonelli, E. G. Cerrella, A. L. Cukierman, *Bioresour. Technol*., **83**, 95 (2002).
3. M. Danish, T. A. Ahmad, *Sust. Energ. Rev*., **87**, 1 (2018).
4. S. Chatterjee, T. Saito, *Chem. Sus. Chem*., **8**, 3941 (2015).
5. P.J. M. Suhas Carrott, M. M. L. Ribeiro Carrott, *Bioresour. Technol.*, **98**, 2301 (2007).
6. J. I. Hayashi, K. Muroyama, V. G. Gomes, A. P. Watkinson, *Carbon*, **40**, 630 (2002).
7. Y Diao, W. P. Walawender, L, P. Fan, *Bioresour. Technol.*, **81**, 45 (2002).
8. E. Gonzalez-Serrano, T, Cordero, J. Rodriguez-Mirasol, L. Cotoruelo, J. J. Rodriguez, *Water Research*, **38**, 3043 (2004).
9. D. Vladov, L. Raicheva, R. Nikolov, T. Hr. Radoykova, S. K. Nenkova, *Cellulose Chem. Technol*., **53**, 731 (2019).
10. L. Raicheva, G. Radeva, S. Nenkova, R. Nikolov, *Bulg. Chem. Commun.*, **49**, 139 (2017).
11. A. A. Palant, I. D. Troshkina, A M. Chekmarev, Metallurgy Rhenium, Moskva, Nauka, 2007.
12. M. B. Fathi, B. Rezai, E. K. Alamdari, R. D. Alorro, *Journal of Mining & Environment,* **9**, 1, 243 (2018).
13. G. V. Petrov, A. Boduen, S. Fokina, M. Sodorova, *Metallurgy of Rare and Noble Metals*, **4**, 9 (2015).
14. C. D. Anderson, P. R. Taylor, C. G. Anderson, *Minerals & Metallurgical Processing*, **30**, 59 (2013).
15. O. Bozhkov, L. Borisova, *Analyt. Commun.*, **33**, 133 (1996).
16. R. Draganova, S. Nenkova, Chemistry and Structure of Vegetable Tissues, Sofia, UCTM, 2002.
17. H. Saygili, F. Guzel, *J. Clean Prod*., **113**, 995 (2016).
18. H. Hu, B. Jiang, J. Zhang, X. Chen, *RSC Advances*, **5**, 104769 (2015).
19. R. Saad, J. Hawari, *J. Porous Mater*., **20**, 227 (2013).
20. L. Klapiszewski, T. J Szalaty, J. Zdarta, T. Jesionowski, *Physicochem. Probl. Miner. Process*., **52**(1), 459 (2016).

Bulgarian Chemical Communications, Volume 53, Issue 3 (pp. 294 - 306) 2021 *DOI: 10.34049/bcc.53.3.5344*

Preparation of polymer-coated aggregate by utilization of waste plastic for pavement of roads

S. M. Tariq[1], A. Mushtaq[2]*, A. Ullah[1], R. A. Qamar[1], Z. U. Ali[1], S. Afshan[1]

[1]*Chemical Engineering Department, NED University of Engineering & Technology, Karachi, Sindh, Pakistan*
[2]*Polymer and Petrochemical Engineering Department, NED University of Engineering & Technology, Karachi, Sindh, Pakistan*

Received: October 30, 2020; Revised: June 07, 2021

Pakistan, being an underdeveloped country, is highly facing waste disposal and especially waste plastic which lasts for hundreds of years without degradation. Many factors may be involved in it, but we need to purpose and try to urgently implement a constructive idea of using this non-biodegradable waste. The contaminated rain or sewage water and the potholes are the great problems in trafficking and shipping. The idea of preparation of polymer coated aggregate (PCA) is not new, but for our country, it is a whole new process. This study is the country's contribution that is proposing and building not even the idea but the whole process for utilizing the waste plastic in preparation of PCA, which will further be used as road construction material. This study aims at the most suitable solution to these problems, as it was aligned to solve both problems related to the waste plastic and the deteriorated roads, which simultaneously manages waste and improves the road life. The coating of molten plastic over the aggregate supports to recover the value of the aggregate. The binding strength of 290 tons is achieved by 25 wt. % polyethylene while higher binding strength can be achieved by using different plastics. Higher plastic weightage leads to lower moisture absorption, less voids, better soundness and impact value. At the same time, abrasion value is also lowered by higher plastic content thus causing lower friction and skidding of automobiles.

Keywords: Non-biodegradable; waste plastic; polymer-coated aggregate; bitumen; binding strength.

INTRODUCTION

Due to the increased use of plastic and modernization of the world, humans cannot protect themselves from vanishing plastic, so it has to be used constructively. Waste plastic disposal is a major problem of our environment, causing drastic damage to all habitats and increasing pollution, global warming, and is a threat to the existing and the future life. It should be recycled or reused to prevent everyone from all of its hazards. Many ideas have been proposed yet, related to reusing, recycling, pyrolysis of waste plastic, but our idea of using the waste plastic for preparation of road material shall help us to provide better binding property and increased road life. Many researchers have worked on it, and this idea has been adopted successfully throughout the world. Many countries are paving their roads by using their trash, and this is not only an economic way, but it also adds beauty to their environment, supporting tourism and ultimately supporting their economy [1, 2].

A material, which is made from many small monomers having large molecular weights, can be shaped into various things called organic polymer or plastics. Plastics are strong, durable, and degrade very slowly. They are made up of long-chained molecules (polymers) containing repeated units of carbon atoms (monomers). These polymers have extremely strong intermolecular carbon-carbon bonds. If plastic is durable on the one hand, then, on the other hand, it is resistant to degradation [2, 3].

Transportation is one of the most important factors that contribute a lot to the development of a country. As regards transportation, the flexible pavement is very important in constructing roads by using polymer coated aggregate (PCA). It can achieve all requirements of strength, durability, flexibleness, and cost-effectiveness.

This study is based on the usage of waste plastic in an innovative way to prepare road construction material. By adding the waste plastic polymer over the hot aggregate; which will eventually get coated on continuous agitation yielding the PCA, it is further used in the preparation of road construction material by mixing the PCA with heated molten bitumen [1, 4].

In 1907 the advancement of Bakelite accomplished a boom in materials by bringing designed plastic into world trade. Before the completion of the 20th century, plastics were found to be persevering polluters of various ecological fortes, from Mount Everest to the sea level. On

*To whom all correspondence should be sent:
E-mail: engrasimmushtaq@yahoo.com

© 2021 Bulgarian Academy of Sciences, Union of Chemists in Bulgaria

account of being mistaken for food by animals, flooding low-lying areas by plugging up squander systems, or causing immense revile, plastics have pulled in growing thought as a tremendous poison [2, 5].

Plastic is a polymeric material, that is, a material whose particles are huge, often taking after long ties containing an unending course of action of interconnected associations. For instance, silk exists in abundance, yet nature's "plastics" have not been entangled in environmental tainting since they don't continue on the Earth. Since fabricated plastics are, for the most part, non-biodegradable, they will, by and large, pollute natural surroundings. Likewise, various lightweight single-use plastic things and packaging materials, which speak to around half of all plastics made, are not put away in compartments for the following departure to landfills, reusing centers, or incinerators. They may be improperly disposed of at or near the territory where they end their comfort to the buyer. Dropped on the ground, removed from a vehicle window, heaped onto a successfully full garbage holder, or unexpectedly took away by a tornado, they immediately begin to defile the Earth. Unquestionably, scenes littered with plastic packaging have gotten ordinary in various bits of the world [6, 7].

Materials utilized in the principal half of the twentieth century, for example, glass, iron, aluminum, paper, and plastics have a low recuperation rate. They are generally wasteful to recycle as reused scrap in the assembling cycle, because of noteworthy preparing troubles, for example, a low softening point, which keeps toxins from being driven off during warming and reusing. Most reused plastics are financed underneath the expense of crude materials by different store plans, or government guidelines just commanding their reusing. Reusing rates change drastically from nation to nation, with nations getting rates more prominent than 50%. Regardless, reusing doesn't generally address plastic contamination since reused plastic is "appropriately" discarded, while plastic contamination originates from inappropriate removal [8].

With the increase of advancement and the role of technology in the daily life of humans, polymer plastics have played an important role in facilitating us in every aspect of life. They had taken over the place of metals, ceramics, wood, and all other materials used before, which were far more hygienic and easy to dispose of or reuse than plastic. As time passes, it has become crucial to find robust, long-lasting, and economic way to dispose of or innovatively reuse plastic waste. Several researchers worked on it for a long time and proposed different processes for constructively reusing plastic. Our country is facing the same plastic disposal problem since the start of its use.

Despite being nonnutritive and unappetizing, plastics have defilements up to multiple times. They enter the seawater and a while later pass on to the species that ingest them. In one assessment, levels of polychlorinated biphenyl (PCB), a salve, and ensuring material that is right now commonly precluded, seemed to have extended essentially in the dress organ oil of streaked shearwaters after seabirds had been dealt with plastic pellets winnowed from Tokyo Bay for simply a solitary week [1, 3].

Plastic Contamination Break Down into Microplastic

Afloat, sunlight, wind, and wave action separate plastic waste into little particles, routinely short of one-fifth of an inch over. These alleged microplastics are spread all through the water section and found in each edge of the globe, from Mount Everest, the most raised top, to the Mariana Trench, the most significant box [9].

Microplastics are further disintegrated into tinier and humbler pieces. Plastic microfibers, at that point, have been found in metropolitan drinking water structures and coasting through the air. Sunlight and seawater embrittle plastic, and the conceivable breakdown of greater articles into microplastics makes plastic available to zooplankton and other marine animals.

Plastics changed prescription with life-saving contraptions, made space travel possible, helped vehicles and planes—saving fuel and tainting—and saved carries on with defensive covers, incubators, and equipment for clean drinking water [9, 10].

The facilities plastics offer, regardless, provoked a disposable culture that reveals the material's obfuscated side today; single-use plastics speak to 40% of the plastic made every year. A critical number of these things, for instance, plastic sacks and food covers, have a future of just minutes to hours, yet they may proceed in nature for a long time.

A huge part of the plastic waste is found in the oceans, Earth's last sink, streams from land. Deny is furthermore passed on to the sea by noteworthy streams, which go about as transport lines, getting progressively more garbage as they move downstream. When uncontrolled, a huge aspect of the plastic junk remains in waterfront waters. Nevertheless, when found a workable pace in ocean streams, it might be delivered all over.

The arrangement is to keep plastic waste from entering waterways and oceans in any case. It could be refined with improved waste administration frameworks and reusing a better item plan that considers the short existence of dispensable bundling and a decrease in the assembling of pointless single-use plastics. The second major problem of concern is deteriorated roads, showing poor management and a lack of technology [11, 12].

This research aligned these two major problems by using plastic waste in the production of polymer-coated aggregate (PCA) for road construction material to solve two major problems in a combination, to contribute towards the betterment of society. With the increasing use of plastic, the problems increased, not only related to human health, but due to its toxicity, also related to the environment and all-natural habitats. Humans have troubled not only their lives but also disturbed all creatures. The waste plastic disposed of in oceans is deadly, harming marine life and disturbing the food chain.

Fig. 1. Contamination of waste, mainly plastic, in a local area

The biggest problem for developing countries is the management of solid waste, as shown in Figure 1. Today Pakistan produces about 87,000 tons of solid waste every day, estimated up to 48.5 million tons of solid waste every year. So, it is a matter of great concern because the death rate is increasing due to waste-related diseases, and it causes serious environmental effects. Only a little waste is recycled. Out of 48.5 million tons of solid waste, plastic waste is about 9% of the total waste produced in Pakistan. Because of its non-biodegradability, it produced water stagnation and was associated with hygienic problems [12, 13].

Deterioration of Roads

According to a report by the Permanent International Association of Road Congress (PIARC) and National Highway Authority (NHA), the total length of roads in the country is 264,401 km long Highway network - that is 3.65 % of the total road network carrying 80 percent of the total traffic of Pakistan. Over the past decade, road traffic, including both passengers and freight, has significantly promoted the national economy. Currently, it is 91 percent of national passenger traffic and 96 percent of the cargo. Roadways, highways, and even pathways in Pakistan are generally in very poor condition. The distresses like rutting and fatigue cracking have degraded the condition of the available roads and the current heavy rain makes transportation more unsafe and dangerous for travelers.

(a) (b)

Fig. 2. (a) Small potholes, deterioration of the road (b) Large pothole (contamination resulting in water)

Pavement conditions suggested that 41% of the National Highway (NHA) lost its structural coherence and load-bearing capacity. 58% of the NHA network is suffering from rutting that is affecting transportation and traveler's safety. Nearly 27% of the NHA network has a serious safety hazard where the wheel path ruts more than 25 mm. Even on a smaller scale, the condition of roads is very poor, the potholes and stagnate rain or sewage water are always a trouble for the countrymen, as shown in Figure 2 (a, b) [1, 8].

The major objectives of this research are to recycle plastic waste by reusing it by coating it over the surface of aggregate, which is further used in road construction material. It can improve durability, flexibility, stability, and economy of the road. Strength characteristics of PCA itself and also with bitumen are studied. The polymer coating reduces the voids and cracks, thus having good resistance towards water stagnation and rainwater. The abrasion, weathering, and pothole formations are also reduced. The purpose is to improve and enhance the properties, including binding strength, penetration value, tensile strength, stripping (potholes) seepage of water, better resistance, Marshall stability value, and check the durability for the pavement of roads.

With the rapid increase in the world population, the demand for such a versatile material could automatically increase. The countries are in dire desire of such ideas and implementation of them, which helps to get rid of problems and this idea of

using waste into road construction is like converting the waste into treasure, as facing both problems of increasing waste and the poor condition of roads. The waste plastic is either left on roads or dumped in land or oceans. Both ways are harmful. The contribution of plastic cannot be denied in our daily life; rather, it has to be utilized in a constructive way for the nation's prosperity [10, 14].

This study envisages improvements in these parameters after the preparation of PCA, solid waste management, usage of unwanted trash, reducing voids and potholes formation, moisture absorption, and improving cost-effectiveness, compression strength, binding strength. Plastic waste could be classified in several ways, but most often by its physical properties. Based on chemical sources, general groups of plastics are cellulose plastics, protein plastics, natural resin, elastomers, and synthetic resin plastic fibers. According to physical properties, plastic is of two types: thermoplastics and thermosetting plastic.

Upon application of heat, the thermoplastics could be molded into different shapes and become solid on cooling. Common examples are polyethylene, polypropylene, polystyrene, polyvinyl chloride, Teflon, and nylon.

Thermosetting plastics, when once shaped, could not be softened or remolded on the application of heat. Common examples are Bakelite, epoxy resins, polyesters, and polyurethane. According to the property of remolding on heat application, we are using thermoplastics as waste plastic raw material, in our project. Generally, some of the thermoplastics are softened at a temperature of around 130-150°C. It is noticed that at a temperature of around 120-180°C, there is no gas evolution, but beyond this temperature, thermal degradation and gas evolution may occur [6, 15].

Sources of generation of waste plastic are HDPE and LDPE (carry bags, cosmetic bottles, sacks, milk pouches), polyethylene terephthalate (drinking water bottles), polypropylene (wrappers of biscuits detergents, caps of bottles), polystyrene (yogurt pouches, food trays, egg boxes) and polyvinyl chloride (pipes, building, and constructions, electrical fittings).

The waste plastic polymer exhibits good binding properties. When coating the aggregate with molten waste plastic polymer, it will cover the surface of the aggregate. The required PCA is already there. Adding molten bitumen to it will provide a road construction material, whose properties have been improved from the conventional road construction material. The voids will have been filled, and the binding will also have been strengthened, as the molten plastic will cover the surface of the aggregate, that is, attached to it completely, and afterward, this mixture is covered by bitumen. This result will further be confirmed by several testings [3, 12].

To resist the drastic weather conditions and the friction between wheels and roads, the surface layers of pavement may contain the strongest and most expensive material as it is necessary to build roads which have high strength. Roads must have the ability to drain off the surface water, which is the requirement to improve road life, and it is important for vehicle safety also. Asphalt performance strongly depends upon the polymer-coated aggregate.

METHODOLOGY

The basic raw material utilized for this research is easily and cheaply available. Raw materials for lab or commercial basis synthesis are waste plastic (polyethylene, polypropylene, polystyrene), aggregate, and bitumen. In this research, the raw materials for lab and commercial basis synthesis were the same.

The product was obtained in two stages. In the first stage, the waste plastic was melted and coated over the aggregate in the reactor yielding the PCA. In the second stage, the raw material bitumen was mixed with PCA to obtain the final product (the actual road laying material).

Plastic is easily accessed and useful material on the one hand, but on the other hand, it is one of the world's greatest environmental problems. Yet, both society and the industrial sector are highly dependent on plastic. Since it is lightweight, a good insulator and resistant to corrosion, so vast use is undeniable in every sector. Due to its vast use, kinds of research have been made and are in progress to overcome its waste-causing pollution. Scientists are switching towards biodegradable bioplastic made from renewable biomasses or agricultural byproducts. Still, it will take our country, a whole century or more, to shift towards it, and before, we have to reduce our present plastic waste in a useful way, for which our project will play a key role.

Aggregate mainly comprises a broad category of coarse to medium-grained materials. This study uses crushed stones mixed with sand as an aggregate. Bitumen is a highly viscous liquid and a mixture of various products whose main constituent is carbon. For transportation of bitumen through pipes, it must be heated or diluted with a lighter oil. For paving the roads and roofing tiles, far more refined bitumen is used. Desirable properties of bitumen include good adhesion and cohesion. It is water repellant. Its nature is thermoplastic. Drawbacks include

oxidation that may occur, which leads to cracks. Water absorption may cause potholes formation. Bitumen is a petroleum product, so its cost is high [13, 16].

This work emphasizes preparing a material that will be used in road construction. It has improved strength than conventional roads, lower water absorption due to lesser voids, lower abrasion between tires and roads, improved life of both tires and the road, and lesser cracks due to better binding.

The selection of appropriate raw materials is the key to achieving the desired product. This project uses a pre-processed raw material (crushed aggregate), and before use, no further processing is required except the waste plastic, which is shredded manually before its use. All the raw materials can be easily stored in atmospheric conditions. The handling of materials can be done properly as the process is done at a high temperature.

This process is an innovative way to find the solution of increasing waste plastic and utilizing it in paving the roads. The prepared PCA is the raw product for road construction material. The heated bitumen is added after the preparation of our desired PCA. We have done some amendments like varying the properties of PCA by varying temperature. This research designs equipment that can bear high temperatures and will also give good mixing for the required product.

Process Description

There is only one process available to prepare PCA that has been adopted. The process is the same as the conventional road construction material process. Still, the modification did find the optimum condition for the best PCA. A new innovative method was proposed by coating waste plastic over the hot aggregate and mixing it with molten bitumen to get the desired high-strength road construction material by designing the reactor to achieve the required temperature and agitating condition. After the preparation of the sample, it will be exposed to different tests to check different parameters. Before starting the actual process, some pretreatments are to be carried to achieve the desired results of PCA.

Segregation

The waste plastic is collected from numerous sources, and non-organic waste is separated from it (if any). For this study, the waste plastic was collected from homes. Later, it will be collected from the neighborhood to initiate the constructive use of waste plastic. For further requirements, it can be bought from the scrap market.

Shredding of Waste Plastic

The waste plastic collected is shredded into small pieces to avoid lumping, so uniform coating will be achieved. Shred the plastic manually in small pieces by using a scissor. The pieces were not single-sized, but this will not cause any trouble as at high temperature it will steadily coat if provided appropriate mixing.

Crushing of Aggregate

The stone aggregate used for road construction was crushed to get a uniformly sized aggregate, so uniform heating and coating will be done simultaneously. For this research, crushed stone aggregate was bought. The plastic waste collected consisted of shoppers, plastic bottles, discarded disposable utensils. We are innovatively using this waste plastic. It was shredded and mixed with hot aggregate, quickly melted and got coated over the hot aggregate. The bitumen was heated separately and was subsequently mixed with this coated aggregate.

Preparation of Polymer-Coated Aggregate (PCA)

The aggregate has to be heated to the highest temperature of nearly 200°C (just to soften the plastic and not decomposing it, to prevent degradation of plastic which causes a great hazard to the environment by producing toxic gases). The shredded waste plastic was added over the heated aggregate with continuous agitation to give a uniform coating of molten polymer. The plastic was softened on heating and coated over the aggregate (monitoring of temperature is crucial). Within a few seconds or a minute, plastic melts and gets coated over the hot aggregate, so PCA is obtained. Plastic gives an oily look to the aggregate and, ultimately, to the PCA. Molten bitumen is mixed with PCA, and the resulting PCA-bitumen mix is ready to pave a road, as shown in Figure 3. The temperature and agitation must be controlled and monitored continuously to achieve the best strength, quality, and durability.

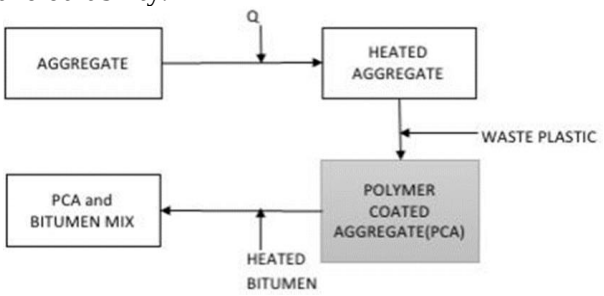

Fig. 3. Bitumen flow diagram for preparation of road construction material through PCA.

Equipment Design

The equipment used for this experiment was not previously available. The prime functions required for PCA are temperature controlling and continuous agitation, for which a heating and mixing chamber was designed as displayed in Figure 4. The non-reactive heating and mixing chamber includes the components shown in Figure 4.

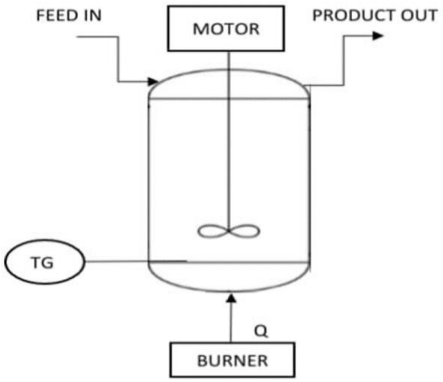

Fig. 4. Process instrumentation diagram for designed equipment.

Vessel. This equipment mainly consists of a vessel in which the raw material is mixed and heated. It is a combination of heater and mixer as required for the simultaneous heating and mixing of polymer and aggregate.

Agitator. The agitator is used for continuous mixing to achieve homogeneous heat transfer and uniform coating of the molten polymer over the hot aggregate. For this purpose, a curved blade turbine impeller is used.

Temperature gauge. As temperature control is the main factor in the preparation of PCA, a temperature gauge is used to observe the temperature readings of the sample. It is placed on the wall of the chamber.

Burner. To provide heat in the vessel's base. The burner is used as a heating source, and the flame is controlled manually for PCA temperature.

Electric Motor. A high-power motor is used to rotate the agitator. As solid raw materials are used, so the motor must be powered enough to continually agitate the mix.

Lid. A lid is used to cover the vessel having a motor mounted on it and the shaft of the agitator fixed in it.

Designed Parameters

Figure 5 (a) shows the designed equipment to achieve that desired product has these designed parameters: minimum required reaction temperature (T) = 100°C; the desired temperature is between 100°C -200°C; material is stainless steel, diameter d ≈ 0.45 m, height ≈ 0.75 m, and impeller = curved blade turbine.

Initially, pre-designed equipment was used, which can do simultaneous heating and mixing, as shown in Figure 5 (b). This pre-designed equipment consists of a closed chamber, insulation of glass wool, impeller, lid mounted with an electric motor, heater rod attached to the lid, temperature sensors, and speed controller for the impeller, mainframe where the reactor and control panel are mounted. A control panel is attached to the reactor to control the temperature and speed of the impeller.

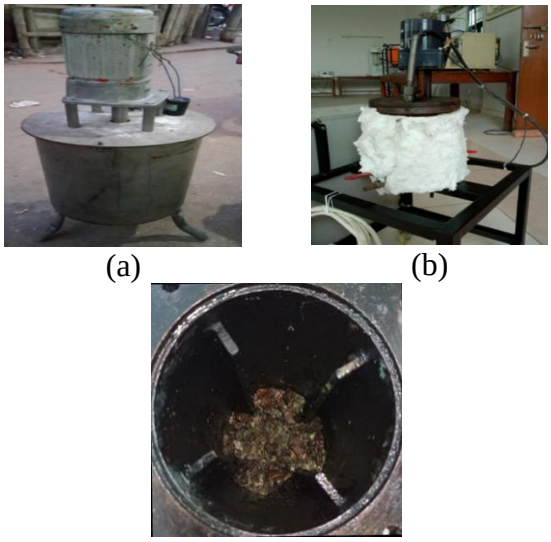

Fig. 5. (a) Newly design equipment (b) Setup of the pre-designed equipment (c) Experimental result (stuck product in pre-design equipment)

While experimenting with this designed equipment, the following observations were made: maximum reaction temperature (T) = 800 ºC; the desired temperature is within this range, volume (V) =2 L, D = 0.108 m, impeller = 45’ tilted pitched blade turbine - 4 blades. This equipment was designed for liquids and had to be modified for the required reactor. During the experiment, the temperature range was appropriate but faced problems and troubleshooting while using this equipment. The capacity of the reactor was too small; also, the diameter was small. The melting rate of the polymer was too slow due to a single heater rod, which results in inappropriate heat transfer - lumps of the molten polymer formed owing to inappropriate heating and mixing due to small blades. As a result, choking of PCA happened after processing, which was cleaned by us but will be difficult in the future as it was a time-consuming process, especially for a reactor having a small opening. Figure 5 (c) shows the stuck product in the pre-design equipment.

Open Flame Process

Figure 6 (a) displays the open flame process, a trial process for the preparation of PCA before designing our equipment. The objective of this open-flame process was to check the melting property and the binding strength of waste plastic while achieving the desired temperature.

Fig. 6. (a) Open flame setup; (b) PCA and bitumen mix in the process; (c) Product of open flame process (d) Block of PCA-bitumen mix prepared in the newly designed equipment

The open flame equipment consists of a circular cooking pot, simultaneously heating and mixing aggregate and polymer. The heating source was the wood logs confined in bricks, and an open stove was used. Two heating sources were made to heat the polymer-aggregate mix and bitumen separately. A large porous cooking spoon was used as a spatula, and a steel container was used for heating bitumen. The thermometer was used to note temperature manually from time to time. Raw materials were the same as defined above. Small mold was used for molding the finished product, as given in Figure 6 (b) to place the cooking pot on the heating source. Add aggregate to the cooking pot and start heating. Check the temperature of the cooking pot using a thermometer; when the desired temperature is achieved, add shredded waste plastic over hot aggregate. It takes a minute to melt the waste plastic and to coat it over the aggregate. Use a spatula to mix the aggregate and the melted plastics for uniform distribution. Add some more plastic; mix it uniformly using the spatula. Heat the bitumen to melt it in the container to about 160°C as hot bitumen has to be added over the hot aggregate for better binding. Then add the melted bitumen over the polymer-coated aggregate to obtain the final product – a uniform mix of the bitumen and the PCA as shown in Figure 6 (c). Put the sample in a mold. Compress it using some weights and wait to get it dry.

While experimenting with open flame equipment, the problem faced was the uncontrolled temperature, as logs surrounded by bricks were used as heating source. The fluctuating direction of the wind was disturbing the flame. One sample was prepared by this method. By observing the failure of achieving the desired temperature and binding, it worked on the fabrication of our equipment to get a better sample of PCA. The newly developed reactor consists of an assembly having the following components:

Reactor (cylindrical vessel made up of stainless steel) designed for heating aggregate and polymer and mixing them simultaneously. *Lid* with a mounted electrical motor. *Impeller* fitted in the lid, its rod attached to the motor used to mix PCA electrically. The heating source (gas stove) is placed under a cylinder as an external heating source. A gas cylinder is connected to the heating source as a fuel source. An open flame process was used for heating and mixing bitumen with PCA. Place the heating source under the reactor and turn it on. Add aggregate in the reactor and start heating on high flame. Add plastic after some time and let aggregate and plastic heat and mix till the plastic is uniformly coated over aggregate using continuous mixing. Check the temperature of the cooking pot using a thermometer; when the desired temperature is achieved, add shredded waste plastic over hot aggregate. It takes a few minutes to melt the waste plastic and to coat it over aggregate. Heat the bitumen to melt to a temperature of about 160°C. Put the sample in a mold. Compress it using some weights and wait to get it dry, as shown in Figure 6 (d).

The sample prepared in this reactor had the following composition: aggregate = 799.6 g, bitumen = 252.6 g, plastic = 140.4 g. It is 9.36% of the total sample, and the remaining from 1500 g was sand that is 307.4 g. Table 1 shows different temperatures and plastic percentages for the various samples.

Table 1. Different temperatures and plastic percentages for various samples

Temperature (°C)	Polymer wt.%	Temperature (°C)	Polymer wt.%	Temperature (°C)	Polymer wt.%
130	2	140	2	150	2
	5		5		5
	10		10		10
135	2	145	2	155	2
	5		5		5
	10		10		10

While experimenting with the newly designed reactor, the following problems were faced: the temperature was slightly deviating from the desired value as it was controlled manually. The fluctuating direction of the wind was disturbing the flame. Electrical heating will give accurate temperature and will be unaffected by wind direction, but it is not economic to use. Due to the mounted motor, the lid becomes too heavy, has to be removed for inlet/outlet of material and to check uniform coating of polymer over aggregate. A small inlet must be designed in the lid that prevents the removal of the whole lid. This study prepared only one sample of this reactor at T = 120°C and 9.36 wt. % polymer (by wt. % of the total sample). The thermal characteristics of the polymer used are given in Table 1. The softening point test is done through ball and ring equipment.

Characteristics of Polymer-Coated Aggregate (PCA)

The main product of this research, PCA, was characterized by property tests.

Binding Strength. The molded block of PCA is subjected to compression by a universal testing machine to check the binding strength of the sample. The addition of plastic in aggregate improves the binding strength of the material [17].

Moisture Absorption. A known amount of PCA block is placed in water for 24 hours and weighed after taking it out. The amount of water absorbed is found by subtracting the mass before and after the immersion of PCA in water. The difference will be the mass of water absorbed. It is expected to realize that the water absorption had been reduced by improving the arrangement, covering plastic over the hot aggregate. This coating of plastic shows a decrement in voids. Therefore, the coating of molten plastic over aggregate supports to recover the aggregate value [17, 18].

Soundness Test. A soundness test is done for checking the protection of aggregate to withstand action. The low-value aggregate causes weight loss. The plastic-coated aggregate is expected to present no or low amount of weight loss, thus approving the enhancement in aggregate value. The soundness directly depends upon the amount of porosity and voids of the aggregate that is decreased by the addition of polymer. It is determined by doing an enhanced weathering test cycle. The net loss in aggregate weight for five cycles must not exceed 12 %, tested with sodium sulfate.

Aggregate Impact Test. Here, resistance or durability of the aggregate is determined to break under rehashed impacts. The total was exposed to 15 blows with a mallet of weight fourteen kg, and the squashed total was sieved on a 2.26 mm sifter. The total effect esteem is the proportion of fines (going through the 2.36 mm strainer size) to the complete load of the example in percent. The aggregate effect esteem must not surpass 30% for its application in asphalts.

Los Angeles Abrasion Test. The repeated motion of the vehicle with a rubber tire will have specific wear and tear done by the external surface of the pavement. For the Los Angeles abrasion (LAR) test, a PCA sample that remained on the 1.70 mm (No. 12) sieve is placed in a huge rotating drum which includes a shelf plate attached to the outer wall of the drum. A detailed amount of steel spheres was then placed in the machine, and the drum was revolved for 500 revolutions at a speed of 30 - 33 rpm. The solid material was taken out and separated from the material passing through the 1.70 mm (No. 12) sieve. The weight of remained material (bigger elements) was then compared to the actual sample weight. The difference in weight was stated as a percent of the original weight and called the percentage loss. For pavements, the LAR value must be less than 30%. The LAR values were less for PCA than for the plain aggregate.

Characteristics of the PCA-Bitumen Mix

Marshall Stability ASTM D 1559. It is the characteristic of the load-bearing capacity of the adjustable pavement of the bituminous PCA at a loading rate of 50.8 mm/min. It is associated with the resistance of bituminous PCA materials to rutting, shearing stress, and displacement.

Bitumen Extraction Test ASTM D2172. The extraction tests are executed as bituminous PCA, mixed with TCE (trichloroethylene), and bitumen separation. Here the separation or extraction of bitumen was almost done. Bituminous PCA was first mixed with TCE, and the mixed bitumen was then extracted, separated, and estimated. The entire elimination of bitumen was not done. A better separation of bitumen was executed using another solvent, such as decalin that also acts as a plastic extractor. The bituminous PCA obtained from step 2 is mixed with decalin for another 30 min, and extracted bitumen was approximated. The extraction was again repeated by refluxing the mix for five min. More separation took place.

Penetration Index Test. This test is done by using a penetrometer. The penetration of a bituminous PCA is the length penetrated in 10 mm. A standard needle would penetrate or enter vertically into a material sample under standard temperature conditions, load applied, and time.

Ductility Index Test. The distance in centimeters determines the ductility of the bituminous PCA material. It can be elongated before fracture when a standard briquette specimen of the material is hauled separately at a definite temperature and speed.

Stripping Test. The stripping value measures the binding strength of the PCA and the bitumen by submerging the mixture in water for 24 h at 40°C. So the water penetrates the pores and voids of the stone resulting in shedding off the bitumen. The outcome results in the release of the aggregate material, and potholes are also formed. The molten polymer that fills the voids of the aggregate also binds the aggregate together and with the bitumen. Now the water does not penetrate over the PCA material, therefore peeling off the bitumen from the PCA stopped and so stripping value enhanced.

Material and Energy Balances

Variables to be used: A = polymer; B = aggregate; 2 = PCA; m = mass flowrate, $kg.s^{-1}$; x_A = mass fraction of polymer ($x_A = 1$; as A is pure); x_B = mass fraction of A in B ($x_B = 0$); T = temperature, °C; $T_A = T_B$ = troom; T_2 = outlet temperature of PCA = temperature of contents of vessel; T_b = temperature of burner; controlled manually; Q = heat added to the system, $J.s^{-1}$ = W; Y = height of mixture (sample) within the vessel, m; V = volume of mixture, m^3; D = mean density of PCA, (mean of density at all stages; at inlet, within the vessel and at outlet of vessel), $kg.m^{-3}$.

Constants: U = overall heat transfer coefficient, $W.m^{-2}.°C^{-1}$; A = over all heat transfer area, m^2 and C = specific heat, $J.kg^{-1}.°C^{-1}$.

The assumptions made while carrying out material and energy balances are: the mixture is non-reactive, perfect mixing takes place; no spatial variations. The density of the polymer is only varying on the application of heat within the vessel and remains constant at the inlet and outlet, assuming constant D. Figure 7 shows the schematic diagram of the designed equipment.

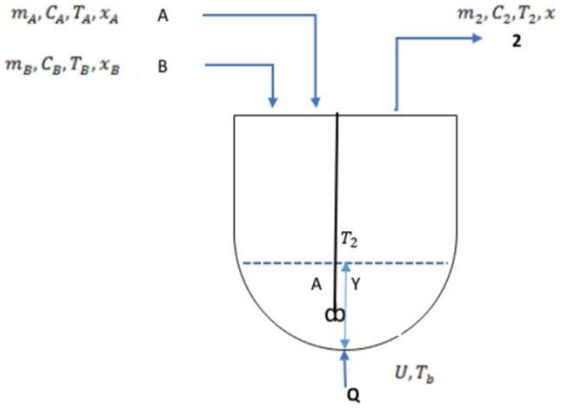

Fig. 7. Schematic diagram of designed equipment

Mass Balance:

Overall balance:

$$\Rightarrow \frac{d(DV)}{dt} = m_A + m_B - m_2$$

$$\Rightarrow \frac{D\,d(V)}{dt} = m_A + m_B - m_2$$

Since, V = A*Y

$$\Rightarrow D * A\frac{dY}{dt} = m_A + m_B - m_2$$

$$\Rightarrow \frac{dY}{dt} = \frac{m_A + m_B - m_2}{D*A} \quad \text{..... (1)}$$

Component balance:

$$\Rightarrow \frac{d(D*V*x)}{dt} = m_A * x_A + m_B * x_B - m_2 * x$$

Since, $x_A = 1$ and $x_B = 0$

$$\Rightarrow \frac{d(D*V*x)}{dt} = m_A - m_2 * x$$

$$\Rightarrow D * x\frac{dV}{dt} + D * V\frac{dx}{dt} = m_A - m_2 * x$$

$$\Rightarrow D * V\frac{dx}{dt} = m_A - m_2 * x - D * x\frac{dV}{dt}$$

$$\Rightarrow D * A * Y\frac{dx}{dt} = m_A - m_2 * x - D * A * x\frac{dY}{dt}$$

Using the value of $\frac{dY}{dt}$ from (1)

$$\Rightarrow D * A * Y\frac{dx}{dt} = m_A - m_2 * x - D * A * x\left(\frac{m_A + m_B - m_2}{D * A}\right)$$

$$\Rightarrow D * A * Y\frac{dx}{dt} = m_A - m_2 * x - x(m_A + m_B - m_2)$$

$$\Rightarrow D * A * Y\frac{dx}{dt} = m_A - m_2 * x - m_A * x - m_B * x + m_2 * x$$

$$=> D*A*Y\frac{\mathrm{dx}}{\mathrm{dt}} = m_A - m_A*\mathrm{x} - m_B*\mathrm{x}$$

$$=> D*A*Y\frac{\mathrm{dx}}{\mathrm{dt}} = m_A(1-\mathrm{x}) - m_B*\mathrm{x}$$

$$=> \frac{\mathrm{dx}}{\mathrm{dt}} = \frac{m_A(1-\mathrm{x}) - m_B*\mathrm{x}}{D*A*Y} \quad \text{.. (2)}$$

Energy balance:

$$=> \frac{d(D*V*C_2*T_2)}{dt} = m*C_A*T_A + m_B*C_B*T_B + Q - m_2*C_2*T_2$$

$$=> \mathrm{D}*\mathrm{C}_2*\mathrm{A}\frac{d(Y*T_2)}{dt} = m_A*C_A*T_A + m_B*C_B*T_B + Q - m_2*C_2*T_2$$

$$=> \frac{d(Y*T_2)}{dt} = \frac{m_A*C_A*T_A + m_B*C_B*T_B + Q - m_2*C_2*T_2}{\mathrm{D}*C_2*\mathrm{A}}$$

$$=> Y\frac{dT_2}{dt} + T_2\frac{dY}{dt} = \frac{m_A*C_A*T_A + m_B*C_B*T_B + Q - m_2*C_2*T_2}{\mathrm{D}*C_2*\mathrm{A}}$$

$$=> \frac{dT_2}{dt} + \frac{T_2}{Y}\frac{dY}{dt} = \frac{m_A*C_A*T_A + m_B*C_B*T_B + Q - m_2*C_2*T_2}{\mathrm{D}*C_2*\mathrm{A}*\mathrm{Y}}$$

$$=> \frac{dT_2}{dt} = \frac{m_A*C_A*T_A + m_B*C_B*T_B + Q - m_2*C_2*T_2}{\mathrm{D}*C_2*\mathrm{A}*\mathrm{Y}} - \frac{T_2}{Y}\frac{dY}{dt}$$

Using the value of $\frac{dY}{dt}$ from (1)

$$=> \frac{dT_2}{dt} = \frac{m_A*C_A*T_A + m_B*C_B*T_B + Q - m_2*C_2*T_2}{\mathrm{D}*C_2*\mathrm{A}*\mathrm{Y}} - \frac{T_2}{Y}\frac{m_A + m_B - m_2}{D*A}$$

$$=> \frac{dT_2}{dt} = \frac{m_A*C_A*T_A + m_B*C_B*T_B + Q - m_2*C_2*T_2}{\mathrm{D}*C_2*\mathrm{A}*\mathrm{Y}} - \frac{m_A*T_2 + m_B*T_2 - m_2*T_2}{D*A*Y} \quad \text{.. (3)}$$

where:

$$\mathrm{Q} = \mathrm{U}*\mathrm{A}*(T_b - T_2)\text{..... .... (4)}$$

Mathematical Modeling

Based on the above-derived equations, the following mathematical model was made as given in Figure 8:

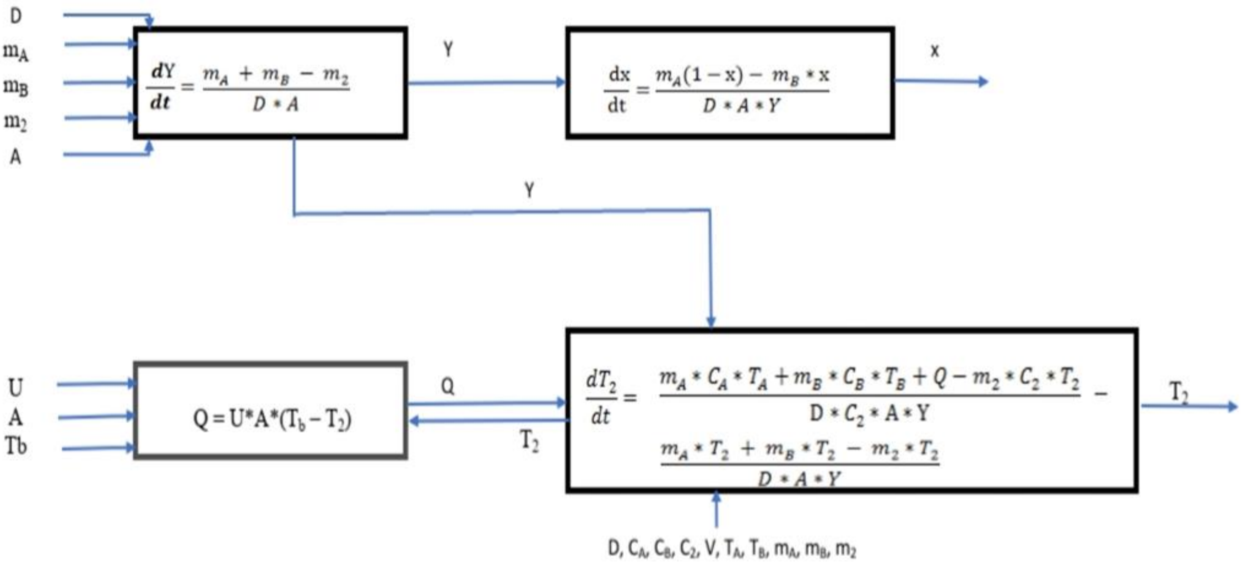

Fig. 8. Derived mathematical model

RESULTS AND DISCUSSION

PCA is an alternative to a bitumen-asphalt mixture and offers great resistance to potholes formation. In PCA, the term aggregate refers to the gravels and sand, while polymer-coated refers to the coating of the gravels by recycled polymers. The data of various test results were taken to support this research to prove the importance of PCA and utilization in the pavement of roads. Table 2 shows the thermal properties of the polymer [18, 19].

Binding strength was tested by varying plastic composition; the maximum binding strength was achieved for the maximum plastic composition, as given in Table 3. The binding strength of 290 tons was achieved by 25 wt. % polyethylene while higher binding strength can be achieved by using different plastics. It was concluded that binding strength is sensitive to the type and composition of the plastic.

Different methods test the physical properties of PCA, and by changing compositions, different results with different physical properties were achieved by altering temperatures and process parameters, as shown in Table 4 [4, 6, 20].

Evolution of harmful gases at different temperatures was tested by varying the temperature and it was concluded that by keeping the temperature below 200°C there is no evolution of toxic gases. Table 5 shows the Marshall stability value for the PCA-bitumen mix [21, 22]. Table 6 shows the results of the bitumen extraction test, and the physical properties of waste plastic are given in Table 7 [14, 17]. Table 8 shows the stripping value

of the PCA-bitumen mix. Higher plastic weightage leads to lower moisture absorption, less voids, better soundness and impact value. At the same time, abrasion value is also lowered by higher plastic compositions, which is one of the disadvantages of higher plastic content as lower abrasion value offers lower friction and causes skidding of automobiles.

Table 2. Thermal properties of polymer

Type of polymer	Solubility in water	Softening temperature range (°C)	Products reported	Decomposition temperature range (°C)	Products reported	Ignition temperature range (°C)	Products reported
PE	nil	100-120	no gas	270-350	CH_4, C_2H_6	>700	CO, CO_2
PP	nil	140-160	no gas	270-350	C_2H_6	>700	CO, CO_2

Table 3. Variation in binding strength

Type of polymer	Plastic wt. %	Binding strength (Kg)	Compression strength (Tons)
Polyethylene (PE)	10	325	250
	20	340	270
	25	350	290
Polypropylene (PP)	10	350	280
	20	370	290
	25	385	310

Table 4. Aggregate technical properties

Plastic coated over aggregate wt. %	Moisture absorption %	Soundness %	Aggregate impact value (AIV)	Los Angel's Abrasion/ Rattler test (LAR) %	Voids %
0	4	5±1	25.4	26	4
1	2	Nil	21.20	21	2.2
2	1.1	Nil	18.50	20	1
3	Traces	Nil	17.00	18	Nil

Table 5. Marshall stability value for PCA-bitumen mix

Bitumen wt.%	Polymer bitumen wt. %	Type of polymer plastic	Marshall value (KN)	Flow value (X) (0.25mm)	Void %	Marshall Quotient (KN/mm)
4.5	5	PP	16	4	53	4
4.5	10	PP	20	5	55	4
4.5	10	PE	20	4	58	5
4.5	15	PE	22.5	4	56	5.63

Table 6. Bitumen extraction test

Plastic wt. %	Bitumen extracted after 5 min %	Bitumen extracted after 10 min %	Bitumen extracted after 15 min %
0	96.0	98.0	99.0
0.5	63.5	88.7	92.3
0.75	63.2	86.7	90.7
1.0	61.3	76.7	83.6

Table 7. Physical properties of waste plastic

Commercial plastic material	Nature of plastic	Thickness (microns)	Softening temperature range (°C)
Carry bag	Polyethylene	10	100-120
Cup		150	100-120
Water bottle		210	170-180
Soft drink bottles		210	170-180
Parcel cover		50	100-120
Film		50	120-130

Table 8. Stripping value of PCA-bitumen mix

	Plain aggregate				PCA			
Time (hours)	2	24	72	96	2	24	72	96
Stripping value	0	0	2	5	0	0	0	0

Process Costing and Economic Analysis

This novel strategy for up-degree streets ends up being valuable and practical, sparing millions of rupees. There are enormous prospects of the street up-degree as far as quality and cost-viability, as the condition and nature of streets are declining day by day. Due to increased waste problems and early damage of roads, especially in Karachi, which occurred due to stagnant wastewater or any other reason, the economic sustainability of the city and even the whole country is declining as health and transportation problems are increasing gradually. This method not only provides the utilization of landfilled waste but also contributes towards the improvement of road properties and lowering the cost of road material with durability, thus economically uplifting the country.

Basic Costs: cost of waste plastics = Rs. 25/- per kg, cost of bitumen per drum (200 Kg) = Rs. 8400/- and cost of bitumen per kg. = Rs. 42.00/. Generally, roads are constructed in a basic width of 3.0 m, 3.75 m, and 4.0 m. Consider a 1 km length road of width 3.75 m.

In terms of aggregate: Let optimum amount of waste plastic used = 10% (by wt. of aggregates). Amount of aggregates used in road construction (1 km length × 3.75 m width) = 3750 m^2 × 12.5 kg per m^2 (avg.) = 46875 kg. So, amount of waste plastic used in road (10% by wt.) = 4687.5 kg. Total cost of waste plastic used = 4687.5 * 25 = Rs. 117,187.5/-. Cost of bitumen saved (4687.5 kg equivalent to plastic used) = 4687.5 * 42 = Rs. 196,875/-

In terms of bitumen: let the optimum percentage of plastic in the blend as per different testing results is around 5% wt. of bitumen. Cost of road (new) / kilometer: bitumen required for work (approximately) 21,300 kg per km, cost of bitumen in new work per km= 21,300 * 42 = Rs. 894,600/-, waste plastic coated over hot aggregate for PCA (5% by wt. of bitumen) = 21,300 * 0.05 = 1,065 kg, cost of waste plastic used = 1,065 * 25 = Rs. 26,625/-, cost of bitumen saved (1065 kg equivalent to plastic used) = 1,065 * 42 = Rs. 44,730/- and total savings per km = 44,730 – 26,625 = Rs. 18,105/-

Cost of road (up gradation) / kilometer, bitumen required for work (approximately) = 11,925 kg per km, cost of bitumen in repairs (up gradation) per km = 11925 * 42 = Rs. 500,850/-, waste plastic coated over hot aggregate for PCA (5% by wt. of bitumen) = 11,925 * 0.05 = 596.25 kg, cost of waste plastic used = 596.25 * 25 = Rs. 14,906.25/-, cost of bitumen saved (596.25 kg equivalent to plastic used) = 596.25 * 42 = Rs. 25,042.5/- and total savings per km = 25,042.5 – 14,905.25 = Rs. 10,137.25/-.

Economic Outcomes

All kinds of waste plastic used are most problematic to the environment. The burning of waste plastic produces hazardous gases that can be limited by using plastic in the proposed process. Landfilling will be reduced to a larger extent by utilizing the waste plastic that contributes to a larger portion of solid waste that is increasing day by day. The non-biodegradable plastic covering prevents composting of organic waste, which will decompose more quickly after eliminating plastic. Once the plastic is separated from the organic waste, farmers can directly utilize the latter instead of purchasing fertilizers. The government expenditure will lower on road construction. The increased life of roads will be the most cost-effective and sustainable benefit. The enhanced road properties by the use of non-biodegradable and durable plastic will ease transportation.

CONCLUSION

This constructive method of obtaining PCA and its utilization to prepare road construction material or any other use will become a definite part of the environment. This study was aligned for the solution of the two major problems faced by the country - increasing waste plastic and increasing and early deterioration of roads - through the utilization of waste plastic polymers in preparation of PCA for construction of road material. The preparation of PCA utilizes the waste plastics and reduces them in the future so that the pollution rate will also be decreased and marine life could be saved. The PCA will be one of the economical and beneficial materials for road preparation because it saves 1 km of road material as the shredded plastic in the form of polymer covers the aggregate and occupies a large portion of the road. The absorption rate of PCA is very low due to the utilization of waste plastic. The life of the road will be increased because of its low porosity, and there will be no pothole formation. The addition of waste plastic in aggregate (PCA) will

help improve the strength (Marshal stability value) and the durability of the pavement. The water absorption was reduced by improving the arrangement, covering plastic over the hot aggregate. This coating of plastic shows a decrement in voids. The plastic-coated aggregate is expected to present no or low amount of weight loss, thus approving the enhancement in aggregate value. For pavements, the Los Angeles abrasion (LAR) value must be less than 30%, showing better water resistance, no water stagnation, no stripping, and no potholes.

Acknowledgement: *The authors would like to acknowledge the Department of Chemical Engineering and Department of Polymer and Petrochemical Engineering, NED University of Engineering & Technology, Karachi, Pakistan, to support this research work.*

REFERENCES

1. D. Bhatt, S. Markuna, *International Research Journal of Modernization in Engineering Technology and Science*, **2**, 639 (2020).
2. P. Neelapala Naresh, V. Suryaprakash, *Int. J. Anal. Exp. Modal Analys.*, **12**, 65 (2020).
3. R. Dharani, N. Uma, *Int. J. Sci. Adv. Res. Tech.*, **4**, 168 (2018).
4. A. B. Crusho, V. Verghese, *Int. Res. J. Multidis. Techno.*, **1**, 668 (2019).
5. A. M. A. Abdo, *ARPN J. Eng. Appl. Sci.*, **12**, 4351 (2017).
6. P. N. A. Asare, F. A. Kuranchie, E. A. Ofosu, F. Verones, *Cogent Environ. Sci.*, **5**, 1 (2019).
7. N. Pramukh, R. L. Prajwal, B. M. Darshan, S. Sunilkumar, C. L. Santhosh, *Int. J. Res. Eng. Sci. Manag.*, **3**, 257 (2020).
8. A. Lulseged, K. Mehantharaja, C.V.S.R. Prasad, *Int. J. Scient. Eng. Tech. Res.*, **5**, 933 (2016).
9. A. Biswas, A. Goel, S. Potnis, *Case Stud. Const. Mat.*, **13**, 1 (2020).
10. R. N. Patil, H. P. Rane, S. D. Kothawade, H. A. Shinde, R. G. Katore, P. Jha, *Int. J. Recen. Trend. Eng. Res.*, **3**, 131 (2017).
11. M. Sharma, A. S. Trivedi, R. Sahu, *Int. J. Civil Eng. Res.*, **7**, 125 (2016).
12. D. Midha, E. S. Sharma, E. Vikram, *Int. J. Tech. Res. Eng.*, **6**, 5674 (2019).
13. M. Sharma, A. S. Trivedi, R. Sahu, *Int. J. App. Env. Sci.*, **12**, 953 (2017).
14. B. Mishra, M. K. Gupta, *Int. J. Eng. Tech.*, **7**, 396 (2018).
15. F. Adou, B. Ampadu, N. K. Agyepong, O. N.-A. Soli, *Civil Environ. Res.*, **10**, 32 (2018).
16. R. Jadon, R. Kansal, *Int. Res. J. Eng. Tech.*, **3**, 3022 (2016).
17. A. Balaguera, G. I. Carvajal, J. Albertí, P. Fullana-i-Palmer, *Resour., Conserv. Recycl.*, **132**, 37 (2018).
18. S. Bhargava, A. K. Raghuwanshi, P. Gupta, *Int. J. Innov. Sci. Eng. Tech.*, **3**, 276 (2016).
19. R. Jadon, R. Kansal, *Int. J. Sci.Tech. Eng.*, **3**, (2016).
20. S. A. Dawale, *Int. J. Adv. Eng. Tech. Manag. App. Sci.*, **3**, 118 (2016).
21. G. Lu, P. Liu, Y. Wang, S. Faßbender, D. Wang, M. Oeser, *J. Cleaner Prod.*, **220**, 1052 (2019).
22. K. K. Sahoo, M. Gupta, R. Sahu, K. Mudgal, Y. S. Shankar, *Adv. Waste Manag.*, **6**, 155 (2019).

Bulgarian Chemical Communications, Volume 53, Issue 3 (pp. 307 - 312) 2021 *DOI: 10.34049/bcc.53.3.5351*

Phytochemical composition and antioxidant activity of Algerian *Astragalus gombo* stems

S. Benferdia*, Z. Rahmani, A. Belfar, R. Cherbi, Z. Rahmani, A. Messaoudi, M. Saïdi

Department of Chemistry, Faculty of Mathematics and Material Sciences, University Kasdi Merbah, Ouargla (30000), Algeria
Laboratoire de Valorisation et Promotion des Ressources Sahariennes

Received: November 19, 2020, Revised: February 18, 2021

Astragalus gombo obtained from Ouargla, Algeria, is first studied in this research for antioxidant activity. Our aim was to evaluate total polyphenol, flavonoid, tannin contents and antioxidant capacity of *Astragalus gombo* stems. Total polyphenol, flavonoid and tannin contents of *Astragalus gombo* stems varied from 4.174 ± 0.034 mg GAE/g DW to 0.213 ± 0.001 mg GAE/g DW, 0.706 ± 0.002 and 0.011 ± 0.000 mg QE/g DW and 0.098 ± 0.005 and 0.0084 ± 0.0001 mg CE/g DW, respectively. The antioxidant activity was measured by two methods: inhibition of DPPH$^{\bullet}$ and total antioxidant capacity by phosphomolybdate assay (PM). The results showed that the extracts display an excellent antioxidant capacity. An excellent relationship between antioxidant activity and total polyphenol content manifested that the phenolic compounds were the most important antioxidant components in the extracts.

Keywords: *Astragalus gombo*; Antioxidant; DPPH$^{\bullet}$; Total polyphenol content

INTRODUCTION

The medicinal use of plants is very old, the researchers demonstrate that remedial use of medicinal plants is known since 4000 - 5000 B.C. and Chinese first employed the natural herbal composition as treatment. In India, sources of use of plants as medicine can be found in Rig-Veda, which is said to be written between 1600-3500 B.C. [1]. The expression of medicinal plants comprises a different kind of plants and several of these plants possess medicinal activities [2]. These medicinal plants are rich of ingredients, which can help in developing drugs.

The genus *Astragalus* is the biggest in the Fabaceae family, with more than 2500-3000 species [3]. The species are spread in Central Asia, South and North America and North and South Africa. One of these species, *Astragalus gombo* bunge, is present in Septentrional Algerian Sahara. It is a perennial plant, common and endemic, frequently used as animal fodder [4]. Astragalus roots are used in traditional medicine as an anti-tonic. It has also been used to treat diabetes, leukemia and treating female irregular menstruation and amenorrhea [5]. Some astragalus species like *Astragalus mongholicus* and *A. membranaceus* are used in traditional Chinese medicine due to their anti-cancer properties [5, 6].

Free radicals are atoms or molecules with an unpaired electron and are important intermediates in natural processes, involving regulating biological functions such as vasodilation, and neurotransmission. However, an excessive amount causes many diseases like cancer [7].

Free radicals are not stable and react rapidly with other compounds, aiming to take the necessary electron to achieve stability. The human body possesses a complex system of enzymatic and non-enzymatic antioxidant defenses which neutralize the deleterious consequences of free radicals [8]. The term antioxidant designates any substance which has a low concentration compared to oxidizable substrates, inhibits or delays the oxidation process [7]. The antioxidants play an important role in the protection from free radicals by donation of hydrogen or electron, which quench the free radicals [9].

The interaction of flavonoids with many radicals has been used in various studies to evaluate the essentials of antioxidant capacity [10].

The aim of this work is to measure the total content of phenolic, flavonoid and tannin compounds of stems *Astragalus gombo* bunge and study the correlation between them and the antioxidant capacity.

MATERIAL AND METHODS

Chemicals and reagents

Folin-Ciocalteu reagent, ascorbic acid, gallic acid, catechin, vanillin, 2,2-diphenyl-1-picrylhydrazyl (DPPH), sulfuric acid, butylated hydroxytoluene (BHT) were purchased from Sigma Aldrich; ammonium molybdate, sodium carbonate,

* To whom all correspondence should be sent:
E-mail: benferdia.rahmani@gmail.com

© 2021 Bulgarian Academy of Sciences, Union of Chemists in Bulgaria

hydrochloric acid, sodium dihydrogen phosphate, were provided by Biochem Chempharma. All other chemicals and solvents used in this research were of analytical grade.

Instrumentation

The proposed work was carried out on a UV/Vis spectrophotometer SPECTROSCAN 80 DV. All weighing was done on an electronic analytic balance. Plant extracts preparation was carried out by using a rotary evaporator ISOLAB GmbH for evaporating the solvent.

Plant collection

Plant stems were collected from the region of Oued N'ssa [32°23'N 5°21'E] (Ouargla, Algeria, arid climate). The collection was in the mornings in the beginning of March 2018. Professor Abdelmadjid Chahma from the University of Ouargla, Algeria, identified the specimen. Stems were cut into small parts and stored in paper containers at 25 °C in darkness until required for use.

Preparation of the extracts

Stems of *Astragalus gombo* were macerated at room temperature with petroleum ether for 24 h, and then the plant was air-dried until all the solvent was evaporated. After that the stems were macerated again with MeOH-H_2O (80:20, v/v) for 24 h three times. After filtration, the filtrate was evaporated until dryness, subsequently the dried filtrate was dissolved with H_2O and successively extracted using different organic solvents dichloromethane, ethyl acetate and butanol. These extracts, as well as the rest water fraction were concentrated under reduced pressure and then redissolved with minimum of methanol or water and kept at 4°C.

Phytochemical screening

The crude extract of stems was used for carrying out the following phytochemical tests using standard procedures to identify the various constituents described in the literature [11-13].

Determination of total phenolic content (TPC)

The total phenolic content in all stems extracts of *Astragalus gombo* was determined spectrophotometrically according to the Folin-Ciocalteu method [14]. Briefly, 0.1 ml of the extract sample was mixed with 0.5 ml of a 10 % Folin-Ciocalteu reagent (diluted in distilled water 1/10). After 5 min, 2.0 ml of 20 % Na_2CO_3 were added, and the mixture was incubated for 30 min at 25°C in the dark. Absorbance at 760 nm was measured. The TPC was determined using linear regression equation obtained from the calibration curve of gallic acid. The content of total phenolic compounds was determined as mean±SD (n=3) and expressed as mg gallic acid equivalent GAE/g of dry weight (DW) of plant.

Determination of total flavonoid content (TFC)

The content of total flavonoids was measured using the aluminum chloride colorimetric assay [15]. Briefly, 0.5 ml of the extract was added to 0.5 ml of 2 % $AlCl_3$ ethanol solution. After 30 min incubation at 25°C, the absorbance at 430 nm was measured. The content of total flavonoids was estimated as mean ± SD (n = 3) and expressed as mg quercetin equivalent QE/g of dry weight (DW).

Determination of total tannin content (TTC)

The total tannin content of the *Astragalus gombo* stems was determined by using the vanillin-acidified method [16]. 3 ml of a freshly prepared solution of vanillin (4% w/v vanillin solution in ethanol) and 1.5 ml of concentrated HCl were added to 0.4 ml of extract sample. After 15 min of incubation, the absorbance at 500 nm was measured. The content of total tannin was estimated as mean ± SD (n = 3) and expressed as mg catechin equivalent CE/g dry weight (DW).

Antioxidant activity

Evaluation of total antioxidant capacity by phosphomolybdate assay (PM). Phospho-molybdate assay was used to estimate the antioxidant activity of the samples [17]. The different extracts and fractions of *Astragalus gombo* were used. Various concentrations of extracts (0.1 ml) were mixed with 1 ml of reagent solution (4 mM ammonium molybdate, 28 mM sodium phosphate and 0.6 M sulfuric acid). The mixture was kept at 95 ºC for 90 min. The absorbance was read at 695 nm against blank after cooling the tubes at 25°C, using ascorbic acid as a positive control, and the results were expressed in mM as the ascorbic acid equivalent antioxidant capacity AEAC. The following equation was employed to determine the values of AEAC:

$$AEAC = \frac{k_{extract}}{k_{ascorbic\ acid}}$$

where, $k_{extract}$: slope of the curve *absorbance = f(1/dilution number)*, $k_{ascorbic\ acid}$: slope of the curve *absorbance = f(concentration of ascorbic acid).*

DPPH radical scavenging activity. The power to scavenge the free radical DPPH• was estimated as the decrease in absorbance at 517 nm according to

[10]. Sample solution (1.5 ml) at various concentrations was added to methanolic DPPH (1.5 ml of a 0.25 mM solution) . The mixture was incubated for 30 min in dark, and then the absorbance was measured at 517 nm against a control. The antioxidant capacity of the extract was expressed as an IC_{50} value defined as the concentration (mg/ml) of the extract that inhibited $DPPH^{\bullet}$ radicals by 50%. The following equation was employed to determine the % DPPH radical scavenging activity:

$$\%\ \text{DPPH radical scavenging} = \frac{(\ control\ absorbance - extract\ absobance)}{(control\ absorbance)}\ x100$$

RESULTS AND DISCUSSION

The recovery percentage of extractable compounds of stems ranged from 4.8852 to 0.1387%. The extraction yields of dichloromethane and of ethyl acetate were low, however, the yield of butanol extraction was significant. The results revealed that the highest yield extracts were obtained by the crude (methanol) (4.8852%) and butanol (1.2947%). This can be related to the richness of the plant in polar compounds. The variation in the yields of extracts could be attributed to the difference in solvent polarities used, which also plays a key role in increasing the solubility of phytochemical compounds.

The curative properties of *Astragalus gombo* are probably due to the existence of various secondary metabolites like polyphenols, flavonoids, coumarins, saponins, quinones, tannins, etc. The phytochemical screening of the extracts from the stems of *Astragalus gombo* is illustrated in Table 1.

The results of phytochemical tests detected the presence of flavonoids, tannins, protein, glycosides, terpenoids, coumarins, saponins and quinones. The existence of these compounds has been proved and six new cycloartane-type triterpene glycosides have been isolated in *Astragalus gombo* [18].

Table 1. Phytochemical screening of extracts from stems of *Astragalus gombo*

Phytochemical components	Stems
Flavonoids	++
Steroids	-
Tannins	+
Saponins	+++
Terpenoids	+
Alkaloids	-
Glycosides	++
Cardenolides	-
Protein	+
Quinones	+
Polyphenols	+++
Coumarins	+++

+ = Present, - = Absent

Another study [19] revealed the presence of protein in the aerial parts of *Astragalus gombo* from a semi-aride region in Algeria. On the other hand, Kim *et al.* [20] isolated protein of *Astragalus membranaceus* which acts as an allergen.

The richness of the *Astragalus* species in polysaccharides and saponins explains the use of this plant for their hepatoprotective, immune-stimulant, antioxidative, and antiviral properties [21].

In addition, this plant contains coumarins which are used as anticoagulants [22], antioxidants, antimicrobial (antiviral, antifungal, and anti-parasitic), anticancer, antidiabetic, analgesic, anti-neurodegenerative, and anti-inflammatory agents [23].

Preliminary tests have shown the existence of phenolic compounds. These compounds have a wide range of biological activities [24]. Therefore, our choice focused on this family of compounds that were obtained by the methods of extraction of polyphenols. The results are shown in Table 2.

The TPC of the various stems extracts is expressed in terms of GAE and is presented in Table 2. The TPC were calculated using the following linear regression equation derived from the standard curve of gallic acid: $y = 3.326x$, $R^2 = 0.992$, where y is absorbance and x is the concentration of gallic acid in g/L. Total phenolics ranged from 4.174 ± 0.034 mg GAE/g DW to 0.213 ± 0.001 mg GAE/g DW (Table 2). The highest content was found in the aqueous phase of stems; the lowest content was registered in the ethyl acetate phase of stems.

Ethyl acetate was applied to extract medium polar flavonoids and glycosides while butanol and water were utilized for extracting polar compounds like phenolic acids, aglycones. The TFC of the various crude extracts are expressed in terms of QE and are presented in Table 2. The TFC were calculated using the following linear regression equation obtained from the standard plot of quercetin: $y = 36.37x$, $R^2 = 0.999$, where y is absorbance and x is the concentration of quercetin in g/L.

Table 2. Yields of the extracts, total phenolic, flavonoid, tannin and antioxidant activity of various extracts of *Astragalus gombo*

Extracts	Yield %	TPC mg GAE/g DW	TFC mg QE/g DW	TTC mg CE/g DW	IC_{50} mg/ml	AEAC mM
Crude	4.8852	3.104±0.011	0.548±0.001	0.029±0.001	1.586±0.011	271.5±0.3
Dichloromethane	0.1387	0.254±0.001	0.011±0.000	0.008±0.000	0.073±0.005	099.1±1.8
Ethyl acetate	0.1508	0.213±0.001	0.518±0.002	0.008±0.000	0.300±0.026	099.2±1.1
Butanol	1.2947	1.209±0.008	0.706±0.002	0.039±0.003	0.616±0.021	194.7±22
Aqueous	ND	4.174±0.034	0.593±0.002	0.098±0.005	0.890±0.080	229.1±1.4
BHT	/	/	/	/	0.004±0.000	004.9±1.5
Vitamin C	/	/	/	/	0.009±0.000	/

ND, not determined

TFC of the crude extract and the fractions of *Astragalus gombo*, expressed as quercetin equivalent per gram dry weight mg QE/g DW, was between 0.706± 0.002 and 0.011 ± 0.000 mg QE/g DW. The highest content was found in butanol stems extracts; the lowest content was registered in dichloromethane stems extracts. Total tannin equivalents of the various extracts are expressed in terms of catechin equivalent and are presented in Table 2. The TTC were calculated using the following linear regression equation obtained from the standard plot of catechin: $y = 4.378x$, $R^2 = 0.997$, where y is absorbance and x is the concentration of catechin in mg/mL. TTC in the fractions and the crude extract of *Astragalus gombo*, varied between 0.098 ± 0.005 and 0.0084±0.0001 mg CE/g DW. The highest content was found in aqueous stems fractions, while the lowest was found in dichloromethane stems fractions.

The role of an antioxidant is to scavenge free radicals. One mechanism out of which this is done includes donating hydrogen to a free radical and hence its reduction to an unreactive species. Addition of hydrogen removes the odd electron feature, which is responsible for radical reactivity. The antiradical activity of ten crude extracts of *Astragalus gombo* leaves and stems was investigated by radical scavenging methods such as DPPH$^{\bullet}$.

The scavenging effect of different concentrations of *Astragalus gombo* leaves and stems extracts on the DPPH$^{\bullet}$ free radical was compared with that of a standard antioxidant, (ascorbic acid and BHT). The results, expressed as IC_{50} (mg/ml), are shown in Table 2.

The method of DPPH$^{\bullet}$ is based on the reduction of the stable radical DPPH$^{\bullet}$ with a violet color to DPPH-H with a yellow color. The disappearance of the violet color can be monitored spectrophotometrically at 517 nm. The values of IC_{50} varied between 1.586±0.011 and 0.073±0.005 mg/ml (Table 2). The best activity was found in the dichloromethane stems fraction with an IC_{50} value of 0.073±0.005 mg/ml followed by ethyl acetate with an IC_{50} value of 0.3±0.026 mg/ml. BHT and ascorbic acid showed a good antiradical activity, better than all extracts.

The total antioxidant activity of the different extracts of *Astragalus gombo* was measured by the phosphomolybdenum method, which is based on the reduction of Mo (VI) to Mo (V).

The formation of green phosphate/Mo (V) compounds was measured at 695 nm. Total antioxidant activity of all extracts varied between 271.5 ± 0.3 and 99.1 ± 1.8 mM. Crude fraction had a strong antioxidant activity with a value of 271.5 ± 0.3 mM followed by aqueous stems extract with a value of 229.1 ± 1.4 mM. The lowest antioxidant activity was recorded in the dichloromethane fraction with a value of 99.1 ± 1.8 mM.

Recently interest in food phenolics has highly increased, for their antioxidant capacity and their possible beneficial effects in human health, such as in the treatment and prevention of cancer, cardiovascular disease, and other pathologies [25]. Phenolic compounds undergo a complex redox reaction with the phosphotungstic and phosphomolybdic acids present in the Folin-Ciocalteu reagent [26]. Under alkaline conditions, phenolic compounds reduce the Folin reagent to form a blue color; however, the assay is *not specific for phenolic compounds*. Tryptophan, ascorbic acid, thiols, redox-active metal ions, and nucleotide bases all reduce the Folin reagent and increase the final values [27].

Flavonoids, as a class of polyphenolics, are one of the most diverse, and most extensively present in plants. Numerous studies have established positive effects of flavonoids as potent antioxidants. These compounds exert a wide range of anticancer effects [28].

We have observed that phenolic and flavonoid contents are higher in the polar fractions (aqueous

and butanol fractions), which may indicate that these polyphenol compounds are more hydroxylated and/or glycosydated. The content of phenolic or flavonoid compounds in the fractions was affected by their solubility in the solvent used for extraction. Polar fractions had more polyphenols than non-polar fractions. Other studies showed that the content of phenolics in leaflets in different *Astragalus* species was higher than that in roots and seeds [29].

Comparing our results with previous studies specific for *Astragalus gombiformis* we noted that the values of IC_{50} obtained by Teyeb *et al*. [30] are higher. By way of example, for the aerial parts they give 0.473 mg/ml; and for the roots - 0.626 mg/ml. We recall that the extraction system used in this study is methanol.

Other studies on the *Astragalus chrysostachys* Boiss. roots show that the inhibition of $DPPH^{\bullet}$ is better than our results - in ethyl acetate phase 0.0146 mg/ml and in butanol phase - 0.0517 mg/ml [31].

Antioxidant capacity assays may be in general classified as single electron transfer (SET) and hydrogen atom transfer (HAT) based assays. SET assays measure the capacity of an antioxidant in the reduction of an oxidant. Phosphomolybdenum assay method is based on the redox antioxidant reaction.

Relationships among antioxidant capacity estimates and TPC, TFC, TTC

In the current research, the extracts of stems give an excellent correlation between TTC and TPC with a correlation coefficient R^2 = 0.85 while the extracts give a medium correlation between TPC and TFC with R^2 = 0.46. Moreover, the extracts of stems give a medium correlation between TFC and TTC with R^2 = 0.48. The TTC and TFC give a medium correlation with the antioxidant activity (especially with IC_{50}). On the contrary, a good correlation is shown between TPC and the antioxidant activity especially with IC_{50} (R^2 = 0.78).

Zhang *et al*. [32] estimated the antioxidant activity of a number of extracts from *Astragalus complanatus* obtained under different extraction conditions. They found that the antioxidant capacity, measured by $DPPH^{\bullet}$ test, well correlates to the TPC of the corresponding extracts. The high correlation coefficient (0.95) indicates that the total phenolics in the extracts were the major free radical scavenging compounds.

In addition, a good correlation is shown of TPC, TFC and TTC with the reduction capacity of Mo (VI) to Mo (V). Furthermore, according to some studies, the antioxidant activity depends on the structural conformation of the phenolic compounds. The latter is generally influenced by the phenolic compounds in the samples and by the different mechanisms involved in the radical–antioxidant reactions. These compounds may have a wide set of chemical structures that could react with radicals by hydrogen donation and/or electron transfer. There is an excellent correlation between the two methods of antioxidant activity determination (PM and $DPPH^{\bullet}$) (R^2 = 0.94).

CONCLUSION

In the present study, application of different solvents to extract antioxidant compounds from *Astragalus gombo* stems was investigated. Our results suggest that *Astragalus gombo* bunge could be a potential source of compounds with strong antioxidant potential. In addition, a high content of phenolics and tannin in this plant was determined.

This study indicated that the aqueous fraction has higher phenolic and tannic contents than other fractions. In addition, it exhibited strong antioxidant capacities in PM assay. All extracts exhibited strong reduction of Mo(VI) to Mo(V) comparable to the commercial BHT antioxidant. That is why the *Astragalus gombo* bunge is a suitable plant for treatment of many diseases.

Acknowledgements: *The authors gratefully acknowledge the support provided by Mr Mohamed Hadjadj, Director of VPRS Laboratory, University of Ouargla, Algeria.*

Conflict of interest: *All authors declare no conflict of interest.*

REFERENCES

1. S. Hosseinzadeh, A. Jafarikukhdan, A. Hosseini, R. Armand, *Int. J. Clin. Med*., **6**, 636 (2015).
2. B. A. Rasool Hassan, *Pharmaceut. Anal. Acta*, **3**, 1000e139 (2012).
3. S. Naghiloo, A. Movafeghi, A. Delazar, H. Nazemiyeh, S. Asnaashari, M. R. Dadpour, *BioImpacts*: *BI*, **2**, 106 (2012).
4. T. Chouana, G. Pierre, C. Vial, C. Gardarin, A. Wadouachi, D. Cailleu, D. Le Cerf, Z. Boual, M. D. O. El Hadj, P. Michaud, *Carbohydr. Polym.*, **175**, 388 (2017).
5. A. Dasgupta, *Antiinflammatory Herbal Supplements*, 76 (2019).
6. P. Liu, H. Zhao, Y. Luo, *Aging and Dis.*, **8**, 868 (2017).
7. O. O. Abiodun, M. E. Nnoruka, R. O. Tijani, *Turk. J. Pharm. Sci.*, **17**, 344 (2020).
8. Z. Rahmani, M. Dekmouche, M. Hadjadj, M. Saidi, *Der Pharma Chem.*, **8**, 1 (2016).

9. C. Bakka, M. Hadjadj, O. Smara, H. Dendougui, S. Mahdjar, *Int. J. Pharm. Sci. Res.*, **11**, 3634 (2019).
10. Z. Rahmani, A. Douadi, Z. Rahmani, *Asian J. Chem.*, **12**, 362 (2019).
11. R. N. S. Yadav, M. Agarwala, *J Phytol.*, **3**, 11 (2011).
12. A. J. Harborne, Phytochemical methods a guide to modern techniques of plant analysis, Springer, Netherlands, 1998.
13. W. C. Evans, Pharmacognosy E-book. Elsevier Health Sciences, 2009.
14. N. Stanković, T. Mihajilov-Krstev, B. Zlatković, V. Stankov-Jovanović, V. Mitić, J. Jović, L. Čomić, B. Kocić, N. Bernstein, *NJAS-Wagen J. Life Sc.*, **78**, 23 (2016).
15. M. Abdeldjabbar, D. Messaouda, R. Zhour, B. Cheyma, *Asian J. Chem*., **13**, 2 (2020).
16. D. Djemoui, M. Saidi, Z. Rahmani, A. Djemoui, *J. Fundam. Appl. Sci.*, **11**, 283 (2019).
17. P. Prieto, M. Pineda, M. Aguilar, *Anal. Biochem*., **269**, 338 (1999).
18. L. Maamria, C. Long, H. Haba, C. Lavaud, A. Cannac, M. Benkhaled, *Phytochem. Lett.*, **11**, 286 (2015).
19. S. Medjekal, H. Bousseboua, *Livest. Res. Rural. Dev*., **28** (12), 1 (2016).
20. K.-H. Kim, J. Y. Park, I.-S. Lee, K. J. Lim, W. S. Jung, H.-J. Jang, *BioChip J*., **10**, 95 (2016).
21. J. L. Rios, P. G. Waterman, *Phytother. Res.*, **11**, 411 (1997).
22. J. K. Aronson, Meyler's Side Effects of Drugs 16E: The International Encyclopedia of Adverse Drug Reactions and Interactions, University of Oxford, Oxford, UK, 2015, p. 7674.
23. M. J. Matos, L. Santana, E. Uriarte, O. A. Abreu, E. Molina, E. G. Yordi, Coumarins - an important class of phytochemicals, Phytochemicals - Isolation, Characterisation and Role in Human Health, 2015, p. 113.
24. M. Al-Owaisi, N. Al-Hadiwi, S. A. Khan, *Asian Pac. J. Trop. Biomed.*, **4**, 968 (2014).
25. L. Bravo, *Nutr. Rev.*, **56**, 317 (1998).
26. V. L. Singleton, J. A. Rossi, *Am. J. Enol. Vitic.*, **16**, 144 (1965).
27. R. R. Schendel, Phenol content in sprouted grains, in: Sprouted Grains: Nutritional Value, Production, and Applications, Elsevier, London, UK, 2019, p. 279.
28. D. M. Kopustinskiene, V. Jakstas, A. Savickas, J. Bernatoniene, *Nutrients*, **12**, 1 (2020).
29. V. Niknam, H. Ebrahimzadeh, *Pak. J. Bot.*, **34**, 283 (2002).
30. H. Teyeb, O. Houta, H. Najjaa, A. Lamari, M. Neffati, W. Douki, M. F. Najjar, *Z. Naturforsch.*, **67**c, 370 (2012).
31. J. Ghasemian-Yadegari, S. Hamedeyazdan, H. Nazemiyeh, F. Fathiazad, *Iran J. Pharm. Res.*, **18**, 1908 (2019).
32. Q.-A. Zhang, X.-H. Fan, Z.-Q. Zhang, T. Li, C.-P. Zhu, X.-R. Zhang, W. Song, *Food Chem.*, **141**, 1295 (2013).

Bulgarian Chemical Communications, Volume 53, Issue 3 (pp. 313 - 320) 2021 *DOI: 10.34049/bcc.53.3.5353*

Electrodeposition of HAP/TiO_2 on type 316L stainless steel for orthopedic application

R. Manonmani[1]*, S. Sureshkumar[1], S. Mohandoss[1], B. Venkatachalapathy[2]

[1]*Department of Chemistry, Rajalakshmi Engineering College, Chennai - 602105, India*
[2]*Department of Chemistry, SRM Easwari Engineering College, Ramapuram, Chennai, India*

Received: November 26, 2020, Revised: May 30, 2021

The effect of nano HAP/TiO_2 coating on type 316L stainless steel was investigated. Type 316L stainless steel substrates were electrophoretically coated for various coating time spans and voltages. The coated samples were sintered in an air furnace at 700°C for 1 h. The electrochemical corrosion test was performed in simulated body fluid to evaluate the coating impact on the corrosion behavior of the substrates. The results showed that the coated substrate at 30 V for 60 sec provides a uniform, crack-free coating with enhanced adhesion strength, improving the corrosion resistance of the substrate. *In vitro* study with MC3T3-E1 osteoblast cells showed improved cell attachment and better cells proliferation compared to uncoated sample, by controlling the release of metal ions.

Keywords: Nano biocomposite, Corrosion resistance, Electrophoretic deposition, Type 316L stainless steel.

INTRODUCTION

Metallic implants such as titanium, type 316L stainless steel (316L SS) and magnesium alloy are extensively utilized for load bearing applications, which can provide many solutions to problems such as osteoarthritis, damaged hard tissues and bone fractures in dental and orthopedic applications [1-3]. However, the corrosion behavior of metallic implants such as pitting corrosion, crevice corrosion and fretting corrosion has been observed in the physiological body fluid [4, 5]. It can lead to the release of ions into the tissue environment. Hence, the metal that is to be used as implant must possess high corrosion resistance and better biocompatibility. Till today type 316L SS is the most commonly used biomaterial to orthopedic prostheses due to its excellent corrosion resistance and biocompatibility [6].

In order to enhance the cell-implant material interaction and to increase the longevity of the material, bioactive ceramic-based coating has been applied to type 316L SS. Among the protective and biocompatible coatings, nano hydroxyapatite (HAP) is an attractive biomaterial for human hard tissue implants since it contains a similar chemical composition to that of natural bones and teeth [7, 8]. Nano HAP plays an excellent role in biomedical applications owing to its excellent biocompatible, osteoconductive and bioactive properties, and its close resemblance to the mineral component of bone tissue [9, 10]. Though nano HAP can bond directly to natural bones, its brittle nature and poor strength limit its clinical applications under load-bearing conditions. To overcome these problems and provide better corrosion resistance, incorporation of reinforcing materials like nano TiO_2 is used [11, 12]. Nano TiO_2 is a biocompatible, bioinert material and it was added as a matrix to produce composite coatings possessing higher chemical stability. It has also been reported that TiO_2 coating is biocompatible and improves the calcium and phosphate precipitation onto the metal surface [13].

Many researchers have reported different methods for obtaining of bioceramic coatings on implants, such as sol-gel, micro-arc oxidation, ion beam sputtering, air brush spraying, electrophoretic deposition (EPD), plasma spraying, etc. [14, 15]. Among many techniques, electrophoretic deposition has been found to be an efficient technique to fabricate nano triphasic bioceramic coatings from suspensions and it is an easier process for obtaining nano structural deposits [16, 17]. Thus, nano biocomposite (nano HAP/nano TiO_2) coatings provide the implants with bioactivity, better chemical stability and enhanced adhesion property. So far, there are no reports on nano hydroxyapatite/nano TiO_2 composite coating on type 316L SS. The present work investigates the development of nano biocomposite coating on type 316L SS by electrophoretic deposition process (EPD). EPD was carried out at different voltages from 10 to 40 V for different time intervals (30 to 90 sec) to find out the optimum voltage and its respective time using corrosion studies.

EXPERİMENTAL

Substrate preparation

Type 316L SS substrate was obtained from Steel Authority of India Limited (ASTM F138- 13a).

* To whom all correspondence should be sent:
E-mail: manosenthil.chem@gmail.com

© 2021 Bulgarian Academy of Sciences, Union of Chemists in Bulgaria

Type 316L SS substrate was used as a cathode with a size of 10 mm × 10 mm × 2 mm and 314 SS was used as an anode with a size of 11 mm × 8 mm × 0.5 mm. The substrates were abraded using grit emery paper starting by ranges from 120 to 1000 followed by soap solution treatment, ultrasonically cleaned with acetone and dried at room temperature.

Suspension preparation

A 2% suspension of nano biocomposite in isopropyl alcohol (IPA) was taken in a 100-ml beaker. Iodine (0.1 g) was added to the suspension. Iodine acts as a dispersant to stabilize the suspension and also prevents the agglomeration of the nano particles in the suspension. The suspension was kept for one day in undisturbed condition to get uniform dispersion of the particles. Then, the suspension was sonicated for 30 min to get uniform suspension of particles for the EPD coating process.

Deposition of nano biocomposite

Deposition of nano biocomposite on type 316L SS substrate was achieved by EPD process at room temperature. Two electrodes (type 316L SS and 314 SS) were immersed in a suspension and the distance between these two electrodes was less than 1 cm in order to achieve optimum particle deposition on the exposed electrode surface area. Before deposition one edge of the sample was masked with a Teflon tape and deposition was carried out on other 1 cm^2 surface areas. After the coating process, the coated substrates were dried at room temperature. The dried substrates were subjected to a sintering process at 700°C in an air furnace at a heating rate of 10°C/min for 1 h. The samples were removed after cooling from the furnace and were stored in vacuum desiccators. The coating parameters as voltage and time were optimized by means of electrochemical studies.

Preparation of SBF

Simulated body fluid (SBF) with ion concentration nearly equal to that of human blood plasma, modified fluids with different ion concentrations shown in Table 1, were prepared by dissolving reagent grade NaCl, $CaCl_2$, KCl, $NaHCO_3$, NaH_2PO_4, glucose, $MgSO_4.7H_2O$, $MgCl_2.6H_2O$, $Na_2HPO_4.2H_2O$ in distilled water. In this study, the SBF solution does not contain organic materials which would be appropriate to systems *in vivo*.

Characterization of coated substrate

Electrochemical impedance spectroscopic (EIS) and potentiodynamic polarization studies were performed using a Biologic-SP 240 (EC-lab Version 10.37) interfaced with a computer. A conventional three-electrode cell was used for electrochemical measurements according to ASTM guidelines (G61–86). A graphite electrode, saturated calomel electrode (SCE) and the nano biocomposite coated 316L SS sample were used as a counter electrode, reference electrode and working electrode, respectively. Electrochemical measurements were carried out using an SBF solution with pH of 7.4 at room temperature. EIS was carried out by applying a frequency range from 100 kHz to 10 mHz. Using Nyquist plot, the polarization resistance (R_p) was calculated. Potentiodynamic polarization study was initiated with a starting potential less than 0.250 V of OCP at a scan rate (dE/dt) of 10 mV/min and the parameters like corrosion potential (E_{corr}) and corrosion current density (I_{corr}) were measured. The microhardness properties of the composite coated samples (ASTM E92-17) were measured using Vickers microhardness tester (Ever One Enterprises Limited, India). A loading force of 100 gram Force (gF) was applied for 5 sec to record the measurements.

Table 1. Chemicals used for preparing SBF

Order	Chemicals	Purity (%)	Weight (g/ L)
1	NaCl	99.5	8.00
2	$CaCl_2$	96.0	0.14
3	KCl	99.5	0.40
4	$NaHCO_3$	99.5	0.35
5	NaH_2PO_4	99.5	0.10
6	Glucose	99.5	1.00
7	$MgSO_4.7H_2O$	99.0	0.06
8	$MgCl_2.6H_2O$	96.0	0.10
9	$Na_2HPO_4.2H_2O$	96.0	0.06

The X-ray diffraction (Bruker model D8, Germany) analysis was conducted using Cu kα radiation, and λ of 1.5406Å. The 2θ angles were swept from 10 to 70° in steps of one degree. The surface roughness of the composite coated 316L SS samples was measured by a non-contact optical surface profiler (BRUKER model CONTOUR GT, Germany). Average surface roughness (R_a) measurements were taken at ten various locations on the coated samples to get an accurate assessment. All the measurements were taken perpendicular to the machine markings.

MC3T3-E1 osteoblast cells were obtained from the National Centre for Cell Sciences, Pune (NCCS) and used to assess cell viability on nano biocomposite coated and uncoated 316L SS substrate. *In vitro* cytotoxicity study was carried out using MTT assay [18].

RESULTS AND DISCUSSION

Electrochemical studies

EIS technique was used to characterize the electrochemical nature of uncoated 316L SS and nano biocomposite coated type 316L SS substrates. Figs. 1a and 1b show the Nyquist plots of uncoated 316L SS and nano biocomposite coated type 316L SS substrates at different coating voltages and time spans. The polarization resistance (R_p) and impedance (|Z|) values were higher for coated substrate than for the uncoated type 316L SS.

The presence of nano biocomposite outer coating acts as a barrier layer which prevents the metal ions from corrosive attack due to SBF fluids. Thus, coatings provide protection to metallic substrates in the corrosive body fluid atmosphere mainly due to the presence of chloride ions. Table 2 shows the electrochemical parameters for uncoated and nano biocomposite coated type 316L SS substrate at a coating time of 60 sec and different coating voltages.

From Table 2 it can be observed that the maximum resistance and impedance values obtained for 30 V are due to formation of uniform, crack free coating with strong adhesion on the metal surface. In the case of 20 V a thin coating is produced, which can easily cleave and let the SBF solution enter into the metal surface and stimulate a release of metal ions into the solution. Similarly, coating at 40 V yields a thick layer with hair crack formation, which provides a pathway for body fluids to attack the metal ions. This leads to a decrease in polarization resistance and impedance values at higher voltages. Thick coating with more crack formation was observed on the nano biocomposite coated layer on type 316L SS above 40 V. Thus, the best protective coating was formed on type 316L SS at 30 V.

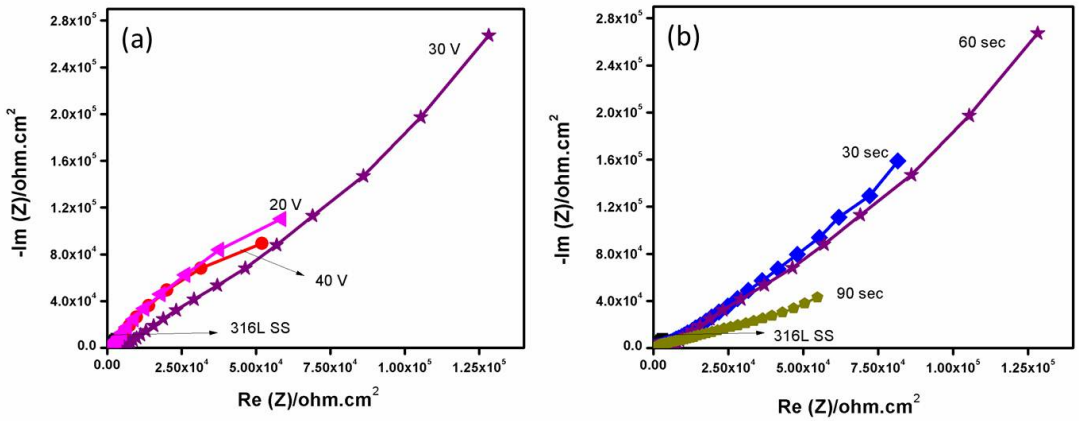

Fig. 1. Nyquist plots of uncoated and nano biocomposite-coated type 316L SS

Table 2. Electrochemical parameters for coated substrates with coating time of 60 sec at different coating voltages

Coating voltage	E_{corr} (mv) *vs* SCE	I_{corr} (mA/cm^2)	R_p (KΩcm^2)	|Z| Ωcm^2
316L SS	-246	-4.33	19.72	17443
20V	-163	-4.91	38.77	123037
30V	-138	-5.81	90.17	266790
40V	-223	-4.76	31.28	91332

Table 3 shows the electrochemical parameters for uncoated and nano biocomposite coated type 316L SS substrate at a coating voltage of 30 V for various coating times. Maximum polarization resistance and impedance was observed at a coating time of 60 sec compared to other coated and uncoated type 316L SS substrates. At coating time spans of 30 sec and 90 sec a thin, respectively, thick coating is produced with crack formation. So, at these coating time spans the SBF solution contacts with the metal surface and initiates a corrosion reaction. Hence, poor resistance and impedance was observed at this condition. With coating times above 90 sec, thick coating with more crack formation was observed on the nano biocomposite coated layer on type 316L SS. However, a highly protective bioceramic coating on type 316L SS substrate was observed at a coating time of 60 sec. Fig. 2a shows the potentiodynamic polarization curves of uncoated 316L SS and nano biocomposite coated type 316L SS substrates at a coating time of 60 sec at different coating voltages. Fig. 2b shows the potentiodynamic polarization curves of uncoated 316L SS and nano biocomposite coated type 316L SS substrates at a coating voltage of 30 V with different coating times. Potentiodynamic polarization curves can be seen in Fig. 2 and the electrochemical parameters including E_{corr} and I_{corr} obtained from the Tafel curves are shown in Tables 2 and 3. It can be noted that all coated substrates showed higher values of I_{corr} and E_{corr} than uncoated ones. It also can be observed that the passivation curves of the coating at 30 V and 60 sec show higher electrochemical stability on the dynamic nature of the corrosion process, when compared with other coated and uncoated substrates. Hence, the best protective coating is obtained on type 316L SS substrate at 30 V for 60 sec.

Mechanical characterization

Implants meeting an intricate physiological environment not only should have good biological properties but also adequate mechanical strength for durable performance [19]. The mechanical strength of nano biocomposite coated and uncoated type 316L SS samples were measured by Vickers microhardness test. The hardness values for bioceramic coated and uncoated type 316L SS substrates are shown in Fig. 3.

Table 3. Electrochemical parameters for coated substrates with coating voltage of 30 V at different coating times.

Coating time	E_{corr} (mv) *vs* SCE	I_{corr} (mA/cm^2)	R_p (KΩcm^2)	|Z| Ωcm^2
316L SS	-246	-4.33	19.72	17443
0 sec	-182	-4.85	47.93	159218
60 sec	-138	-5.81	90.17	266790
90 sec	-234	-4.53	41.01	43458

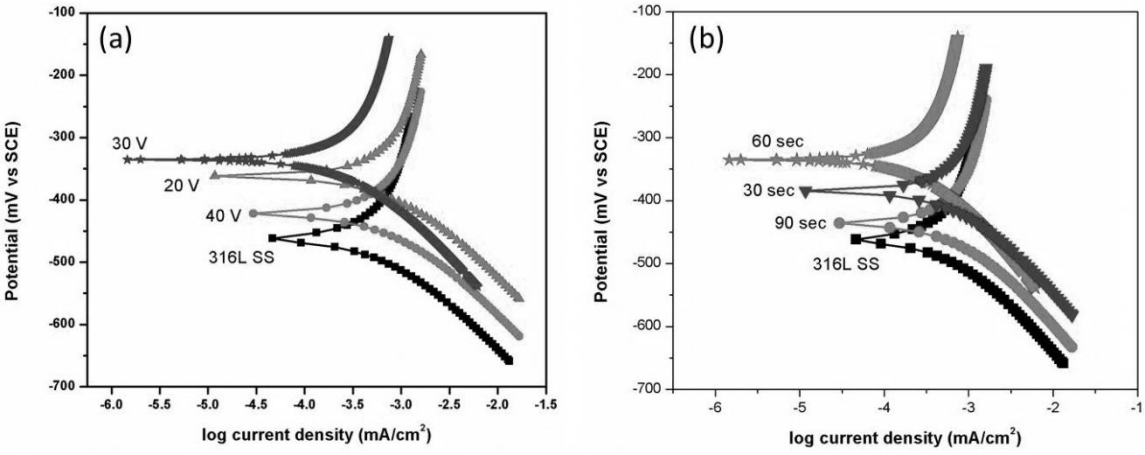

Fig. 2. Potentiodynamic polarization curves

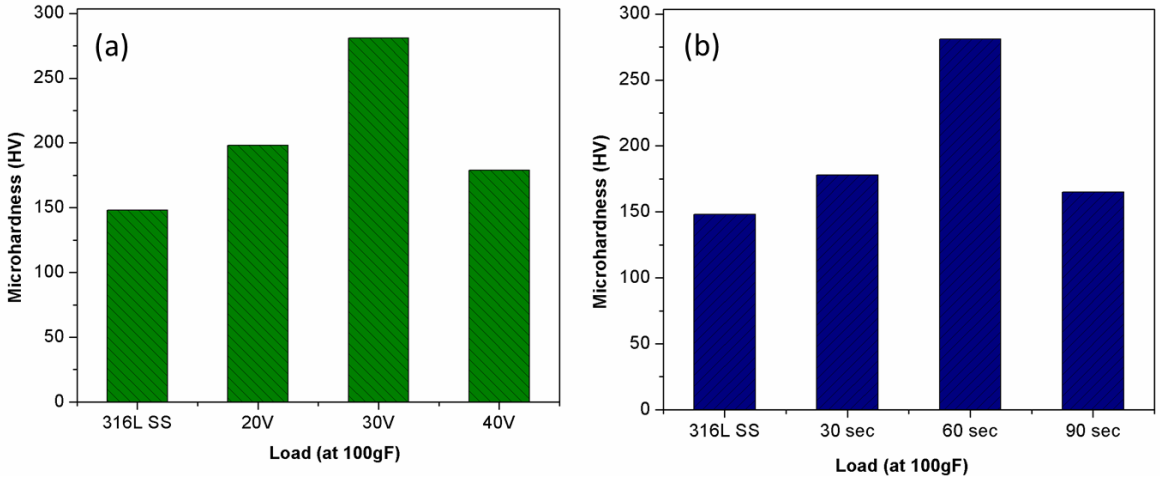

Fig. 3. Vickers microhardness for uncoated and nano biocomposite coated type 316L SS

Fig. 3a shows the Vickers microhardness for uncoated 316L SS and nano biocomposite coated type 316L SS substrates at a coating time of 60 sec with various coating voltages. Fig. 3b shows the Vickers microhardness for uncoated 316L SS and nano biocomposite coated type 316L SS substrates at a coating voltage of 30 V with various coating times. Vickers microhardness test was carried out on nano biocomposite coated type 316L SS after sintering at 700°C in an air furnace. From Fig. 3 it can be observed that coated substrates showed significantly enhanced hardness compared to uncoated 316L SS sample. The higher mechanical strength observed on nano biocomposite coated type 316L SS at 30 V and 60 sec is due to the enhanced adhesion strength of the uniform crack-free coating after sintering. Thus, the coated sample at 30 V and 60 sec was highly suitable for biomedical application.

XRD analysis

Fig. 4 shows the XRD spectra of nano biocomposite coated type 316L SS substrate obtained at 30 V and 60 sec after sintering. The peaks with maximum intensity detected at (002), (210), (211), (300), (202), (310), (222), (213) and (004) reflection planes, were assigned to nano HAP. The obtained results were in good agreement with the JCPDS file card No. 09-0432.

Generally, TiO_2 crystallites are present in three forms: brookite (orthorhombic), anatase (tetragonal), and rutile (tetragonal). Brookite and anatase phases are stable at room temperature and they are transformed to rutile phase at 700°C [20]. The remaining peaks corresponding to rutile nano TiO_2 were observed at (101), (004), (200) and (211) (JCPDS file no.21-1276) [21]. This rutile phase of nanoTiO_2 enhances the bioactivity and cell proliferation when compared to anatase and brookite. No other peak was observed after sintering of nano biocomposite coated type 316L SS substrate. Thus, the XRD spectra confirmed the presence of bioactive nano HAP and bioinert nanoTiO_2 crystalline phases in nano biocomposite coated type 316L SS substrate.

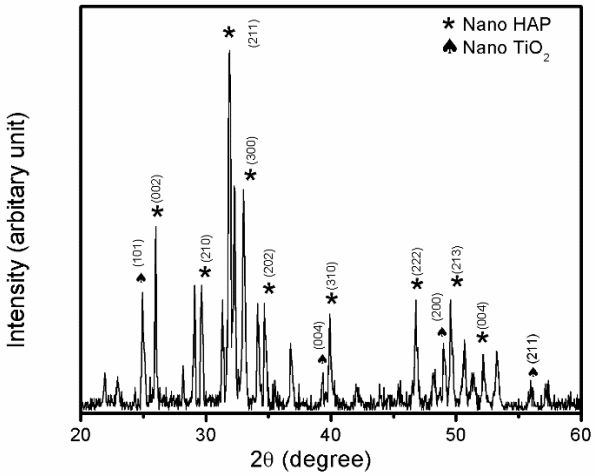

Fig. 4. XRD spectra of nano biocomposite-coated type 316L SS

Surface roughness analysis

Surface profilometer image of nano biocomposite coated type 316L SS substrate obtained at 30 V and 60 sec after sintering is shown in Fig. 5. Overall surface roughness of the coated substrate was recorded using a surface profilometer. The average surface roughness for the nano biocomposite coated substrate was found to be 0.497 ± 0.06 µm. The enhanced surface roughness obtained for the nano biocomposite coated substrate is due to interlocking of the rough porous surface of nano HAP with nano TiO_2 powder. Surface roughness is one of the important characteristics for cell attachment and proliferation.

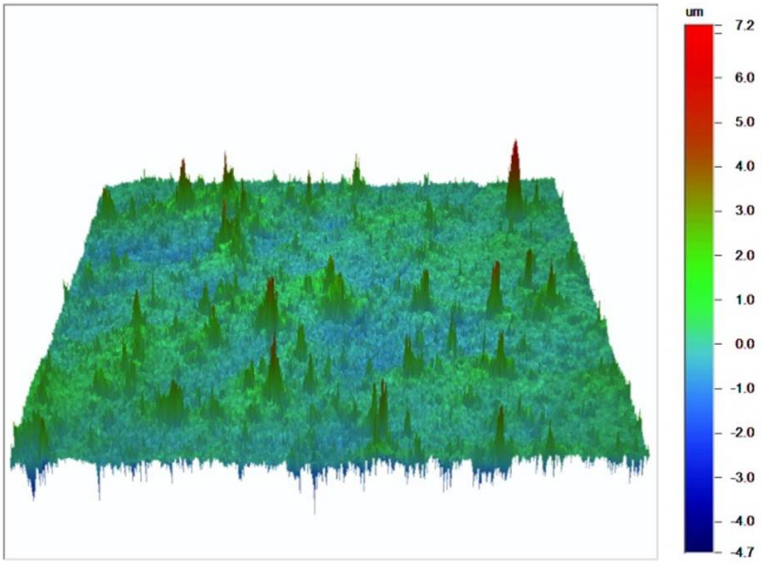

Fig. 5. Surface profilometer image of nano biocomposite coated type 316L SS substrate

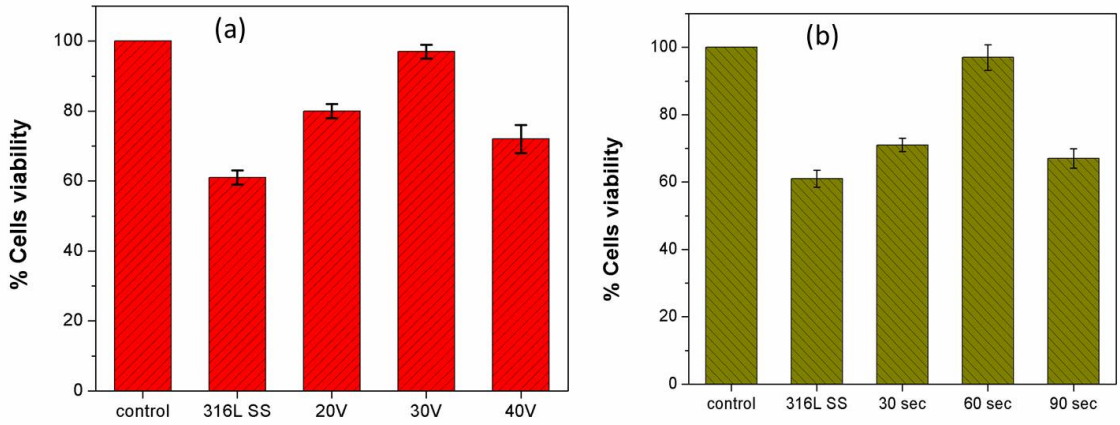

Fig. 6. Cell viability with MC3T3-E1 osteoblast

The stability of the implant can be improved by increasing the surface roughness of the coatings [22]. This can provide a suitable environment for the bone cells to attach on the surface of the implant. Thus, nano biocomposite coated type 316L SS substrate at optimized voltage of 30 V and time of 60 sec is suitable for bone bonding.

Cell culture studies

Surface roughness, corrosion resistance and mechanical property of the coated layer are playing very important roles in cell attachment, proliferation, and diversity of MC3T3-E1 osteoblast cells. In addition to that the greater surface area on the coated substrate can capture more cells [23]. Fig. 6a shows the cell viability of MC3T3-E1 osteoblast cells for uncoated 316L SS and nano biocomposite coated type 316L SS substrates at a coating time of 60 sec with various coating voltages. Fig. 6b shows the cell viability of MC3T3-E1osteoblast cells for uncoated 316L SS and nano biocomposite coated type 316L SS substrates at a coating voltage of 30 V with various coating times. Cell viability was measured using MC3T3-E1 osteoblast cells for uncoated and nano biocomposite coated type 316L SS samples after culturing for 72 h.

The cell viability of the coated substrate was higher than that of the uncoated one. Uncoated substrate easily releases metal ions and affects the cells viability due to non-protected surface. Better performance of the coated substrate was observed when compared with uncoated substrate due to the protective layer of the coating. Crack free coating with a very good protective layer and rougher surface along with superior mechanical strength were achieved at 30 V and 60 sec compared with other coated substrates. It was found that better cell viability (98%) was obtained for the coated type 316L SS substrate at 30 V and 60 sec than for other coated and uncoated substrates. All the above factors lead to improved osseointegration properties of the coated substrate at 30 V and 60 sec.

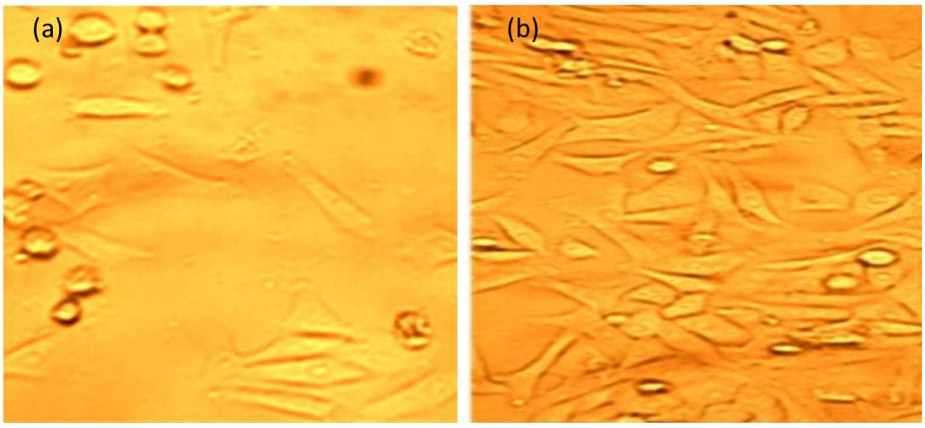

Fig. 7. Histomorphology cell image for nano biocomposite coated type 316L SS

Osteoblast MC3T3-E1 cells exposed to uncoated and coated type 316L SS implants are shown in Fig. 7. The histomorphology cell image for nano biocomposite coated type 316L SS substrate at 30 V and 60 sec is seen. Histomorphology was taken for cell growth using osteoblast MC3T3-E1 cells after 72 h. This histomorphology shows that more cells are present on the coated substrate than on uncoated 316L SS.

The presence of a good number of live cells which proliferate on the coated substrate because bioactive nano HAP is a natural component which is plentifully found in bone matrix, favors osseointegration of cells. The presence of biocompatible nano TiO_2 provides strong adhesion of the bioceramic through the coating on type 316L SS substrate. The number of cells per unit area of the coated substrate increased with surface roughness. Nano biocomposite coating provides uniform crack free coating with strong adhesion and improved corrosion resistance with good surface roughness at 30 V and 60 sec.

Thus, cells which were attached on coated substrate proliferated more actively and covered the entire surface area at the optimized conditions. Thus, higher cell viability and proliferation was achieved on coated type 316L SS substrate at 30 V and 60 sec. Hence, nano biocomposite coated substrate at 30 V and 60 sec could be considered as a better coating to improve the life span of implants in orthopedic applications.

CONCLUSIONS

Nano biocomposite was coated by EPD on type 316L SS substrates using different voltages and coating time spans and was subsequently sintered at 700°C in an air furnace. The electrochemical studies in an SBF solution revealed that coated substrates at 30 V and 60 sec exhibit higher corrosion resistance when compared to other coated and uncoated type 316L SS substrates. The XRD analysis confirms the presence of two bioceramics: nano HAP and nano TiO_2 in the coating. The composite coating at optimized conditions exhibited enhanced microhardness strength. *In vitro* cell culture studies showed that the coated substrate at the optimized conditions facilitated cell viability and enhanced cells proliferation. Hence, nano biocomposite coated type 316L SS substrate at 30 V and 60 sec could improve the life time of implants by enhanced bioactivity and faster bone growth, as well as enhanced corrosion resistance.

REFERENCES

1. M. Geetha, A. K. Singh, R. Asokamani, A. K. Gogia, *Prog. Mater. Sci*., **54 (3),** 397 (2009).
2. I. Gotman, *J. Endourol*., **11(6),** 383 (1997).
3. M. J. Wang, S.C. Chao, S.K. Yen, *Corros. Sci.*, **104 (3)**, 47 (2016).
4. T. Hanawa, *Mater. Sci. Eng. C*, **24 (6),** 745 (2004).
5. M. Niinomi, *Metall. Mater. Trans. A*, **33(3),** 352 (2002).
6. H. Tanigawa, H. Asoh, T. Ohno, M. Kubota, S. Ono, *Corros. Sci.,* **70**, 212 (2013).
7. M. Wang, *Biomaterials*, **24 (13),** 2133 (2003).
8. D. Tadic, F. Peters, M. Epple, *Biomaterials*, **23 (12),** 2553 (2002).
9. X. Li, C. A. Blitterswijk, Q. Feng, F. Cui, F. Watari, *Biomaterials*, **29 (23),** 3306 (2008).
10. X. Li, H. Liu, X. Niu, Y. Fan, Q. Feng, F. Z. Cui, F. Watari, *J. Biomed. Mater. Res.,* **97(1),** 10 (2011).
11. N. Ignjatović, S. Tomić, M. Dakić, M. Miljković, M. Plavšić, D. Uskoković, *Biomaterials*, **20 (9)**, 809 (1999).
12. A. Bigi, E. Boanini, S. Panzavolta, N. Roveri, *Biomacromolecules*, **1(4),** 752 (2000).
13. S. Nagarajan, N. Rajendran, *Appl. Surf. Sci.,* **255 (7),** 3927 (2009).
14. V. Cannillo, L. Lusvarghi, A. Sola, *J. Eur. Ceram. Soc*., **28 (11),** 2161 (2008).
15. Y. Fukada, N. Nagarajan, W. Mekky, Y. Bao, H. S. Kim, P. S. Nicholson, *J. Mater. Sci.,* **39 (3),** 787(2004).
16. L. Besra, M. Liu, *Progr. Mater. Sci.,* **52 (1),** 1 (2007).

17. R. Manonmani, *J. Aust. Ceram. Soc*., (2020), in press.
18. T. Mosmann, *J. Immunol. Methods*, **65 (1),** 55 (1983).
19. B. D. Hahn, J. M. Lee, D. S. Park, J. J. Choi, J. Ryu, W. H. Yoon, H. E. Kim, *Thin Solid Films*, **518 (8),** 2194 (2010).
20. M. S. P. Francisco, V. R. Mastelaro, *Chem. Mater*., **14 (6),** 2514 (2002).
21. Y. F. You, C. H. Xu, S. S. Xu, S. Cao, J. P. Wang, Y. B. Huang, S. Q. Shi, *Ceram. Int.,* **40 (6),** 8659 (2014).
22. R. Manonmani, *J. Iran. Chem. Soc*., (2020), in press.
23. H. Zhang, J. Han, Y. Sun, Y. Huang, M. Zhou, *Mater. Sci. Eng. C*, **56**, 22 (2015).

Bulgarian Chemical Communications, Volume 53, Issue 3 (pp. 321 - 326) 2021 *DOI: 10.34049/bcc.53.3.5368*

Synthesis, characterization and anticancer activity of NiO nanoparticles from a Ni(II) complex derived from chitosan and pyridine derivative

M. S. Al-Fakeh[1,2]

[1]*Department of Chemistry, College of Science, Qassim University, Buraidah 51452, Saudi Arabia*
[2] *Taiz University, Taiz, Republic of Yemen*

Received: December 31 2020; Revised: June 28, 2021

Synthesis of NiO nanoparticles (NPs) by a calcination method is the approach used in this article. Materials utilized were nickel chloride hexahydrate, chitosan (CS) and 2-aminopyridine (2-AMPY) ligands for the preparation of the nickel(II) complex, $[Ni(CS)(2\text{-}AMPY)(H_2O)_3]$. NPs properties were identified by Fourier transform infrared (FTIR) spectroscopy, UV, TG, X-ray powder diffraction and scanning electron microscopy (SEM). The results obtained prove the presence of nickel oxide NPs produced during calcination. Finally, the anti-cancer activity of the nickel oxide NPs was studied. The cytotoxic effectiveness of the NiO NPs was examined in cultured human breast cancer cells. The results of the present study indicate that the NiO NPs could increase the permeability of cancer cell wall.

Keywords: Mixed-ligand complex, NiO nanoparticles, XRD, Anti-cancer activity.

INTRODUCTION

Currently, nanomaterials such as nanoparticles (NPs), nanotubes and nanowires exhibit electronic, magnetic, mechanical, thermal, and catalytic properties, and are used in chemical reduction, photo-reduction, electrochemical reduction, spray pyrolysis, laser and ablation methods [1-5]. Metal oxide nanoparticles (MONPS) preparation and properties constitute a major research field in materials chemistry; mostly relevant is the use of nanoparticles in nanotechnology applications, because metal particles sized in the nanometer scale (1-100 nm) possess specific physical, chemical and biological properties [6-11]. The biological activity of these NPs depends on their stability, concentration and size when added to the microbe's growth medium, so this provides more confinement time for interaction of microbes with nano-particles. Highly ionic nickel oxide NPs may be particularly important antimicrobial, antifungal and anticancer agents as they can be synthesized with extremely high surface areas and unusual crystal shapes [12, 13]. Chitosan (CS), the product of N deacetylation of chitin widely spread in shell fish and cell walls of plants or fungi, is an important renewable natural resource. It is also well-known that chitosan has antifungal activity, biocompatibility and biodegradation due to its chemical and physicalproperties, as well as unusual biological activity, which have been used in food, catalysis, material and pharmaceutical applications [14-17]. Moreover, the complex-forming ability of pyridine and its derivatives with transition metal ions is well-known, 2-aminopyridine acting as a monodentate ligand through its pyridine N-atom [18]. Thus, the chemistry of nickel(II) mononuclear compounds with O- and N-containing groups, especially pyridine ligands, has been widely studied [19, 20]. There are several chemical or mechanical processes developed for synthesizing crystalline metal oxide powders in nanoscale dimensions. The purpose of this work is the synthesis and characterization of a new complex derived from chitosan, a pyridine derivative and nickel(II). The resulting mixed-ligand complex was used as a precursor for preparation of NiO nanoparticles.

EXPERIMENTAL

Material and physical measurements

Chitosan with more than 90% degree of deacetylation and 2-aminopyridine were purchased from Sinopharm chemical reagent Co., Ltd, China and Sigma-Aldrich, respectively. All materials and solvents utilized were commercially available and employed as received without further purification.

The elemental analysis (carbon, hydrogen and nitrogen) was performed using Analyischer Funktionstest Vario El Fab-Nr.11982027 elemental analyzer. For more details of the other physical measurements see [5]. The cytotoxic activity of the synthesized compound was studied at the National Research Center, Cairo, Egypt.

Cytotoxic activity

Materials of the cell lines assay. Cell culture of HCT-116 (human colorectal carcinoma) and MCF-7 (human breast adenocarcinoma) cell lines were purchased from the American Type Culture

*To whom all correspondence should be sent:
E-mail: m.alfakehqu.edu.sa.

© 2021 Bulgarian Academy of Sciences, Union of Chemists in Bulgaria

Collection (Rockville, MD, USA) and maintained in Dulbecco's Modified Eagle Medium (DMEM) which was supplemented with 10% heat-inactivated fetal bovine serum (FBS), 100 U/mL penicillin, and 100 U/mL streptomycin. The cells were grown at 37 ◦C in a humidified atmosphere of 5% CO_2.

MTT cytotoxıc assay. The cytotoxic activities against HCT-116 and MCF-7 human cancer cell lines were estimated using the 3-[4,5-dimethyl-2-thiazolyl)-2,5-diphenyl-2H-tetrazolium bromide (MTT) assay which is based on the reduction of the tetrazolium salt by mitochondrial dehydrogenases in viable cells [21, 22]. Cells were dispensed in a 96-well sterile microplate (1×10^4 cells/well) and incubated at 37 ◦C with a series of different concentrations of each tested compound or doxorubicin (positive control) in DMSO for 48 h in a serum-free medium prior to the MTT assay. After incubation, the media were carefully removed, 40 µL of MTT (2.5 mg/mL) were added to each well and then incubated for additional 4 h. The purple formazan dye crystals were solubilized by the addition of 200 µL of DMSO. The absorbance was measured at 570 nm using a Spectra Max Paradigm Multi-Mode microplate reader. The relative cell viability was expressed as the mean percentage of viable cells compared to the untreated control cells.

Synthesis of [Ni(CS)(2-AMPY)$(H_2O)_3$]$_n$

Chitosan (1 g, 0.5 mmol) was added to 60 ml of distilled water containing 0.4 ml of acetic acid at room temperature and stirred until the chitosan ligand was dissolved. Then 25 ml of $NiCl_2.6H_2O$ (1.47 g, 0.6 mmol) was added into the dissolved chitosan.The solution mixture was then stirred for about 15 min and an ethanolic solution of 2-aminopyridine (0.58 g, 0.5 mmol) was added to the mixture. The solution mixture was heated on a water bath for about 50 min whereupon a light-green precipitate was formed which was filtered and washed with ethanol and dried. Analysis for $C_{11}H_{23}N_3NiO_7$: Theoretical value: C, 35.89; H, 6.31; N, 11.41. Experimental values: C, 34.96; H, 6.22; N, 11.08, melting point 186 °C.

Formation of NiO nanoparticles

By calcining the synthesized complex in air at 450 °C with a calcination time of 4 h NiO nanoparticles were obtained.

RESULTS AND DISCUSSION

The reaction of nickel(II) with chitosan and 2-aminopyridine yields a mixed-ligand complex. This Ni(II) complex is stable in air and insoluble in common organic solvents, but partially soluble in dimethyl sulfoxide (DMSO).

Fourier transform infrared spectroscopy (FT-IR)

Figure 1 shows the FT-IR spectrum of the synthesized Ni(II) complex. The strong and broad band at 3424 cm^{-1} is attributed to OH asymmetrical stretching vibration and amino (NH_2) stretching vibrations; the band at 1418 cm^{-1} is related to $–CH_2$ bending, and the absorption band at 1070 cm^{-1} is due to C-O-C stretching vibration in glucosidic linkage [23]. The FT-IR spectrum of the nickel(II) complex shows at 3434 cm^{-1} –OH, $–NH_2$; at 2928 cm^{-1} and 2862 cm^{-1} –C–H stretching; at 1632 cm^{-1} –C=O, amide; 1460 cm^{-1} ($–CH_2–N$) coupled with 1380 cm^{-1} (–N–H); 1155 cm^{-1} (skeleton C–O and –C–O–C); at 888 cm^{-1} C–O–C bridge, as well as glucosidic linkage. All these vibrational peaks are characteristic for chitosan. On the other hand, for the 2-AMPY, the absorption peaks in the area around 3365 and 3473 cm^{-1} indicate the existence of amino (NH_2) group in the nickel(II) complex [24]. These peaks also indicate that the amino N-atom does not participate in the bonding [25]. 2-Aminopyridine displays two bands at 904 and 1468 cm^{-1} which can be referred to υ(C-N) ring vibrations [26]. Finally, the bands at 576 and 528 cm^{-1} are attributed to (Ni–N–) and that at 425 cm^{-1} to (Ni–O).

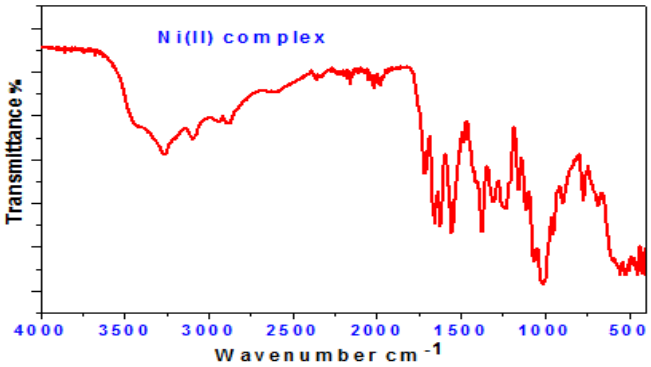

Figure 1. FT-IR spectrum of the Ni(II) complex.

Electronic spectra

Electronic spectra of Ni(II) mixed ligand complex and nickel oxide nanoparticles recorded in the 200-900 nm region in dimethyl sulfoxide (DMSO) solution are shown in Fig. 2. The spectrum of the Ni(II) complex shows two distinct bands at 235 and 434 nm which are referred to (π→π*) and (n→π*) transitions within the 2-ampy and chitosan ligands, respectively [27, 28]. The structure of the nickel complex can be assumed as follows:

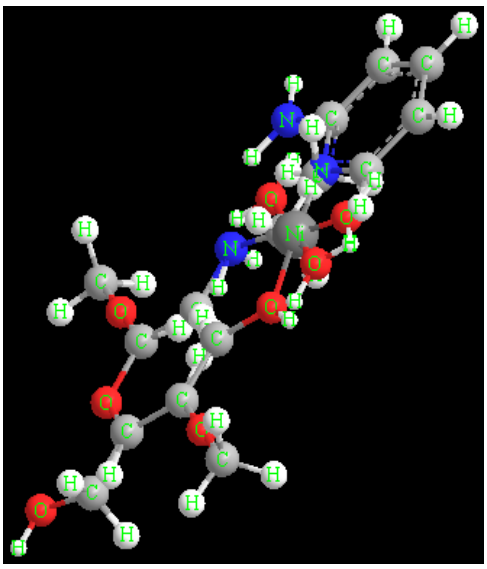

(b)

(a) (c)

Figure 2. (a) Structure of the Ni(II) complex, (b) Estimation view of coordination round Ni(II), (c) DFT (HOMO-LUMO) molecular orbital plots for frontier molecular orbitals of NiO.

Figure 2 (c) shows that the charges being carried by the atoms, cause a dipole moment of 2.9178 debye and total energy of 1575.6 a.u. Fig. 3. displays the UV-vis absorption spectrum of NiO nanoparticles. It is apparent that the spectrum exhibits a band absorption edge at 348 nm [29].

Thermal analysis studies

The thermal decomposition of the nickel(II) compound was inspected from ambient temperature to 650 °C. The thermogram of this complex displays four decomposition steps (Fig. 4), at 28-90, 92-250, 252-390 and 392-650 °C. The first step corresponds to the detachment of the coordinated water (calc. 14.08 %, found 13.87 %). The DTG curve of this step shows a minimum at 56 °C and an endothermic peak at 58 °C in the DTA trace. The mass loss in the second step indicates the release of 2-aminopyridine ligand (calc. 24.50 %, found 24.26 %) (DTG peaks at 225 °C) with a broad exothermic peak in the DTA trace at 227 °C.

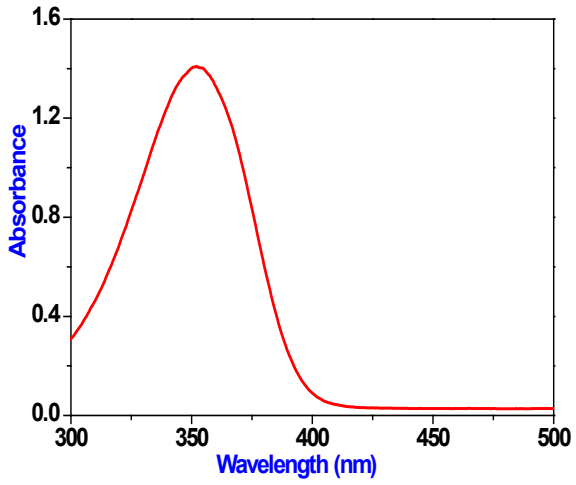

Figure 3. UV-vis absorption spectrum of the NiO nanoparticles.

The third and fourth steps identify the decomposition of the organic ligands (DTG peaks at 350 and 475 °C) with two exothermic peaks in the DTA curve at 352 and 477 °C. The final product was identified as nickel oxide (calc. 19.45 %, found 18.92 %).

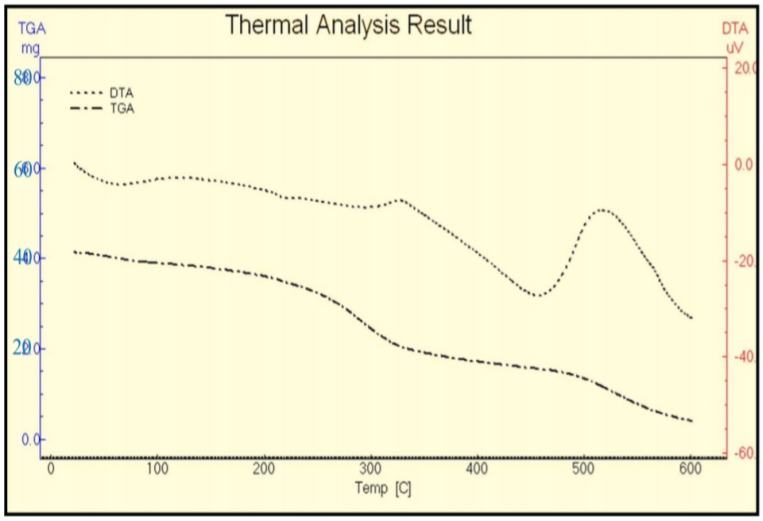

Figure 4. TGA and DTA curves of the Ni(II) complex.

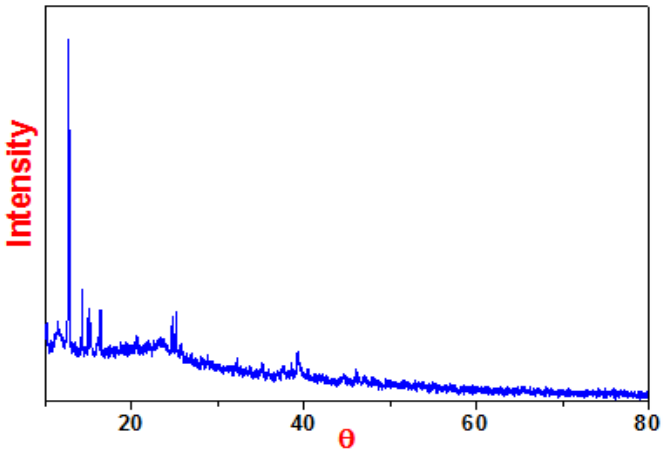

Figure 5. X-ray powder diffraction pattern of the nickel(II) complex.

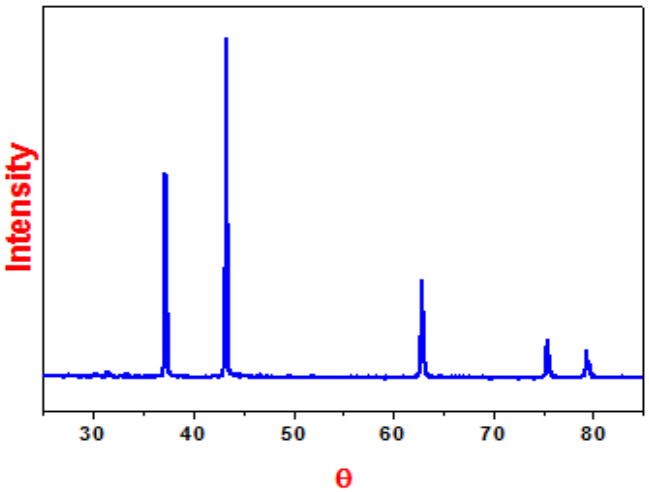

Figure 6. X-ray powder diffraction pattern of the nickel oxide nanoparticles.

Table 1. XRD crystal data of the compounds.

Parameters	Ni(II) compound	NiO
Empirical formula	$C_{11}H_{23}NiN_3O_8$	NiO
Formula weight	384.00	74.68
Crystal system	Triclinic	Hexagonal
a (Å)	8.02	2.95
b (Å)	10.25	2.95
c (Å)	2.74	7.23
α (°)	94.56	90.00
β (°)	99.21	90.00
γ (°)	103.42	120.00
Volume of unit cell (Å^3)	214.83	54.67
Particle size (nm)	156	74

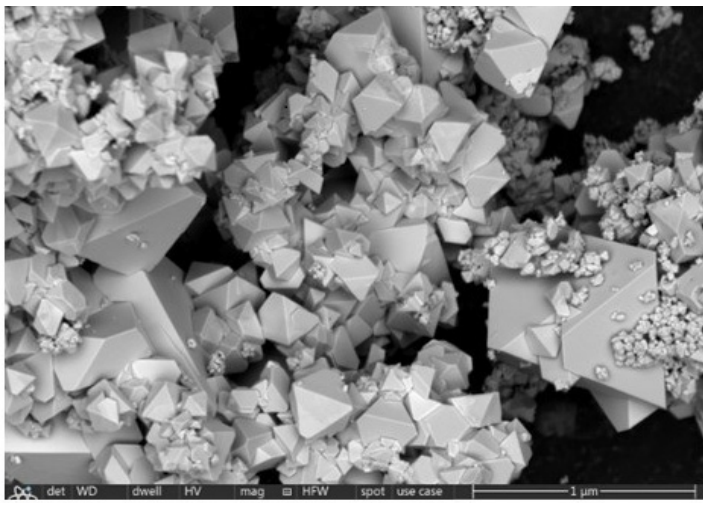

Figure 7. SEM of NiO nanoparticles.

Scanning electron microscopy (SEM)

The scanning electron micrograph of nickel oxide NPs is shown in Fig. 7. SEM is perfect to illustrate the NiO nanoparticles morphology, and clearly shows the formation of NiO nanoparticles in the form of hexagonal groupings.

Cytotoxicity studies

The suggested inducement of intracellular oxidative stress is to be a key event in the toxicity mechanisms of metal oxide nanoparticles (MONPs) such as NiO NPs. The oxide nanoparticles enter inside the cell; this nanomaterial may induce intracellular oxidative stress by annoying the balance between oxidant and antioxidant reactions. On the other hand, the photo-catalysis appears to be the more important anti-cancer mechanism. Reactive oxygen species (ROS) produced on the surface of these nanoparticles in the presence of light cause an oxidative stress in the microbial cell. This eventually leads to the death of the cell. Also the generated NPs can penetrate into the cell membrane and kill the microbes [30]. From the oxidative stress produced by exposure to nanomaterials an increase of the cytosolic Ca^{2+} concentration may be catalyzed or may cause the translocation of transcription factors to the nucleus, which arrange pro-inflammatory genes. Alternatively, overriding oxidative stress may also adjust lipids, proteins and nucleic acids, which further stimulates the anti-oxidant defense system or even leads to cell death [31]. The cytotoxic effect of the NiO NPs was examined on cultured human breast cancer cells by exposing cells for 72 h to the

medium containing the nickel oxide nanoparticles at 5-100 µg/ml concentration. In relation to cell death, a minimum concentration for NiO NPs is well enough to induce it. The micro-organisms carry a negative charge while metal oxides carry a positive charge [32, 33]. This causes electromagnetic attraction between the microbe and the treated surface of nanoparticles. When the metal oxide NPs approach the microbes, the latter oxidize and die immediately. The cytotoxic effect of the NiO nanoparticles at 100 µM on lung adenocarcinoma A549), and prostate cancer (PC3) human tumor cell lines and RPE1 human normal cell line, was 39%, 0% and 41% for A-549, PC3 and RPE1 respectively, compared to doxorubicin taken as 100%. The XRD and SEM demonstrated the decrease in particle size for NiO NPs, which increases the release of Ni^{2+} ions. The more Ni^{2+} ions contact the cell membrane, the higher damage is caused to cancer cell membrane.

CONCLUSIONS

NiO nanopowder was successfully synthesized using nickel chloride hexahydrate and two organic ligands, chitosan (CS) and 2-aminopyridine (2-AMPY) to prepare a Ni(II) complex which was subsequently calcined.

The X-ray pattern shows that all peaks can be well attributed to the phase of NiO. The SEM micrograph manifested that there are some micro-pores between the nanocrystals for the sample calcined at 450 ºC for 4 h. The majority of obtained NiO nanopowders had an average particle size less than 74 nm. The cytotoxic effect of the nickel oxide NPs was examined on cultured human breast cancer cells by exposing cells for 72 h. NiO NPs showed anticancer activity.

REFERENCES

1. O. Długosz, M. Banach, *Colloids and Surfaces A: Physicochemical and Engineering Aspects,* **5 (**12), 606 (2020).
2. M. C. Higgins, S. Ghobadi, J.V. Rojas, C. E. Castano, *Applied Surface Science,* **12 (**4), 146313 (2020).
3. Q. Li, L.-S. Wang, B.-Y. Hu, C. Yang, L. Zhou, L. Zhang, *Materials Letters*, **61 (**8-9), 1615 (2007).
4. X. Xin, Z. Lu, B. Zhou, *Journal of Alloys and Compounds*, **427(**1-2), 251 (2007).
5. M. S. Al-Fakeh, F. M. Alminderej, *International Journal of ChemTech Research,* **11**(5), 442 (2018).
6. Y. Wu, Y. He, T. Wu, T. Chen, W. Weng, H. Wan, *Materials Letters*, **61 (**14-15), 3174 (2007).
7. N. Acacia, F. Barreca, E. Barletta, D. Spadaro, G. Currò, F. Neri, *Appl. Surf. Sci.,* **256,** 6918 (2010).
8. Y. B. M. Mahaleh, S. K. Sadrnezhaad, D. Hosseini, *Journal of Nanomaterials*, **1-4** (2008).
9. A. Aslania, V. Oroojpour, M. Fallahi, *Appl. Surf. Sci.,* **257,** 4056(2011).
10. Kh. S. Khashan, Gh. M. Sulaiman, F. A. K. A. Ameer, and G. Napolitano, *Pak. J. Pharm. Sci*., **29 (**2), 541 (2016).
11. M. A. Gondal, T. A. Saleh, Q. A. Drmosh, *Appl. Surf. Sci.,* **258,** 6982 (2012).
12. J. Hrenovic, J. Milenkovic, N. Daneu, R. M. Kepcija, N. Rajic, *Chemosphere*, **88**, 1103 (2012).
13. A. Azam, A. S. Ahmed, M. Oves, M.S. Khan, A. Memic, *Int. J. Nanomed*., **7,** 3527 (2012).1
14. T. F. Jiao, J. Zh, J. X. Zhou, L. H. Gao, Y. Y. Xing, X. H. Li, *Iranian Polymer Journal*, **20** (2), 123 (2011).
15. K. S. V. Krishna Rao, K. Madhusudana Rao, P. V. Nagendra Kumar, I.-D. Chung, *Iranian Polym. J.*, **19**, 265 (2010).
16. E. Ispir, *Dyes Pigments*, **82**, 13 (2009).
17. N. Velmurugan, G. G. Kumar, S. S. Han, K. S. Nahm, Y. S. Lee, *Iran Polym. J.*, **18**, 383 (2009).
18. B. Dojer, A. Pevec, P. Šegedin, *Inorg. Chim. Acta,* **363**, 1343 (2010).
19. L. Li, F. Yuan, *Synth. React. Inorg., Metal-Org., Nano-Metal Chem*., **42**, 205 (2012).
20. C. Yenikaya, M. Poyraz, M. Sarı, F. Demirci, H. Ilkimen, O. Büyükgüngör, *Polyhedron* **28**, 3526 (2009).
21. A. N. Emam, S. A. Loutfy, A. A. Mostafa, H. M. Awad, M. B. Mohamed, *RSC Adv*., **7**, 23502 (2017).
22. A. K. E. El-Ansary, N. A. Mohamed, Kh. O Mohamed, H. M. W. Abd-Elfattah, M. El-Manawaty, *Research Journal of Pharmaceutical, Biological and Chemical Sciences*, **6 (**4), 1745 (2015).
23. M. R. Kasaai, *Carbohydr. Polym*., **71**, 497 (2008).
24. E. R. Welsh, C. L. Schauer, S. B. Qadri, R. R. Price, *Biomacromolecules***, 3**, 1370 (2002).
25. C. Yenikaya, M. Poyraz, M. Sarı, F. Demirci, H. Ilkimen, O. Büyükgüngör, *Polyhedron,* **28**, 3526 (2009).
26. J. Kim, D. Kim, B. Veriansyah, J. W. Kang, J. D. Kim, *Mater. Lett*., **63**, 1880 (2009).
27. D. L Wilson, D. R Wirz, G. H. Schenk, *Anal. Chem*., **45**, 1447 (1973).
28. O. J. Olaniyan, E. O. Dare, O. R. Adetunji, O. O. Adedeji, Sh. O. Ogungbesan, *Nano Hybrids and Composites,* **11**, 22 (2016).
29. M. El-Kemary, N. Nagy, I. El-Mehasseb, *Materials Science in Semiconductor Processing,* **16**, 1747 (2013).
30. M. Fang, J. H. Chen, X. L. Xu, P. H. Yang, H. F. Hildebrand, *International Journal of Antimicrobial Agents*, **27**(6), 513 (2006).
31. C. Karunakaran, P. Gomathisankar, G. Manikandan, *Materials Chemistry and Physics,* **123**(2), 585 (2010).
32. L. Umaralikhana, M. J. M. Jaffar, *Journal of Advanced Applied Scientific Research*, **1-4** (8), 24 (2016).
33. P. Hosseinkhani, A. M. Zand, S. Imani, M. Rezayi, S. R. Zarchi, *International Journal of Nano Dimension*, **1**(4), 279 (2011).

Bulgarian Chemical Communications, Volume 53, Issue 3 (pp. 327 - 342) 2021 *DOI: 10.34049/bcc.53.3.5375*

Geometrical optimization, PASS prediction, molecular docking, and *in silico* ADMET studies of thymidine derivatives against FimH adhesin of *Escherichia coli*

M. Anowar Hosen[1], A. Alam[1], M. Islam[1], Y. Fujii[2], Y. Ozeki[3], S. M. Abe Kawsar[1*]

[1] *Department of Chemistry, Faculty of Science, University of Chittagong, Chittagong-4331, Bangladesh*
[2] *School of Pharmaceutical Sciences, Nagasaki International University, 2825-7, Huis Ten Bosch-cho, Sasebo, Nagasaki 859-3298, Japan*
[3] *School of Sciences, Yokohama City University, 22-2, Seto, Kanazawa-ku, Yokohama 236-0027, Japan*

Received: January 22, 2021; Revised: July 28, 2021

Thymidine-containing derivatives are some of the most exigent analogs of drug molecules. In this investigation, several 5′-*O*-acyl thymidine derivatives (2–11) having different aliphatic and aromatic groups were employed for optimization, molecular docking, biological prediction, and physicochemical studies. Density functional theory (DFT) with B3LYP/3-21G was employed to demonstrate their thermochemical, atomic partial charge (APC), and molecular electrostatic potential (MEP) properties. Prediction of activity spectra for substances (PASS) revealed promising antibacterial, antiviral, and anti-carcinogenic activities of these thymidine derivatives compared to their antifungal activities. In support of this observation, their cytotoxic prediction and molecular docking studies were performed against FimH adhesin of *Escherichia coli* (PDB: 1TR7). The molecular docking studies exhibited that most of the molecules could bind to the near crucial catalytic binding site, Tyr48, Ile13, Ile52, Phe1, and Tyr137 of the lectin adhesin FimH, and the molecules were surrounded by other active site residues like Gln133, Asp47, Asn46, Asp54, Asn135, Asp140, and Ala6. Besides, these partially acylated thymidine derivatives were analyzed for their pharmacokinetic properties which revealed that the combination of *in silico* ADMET prediction and drug-likeness showed a promising pharmacokinetic profile. Overall, the present study might be useful for the development of thymidine-based potential antimicrobial drugs.

Keywords: Thymidine; adhesin FimH; MEP; PASS; ADMET; DFT

Abbreviations: DFT: density functional theory; ADMET: absorption, distribution, metabolism, elimination, toxicity, QM: quantum mechanical; LYP: Lee, Yang and Parr's; MEP: molecular electrostatic potential; PASS: prediction of activity spectra for substances.

INTRODUCTION

Nucleoside antibiotics have been under investigation for many years [1]. Some of the most clinically effective antiviral agents currently in use are purine or pyrimidine nucleoside analogs [2]. Thymidine, structurally known as deoxythymidine (Figure 1) is a pyrimidine-based nucleoside that constitutes a major part of one of the four nucleosides in DNA and is listed as a chemical teratogen [3]. Modification of hydroxyl (-OH) group at 3′ and 5′ position improves the antimicrobial activity of thymidine derivatives and brings about some potential antimicrobial agents [4-6]. As a result of screening synthetic compounds for potential antimicrobial activity, a study reported that azidothymidine (AZT) has potent bactericidal *in vitro* activity against various members of the family Enterobacteriaceae [7]. Azidothymidine (AZT) is one of the most popular thymidine derivatives (antiviral drug) in which 3′-hydroxyl (-OH) was modified by an azide group and is now used worldwide for the treatment of HIV infection [8]. AZT suppresses the mode of reverse transcription, a ticklish phase in the life cycle of a virus. Edoxudine is another thymidine-derived antiviral drug, strongly working against the herpes simplex virus [3]. Moreover, thymidine is used in cell biology to synchronize cells. Thymidine analog bromodeoxyuridine is often used for the detection of proliferating cells in living tissues. Thymidine is also catabolized to identify TP-expressing tumor xenografts [9]. Furthermore, after alteration of hydroxyl (-OH) group in nucleoside derivatives uridine and cytidine also have potential antimicrobial activity [10-17].

Antagonists of the *Escherichia coli* type-1 fimbrial adhesin FimH are recognized as attractive alternatives for antibiotic therapies and prophylaxes against acute and recurrent bacterial infections. Pyrimidine nucleosides are influential antimicrobial agents that act as a specific inhibitor of the dihydrofolate reductase of bacteria. Some recent computational studies reported that modified thymidine derivatives are also possessing significant thermodynamic stability and pharmacological properties [18]. Pathogenic *E. coli* adheres *via* the FimH adhesin at the tip of their

*To whom all correspondence should be sent:
E-mail: akawsarabe@yahoo.com

© 2021 Bulgarian Academy of Sciences, Union of Chemists in Bulgaria

type-1 fimbriae to mannosylated glycan receptors on epithelial linings [19, 20]. The use of mannose-based anti-adhesives for the selective inhibition of type 1-pilus mediated bacterial adhesion has attracted great interest for the non-antibiotic treatment of urinary tract [19, 21] and intestinal [20, 22, 23] infections caused by pathogenic *E. coli*. These bacteria can express an arsenal of multiple adhesins, lectins with a variable immunoglobulin fold, for their attachment to and colonization of host cells.

Computational chemistry is a popular tool to predict the physicochemical, and biological properties of synthesized chemicals [24-28]. In this context, the potent antimicrobial efficacy of several thymidine derivatives 2–11 (Table 1) with various aliphatic and aromatic chains was investigated by molecular docking against lectin FimH of *Escherichia coli* (PDB: 1TR7) along with the prediction of activity spectra for substances (PASS). In addition, attempts were taken to optimize the acylated thymidine derivatives to predict their physicochemical and thermochemical behavior based on DFT (B3LYP/3-21G) approach with cytotoxicity. Finally, designed thymidine derivatives were analyzed for their pharmacokinetic properties which revealed that the combination of *in silico* ADMET prediction, and drug-likeness calculation gave a promising pharmacokinetic profile. Hence, this research work scintillates on the development of antimicrobial lead molecules from thymidine derivatives against lectin FimH *in silico* tools and studies their pharmacokinetic and toxicity properties.

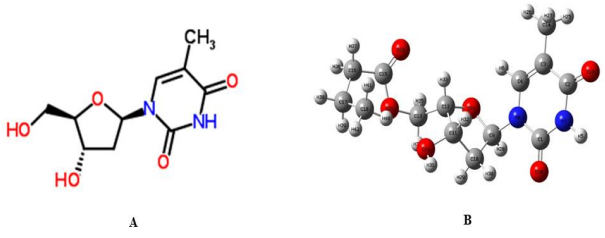

Figure 1. Chemical structure (**A**) and optimized molecular structure (**B**) of thymidine.

EXPERIMENTAL

Materials and methods

Molecular docking has become an increasingly important tool for drug discovery to predict drug interactions with receptor proteins. The blind docking method demonstrates a search throughout the whole surface of the protein molecule for binding sites. The following software was used in the present study: i) Gaussian 09, ii) AutoDock 4.2.6, iii) Swiss-Pdb 4.1.0, iv) Python 3.8.2, v) Discovery Studio 3.5, vi) PyMOL 2.3, and vii) LigPlot þ v.2.2.

Computational Details

Optimization of thymidine derivatives by DFT

In computational drug design study, quantum mechanical (QM) methods have gained attention on the calculation of thermodynamic properties, molecular orbital features, dipole moment, as well as interpretation of different types of interactions [29]. Molecular geometry optimization and further modification of all thymidine derivatives were carried out using the Gaussian 09 program [29]. Density functional theory (DFT) with Beck's (B) [30] three-parameter hybrid model, Lee, Yang, and Parr's (LYP) [31] correlation functional under 3-21G basis set was employed to optimize and predict their thermochemical properties. Molecular weight, heat capacity, entropy, free energy, atomic partial charge, and molecular electrostatic potential were calculated for all the derivatives.

PASS prediction

Web-based prediction of activity spectra for substances (PASS) (http://www.pharmaexpert.ru/PASSonline/index.php) was employed for the prediction of the biological spectrum of these thymidine esters [32]. Firstly, structures of the thymidine derivatives were drawn and converted into their smiles formats by using SwissADME free web tools (http://www.swissadme.ch), which were used to predict the biological spectrum using PASS online software. This program is designed to anticipate more than 4000 forms of biological activity including drug and non-drug actions and can be used to identify the most probable targets with 90% accuracy. PASS results are expressed as Pa (probability for active compound) and Pi (probability for inactive compound). Having probabilities, the Pa and Pi values vary from 0.000 to 1.000, and in general, $Pa + Pi \neq 1$, since these probabilities are calculated freely. The activities with $Pa > Pi$ are only considered as possible for a particular drug. The PASS prediction results were interpreted and used flexibly, *viz*. (i) when $Pa > 0.7$, the chance to find the activity experimentally is high, (ii) if $0.5 < Pa < 0.7$, the possibility to search the activity experimentally is low, but the compound is probably not so similar to known pharmaceutical agents, and (iii) if $Pa < 0.5$, the feasibility to find the activity experimentally is lower, but with a chance to find a structurally similar pharmaceutical agent. So, the prediction of

the activity of the spectrum of a drug is known as its intrinsic property.

Protein preparation and visualization

The 3D crystal structure of lectin FimH of *Escherichia coli* (PDB: 1TR7) was retrieved in pdb format from the protein data bank [33]. All hetero atoms and water molecules were removed using PyMol (version 1.3) software packages [34]. Swiss-Pdb viewer software (version 4.1.0) was employed for energy minimization of the protein [35]. Then optimized thymidine ligands were subjected to molecular docking study against *E. coli* (1TR7) (Figure 2). In fine, molecular docking simulation was rendered by PyRx software (version 0.8) [36] considering the protein as a macromolecule and the drug as a ligand. AutodockVina was employed for docking analysis, and AutoDock Tools (ADT) of the MGL software package was used to convert pdb into pdbqt format to input protein and ligands. The size of the grid box in AutoDockVina was kept at 46.9741, 34.6094, and 41.4160 Å for X, Y, Z directions, respectively. After the completion of docking, both the macromolecule and ligand structures were saved in pdbqt format needed by Accelrys Discovery Studio (version 4.1) to explore and visualize the docking result and search the nonbonding interactions between ligands and amino acid residues of receptor protein [37]. *In vitro*, FimH tends to form amyloid-like aggregates at pH 3, but neither at pH 5, nor 7. Since 1TR7 has its crystal structure in a state that represents the pharmacological target for the development of new drugs, it was selected for computational studies. The validation was checked by PROCHECK online server and it gave 98.08 overall quality factors in ERRAT (http://www.ncbi.nlm.nih.gov/entrez/query.fcgi?cmd=Retrieve&db=PubMed&list_uids=8401235&dopt=Abstract), 96.23% score in VERIFY 3D (https://www.ncbi.nlm.nih.gov/pubmed/1853201?dopt=Abstract). PDBsum online server was also used to check the validation of the main protease receptor with Ramachandran plot (Figure 3) which revealed that 88.07% residues were in the allowed region and no residues were missed.

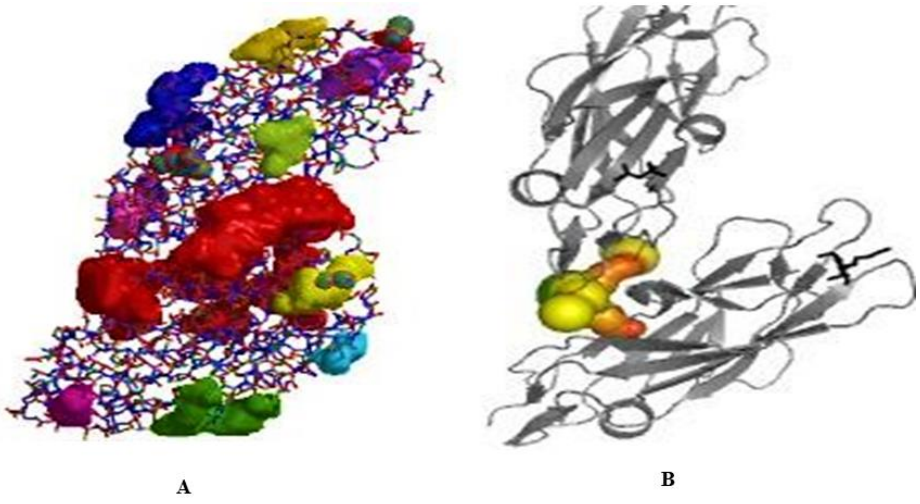

Figure 2. Binding pocket (A) and crystal structure (B) of 1TR7.

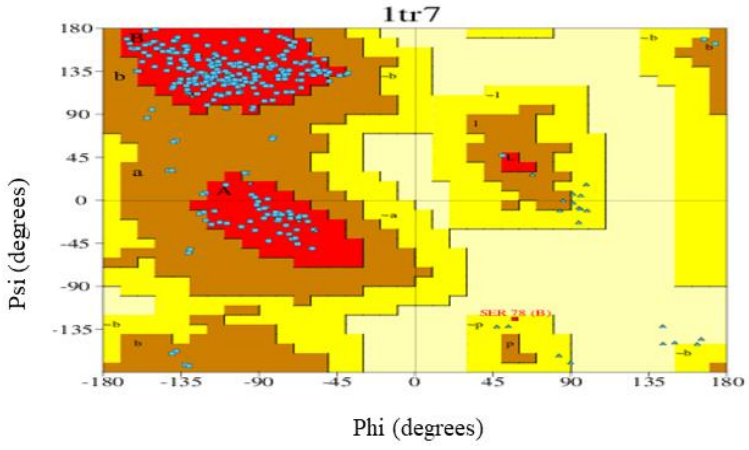

Figure 3. Ramachandran plot for lectin FimH 1TR7.

Docking validation protocol

The docking validation was performed by extracting the co-crystallized ligand (DEG - butyl α-D-mannopyranoside) of the lectin FimH (PDB: 1TR7) and re-docking it into the same position. The lowest energy pose obtained on re-docking and the co-crystallized ligands were superimposed using PyMOL 2.3, and its root means square deviation (RMSD) was calculated between these two superimposed ligands. To validate the docking process, the RMSD must be within a reliable range of 2 Å [38, 39]. It was done to enhance ligand enrichment, which is necessary to test the docking procedure.

In silico pharmacokinetics ADMET and drug-like parameters prediction

To point out potential drug molecules, the ADMET properties were determined for the preliminary prediction of the pharmacokinetic, physicochemical, and drug-like properties in the drug discovery process. *In silico* study suggests an indication to the accession of pharmacokinetic parameters (adsorption, distribution, metabolism, excretion, and toxicity, ADMET) [40], its absorption in the human intestine, percolation of the blood-brain barrier and the central nervous system. The metabolism indicates the chemical biotransformation of a drug by the body, total clearance of drugs and the toxicity levels of the molecules. The drug-likeliness of a molecule is expressed by Lipinski's rule of five parameters (molecular weight <500 Da, no more than 5 hydrogen bond donors, hydrogen bond acceptors should be less than 10 and log P should not be greater than 5). Lipinski's rule of five properties was obtained from the SwissADME server (www.swissadme.ch/index.php) [41]. Prediction of the drug-likeness of the designed thymidine derivatives was also assessed by rule-based filters from Lipinski, Ghose, Veber, and Egan, and the synthetic accessibility difficulty scale was 1–10.

RESULTS AND DISCUSSION

Designed and optimized thymidine derivatives

In the present study, ten thymidine derivatives were modified with different aliphatic and aromatic chains (2–11) (Table 1) and were subjected to a quantum chemical study to realize the mode of their thermochemical properties. Initially, partially acylated derivatives were predicted for biological activities using the PASS program. The observed activities were then rationalized by calculating their physicochemical (DFT method), cytotoxicity (predicted), molecular docking, and with the combination *in silico* ADMET and drug-likeness properties.

Table 1. List of thymidine derivatives 2-11.

Entry	Name of the compound	Acyl groups
1	Thymidine	--
2	5′-*O*-Propionylthymidine	CH_3CH_2CO-
3	5′-*O*-Butyrylthymidine	$CH_3(CH_2)_2CO$-
4	5′-*O*-Hexanoylthymidine	$CH_3(CH_2)_4CO$-
5	5′-*O*-Nonanoylthymidine	$CH_3(CH_2)_7CO$-
6	5′-*O*-Lauroylthymidine	$CH_3(CH_2)_{10}CO$-
7	5′-*O*-Palmitoylthymidine	$CH_3(CH_2)_{14}CO$-
8	5′-*O*-Stearoylthymidine	$CH_3(CH_2)_{16}CO$-
9	5′-*O*-4-Chlorobenzoylthymidine	4-Cl.C_6H_4CO-
10	5′-*O*-3-Bromobenzoylthymidine	3-Br.C_6H_4CO-
11	5′-*O*-Tritylthymidine	$(C_6H_5)_3C$-

Thermochemical study

The spontaneous reaction and stability of a product was elucidated from the free energy and enthalpy values [42]. Highly negative values were more significant for thermal stability. In a quantum chemical study, dipole moment influences non-bonded interactions of hydrogen bond formation smoothly. The binding property can also be improved by increasing of the dipole moment [43]. Free energy (G) is another important factor to display the interaction of binding partners, where a negative value is favorable for spontaneous binding and interaction. Greater negative values reveal better thermodynamic properties. Presences of a bulky acylating group suggesting the possible improvement of free energies are presented in Table 2. In this study, all thymidine derivatives possess a greater negative value for free energy than the parent thymidine, and hence, indicated that the insertion of the acyl group could improve interaction and binding of these molecules with different microbial enzymes. Due to these higher values (–1670.229 to –3774.042 Hartree), halobenzoyl derivatives 9–11 exhibited a better score against *E. coli*. Furthermore, the increased negative values of derivatives 2–8 suggested that these derivatives were thermodynamically more stable.

Table 2. Stoichiometry, molecular weight, heat capacity, entropy, and total free energy of thymidine derivatives.

Entry	Stoichiometry	Formula weight (g/mol)	Heat capacity (cal/mol-kelvin)	Entropy (cal/mol-kelvin)	Total free energy (Hartree)
1	$C_{10}H_{14}N_2O_5$	242.230	59.701	125.981	-870.318
2	$C_{13}H_{18}N_2O_6$	298.291	74.723	144.447	-1061.254
3	$C_{14}H_{20}N_2O_6$	312.120	80.664	156.868	-1100.352
4	$C_{16}H_{24}N_2O_6$	340.371	90.173	169.613	-1178.554
5	$C_{19}H_{30}N_2O_6$	382.451	104.181	182.114	-1295.853
6	$C_{22}H_{36}N_2O_6$	424.530	118.450	213.440	-1413.161
7	$C_{26}H_{44}N_2O_6$	480.585	136.963	240.043	-1569.554
8	$C_{28}H_{48}N_2O_6$	508.693	146.185	246.456	-1647.774
9	$C_{17}H_{17}N_2O_6Cl$	380.780	88.157	168.941	-1670.229
10	$C_{17}H_{17}N_2O_6Br$	425.231	87.893	171.081	-3774.042
11	$C_{29}H_{28}N_2O_5$	484.540	119.760	200.099	-1598.771

Table 3. Predicted biological activities of the thymidine derivatives using PASS software.

Entry	Biological activity							
	Antibacterial		Antifungal		Antiviral		Anti-carcinogenic	
	Pa	Pi	Pa	Pi	Pa	Pi	Pa	Pi
1	0.432	0.024	0.240	0.112	0.806	0.004	0.806	0.005
2	0.463	0.078	0.292	0.084	0.744	0.004	0.797	0.005
3	0.413	0.027	0.300	0.081	0.737	0.004	0.829	0.004
4	0.515	0.027	0.319	0.074	0.724	0.004	0.830	0.004
5	0.515	0.027	0.319	0.074	0.724	0.004	0.830	0.004
6	0.515	0.027	0.319	0.074	0.724	0.004	0.830	0.004
7	0.515	0.027	0.319	0.074	0.724	0.004	0.830	0.004
8	0.515	0.027	0.319	0.074	0.724	0.004	0.830	0.004
9	0.360	0.040	0.258	0.102	0.657	0.005	0.622	0.012
10	0.385	0.034	0.262	0.100	0.648	0.005	0.510	0.018
11	0.348	0.084	0.762	0.011	0.776	0.004	0.659	0.010

Another remarkable change observed was that with the increase of molecular weight, heat capacity, entropy, and free energy sharply increased for compounds 2 to 8 which have a long acyl chain. But fluctuations were found for the aromatic ring-containing derivatives 9–11. In fine, all of these properties may contribute to show higher chemical activity in the drug-related chemical and biochemical fields.

Computational evaluation of antimicrobial activities: PASS

The PASS results were designated as Pa and Pi which are presented in Table 3. It was manifest from prediction Table 3, that thymidine derivatives 2–11 showed $0.34 < Pa < 0.51$ for antibacterial, $0.29 < Pa < 0.76$ for antifungal, $0.64 < Pa < 0.80$ for antiviral and $0.51 < Pa < 0.83$ for anti-carcinogenic activity. This expressly revealed that these molecules were more prone to viruses and bacteria as compared to fungal pathogens. However, attachment of additional aliphatic acyl chains (C-2 to C-18, compounds 2–8) increased the antibacterial activity (Pa ¼ 0.515) compared to thymidine (1, Pa ¼ 0.432), whereas attachment of chloro- and bromo-substituted benzoyl groups did not lead to reasonable improvement (derivatives 9–11). The same scenario was observed for the antiviral activity where acyl chain derivatives 2–8 revealed improved values than the halo-benzoyl derivatives 9 and 10. But compound 11 which has the tri-phenyl group exhibited the highest antiviral activity (Pa ¼ 0.776). We have also predicted the anti-carcinogenic property of these derivatives. Thus, PASS predication exhibited $0.51 < Pa < 0.83$ for anti-carcinogenic activity which indicated that the thymidine derivatives were more potent as anti-carcinogenic agents than previous antimicrobial agents. Significantly, antibacterial, antiviral, and anti-carcinogenic properties of thymidine derivatives with saturated acyl chains (2–8) were found to be more promising than those of halobenzoyl and tri-phenyl derivatives (9–11) [44].

Atomic partial charge

The polarity of chemical bonds often indicates the structures and reactivity [45]. The dipole moment is just a vector, but it does not give the polarity of the molecule. Several methods have been suggested for assigning partial charges to the atoms of a molecule, including both quantum chemical and empirical schemes. Two different methods (Mulliken and NBO) have been utilized to

compute the partial charges of all drug atoms including both quantum chemical and empirical schemes [46]. They are the most recognized population analysis methods and have a significant contribution to the application of quantum chemical calculations to a molecular system because dipole moment and molecular polarizability are also related to atomic charges [47]. Here, all the hydrogen atoms showed a positive charge in both methods, and other electronegative atoms (N and O) negative charge in both methods as expected (Figure 4).

Derivative 6, (C-1 and C-15) showed a greater positive charge due to the presence of highly electronegative oxygen (O-27, O-29, and O-31), nitrogen (N-7) atoms, and H-5 exhibited a higher positive value than another hydrogen because of the oxygen atom of the hydroxyl (-OH) group. Similarly, derivatives **7** (C-1, C-25, and C-40), 8 (C-1, C-24 and, C-36), and 9, 10 (C-6 and C-13) displayed a positive charge in both methods due to the presence of oxygen atom of the carbonyl group and halogen atom (Br) in the aromatic ring.

Molecular electrostatic potential (MEP)

Molecular electrostatic potential (MEP) is globally preferred as a map of reactivity that reveals the most suitable region for organic molecules to perform electrophilic and nucleophilic reactions of charged point-like reagents [48]. It helps to explore the biological recognition process and hydrogen bonding interaction [49]. MEP counter map provides a simple way to predict how different geometry could interact. The MEP of the title compound was obtained based on the B3LYP with basis set 3-21G optimized result and is shown in Figure 5. The MEP is very useful in the study of molecular structure with physicochemical features relationship [50]. MEP was calculated to determine the reactive sites for electrophilic and nucleophilic attacks of the optimized structure of thymidine 1 and its derivatives 2, 4, and 7. The different colors of the electrostatic potential indicate different values. The potentiality of the attacking zone decreases in the sequence: blue > green > yellow > orange > red. The maximum negative area is displayed by red color where electrophiles can easily attack and the maximum positive area is indicated by blue color which is suitable for nucleophilic attack. Moreover, the green color showed zero potential zones.

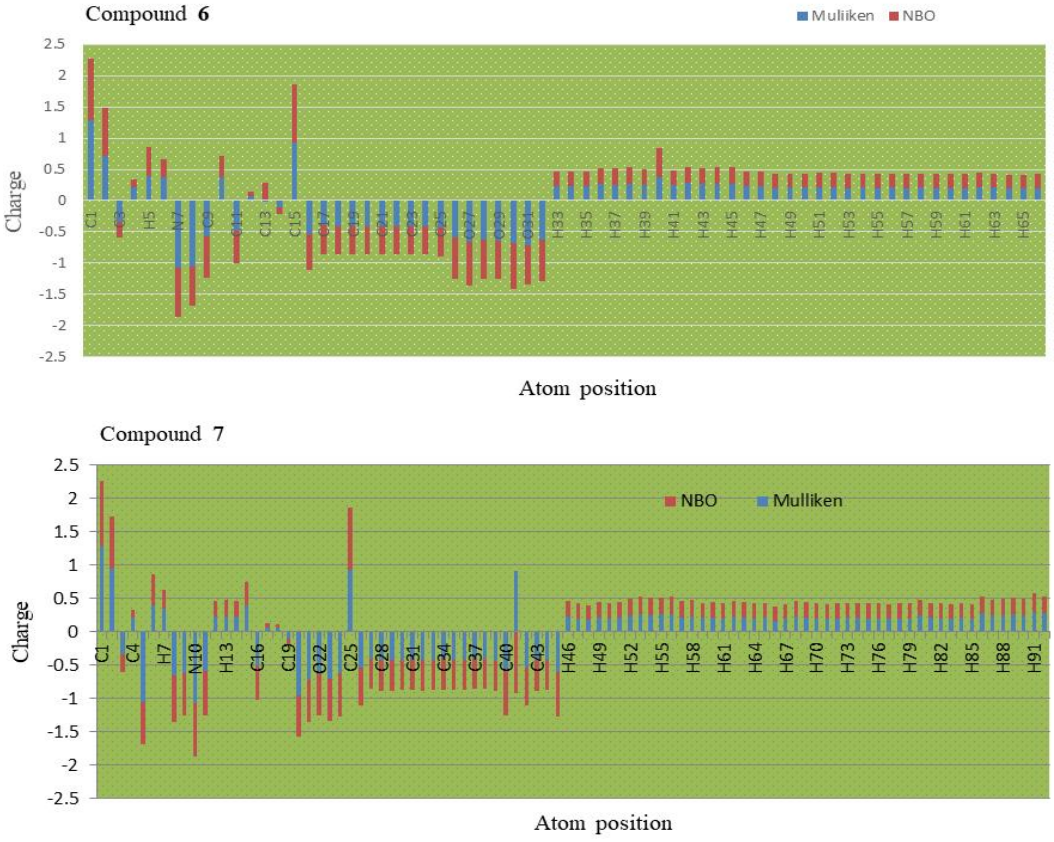

Figure 4. Atomic partial charges of compounds 6 and 7.

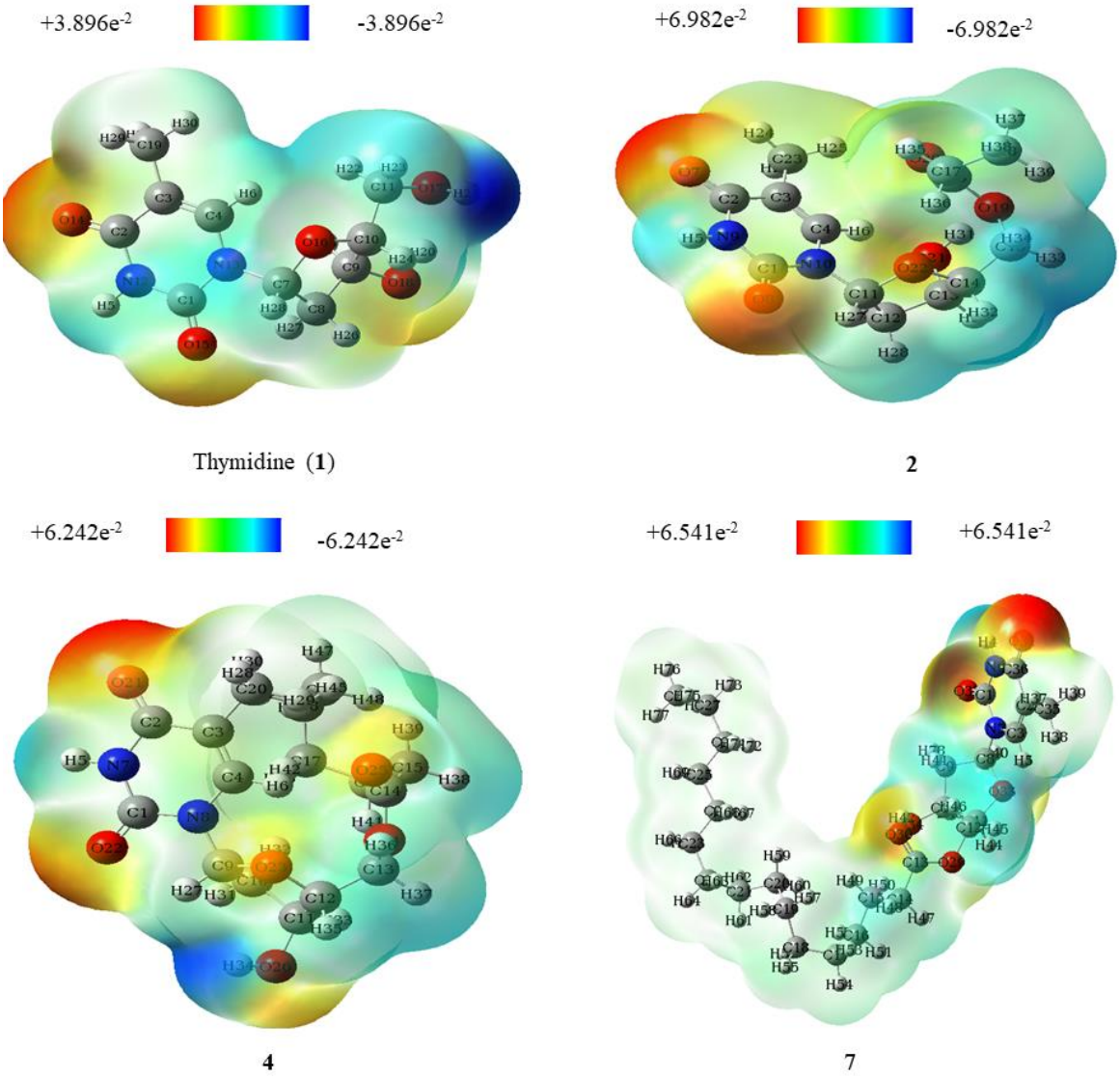

Figure 5. Molecular electrostatic potential map of thymidine and its derivatives **2**, **4**, and **7**.

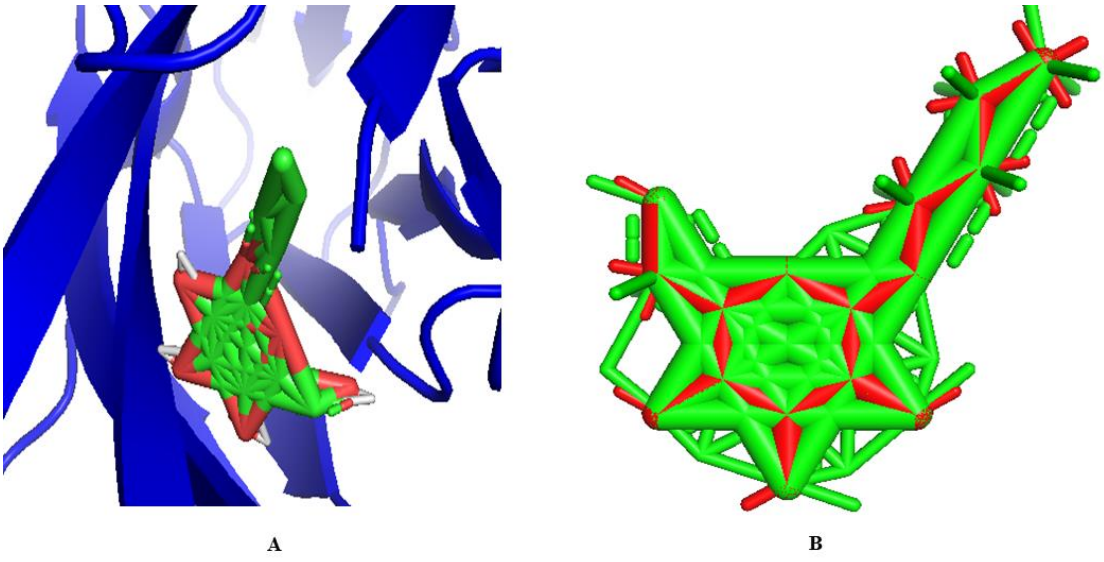

Figure 6. Re-docking pose with the RMSD value of 0.402 Å (red = original, green = docked).

Docking validation study

To identify the ability of docking algorithms to determine the conformation of the protein-bound ligand, re-docking of the co-crystallized ligand was employed to validate the accuracy of the docking procedure. Figure 6 indicates the superimposed view between the docked ligand conformation and the co-crystallized ligand conformation and the RMSD value is 0.402 Å. The complex was found to interact with the same amino acid residues compared to those reported in the present study. The bulky symmetric molecules could be exchanged in the binding site during docking, as is the case in this investigation; the RMSD would be at a very high level. On the contrary, the small compounds could gain low RMSD easily even when placed randomly. Some reported studies [51-53] have suggested a new benchmark for the quality of docking poses based on visual inspection. For visual inspection, Figure 7 shows the 2D visualization of the interactions between a generated docking pose and the experimental ligand conformation. The results of this visual inspection showed the same interactions as in the experimental binding mode, as observed in Figure 7. This result revealed that only visual inspection is not a reliable parameter for the quality of docking poses for docking validation, and the use of visual inspection as a new reference is essential. These partially proved the efficacy and validity of the docking protocol.

Molecular docking studies

Estimation of the feasible binding geometries and interactions between ligand and the active site of proteins was obtained from molecular docking [54]. All selected molecules were subjected to docking into the same binding pocket of lectin FimH of *E. coli* (PDB: 1TR7) using similar optimized docking conditions to identify their binding mode. The results of the docking exploration showed that all thymidine derivatives, along with the parent molecule, gain binding affinities ranging from -5.8 to -6.9 kcal/mol. As shown in Table 4, all the derivatives 2–11 showed comparatively higher binding affinities compared to the parent drug, thymidine 1. These results indicated that modification of the –OH group, along with an aromatic ring or an aliphatic chain molecule improved the binding affinity, while the insertion of halo-benzoyl groups like -Cl and -Br, made some fickleness in binding affinities. However, modification with halogenated aromatic rings increased the binding affinity. The docked pose showed that the drug molecules bind within the active site of the *E. coli* (1TR7) macromolecular structure (Figure 7). Figures 8 and 9 show that thymidine derivatives 9, 10, and 11 (binding affinities -6.7, -6.9, and -6.7 kcal/mol, respectively) bind firmly through hydrophobic bonds with the catalytic binding site Tyr48, Ile52, Ala6, and Ile13, where these residues exhibited alkyl, pi-alkyl pi-sigma and pi-pi stacked interaction. The pi-pi interaction revealed the tight binding with the active site. Besides, Gln133, Asn46, Asp47, Tyr137, and Phe1 which were the highly specific binding pocket of FimH were also found to form hydrogen and electrostatic bonds. It is evident from the structural contrast that compounds 9–11 have an additional aromatic (halogenated ring and tri-phenyl ring) substituent in the parent structure, indicating a high density of electrons in the molecule leading to a comparatively higher binding affinity (6.7 to -6.9 kcal/mol). On the other hand, thymidine derivatives 2, 3, and 4 revealed three similar binding pockets with tyrosine gate Tyr48, Asn46, Asp47, and Pro49 through both hydrogen and hydrophobic bonds. These ligands were bonded in a deep and polar pocket at the N-terminal end of FimH, in which the amino acids Asn46, Asp47, Gln41, and Asn135 create a dense network of nine hydrogen bonds with each hydroxyl group of the ribose ring. In addition, Asn46 showed a closer distance of 1.831 Å for derivative 4.

The derivatives 5–8, which were modified with a long aliphatic chain (nonanoyl, lauroyl, palmitoyl, and stearoyl), enhanced the binding affinities by specific recognition events at post-glycosidic linkage atomic positions two to three with Ile52 and Tyr48 of the tyrosine gate. Interestingly, these derivatives specifically bind through the hydrogen bond with the specific pocket Ile13, Ile52, Asn46, Asn135, Asp47, Asp54, and Gln133. Among all of these residues, Ile52 was found in a close interaction (1.770 Å). Besides, derivatives 9–11 (along with Phe1) displayed the maximum π-alkyl, π-cation, and π- π interactions with the Tyr48 Ile52 and Ile13 indicating a tight binding with the active site.

Table 4. Binding affinities and non-bonding interactions of thymidine and its derivatives.

Entry	Protein	Binding affinity (kcal/mol)	Bond category	Residues in contact	Interaction types	Distance (Å)
1	1TR7	-5.8	Hydrogen	ASN135	H	2.387
			Hydrogen	ASP140	H	2.549
			Hydrogen	THR53	C	3.417
			Hydrophobic	THR134	PS	3.621
2	1TR7	-6.0	Hydrogen	ASN135	H	2.168
			Hydrogen	ASP47	H	2.406
			Hydrogen	GLN41	H	2.911
			Hydrogen	TYR48	H	2.140
			Hydrophobic	ALA6	A	3.602
			Hydrophobic	ALA6	PA	5.462
3	1TR7	-6.1	Hydrogen	ASP47	H	2.336
			Hydrogen	TYR48	H	2.204
			Hydrophobic	PRO49	A	4.583
			Hydrophobic	PRO49	PA	4.863
			Hydrophobic	PRO104	PA	5.223
4	1TR7	-6.4	Hydrogen	ASP47	H	2.725
			Hydrogen	TYR48	H	2.920
			Hydrogen	ASN46	H	1.831
			Hydrophobic	LYS76	A	3.716
			Hydrophobic	PRO49	PA	4.858
5	1TR7	-6.5	Hydrogen	ILE52	H	1.951
			Hydrogen	ASN46	H	2.368
			Hydrogen	ASN46	H	2.447
			Hydrogen	ILE13	H	2.805
			Hydrogen	ASP54	H	1.898
			Hydrogen	GLN133	H	2.849
			Hydrogen	ASN135	H	2.431
			Hydrophobic	TYR48	PA	4.499
6	1TR7	-6.5	Hydrogen	ASP47	H	2.531
			Hydrogen	PRO49	H	4.926
			Hydrogen	SER39	H	2.914
			Hydrophobic	ASN46	PS	3.970
			Hydrophobic	ILE52	A	1.770
7	1TR7	-6.6	Hydrogen	ILE52	H	2.334
			Hydrogen	GLY79	H	2.630
			Hydrogen	ILE13	H	3.040
			Hydrogen	PRO104	H	1.832
			Electrostatic	ASP47	PAn	3.554
			Hydrophobic	ALA6	PA	5.286
8	1TR7	-6.4	Hydrogen	ILE52	H	2.996
			Hydrogen	TYR48	H	2.747
			Hydrophobic	ALA106	PA	5.445
9	1TR7	-6.7	Hydrogen	ASP47	H	1.875
			Hydrogen	SER39	C	3.716
			Hydrophobic	LYS101	A	4.696
			Hydrophobic	ILE13	A	4.050
			Hydrophobic	PHE1	A	4.553
			Hydrophobic	PRO102	PA	4.855
			Hydrophobic	ILE52	PA	5.458
10	1TR7	-6.9	Hydrogen	GLN133	H	2.358
			Electrostatic	PHE1	PCa	4.219
			Hydrophobic	TYR48	PPS	3.883
			Hydrophobic	ILE52	A	3.848
			Hydrophobic	TYR48	PA	4.781
			Hydrophobic	ILE13	PA	5.277
11	1TR7	-6.7	Hydrogen	TYR137	H	2.009
			Hydrogen	ASN46	H	2.322

	Hydrogen	THR40	H	2.212
	Hydrogen	GLN133	H	2.940
	Hydrogen	ASP47	PDH	3.069
	Hydrophobic	ILE13	PS	3.560
	Hydrophobic	ALA6	A	3.796
	Hydrophobic	ALA6	PA	5.423

H = Conventional hydrogen bond; C = Carbon hydrogen bond; A= Alkyl; PA = Pi-alkyl; PAn = Pi-Anion; PCa = Pi-cation; PS = Pi-sigma; PPS = Pi-Pi stacked; PDH = Pi-donor hydrogen bond.

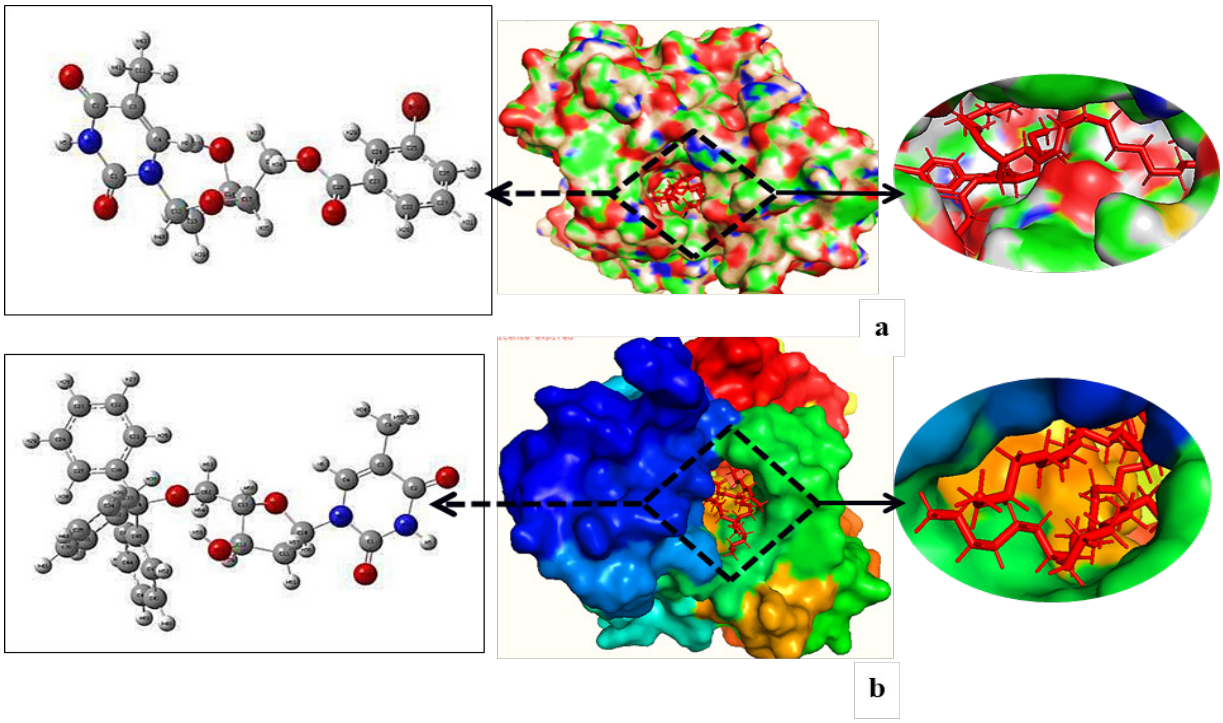

Figure 7. Docked conformation of derivative 10 at inhibition bounding site of 1TR7 (**a**) and docked conformation of derivative 11 at inhibition bounding site of 1TR7 (**b**).

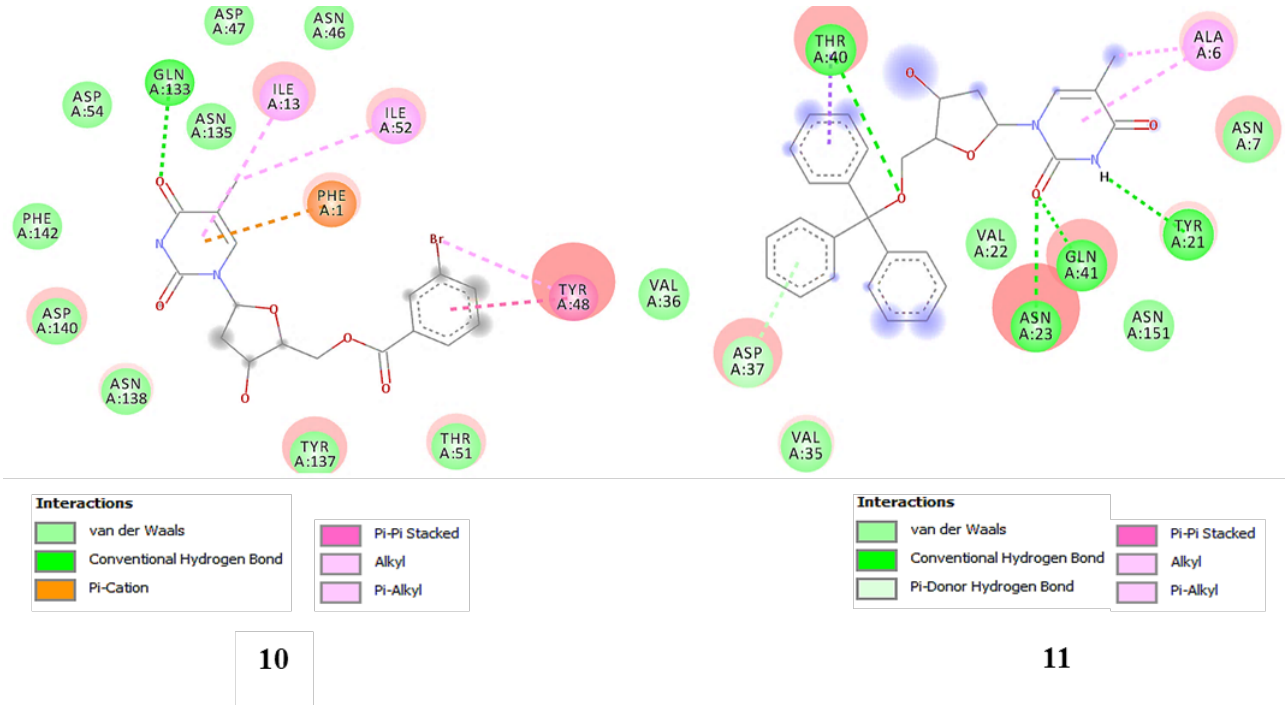

Figure 8. Non-bonding interactions of compounds 9 and 10 with the amino acid residues of 1TR7 generated by Discovery Studio.

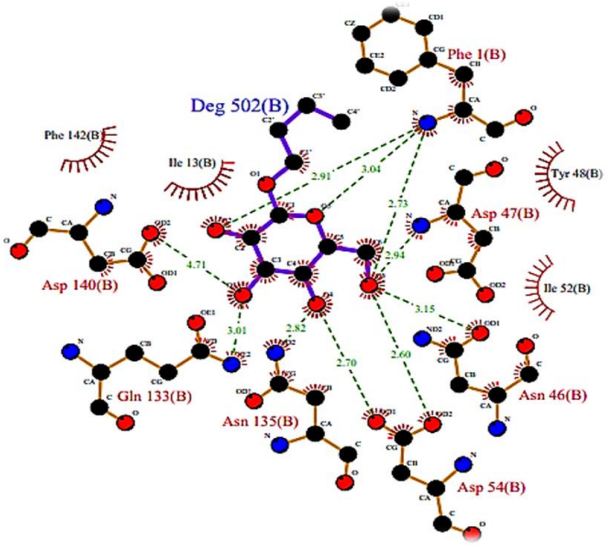

Figure 9. Two-dimensional LigPlot image of FimH complex generated by PDBsum.

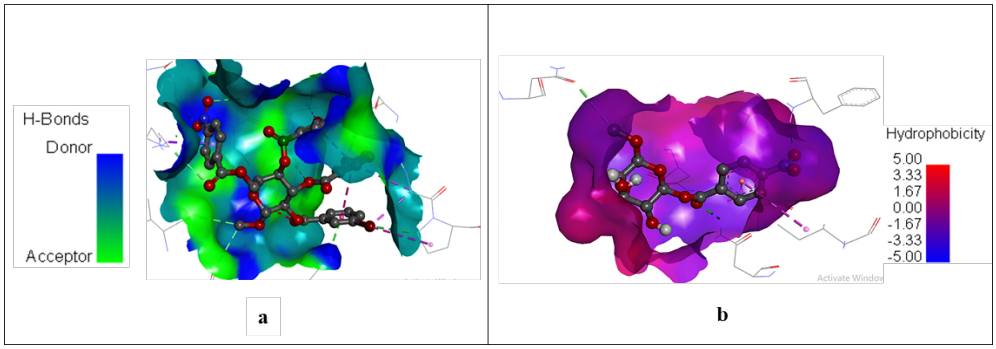

Figure 10. Hydrogen bond surface and hydrophobic surface of 1TR7 with compound 5 (**a**) and compound 9 (**b**).

Recent studies reported that the Tyr48 is considered as the principal component of the PPS, responsible for the accessibility of small molecules to the active site. Binding affinity and binding specialty were improved in the case of 2, 4, 5, 6, 7, and 11 due to significant hydrogen bonding. It was observed that modifications of the –OH group of thymidine 1 enhanced the π-π interactions with the residues of the active site while increasing their polarity resulted in the formation of hydrogen bonding interactions. The most prominent H-bonds were obtained for the derivative 5, formed with Asp54, Gln133, Asn46, Ile13, and Asn133. Hydrogen bonds executed a vital function in shaping the specificity of ligand binding with the receptor, drug design in chemical and biological processes, molecular recognition, and biological activity [55]. The hydrogen bond surface of derivative 5 and the hydrophobic surface of derivative 9 are consequently represented in Figure 10. We realize that the analyzed thymidine derivatives were bound within some of the catalytic binding sites such as isoleucines (Ile13 and Ile52), Tyr48, Tyr137, Asp46, Asp54, Asp140, Asn46, Asn135, Gln133, and Phe1 of the FimH, which is responsible for acute and recurrent bladder infections and chronic inflammatory bowel diseases such as Crohn's disease. Among all the molecules, the inhibition activity of the derivative 10 was found to be the highest (-6.7 kcal/mol). The results were summarized into a set of structural changes to be used in FimH-targeted inhibitor design: thymidine derivatives gave an improved affinity and inhibitory potential; because of their relative flexibility combined with a favorable interaction with isoleucine-52 located in the middle of the tyrosine gate.

Pharmacokinetic prediction and Lipinski's rule

In order to predict that the modified derivatives are potential drugs, we used the *in silico* pharmacokinetic parameters ADMET. The pkCSM online server [56] was employed to calculate *in silico* ADMET properties (Table 5). The absorbance value below 30% indicated poor absorbance; most of the compounds displayed a value above 60%, which revealed a good absorbance in the human intestine.

Table 5. *In silico* ADMET prediction of thymidine and its derivatives.

Entry	Absorption	Distribution			Metabolism					Excretion		Toxicity
	Intestinal absorption (human)	VDss (human)	BBB permeability	CNS permeability	Substrate		Inhibitor			Total Clearance		AMES toxicity
					CYP							
					2D6	3A4	1A2	2C19	2D6	3A4		
	Numeric (% Absorbed)	Numeric (Log L/kg)	Numeric (Log BB)	Numeric (Log PS)	Categorical (Yes/No)					Numeric (Log ml/min/kg)		Categorical (Yes/No)
1	60.686	0.395	-0.982	-2.649	No	Yes	Yes	Yes	No	Yes	0.729	No
2	61.061	0.409	-0.950	-3.646	No	Yes	No	Yes	No	Yes	1.446	No
3	61.802	0.405	-0.380	-3.634	No	Yes	Yes	Yes	No	Yes	1.454	No
4	62.236	0.494	0.334	-2.615	No	Yes	Yes	Yes	No	Yes	1.507	No
5	63.364	0.459	0.323	-2.919	No	Yes	Yes	Yes	No	Yes	1.585	No
6	65.540	0.439	0.310	-2.884	No	Yes	Yes	Yes	No	Yes	1.664	No
7	68.304	0.465	0.327	-2.837	No	Yes	No	Yes	No	Yes	1.357	No
8	69.892	0.506	0.385	-2813	No	Yes	Yes	Yes	No	Yes	1.388	No
9	69.418	0.402	0.274	-2.147	No	Yes	Yes	Yes	No	Yes	-0.109	No
10	69.227	0.409	0.305	-1.146	No	Yes	Yes	Yes	No	Yes	-0.071	No
11	89.906	0.525	0.920	-1.676	No	Yes	Yes	Yes	No	Yes	0.650	No

It is evident that the volume of distribution (VDss) was supposed to be high if the value was higher than 0.45. In addition, blood-brain barrier (BBB) and central nervous system (CNS) permeability had standard values (>0.3 to < -1 log BB, and > -2 to < -3 log PS), respectively. A given compound with a log BB < -1 is poorly distributed to the brain, while that with log BB >0.3 means a potential to cross BBB and with log PS > -2 is considered to penetrate the CNS, while with log PS < -3 it is difficult to move in the CNS [57]. It was observed that most of the compounds exhibited a significant potential to cross the barriers except derivatives 2, and 3. The enzymatic metabolism ensures the chemical biotransformation of a designed drug in the body, which plays a key role in the transformation of drug compounds. In the body, drugs produce several enzymatic metabolites which play a role in catalyzing the reaction with several drug concentrations [58]. It is essential to consider the metabolism of drugs, which may show several physicochemical and pharmacological parameters. The cytochrome P450 (CYP450) plays a major role in drug metabolism because of the major liver enzyme system involved in phase 1 metabolism. Some selective CYP genes of CYP1, CYP2, CYP3, and CYP4 families were found to be involved in drug metabolism, with CYP (1A2, 2C19, 2D6, and 3A4) causing the biotransformation of more than 90% of drugs undergoing phase I metabolism. Therefore, among these members, CYP3A4 is the most important inhibition in this study [59]. All designed derivatives were found to be the substrate and the inhibitor of CYP3A4. Clearance is a constant that indicates the relationship between drug concentration in the body and the rate of elimination of the drug. Therefore, all modified derivatives showed a somewhat high value but were still acceptable in the persistence of the drug in the body. Moreover, it is essential to test whether the calculated derivatives are non-toxic because this plays a critical role in the selection of drugs. All the derivatives we designed are non-toxic. Overall, derivatives 4–11 have better *in silico* pharmacokinetic properties.

Generally, drug-likeness is evaluated using Lipinski's rule of five [60]. As a matter of principle, an orally active drug should have no more than one interruption of the following conditions: (1) no more than five hydrogen bond donors, (2) no more than ten hydrogen bond acceptor, (3) molecular mass of less than 500 Da, (4) an octanol-water partition coefficient of not more than five, and (5) molar refractivity <140. If two or more of the guidelines are disrupted, reduced absorption can be estimated. All of the thymidine derivatives did not violate any of Lipinski's rule of five (Tables 6 and 7). However, topological polar surface area (TPSA) is a contributing factor for oral absorption and blood-brain barrier permeation capacity and the screened drug-likeness of a molecule should have TPSA between 20 and 130 Å^2. The SwissADME web tool prediction ravels that only derivative 11 violates this TPSA standard and all others ligands

are anticipated to be orally bioavailable. In addition, Pan-assay interference derivatives (PAINS) revealed no violation with these thymidine derivatives. PAINS are chemical compounds that often give false-positive results in high-throughput screens. PAINS tend to react nonspecifically with numerous biological targets rather than specifically affecting one desired target. The derivatives designed were evaluated for their synthetic accessibility, the synthetic accessibility values for all derivatives designed are about 3 to 5, therefore, they are easy to synthesize. In fine, the new compounds 2–4 and 9–11 respect all drug-likeness rules.

Table 6. Drug-likeness prediction of thymidine and its derivatives.

Entry	Molar Refractivity (Å)	Log $P_{o/w}$ (XLOGP3)	NRB	NHA	NHD	TPSA (Å²)	Csp3
1	58.070	-1.510	2	5	3	104.550	0.601
2	72.621	0.391	5	6	2	110.620	0.620
3	77.422	1.874	6	6	2	110.620	0.640
4	87.044	1.940	8	6	2	110.620	0.691
5	101.460	3.322	11	6	2	110.620	0.744
6	115.882	4.954	14	6	2	110.620	0.772
7	135.119	7.110	18	6	2	110.620	0.814
8	144.722	8.202	20	6	2	110.620	0.821
9	92.720	1.755	5	6	2	110.620	0.350
10	95.412	1.814	5	6	2	110.620	0.350
11	93.556	3.491	7	5	2	136.151	0.244

Table 7. Drug-likeness prediction of the thymidine esters basing on Lipinski, Muegge, Veber, Egan, Ghose, and their synthetic accessibility.

Entry	Lipinski	Muegge	Veber	Egan	Ghose	Synthetic accessibility	PAINS alert
1	Yes	Yes	Yes	Yes	Yes	3.641	0
2	Yes	Yes	Yes	Yes	Yes	3.960	0
3	Yes	Yes	Yes	Yes	Yes	4.064	0
4	Yes	Yes	Yes	Yes	Yes	4.281	0
5	Yes	Yes	No	Yes	Yes	4.625	0
6	Yes	Yes	No	Yes	Yes	4.972	0
7	Yes	No	Yes	Yes	No	5.454	0
8	Yes	No	No	Yes	No	5.701	0
9	Yes	Yes	Yes	Yes	Yes	4.025	0
10	Yes	Yes	Yes	Yes	Yes	4.106	0
11	Yes	Yes	Yes	Yes	Yes	5.040	0

Table 8. Predicted cytotoxic activity of the thymidine derivatives.

Entry	Cancer cell line prediction result			
	Blood (Leukemia)		Lung (Carcinoma)	
	Pa	Pi	Pa	Pi
1	0.640	0.007	0.569	0.024
2	-	-	0.502	0.016
3	0.515	0.013	0.570	0.024
4	0.505	0.014	0.568	0.024
5	0.505	0.014	0.568	0.024
6	0.505	0.014	0.568	0.024
7	0.505	0.014	0.568	0.024
8	0.505	0.014	0.568	0.024
9	-	-	0.503	0.048
10	-	-	-	-
11	0.522	0.013	0.523	0.039

Cytotoxic prediction

Web-based PASS was used to predict the cytotoxicity of modified thymidine derivatives. Childhood T acute lymphoblastic leukemia and non-small cell lung cancer -3 stages were predicted to suggest the maximum nontoxic bioactive drug molecule. It was evident from prediction Table 8 that thymidine derivatives 2–11 showed 0.50 < Pa < 0.52 for lymphoblastic leukemia, 0.50 < Pa < 0.56 lung cancer. There is a clear concept from the predicted data that these molecules have an equal potentiality to work against both of the cancer cells. Derivatives 3–8 exhibited the same types of activity (Pa ¼ 0.505) and (Pa ¼ 0.568) in spite of having a different aliphatic chain. Finally, derivative 11 which has a tri-phenyl ring revealed a comparatively higher activity (Pa ¼ 0.523) in both predictions. We hope to conduct such studies for a more drug-related validation of these promising thymidine derivatives.

CONCLUSION

In conclusion, several thymidine derivatives were successfully analyzed *in silico* for their antimicrobial, thermodynamic, molecular docking, pharmacokinetic, and drug-likeness properties. Quantum mechanical (QM) calculations of all the thymidine derivatives were performed to determine the thermodynamic parameters, atomic partial charge, and molecular electrostatic potential which revealed that insertion of aliphatic chains and halobenzoyl ring increased the stability of the thymidine derivatives. PASS prediction values of the thymidine derivatives 2–11 were Pa < 0.51 in antibacterial, Pa < 0.76 in antifungal, Pa < 0.77 in antiviral and Pa < 0.83 in anti-carcinogenic activity which revealed the antimicrobial potency of the modified derivatives. Molecular docking was employed to suggest the best antibacterials against *E. coli* (1TR7). Thymidine derivatives showed an interesting range of binding affinity -6.0 to -6.9 kcal/mol and strong interactions with at least one of the catalytic residues (Tyr48, Tyr137, Ile13, Ile52, Asp47, Asp54, Asp140, Asn46, Asn135, and Gln133) of the lectin FimH (1TR7). These derivatives showed several non-covalent interactions, such as hydrogen bonding, hydrophobic, and electrostatic interactions. These blind molecular docking analyses may provide a potential approach for the application of antibacterial drugs as expected inhibitors of *E. coli* protein lectin FimH. The docking validation process revealed that RMSD is in the standard range. Visual inspection exhibited very convincing results in the molecular docking validation process. In fine, these derivatives were analyzed for their pharmacokinetic properties which expressed that the combination of cytotoxic prediction, *in silico* ADMET prediction, and drug-likeness had shown promising results because the newly designed molecules have improved kinetic parameters and maintain all drug-likeness rules, as well as an interesting result in terms of biological activity. So, it could be concluded that most of the selected antibacterials showed promise and can be used to design effective antibacterial drugs against *E. coli* protein lectin FimH. More drug-likeness *in vitro* and *in vivo* studies such as nontoxic concentration towards healthy cells may be conducted in the near future.

Acknowledgement: *The authors are grateful to the Research and Publication Cell (Ref.: 6322/gobe/pari/proka/doptor/C.U./2018), University of Chittagong, Bangladesh for providing financial support to carry out this piece of research.*

REFERENCES

1. G. Niu, H. Tan, *Trends Microbiol*., **23** (2), 110 (2015).
2. K. L. Seley-Radtke, M. K. Yates, *Antiviral Res*., **154**, 66 (2018).
3. J. E. Polifka, J. M. Friedman, *Teratology*, **65** (5), 240 (2002).
4. M. Arifuzzaman, M. M. Islam, M. M. Rahman, M. A. Rahman, S. M. A. Kawsar, *Acta Pharm. Sci.*, **56** (4), 7 (2018).
5. T. S. Chowdhury, J. Ferdous, M. M. H. Misbah, M. Z. H. Bulbul, S. M. A. Kawsar, *J. Bangladesh Chem. Soc.*, **31** (2), 40 (2019).
6. A. Alam, M. A. Hosen, A. Hosen, Y. Fujii, Y. Ozeki, S. M. A. Kawsar, *J. Mexican Chem. Soc.*, **65**, 256 (2021).
7. L. P. Elwell, R. Ferone, G. A. Freeman, J. A. Fyfe, J. A. Hill, P. H. Ray, C. A. Richards, S. C. Singer, V. B. Knick, J. L. Rideout, *Antimicrob. Agents Chemother*., **31**(2), 274 (1987).
8. A. A. Krayevsky, K. A. Watanabe, Modified Nucleosides as Anti-AIDS Drugs: Current Status and Perspectives, Bioinform., Moscow, 1993.
9. S. Tabata, M. Yamamoto, H. Goto A. Hirayama, M. Ohishi, T. Kuramoto, A. Mitsuhashi, R. Ikeda, M. Haraguchi, K. Kawahara, Y. Shinsato, K. Minami, A. Saijo, M. Hanibuchi, Y. Nishioka, S. Sone, H. Esumi, M. Tomita, T. Soga, T. Furukawa, S.-I. Akiyama, *Cell Report*, **19** (7) 1313 (2017).
10. M. Z. H. Bulbul, T. S. Chowdhury, M. M. H. Misbah, J. Ferdous, S. Dey, I. Hasan, Y. Fujii, Y. Ozeki, S. M. A. Kawsar, *Pharmacia*, **68** (1), 23 (2021).
11. K. M. Rana, J. Ferdous, A. Hosen, S. M. A. Kawsar, *J. Sib. Fed. Univ. Chem.*, **13** (4), 465 (2020).

12. M. Z. H. Bulbul, M. A. Hosen, J. Ferdous, T. S. Chowdhury, M. M. H. Misbah, S. M. A. Kawsar, *Int. J. New Chem.,* **8** (1), 88 (2021).
13. J. Maowa, M. A. Hosen, A. Alam, K. M. Rana, Y. Fujii, Y. Ozeki, S. M. A. Kawsar, *Phys. Chem. Res*., **9**, 385 (2021).
14. M. I. Mirajul, M. Arifuzzaman, M. R. Monjur, M. R. Atiar, S. M. A. Kawsar, *Hacettepe J. Biol. Chem.*, **47**, 153 (2019).
15. S. R. Devi, S. Jesmin, M. Rahman, M. A. Manchur, Y. Fujii, R. A. Kanaly, Y. Ozeki, S. M. A. Kawsar, *Acta Pharm. Sci*., **57**, 47 (2019).
16. J. Maowa, A. Alam, K. M. Rana, S. Dey, A. Hosen, Y. Fujii, I. Hasan, Y. Ozeki, S. M. A. Kawsar, *Ovidius Univ. Annals Chem.,* **32**, 6 (2021).
17. K. M. Rana, J. Maowa, A. Alam, S. Dey, A. Hosen, I. Hasan, Y. Fujii, Y. Ozeki, S. M. A. Kawsar, *In Silico Pharmacol.,* **9**, 1 (2021).
18. S. M. A. Kawsar, M. A. Hosen, *Turk. Comput. Theor. Chem.,* **4** (2), 59 (2020).
19. A. L. Kau, D. A. Hunstad, S. J. Hultgren, *Curr. Opin. Microbiol*., **8** (1), 54 (2005).
20. F. A. Carvalho, N. Barnich, A. Sivignon, C. Darcha, C. H. Chan, C. P. Stanners, A. Darfeuille-Michaud, *J. Exp. Med*., **206** (10), 2179 (2009).
21. C. S. Hung, J. Bouckaert, D. Hung, J. Pinkner, C. Widberg, A. DeFusco, C. G. Auguste, R. Strouse, S. Langermann, G. Waksman, S. J. Hultgren, *Mol. Microbiol.*, **44** (4), 903 (2002).
22. A. Sivignon, X. Yan, D. Alvarez Dorta, R. Bonnet, J. Bouckaert, E. Fleury, J. Bernard, S. G. Gouin, A. Darfeuille-Michaud, N. Barnich, *mBio*., **6** (6), e01298 (2015).
23. N. Dreux, J. Denizot, M. Martinez-Medina, A. Mellmann, M. Billig, D. Kisiela, S. Chattopadhyay, E. Sokurenko, C. Neut, C. Gower-Rousseau, J-F. Colombel, R. Bonnet, A. Darfeuille-Michaud, N. Barnich, *PLoS Pathog*., **9** (1), e1003141 (2013).
24. D. Chatfield, J. Christopher, *Theoretical Chem. Acc*., **108**, 367 (2002).
25. S. M. A. Kawsar, M. A. Hosen, Y. Fujii, Y. Ozeki, *J. Comput. Chem. Mol. Model.,* **4** (4), 452 (2020).
26. F. Yasmin, M. R. Amin, M. A. Hosen, M. Z. H. Bulbul, S. Dey, S. M. A. Kawsar, *Cellulose Chem. Technol.,* **55**, 477 (2021).
27. S. M. A. Kawsar, A. Kumar, *J. Chilean Chem*. Soc., **66**, 5206 (2021).
28. F. Yasmin, M. R. Amin, M. A. Hosen, M. Z. H. Bulbul, S. Dey, S. M. A. Kawsar, *J. Sib. Fed. Univ. Chem.*, **14**, 171 (2021).
29. R. A. Gaussian, M. J. Frisch, G. W. Trucks, H. B. Schlegel, G. E. Scuseria, et al., Gaussian Inc., Wallingford, CT, 2009, https://gaussian.com/g09citation/.
30. A. D. Becke, *Phys. Rev., A*, **38**, 3098 (1988).
31. C. Lee, W. Yang, R. G. Parr, *Phys. Rev., B*, **37**, 785 (1988).
32. S. Kumaresan, V. Senthilkumar, A. Stephen, B. S. Balakumar, *World J. Pharmaceut. Res*., **4** (1) 1035 (2015).
33. H. M. Berman, J. Westbrook, Z. Feng, G. Gilliland, T. N. Bhat, H. Weissig, *Nucleic Acids Res*., **28**, 235 (2000).
34. W. L. Delano, The PyMOL molecular graphics system. De-Lano Scientific, San Carlos, CA, USA, 2002.
35. N. Guex, M. C. Peitsch, *Electrophoresis*, **18**, 2714 (1997).
36. S. Dallakyan, A. J. Olson, Small-molecule library screening by docking with Py Rx, in: J. E. Hempel, C. H. Williams, C. C. Hong (eds.), Chemical biology: methods and protocols. Springer, New York, USA, 2015, p. 243.
37. Version ADS 4.0, Accelrys, San Diego, USA, 2017.
38. K. Onodera, K. Satou, H. Hirota, *J. Chem. Inf. Model.,* **47**, 1609 (2007).
39. G. L. Warren, C. W. Andrews, A. M. Capelli, B. Clarke, J. LaLonde, M. H. Lambert, M. Lindvall, N. Nevins, S. F. Semus, S. Senger, G. Tedesco, I. Wall, J. M. Woolven, C.E. Peishoff, M. S. Head, *J. Med. Chem.,* **49** (20), 5912 (2006).
40. L. L. G. Ferreira, A. D. Andricopulo, *Drug Discov. Today*, **24**, 1157 (2019).
41. A. Daina, O. Michielin, V. Zoete, *Sci. Rep*., **7**, 1 (2017).
42. N. Cohen, S. W. Benson, *Chem. Rev*., **93**, 2419 (1993).
43. E. J. Lien, Z. R. Guo, R. L. Li, C. T. Su, *J. Pharm. Sci.,* **71**, 641 (1982).
44. M. M. Matin, P. Chakraborty, M. S. Alam, M. M. Islam, U. Hanee, *Carbohydr. Res*., **496**, 108130 (2020).
45. H. Heinz, U. W. Suter, *J. Phys. Chem*., *B*, **108**, 18341 (2004).
46. K. C. Gross, P. G. Seybold, C. M. Hadad, *Int. J. Quantum Chem*., **90**, 445 (2002).
47. R. S. Mulliken, *J. Chem. Phys*., **23**, 1833 (1955).
48. M. L. Amin, *Drug Target Insights*, **7**, 27 (2013).
49. P. Politzer, J. S. Murray, *Rev. Comput. Chem*., **2** 273 (1991).
50. P. Politzer, D. G. Truhlar (eds.), Chemical applications of atomic and molecular electrostatic potentials. Reactivity, structure, scattering, and energetics of organic, inorganic, and biological systems, Springer USA, 1981.
51. R. T. Kroemer, A. Vulpetti, J. J. McDonald, D. C. Rohrer, J. -Y. Trosset, F. Giordanetto, S. Cotesta, C. McMartin, M. Kihlen, P. F. W. Stouten, *J. Chem. Inf. Comput. Sci.,* **44** (3), 871 (2004).
52. G. Jones, P. Willett, R. C. Glen, A. R. Leach, R. Taylor, *J. Mol. Biol.,* **267** (3), 727 (1997).
53. M. Kontoyianni, L. M. McClellan, G. S. Sokol, *J. Med. Chem.,* **47** (3), 558 (2004).
54. R. Ghosh, A. Chakraborty, A. Biswas, S. Chowdhuri, *J. Biomol. Struct. Dyn*., 1 (2020).
55. J. Perlstein, *J. American Chem. Soc.,* **123**, 191 (2001).
56. D. E. V. Pires, T. L. Blundell, D. B. Ascher, *J. Med. Chem.,* **58**, 4066 (2015).
57. D. E. Clark, *Drug Discov. Today,* **8**, 927 (2003).

58. S. Kok-Yong, L. Lawrence, Drug distribution and drug elimination. Basic pharmacokinetic concepts, some clinical applications, InTechOpen, London, SW7 2QJ, UK, 2015.
59. M. M. Thapar, Pharmacokinetics and Dynamics of Atovaquone and Proguanil, Malarone®, Karolinska University Press, Stockholm, Sweden, 2004.
60. C. A. Lipinski, F. Lombardo, B. W. Dominy, P. J. Feeney, *Adv. Drug Deliv. Rev.,* **46**, 3 (2001).

Bulgarian Chemical Communications, Volume 53, Issue 3 (pp. 343 - 354) 2021 *DOI: 10.34049/bcc.53.3.5390*

Radiative analysis of entropy generation on MHD Walters-B fluid with heat and mass transfer

S. Asad

Department of Mathematics, College of Science, Majmaah University, Al-Majmaah, 11952, Saudi Arabia

Received: March 01, 2021, Revised: May 31, 2021

Boundary layer flow of Walters-B liquid by an inclined unsteady stretching sheet was investigated. Simultaneous effects of heat and mass transfer on entropy generation were considered. Analysis was carried out in the presence of thermal radiation and viscous dissipation. Convective condition was employed for the heat transfer process. Resulting problems were computed for the convergent solutions of velocity, temperature and concentration fields. The effects of different physical parameters on entropy generation, velocity, temperature and concentration fields are discussed. It was observed that angle of inclination and Weissenberg number decay the velocity field whereas the velocity field is an increasing function of mixed convection parameter. Temperature field rises for larger values of Eckert number and Biot number. The concentration field decreases when Sc increases. Numerical values of skin friction coefficient, local Nusselt number and local Sherwood number were computed and analyzed. We concluded from Table 1 that the magnitude of skin friction coefficient decays for larger values of mixed convection parameter, radiation parameter and Eckert number. Entropy generation decreases when temperature/parameter ratio increases while magnetic parameter boosts the entropy generation. It was also noted that entropy generation rises with larger Reynolds numbers.

Keywords: MHD Walters-B fluid, entropy generation, viscous dissipation, thermal radiation, unsteady inclined stretching sheet, convective boundary condition.

INTRODUCTION

It is a commonly accepted argument now that the fluids in numerous technological and biological applications do not follow the commonly assumed relationship between the stress and the rate of strain at a point. Such fluids have come to be known as non-Newtonian fluids. Materials like molten plastics, polymers, shampoos, certain oils, personal care products, pulps, mud, ice, foods and fossil fuels, which may saturate in underground beds, display non-Newtonian behavior. In recent times, there has been a great deal of interest in understanding the behavior of viscoelastic fluids. Such fluids are of great interest to the applied mathematicians and engineers, essentially from the points of view of theory and simulation of differential equations. On the other hand, in applied sciences such as rheology or physics of the atmosphere, the approach to fluid mechanics is in an experimental set up leading to the measurement of material coefficients. In theoretically studying how to predict the weather, the ordinary differential equations represent the main tool. Since the failures in the predictions are strictly related to a chaotic behavior, one may find it unessential to ask whether the fluids are really Newtonian. Constitutive equations describe the rheological properties of viscoelastic fluids. Most of the models or constitutive equations are empirical or semi-empirical. Also the extra rheological parameters in such relations add more nonlinear terms to the corresponding differential systems. The order of the differential systems involving non-Newtonian fluids is higher in general than the Navier-Stokes equations. In view of all these challenges there is paucity of approximate, analytic and numerical solutions of the nonlinear flow problems of viscoelastic fluids. Keeping this in view, the various investigators are still developing such solutions (see [1-10] and some relevant papers therein).

No doubt, there have been significant advances in the mathematical modeling and analysis of steady boundary layer flows of non-Newtonian fluids over a stretching surface with/without heat and mass transfer. Such flow analysis in presence of heat transfer is important in polymer extrusion, paper production, continuous casting, cooling of metallic plates in a bath, etc. Further, not much attention in this direction is focused on the unsteady flow of MHD non-Newtonian fluids with entropy generation over a stretching sheet. Hayat *et al.* [11] investigated the unsteady flow with heat and mass transfer characteristics in a third-grade fluid bounded by a stretching sheet. They found a series of solutions of the problem.

To whom all correspondence should be sent:
E-mail: asadsadia@ymail.com

© 2021 Bulgarian Academy of Sciences, Union of Chemists in Bulgaria

Flow of Maxwell fluid over a stretching surface in the presence of a first-order constructive/destructive chemical reaction has been reported by Mukhopadhyay and Bhattacharyya [12]. Mukhopadhyay [13] studied the unsteady two-dimensional flow of a non-Newtonian fluid over a stretching surface with prescribed surface temperature. The heat transfer in unsteady boundary layer stagnation-point flow over a shrinking/stretching sheet is investigated by Bhattacharyya [14]. Mishra and Singh [15] investigated the fluid flow along a vertical unsteady stretching sheet with a combined effect of heat and mass transfer. They formulated the problem in the presence of heat generation and a transverse magnetic field.

In this study, we focus on entropy generation, heat and mass transfer, with MHD non-Newtonian fluid. Heat and mass transfer are some of the most interactive factors of energy consumption. Entropy generation in a magnetohydrodynamic flow of non-Newtonian fluid is an efficient method for enhancing the heat transfer, which is very useful to enhance the performance of industrial processing. Initially the concept of entropy generation minimization is given by Bejan [16, 17]. After that many researchers discuss this concept with different physical aspects and different fluid models. Effect of entropy generation on the convective MHD flow of a third-grade fluid is investigated by Rashidi *et al.* [18]. They discussed influences of different physical parameters on the entropy generation. Sithole *et al.* [19] studied a nano fluid flow with entropy generation and nonlinear thermal radiation. They focused on the effects of nonlinear radiation on entropy generation. Naz *et al.* [20] analyzed the cross nanofluid with entropy generation and gyrostatic motile microorganisms. They observed that Brownian motion parameter and temperature difference parameter play an important role to control the concentration of nano particles and the process of entropy generation, respectively.

The purpose of the present investigation is to examine the effect of entropy generation on the boundary layer flow of MHD Walters-B liquid over an unsteady inclined stretching sheet. Simultaneous effects of heat and mass transfer are taken into account. Energy equation in presence of viscous dissipation and thermal radiation effects is considered. Resulting nonlinear problems are formulated first and then solved for the convergent solutions. Contributions of involved parameters on the flow, temperature, concentration and entropy generation are examined. Skin friction coefficient and Nusselt number are computed and analyzed.

Problem formulation

Here we investigate the flow of an incompressible Walters' B fluid due to an inclined stretching sheet with convective boundary condition. The effects of viscous dissipation and thermal radiation are present. The sheet is inclined at an angle α with the horizontal axis, i.e. x-axis and y-axis is taken normal to it. The extra stress tensor S in Walters' B fluid is given by:

$$S = 2\eta_0 A_1 - 2k_0 \frac{DA_1}{Dt}, \tag{1}$$

$$\frac{DA_1}{Dt} = \frac{\partial A_1}{\partial t} + V.\nabla A_1 - A_1.\nabla V - (\nabla V)^T.A_1. \tag{2}$$

In the above equations A_1 is the rate of strain tensor, $\frac{DA_1}{Dt}$ is the covariant derivative of the rate of strain tensor in relation to the material in motion and η_0 and k_0 denote the limiting viscosity at small shear rates and a short memory coefficient, respectively, i.e. :

$$\eta_0 = \int_0^\infty N(\tau)d\tau, \tag{3}$$

$$k_0 = \int_0^\infty \tau N(\tau)d\tau, \tag{4}$$

where $N(\tau)$ is the distribution function with relaxation time τ. Taking short memory into account the terms involving

$$\int_0^\infty \tau^n N(\tau)d\tau, \quad n \geq 2, \tag{5}$$

are neglected in case of Walter's B fluid 11]. The subjected boundary layer equations are given by:

$$\frac{\partial u}{\partial x} + \frac{\partial v}{\partial y} = 0, \tag{6}$$

$$\frac{\partial u}{\partial t} + u\frac{\partial u}{\partial x} + v\frac{\partial u}{\partial y} = \frac{\eta_0}{\rho}\left(\frac{\partial^2 u}{\partial y^2}\right) - \frac{k_0}{\rho}\left[\frac{\partial^3 u}{\partial t \partial y^2} + u\frac{\partial^3 u}{\partial x \partial y^2} + v\frac{\partial^3 u}{\partial y^3} + \frac{\partial u}{\partial x}\frac{\partial^2 u}{\partial y^2} - \frac{\partial u}{\partial y}\frac{\partial^2 u}{\partial x \partial y}\right] + g_0\beta_T(T - T_\infty)\cos\alpha - \frac{\sigma B_0 u}{\rho}, \tag{7}$$

$$\rho c_p\left(\frac{\partial T}{\partial t} + u\frac{\partial T}{\partial x} + v\frac{\partial T}{\partial y}\right) = k\frac{\partial^2 T}{\partial y^2} - \frac{\partial q_r}{\partial y} + \eta_0\left(\frac{\partial u}{\partial y}\right)^2 - 2k_0\left[\frac{\partial u}{\partial y}\frac{\partial^2 u}{\partial t \partial y} + u\frac{\partial u}{\partial y}\frac{\partial^2 u}{\partial x \partial y} + v\frac{\partial u}{\partial y}\frac{\partial^2 u}{\partial y^2}\right] + \sigma B_0 u^2, \tag{8}$$

$$\frac{\partial C}{\partial t} + u\frac{\partial C}{\partial x} + v\frac{\partial C}{\partial y} = De\frac{\partial^2 C}{\partial y^2}, \tag{9}$$

$$u = u_s(x),\ v = 0,\ -k\frac{\partial T}{\partial y} = h(T_f - T)\ ,C = C_w \text{ at } y = 0, \tag{10}$$

$$u \to 0,\ T \to T_\infty,\ C \to C_\infty \text{ as } y \to \infty, \tag{11}$$

in which u and v represent the velocity components along and normal to the sheet, $u_s = \frac{bx}{1-at}$ is the velocity of the stretching sheet, T is the fluid temperature, $\nu = (\mu/\rho)$ is the kinematic viscosity, ρ is the density of the fluid, k is the thermal conductivity of the fluid, h is the convective heat

transfer coefficient, $T_f = T_\infty + T_{ref}\frac{bx^2}{2v}(1-at)^{-3/2}$ is the surface temperature, C is the concentration of fluid, D is the effective diffusion coefficient and $C_w = C_\infty + \frac{cx}{1-at}$ is the fluid concentration.

We introduce:

$$\psi = x\left(\frac{vb}{1-at}\right)^{-1/2} f(\eta), \theta(\eta) = \frac{T-T_\infty}{T_s-T_\infty}, \varphi(\eta) = \frac{C-C_\infty}{C_s-C_\infty}, \eta = y\left(\frac{b}{v(1-at)}\right)^{1/2}, \tag{12}$$

and the velocity components $u = \frac{\partial\psi}{\partial y}$, $v = -\frac{\partial\psi}{\partial x}$, where ψ is the stream function. Now Eq. (6) is identically satisfied and Eqs. (7-11) are reduced into the following forms:

$$f''' + ff'' - f'^2 + -\varepsilon\left(f' + \frac{1}{2}\eta f''\right) + We\left[\varepsilon\left(2f'' + \frac{1}{2}\eta f^{iv}\right) + f''^2 - 2f'f''' + ff^{iv}\right] + G\theta\cos\alpha - Mf' = 0, \tag{13}$$

$$(1+\frac{4}{3}R)\theta'' - Pr\left[\frac{1}{2}\varepsilon(3\theta + \eta\theta') - f\theta' + 2f'\theta\right] + PrE_cf''^2 - PrE_cWe\frac{1}{2}\varepsilon(3f''^2 + \eta f''f''')$$

$$-PrE_cWe(f'f''^2 - ff''f''') + PrEcMf'^2 = 0, \tag{14}$$

$$\varphi'' + Sc(f\varphi' - f'\varphi) - \varepsilon Sc\left(\varphi + \frac{1}{2}\eta\varphi'\right) = 0, \tag{15}$$

$$f = 0,\ f' = 1,\ \theta' = -Bi[1-\theta(0)]\ \varphi = 1 \text{ at } \eta = 0, \tag{16}$$

$$f' \to 0,\ \theta \to 0\ \varphi \to 0 \text{ at } \eta \to \infty. \tag{17}$$

Here $We = \frac{k_0}{\eta_0}\frac{b}{1-at}$ is the Weissenberg number, $Pr = \frac{\nu}{\sigma}$ is the Prandtl number, $\varepsilon = \frac{b}{a}$ is the ratio parameter, $G = \frac{g_0\beta_T(T_s-T_\infty)x^3/\nu}{u_s^2x^2/\nu}$ is the mixed convection parameter, $E_c = \frac{u_s^2}{c_p(T_s-T_\infty)}$ is the Eckert number, $R = \frac{4\sigma^*T_\infty^3}{kk^*}$ is the radiation parameter, $M = \frac{\sigma B_0^2(1-at)}{\rho b}$ $Bi = \frac{h}{k}\sqrt{\frac{\nu(1-at)}{b}}$ is the Biot number and $Sc = \frac{\nu}{D}$ is the Schmidt number.

The skin friction coefficient C_f, the local Nusselt number Nu_x and the local Sherwood number Sh can be expressed in the following forms:

$$C_f = \frac{\tau_w}{\frac{1}{2}\rho u_s^2},\ Nu_x = \frac{xq_w}{k(T_s-T_\infty)},\ Sh = \frac{\sqrt{t}M_w}{D_w(C_s-C_\infty)}, \tag{18}$$

Hence,

$$\tau_w = \mu_0\frac{\partial u}{\partial y}\Big|_{y=0} - k_0\left\{\frac{\partial^2 u}{\partial t\partial y} + u\frac{\partial^2 u}{\partial x\partial y} - 2\frac{\partial u}{\partial x}\frac{\partial u}{\partial y} + v\frac{\partial^2 u}{\partial y^2}\right\}\Big|_{y=0}, \tag{19}$$

Dimensionless forms of skin friction coefficient C_f, local Nusselt number Nu_x and local Sherwood number Sh can be represented by the relations:

$$C_f = 2(Re_x)^{-1/2}\left[(1+3We)f''(\eta) - We\varepsilon\frac{1}{2}(3f''(\eta) + \eta f'''(\eta))\right]\Big|_{\eta=0},$$

$$Nu/Re_x^{1/2} = -(1+\tfrac{4}{3}R)\theta'(0) \qquad Sh/Re_x^{1/2} = -\varphi'(0), \tag{20}$$

in which $(Re_x)^{-1/2} = \sqrt{\frac{\nu}{xu_s}}$.

Convergence of the homotopy solutions

It is well known that the convergence of series (37 - 39) depends on the auxiliary parameters $\hbar_f$, $\hbar_\theta$ and $\hbar_\phi$. These parameters are useful to control and adjust the convergence of series solutions. In order to find the admissible values of $\hbar_f$, $\hbar_\theta$ and $\hbar_\phi$ the $\hbar$ − curves of $f''(0)$, $\theta'(0)$ and $\phi'(0)$ are displayed. Figs. (1-3) depict that the range of admissible values of $\hbar_f$, $\hbar_\theta$ and $\hbar_\phi$ are $-1.25 \le \hbar_f \le -0.26$, $-1.23 \le \hbar_\theta \le -0.27$ and $-1.26 \le \hbar_\phi \le -0.4$. The series converge in the whole region of η when $\hbar_f = \hbar_\theta = -0.8$ and $\hbar_\phi = -0.9$. Table 1 displays the convergence of homotopy solutions for different orders of approximations. Tabulated values clearly indicate that the 25^{th} order of approximations is enough for the convergent solutions.

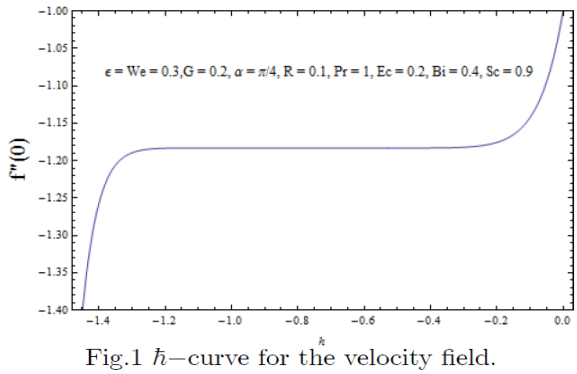

Fig.1 $\hbar-$curve for the velocity field.

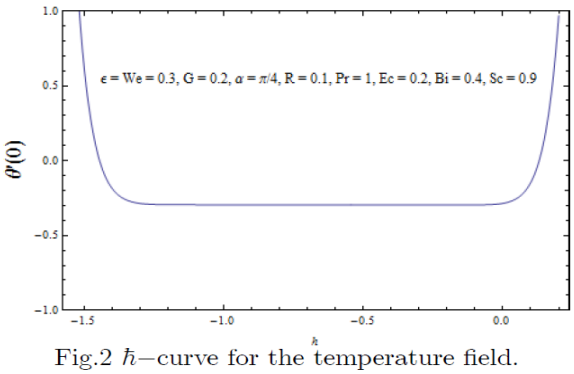

Fig.2 $\hbar-$curve for the temperature field.

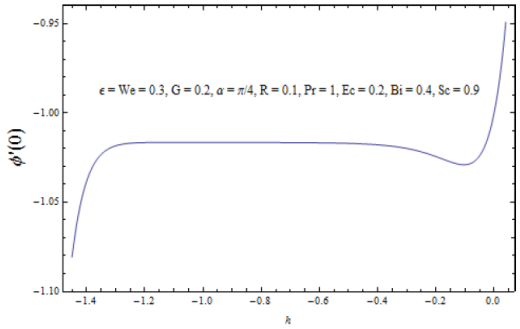

Fig.3 $\hbar-$curve for the concentration field.

Entropy generation

This section discloses the influence of MHD Walter's B fluid with heat and mass transfer on entropy generation. Local volumetric rate of entropy generation is defined as:

$$S_{gen}''' = \frac{k}{T_\infty^2}\left[\left(\frac{\partial T}{\partial y}\right)^2 + \frac{16\sigma^* T_\infty^3}{3k^*}\left(\frac{\partial T}{\partial y}\right)^2\right] + \frac{\sigma B_0^2 u^2}{T_\infty} + \frac{\mu}{T_\infty}\left[\left(\frac{\partial u}{\partial y}\right)^2 - 2k_0\left\{\frac{\partial u}{\partial y}\frac{\partial^2 u}{\partial t \partial y} + u\frac{\partial u}{\partial y}\frac{\partial^2 u}{\partial x \partial y} + v\frac{\partial u}{\partial y}\frac{\partial^2 u}{\partial y^2}\right\}\right], \quad (21)$$

Above equation is the combination of three different phenomena. First is heat transfer, second due to magnetic field and third one is due to viscous dissipation of Walter's B fluid. Characteristic entropy generation rate is defined as:

$$\dot{S}_0''' = \frac{k(\Delta T)^2}{l^2 T_\infty^2}, \quad (22)$$

Thus, the dimensionless form of entropy generation is obtained by taking ratio of Eq. (21) and Eq. (22).

$$N_G = \frac{S_{gen}'''}{\dot{S}_0'''} = Re\left(1 + \frac{4}{3}R\right)\theta'^2 + \frac{1}{\theta_w^2} Re\, Br (f''^2 + Mf'^2) - \frac{1}{\theta_w^2} Re\, Br We\left[\frac{1}{2}\varepsilon(3f''^2 + \eta f'' f''') + f' f''^2 - f f'' f'''\right]. \quad (23)$$

where $Re = \frac{u_s x}{\upsilon}$, $Br = \frac{\mu (u_s)^2}{k\Delta T}$ and $\theta_w = \frac{\Delta T}{T_\infty}$.

GRAPHICAL RESULTS AND DISCUSSION

The arrangement of this section is to disclose the impact of different physical parameters, including ratio parameter, the Biot number, the Weissenberg number, the Prandtl number, the Sherwood number, the Eckert number, the mixed convection parameter, the angle of inclination and the radiation parameter. The variation of aforementioned parameters is seen for the velocity, temperature and concentration fields. It is observed that the effects of α and ε on the velocity field are quite opposite (see Figs. 4 and 5). Velocity field and boundary layer thickness decay for larger values of α. The influence of Weissenberg number We on $f'(\eta)$ is shown in Fig. 6. Here the velocity field is a decreasing function of We. For large values of the mixed convection parameter G, the velocity field increases (see Fig. 7). Effects of radiation parameter R and Eckert number E_c are qualitatively similar for the velocity field $f'(\eta)$ (see Figs. 8 and 9). It is also noticed that the variation of R between 0 and 1 is insignificant on the temperature. Fig. 10 depicts the influence of ε on the temperature field. Apparently, both the temperature field and the thermal boundary layer thickness are decreased *via* ε. Fig. 11 gives the influence of Weissenberg number We on the temperature field. Here the temperature field is an increasing function of We. Fig. 12 shows that the temperature field decays very slowly when the mixed convection parameter G increases. Fig. 13 presents the influence of α on the temperature field. Both the temperature field and the thermal boundary layer thickness decrease when α increases. Fig. 14 witnesses that the temperature field is more pronounced when

radiation effects strengthen. Fig. 15 depicts the variation of **Pr** on temperature field. For larger values of the temperature and thermal boundary layer thickness it decreases. This is since enhancement in **Pr** causes a reduction in thermal conductivity. Effect of Eckert number Ec is displayed in Fig. 16. When we increase the Eckert number then the fluid kinetic energy increases and thus the temperature field increases for larger values of Eckert number. Fig. 17 shows the influence of Biot number on the temperature field. Larger Biot numbers correspond to more convection than conduction and this leads to an increase in temperature, as well as in thermal boundary layer thickness. Influence of parameter ε on the concentration field is displayed in Fig. 18. It is noticed that the concentration field decreases when ε is increased. Fig. 19 shows the influence of Weissenberg number We on the concentration field. It is clearly seen from this figure that the concentration field increases when the Weissenberg number We increases. Fig. 20 gives the influence of α on the concentration field. The angle of inclination α increases the concentration field. The effect of Sc on the concentration field is plotted in Fig. 21. The concentration field decreases when Sc increases. Here a larger Sc number corresponds to lower molecular diffusivity.

Deviation of entropy generation with η is depicted in Fig. 22 for different values of the radiation parameter. Increase in radiation parameter leads to an increase in entropy generation. It is also observed that near the surface variation is almost negligible. Fig. 23 shows the dual behavior of the fluid parameter; small increment is observed near the wall but far away from the wall entropy generation decreases rapidly. The effect of the temperature ratio parameter on entropy generation is displayed in Fig. 24. It is clearly seen from this figure that entropy generation is decreases when the temperature ratio parameter enhances. Dispersion of magnetic parameter on entropy generation is displayed in Fig. 25. Magnetic parameters persuade Lorentz force which boosts the entropy generation. Fig. 26 exhibits the influence of the unsteady parameter, which decays the entropy generation. The effect of Brickman number is displayed in Fig. 27. Brickman number produced heat transport by viscous heating, which makes an improvement in entropy generation. Variation of entropy generation with Reynolds number is shown in Fig. 28. It is noted that entropy generation rises with larger Reynolds numbers because larger Reynolds numbers correspond to larger inertia and smaller viscous force.

Tables 1-3 include the numerical values of skin friction coefficient, local Nusselt number and Sherwood number. The magnitude of the skin friction coefficient decreases for larger values of R, G, ε and Ec. However, it increases when We, α and Pr are increased. It is noticed that the heat transfer at the wall $-\theta(0)$ increases for larger values of ε, G, Bi and it decreases for larger We, α, R and Ec. Table 2 shows that the local Sherwood number increases when radiation parameter R and Schmidt number Sc are increased.

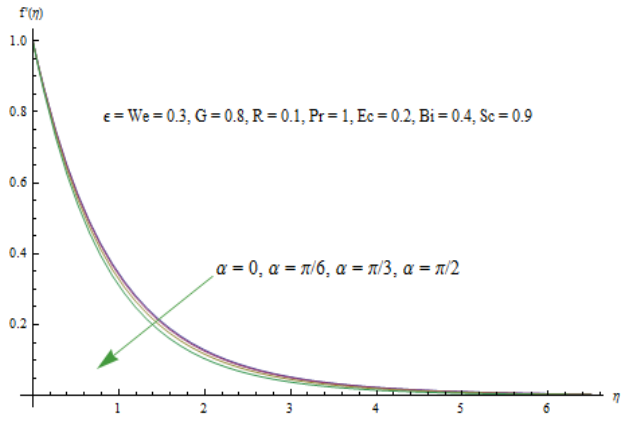

Fig. 4. Influence of α on $f'(\eta)$.

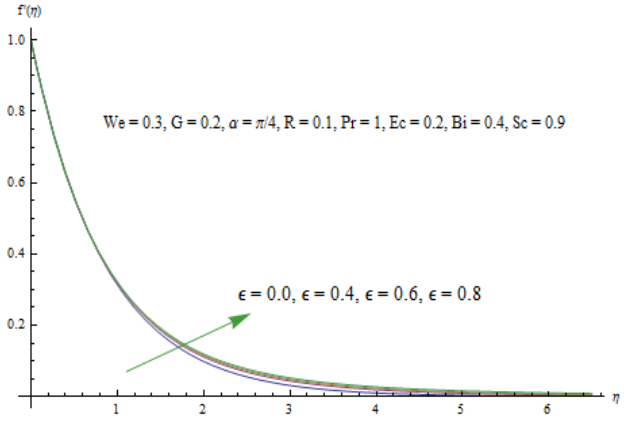

Fig. 5. Influence of ϵ on $f'(\eta)$.

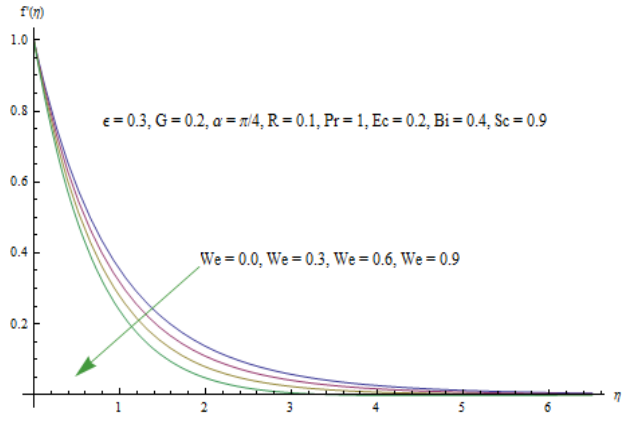

Fig. 6. Influence of We on $f'(\eta)$.

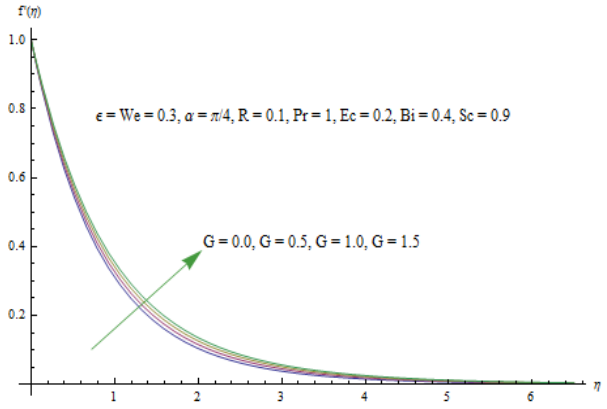

Fig. 7. Influence of Go n $f'(\eta)$.

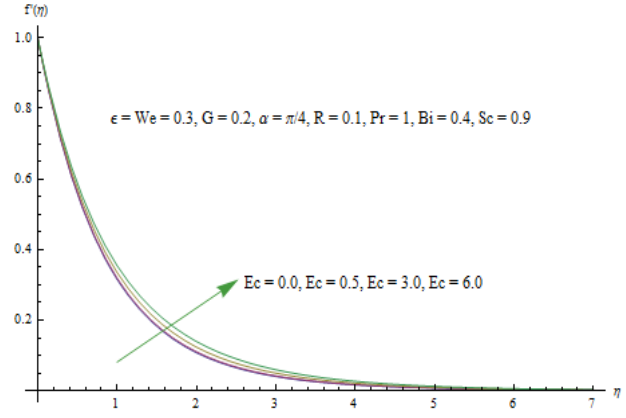

Fig. 8. Influence of E_c on $f'(\eta)$.

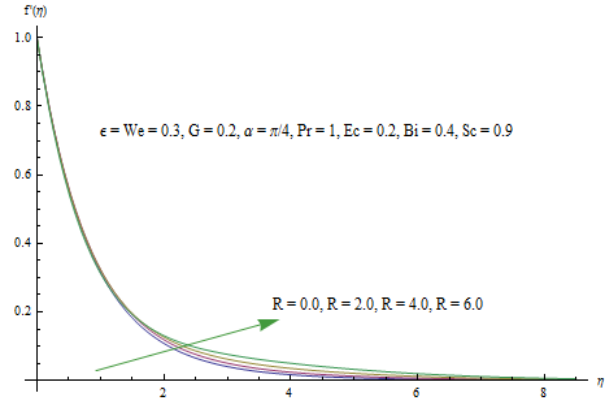

Fig. 9. Influence of R on $f'(\eta)$.

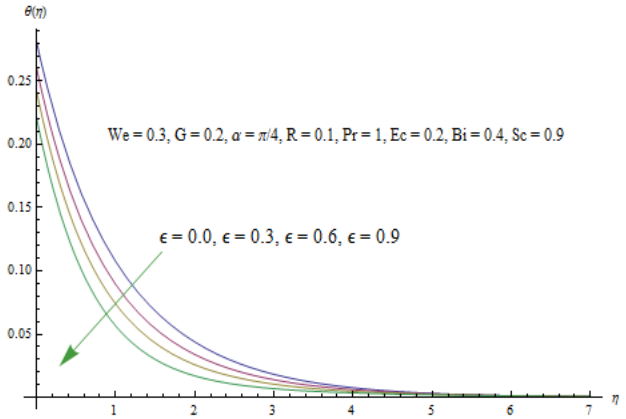

Fig. 10. Influence of ϵ on $\eta(\theta)$.

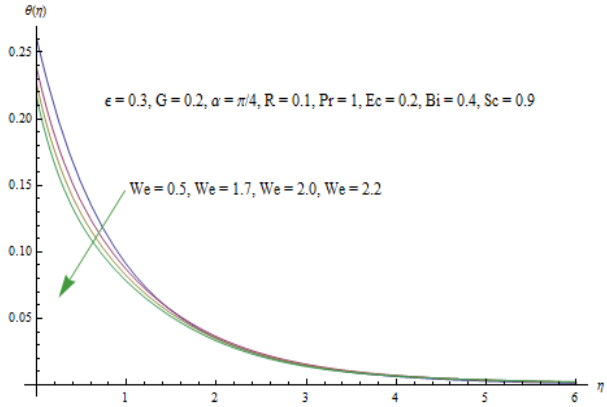

Fig. 11. Influence of We on $\eta(f)$.

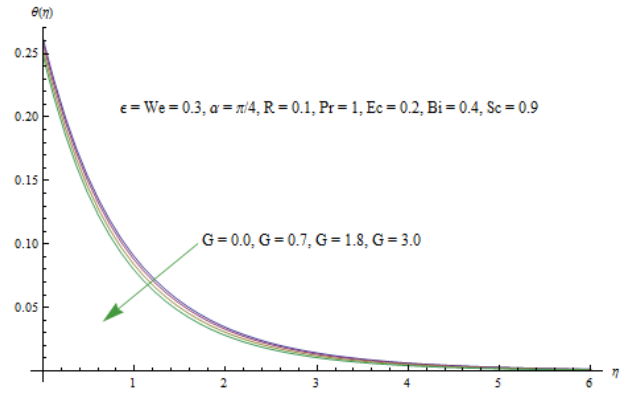

Fig. 12. Influence of G on $\eta(\theta)$.

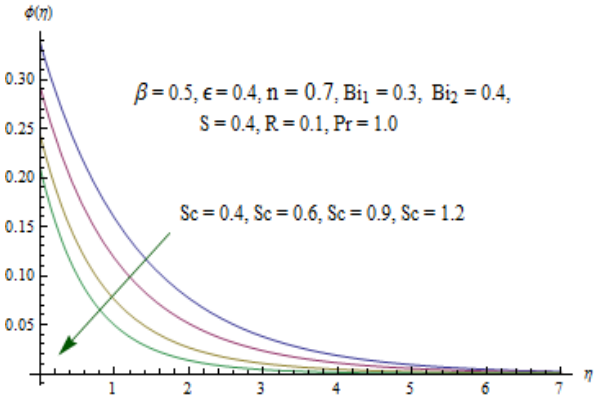

Fig. 13. Influence of α on $\eta(\theta)$.

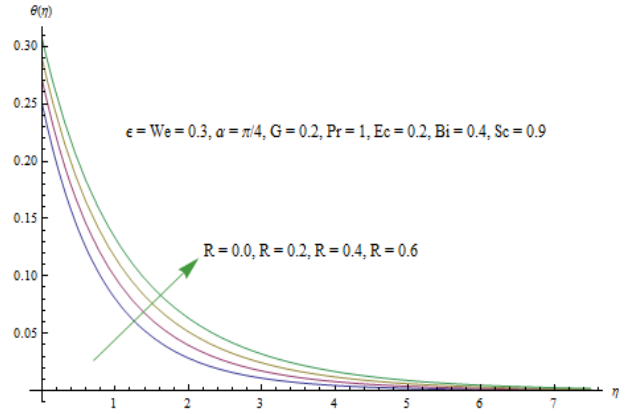

Fig. 14. Influence of R on $\eta(\theta)$.

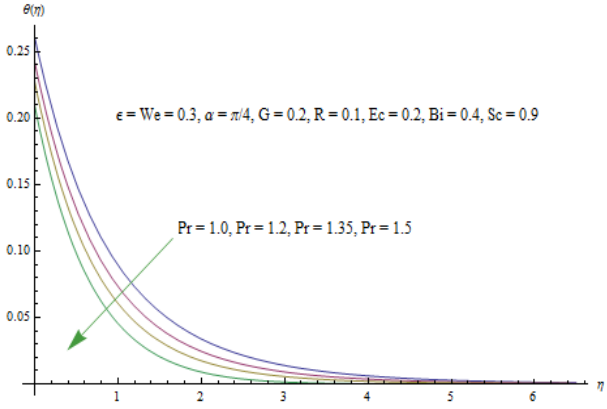

Fig. 15. Influence of Pr on $\eta(\theta)$.

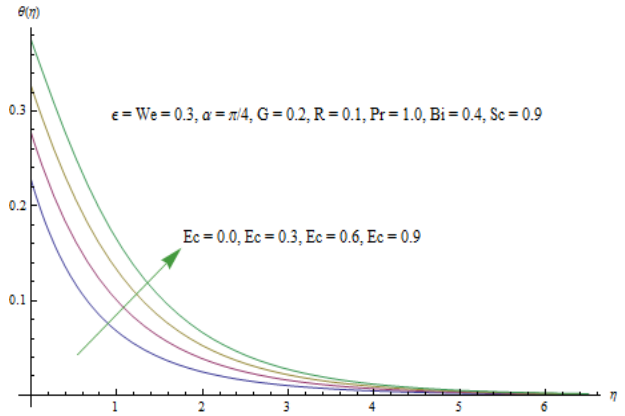

Fig. 16. Influence of E_C on $\eta(\theta)$.

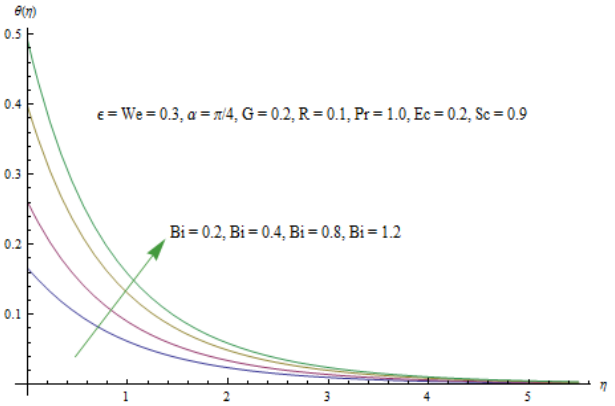

Fig. 17. Influence of Bi on $\eta(\theta)$.

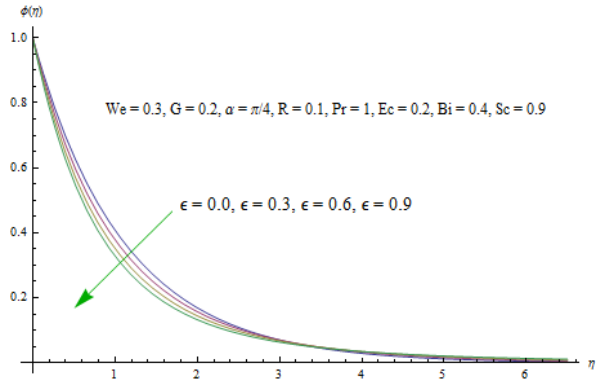

Fig. 18. Influence of ϵ on $\eta(\phi)$.

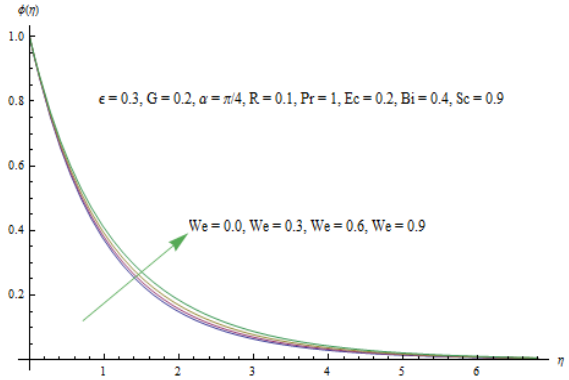

Fig. 19. Influence of We on $\eta(\phi)$.

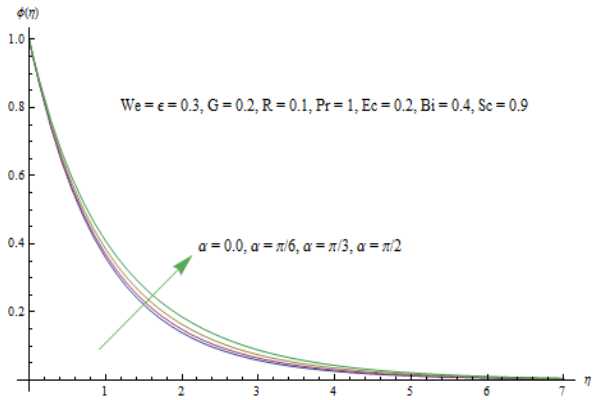

Fig. 20. Influence of α on $\eta(\phi)$.

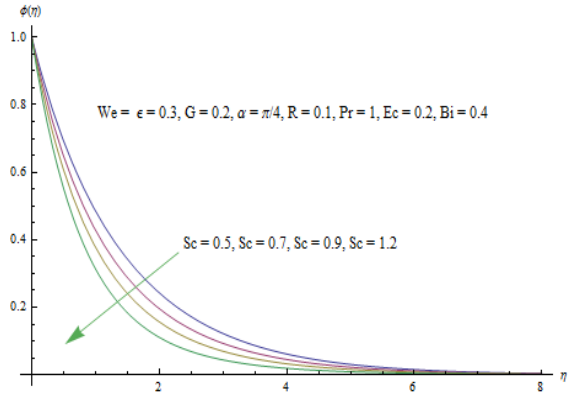

Fig. 21. Influence of Sc on $\eta(\phi)$.

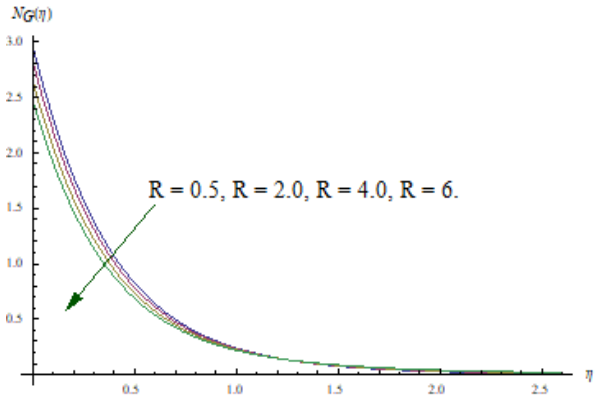

Fig. 22. Influence of R on $N_G(\eta)$.

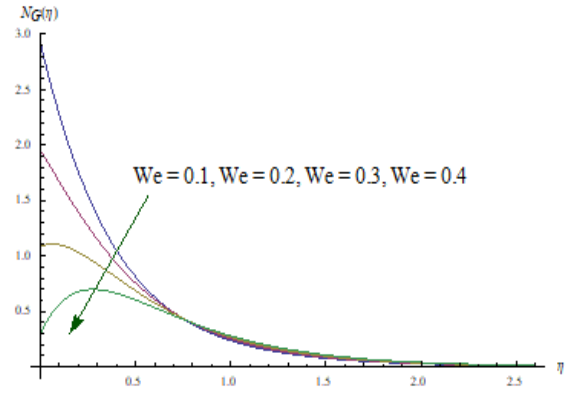

Fig. 23. Influence of We on $N_G(\eta)$.

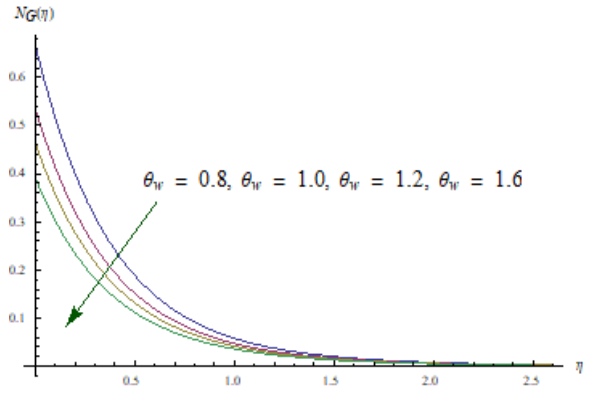

Fig. 24. Influence of θ_∞ on $N_G(\eta)$.

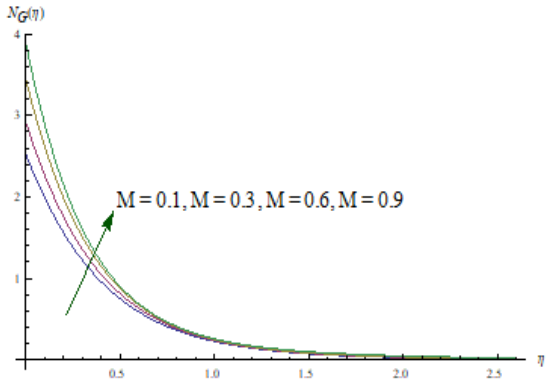

Fig. 25. Influence of M on $N_G(\eta)$.

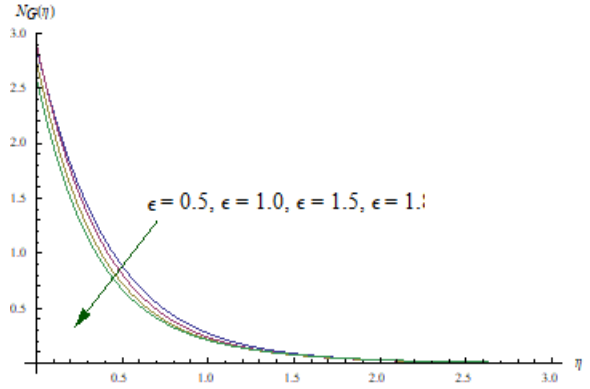

Fig. 26. Influence of ϵ on $N_G(\eta)$.

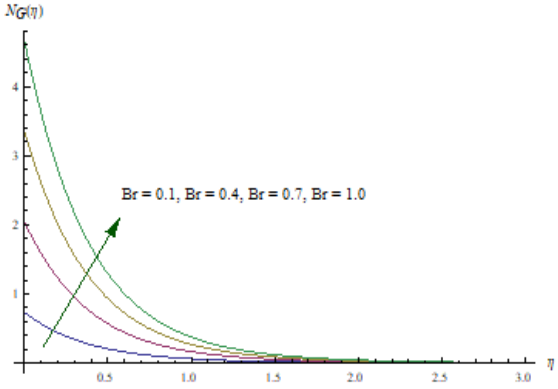

Fig. 27. Influence of Br on $N_G(\eta)$.

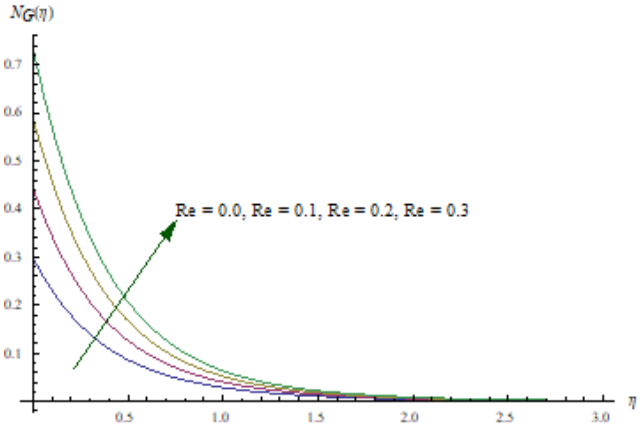

Fig. 28. Influence of Re on $N_G(\eta)$.

Table 1. Values of skin friction coefficient $Re_x^{1/2}C_f$ for the parameters ε, We, G, α, R, *Pr*, E_c, and *Bi*

ε	We	G	α	R	Pr	E_c	Bi	$-\frac{1}{2}Re_x^{1/2}C_f$
0.0	0.3	0.2	$\pi/4$	0.1	1.0	0.2	0.4	2.22135
0.2								2.13488
0.4								2.04054
0.3	0.0							1.08510
	0.2							1.73555
	0.4							2.46015
	0.3	0.0						2.12112
		0.2						2.08842
		0.4						2.05607
			0.0					2.07498
			$\pi/6$					2.08112
			$\pi/3$					2.09796
				0.0				2.09047
				0.3				2.08459
				0.6				2.07940
					0.5			2.07403
					0.9			2.08657
					1.1			2.08999
						0.0		2.09390
						0.3		2.08569
						0.6		2.07760
							0.2	2.09969
							0.6	2.07946
							1.0	2.06611

Table 2. Values of local Nusselt number $Nu/Re_x^{1/2}$ for the parameters ε, *We, G, α, R, Pr*, E_c E_c and *Bi*

ε	We	G	α	R	Pr	E_c	Bi	$-\left(1+\frac{4}{3}R\right)\theta'(0)$
0.0	0.3	0.2	$\pi/4$	0.1	1.0	0.2	0.4	0.286182
0.3								0.295144
0.6								0.301292
0.3	0.0							0.295985
	0.2							0.295379
	0.5							0.294885
		0.0						0.294608
		0.3						0.295403
		0.5						0.295907
			0.0					0.295359
			$\pi/6$					0.295261
			$\pi/3$					0.294989
				0.0				0.299395
				0.1				0.295144
				0.3				0.287178
					0.7			0.281292
					1.1			0.298509
					1.4			0.306404
						0.0		0.308526
						0.2		0.295144
						0.6		0.268771
							0.2	0.166532
							0.5	0.349078
							0.9	0.517163

Table 3. Values of local Sherwood number Sh for the parameters *R*, *We*, α and *Sc*.

R	We	α	Sc	$-\varphi'(0)$
0.0				0.94588
0.3				0.94707
0.9				0.94930
	0.0			0.96707
	0.2			0.95358
	0.3			0.94628
		0.0		0.94783
		$\pi/6$		0.94713
		$\pi/4$		0.94628
			$\pi/40.7$	0.87195
			0.9	0.94628
			1.1	1.14703

Main points

Boundary layer flow of MHD Walters' B liquid by an inclined stretching sheet is discussed in the presence of viscous dissipation and thermal radiation. The main observations are mentioned below:

- Velocity field $f'(\eta)$ is a decreasing function of parameter ε.
- Effects of ε on the temperature and concentration fields are qualitatively similar.
- Weissenberg number We decreases both the velocity and associated boundary layer thickness. Visible number contains viscoelasticity that produces tensile stress which contracts the boundary layer and consequently velocity decreases.
- Weissenberg number We increases the temperature and concentration fields. Velocity field f' is a decreasing function through larger α. On the other hand, when $\rightarrow$ changes from 0 to 2, i.e. when the sheet moves from vertical to horizontal direction, the strength of buoyancy force decreases and consequently the velocity and the boundary layer thickness decrease. Effects of Ec, G and R on velocity field are qualitatively similar. Physically this is because of increase in radiation parameter P, the rate of radiative heat transfer to the fluid increases. For Eckert number the kinetic energy increases by increasing Eχ and so the temperature profile increases.
- From physical point of view, the larger Prandtl number coincides with the weaker thermal diffusivity and thinner boundary layer. This is because a higher Prandtl number fluid has a relatively lower thermal conductivity which reduces conduction and thereby increases the variation of thermal characteristics. There is an enhancement of temperature for larger values of Eckert number E_c, thermal radiation R and Biot number Bi. It is due to the reason that stronger convective heating rises the temperature and thermal boundary layer thickness.
- Variations of ε and Sc on the concentration field are qualitatively similar.
- For a larger Schmidt number viscosity increases and concentration decreases.
- Magnitude of skin friction coefficient is a decreasing function of α, We, Ec and R.
- Influences of ε, G and Bi on the temperature gradient at the surface are qualitatively similar.
- The temperature gradient at the surface decreases when We, E_c and R are enhanced.
- Entropy generation boosts up with magnetic parameter, Reynolds number and Brinkman number, while the reverse behavior is observed for larger values of radiation parameter, temperature ratio parameter, unsteady parameter, and Weissenberg number.

Conflict of interest: *There is no conflict of interest.*

REFERENCES

1. M. R. Krishnamurthy, B. C. Prasannakumara, B. J. Gireesha, R. S. R. Gorla, *Eng. Sci. Tech., Int. J.*, **19,** 53 (2016).
2. N. Balazadeh, M. Sheikholeslami, D. D. Ganji, Z. Li, *J. Molec. Liqs.*, **260,** 30 (2019).
3. T. Hayat, A. Qayyum, F. Alsaadi, M. Awais, A. M. Dobaie, *European Phys. J. Plus*, **128,** 85 (2013).
4. C. Fetecau, A. M. Imran, A. Sohail, *Ann. Acad. Rom. Sci. Ser. Math. Appl.*, **6**, 74 (2014).
5. C. Fetecau, M. Rana, N. Nigar, C. Fetecau, *ZNA Physical Sci.*, **69,** 232 (2014).
6. M. Turkyilmazoglu, *Int. J. Mech. Sci.*, **77,** 263 (2013).
7. R. Ellahi, *Appl. Math. Modell.*, **37,** 1451 (2013).
8. M. Waqas, S. A. Shehzad, T. Hayat, M. I. Khan, A.

Alsaedi, *J. Phys. Chem. Solids*, **133.** 45 (2019).
9. T. Hayat, S. Asad, M. Qasim, A. A. Hendi, *Int. J. Num. Meth. Fluid*, **69,** 1350 (2012).
10. M. M. Rashidi, M. Ali, N. Freidoonimehr, B. Rostami, A. Hossian, *Adv. Mech. Eng*. **2014,** 10 (2014).
11. T. Hayat, M. Mustafa, S. Asghar, *Nonlinear Analysis: Real Word Appl.*, **11**, 3186 (2010).
12. S. Mukhopadhyay, K. Bhattacharyya, *J. Egyptian Math. Soc*., **12,** 229 (2012).
13. S. Mukhopadhyay, P. Ranjan De, K. Bhattacharyya, G. C. Layek, *Ain Shams Eng. J.*, **4**, 933 (2013).
14. K. Bhattacharyya, *Ain Shams Eng. J*., **4,** 259 (2013).
15. T. Hayat, S. Asad, M. Mustafa, A. Alsaedi, *Computer Fluid*, **108**, 179 (2015).
16. A. Bejan, Entropy generation minimization, New York, CRC press, 1996.
17. A. Bejan, Entropy generation through heat and fluid flow, Wiley, 1982.
18. M. M. Rashidi, S. Bagheri, E. Mamoniat, N. Freidoonimeh, *Ain Shams Eng. J.*, **8,** 77 (2017).
19. H. Sithole, H. Mondal, P. Sibanda, *Result in Physics*, **9**, 1077 (2018).
20. R. Naz, M. Noor, T. Hayat, M. Javed, A. Alsaedi, *Comm. Heat Mass Transfer*, **110**, 104431 (2020).
21. M. Turkyilmazoglu, *Int. J. Therm. Sci.*, **50,** 88 (2011).
22. M. Turkyilmazoglu, *J. Heat Transfer*, **137**, 71701 (2012).
23. M. Turkyilmazoglu, *Applied Math. Modell.*, **71**, 1 (2019).
24. B. J. Akinbo, B. I. Olajuwon, *Int. Commun. Heat Mass Transfer*, **121,** 105115 (2021).
25. M. I. Khan, M. Waqas, T. Hayat, A. Alsaedi, M. I. Khan, *Int. J. Hydrogen Energy*, **42,** 26408 (2017).
26. M. Turkyilmazoglu, *Int. J. Thermal Sci*., **50,** 2264 (2011).

Bulgarian Chemical Communications, Volume 53, Issue 3 (pp. 355 - 364) 2021 *DOI: 10.34049/bcc.53.3.5394*

Influence of blend wax additives on the properties of natural rubber composites containing 2,2,4-trimethyl-1,2-dihydroquinoline as antioxidant

P. A. Malinova, N. T. Dishovsky*

Department of Polymer Engineering, University of Chemical Technology and Metallurgy, 1756 Sofia, Bulgaria

Received: December 20, 2020, Revised: June 07, 2021

The paper presents our investigations on the influence of waxes on a very large number of properties of composites based on natural rubber and containing 2,2,4-trimethyl-1,2 dihydroquinoline (TMQ) as an antioxidant. The hypothesis of the present study is that by changing the composition of waxes, respectively wax blends (the ratio between the microcrystalline and the macrocrystalline part) one can control their impact on the properties of rubber mixtures and vulcanizates containing TMQ as antioxidant. Different properties of the composites were studied - rheological, vulcanization, physicomechanical (stress at 100 and 300% deformation, tensile strength, elongation at break, Shore A hardness, tear resistance, etc.), abrasion resistance, thermal and light aging resistance. The combination of TMQ with an optimized mixture of paraffin and microcrystalline waxes can be used successfully for the production of rubber items for various purposes.

Keywords: natural rubber-based composites; wax blends; 2,2,4-trimethyl-1,2-dihydroquinoline; gas chromatographic characterization

INTRODUCTION

For a long time, waxes have been used as additives in rubber processing. They have turned to be cost-effective in terms of internal lubrication energy efficiency; acceleration of the mixing process, improvement of the flow of mixtures and release from matrices. In addition, the elastomeric macromolecules of all rubber compounds based either on natural rubber, butadiene styrene rubber or butadiene acrylonitrile rubber have unsaturation spots (mainly double bonds) which are attacked by atmospheric oxygen, ozone and UV rays [1]. Paraffin and blends being of adaptive molecular structure, are ideal for use as protection against atmospheric influences in rubber processing industry. The migration properties of the former provide continuous oxidative, ultraviolet and ozone protection of finished rubber products [2]. That is why wax blends are a mandatory ingredient in compounds for the production of a number of rubber articles inclusive tire treads.

According to their structure, waxes are divided into macrocrystalline (paraffin) and microcrystalline (ceresin).

Macrocrystalline waxes consist almost entirely of saturated normal hydrocarbons and small amounts of branched hydrocarbons. They are transparent or white in color, hard, shiny and brittle and form large crystals. They differ in melting temperature (relatively low (45-65 ºC)), as well as in the oil content. The number of carbons in their chains ranges from 18 to 50 carbons (commercial paraffins are mostly in the 22 to 38 range) [2].

Microcrystalline waxes are opaque, soft, plastic, sticky and amorphous. They have a higher melting point (65-100ºC). The crystals they form are irregular in shape and small in size. Microwaxes contain significant amounts of branched and cyclic hydrocarbons which distinguish them from paraffins and give them different properties. Microcrystalline waxes have molecular weight higher than that of paraffins with a number of carbons between 30 and 80. The majority have between 45 and 55 carbons [3].

However, wax blends are most commonly used in the rubber processing industry. These are blends of macrocrystalline and microcrystalline waxes. Usually the macrocrystalline wax predominates, the microcrystalline being present at 30% or less. These waxes are formulated so that specific results are achieved, namely tailoring the specific influence on the properties of the elastomeric composites that contain them. The main reason for using wax blends can be stated as follows: To protect the rubber, there must be a wax film present on the surface of the rubber regardless of the ambient temperature. On the other hand, depending on molecular weight and structure, each wax has an optimum temperature at which it will migrate on the surface and form a film [4, 5]. These two requirements (to migrate and to form a film) are met easier, if wax blends are used rather than individual waxes. 2,2,4-Trimethyl-1,2-dihydroquinoline (TMQ) is a very important category of rubber antioxidants (Fig. 1). It has a good

* To whom all correspondence should be sent:
E-mail: dishov@uctm.edu

© 2021 Bulgarian Academy of Sciences, Union of Chemists in Bulgaria

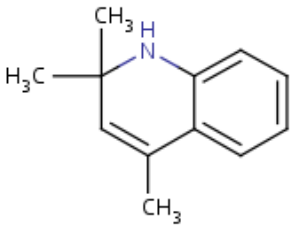

Fig. 1. Structural formula of TMQ

protective effect against heat and oxygen and a stronger inhibitory effect against metal catalytic oxidation, used widely in the manufacture of tyres, different technical rubber goods, adhesive tape, cables, etc. TMQ has limited to medium-strength activity as an antiozonant, medium effectiveness as an anti-fatigue agent, and low effectiveness against crack growth [6].

In this regard, the thesis of the present study is that changing the composition of waxes, respectively wax blends (the ratio between the microcrystalline and macrocrystalline part) we can control the impact of those blends onto the properties of rubber mixtures and vulcanizates containing TMQ as antioxidant, and thus enhance their effectiveness as antiaging agents.

The aim of the present work is to study how the composition of various wax blends, evaluated by the amount of normal and branched iso-hydrocarbons in them, affects a significant number of properties of natural rubber-based composites containing TMQ as an antioxidant. The evaluation can also be made by the number of carbon atoms in the normal and iso-hydrocarbons present in the largest quantities in the wax blends, according to data from their gas chromatographic characterization.

Other authors [4, 7] have also investigated the influence of waxes on a very large number of properties of natural rubber-based composites (rheological, vulcanization, physicomechanical (stress at 100 and 300% deformation, tensile strength, elongation, Shore hardness, tear resistance, fatigue during cyclic deformations, etc.). In [4] the authors came to the conclusion that the optimal properties are achieved by combining paraffin and microcrystalline waxes. In [7], only the individual influence of paraffinic hydrocarbons on the properties listed above was studied. It was compared with the influence of an antioxidant from the group of p-phenylenediamines. In [8] the individual influence of an antioxidant from the group of p-phenylenediamines on a very large number of composite properties was compared to that of TMQ. The effect was demonstrated to be dependent on the concentration of the antioxidants and on the time of their mixing with the elastomeric matrix.

We did not find anything like our study in the literature.

EXPERIMENTAL

Materials

Natural rubber TSR-10, made in Thailand, was used as an elastomeric matrix. Its strictly standardized content of non-rubber substances is given in Table 1.

Table 1. Characteristics of natural rubber TSR-10 used.

Parameters	Value
Mechanical impurities, % by mass	not more than 0.10
Ash content, % by mass	not more than 0.75
Nitrogen, % by mass	not more than 0.6
Volatile substances, % by mass	not more than 0.8
Plasticity retention index (PR)	not less than 50
Wallace plasticity	not less than 30

Furnace carbon black N 220, produced in Russia, was used as a filler of the rubber composites. The other ingredients were stearic acid, zinc oxide, N-tert-butyl-2-benzothiazolylsulfenamide (TBBS) with a density of 1.29 g/cm^3 and a melting point of 105°C; diphenylguanidine - DPG (medium active vulcanization accelerator with a density of 1.19 g/cm^3 and a melting point of 145 ºC); sulfur, processing oil, 1,2-dihydro-2,2,4-trimethylquinoline (TMQ). Blends of different individual brands of paraffin and microcrystalline waxes, manufactured by Evricom Ltd., Bulgaria, with the compositions and characteristics shown in Tables 2 and 3, were used as additives.

Table 2. Characteristics of the individual wax brands used.

Product	Type of the wax	Melting point, °C	Oil content, %	Penetration, 0.1 mm
E4	paraffin	53-55	0.5-0.8	18-20
E57	paraffin	55-57	1.0-1.5	30-36
E58	paraffin	58-60	0.3-0.5	17-19
E62	paraffin	60-64	0.5-0.7	14-16
EC35	microcrystalline	76-78	2.0-3.0	30-35

Table 3. Compositions of the wax blends used.

Sample	E4 %	E57 %	E58 %	E62 %	EC35 %
1	-	20	30	30	20
2	-	-	-	70	30
3	-	-	80	-	20
4	-	80	-	-	20
5	80	-	-	-	20

Table 4. Compositions of natural rubber-based compounds - TSR-10 (all ingredients are in parts by weight per 100 parts by weight of rubber).

Compounds / Ingredients	NR-0	NR-1	NR-2	NR-3	NR-4	NR-5
NR (TSR-10)	100	100	100	100	100	100
Carbon black N 220	50	50	50	50	50	50
Wax blend 1	-	1	-	-	-	-
Wax blend 2	-	-	1	-	-	-
Wax blend 3	-	-	-	1	-	-
Wax blend 4	-	-	-	-	1	-
Wax blend 5	-	-	-	-	-	1
Processing oil	3	3	3	3	3	3
TMQ	1	1	1	1	1	1
Stearic acid	2	2	2	2	2	2
ZnO	5	5	5	5	5	5
Sulfur	1.2	1.2	1.2	1.2	1.2	1.2
TBBS	0.95	0.95	0.95	0.95	0.95	0.95
DPG	0.35	0.35	0.35	0.35	0.35	0.35

NR-0 denotes the rubber of the compound and the vulcanizate, which do not contain a wax mixture, but only TMQ antioxidant.

Production of rubber compounds

The rubber compounds were made on an open laboratory rubber mixer (two-roll mill) with dimensions: L/D 320×160 mm and friction 1.27 (non-dimensional). The speed of the slower rotating roll was 25 min^{-1}. The finished compound was removed from the rollers in the form of a sheet and left to stay for 24 hours before being vulcanized.

Basic compositions

Table 4 shows the compositions of the tested natural rubber based compounds.

Vulcanization procedure

The test specimens were vulcanized on a hydraulic press with electric heating at a temperature of 150 °C. Vulcanization was performed in the vulcanization optimums for each compound determined using an MDR 2000 oscillating disk vulcameter (Alpha Technology) by applying a pressure of 10.0 MPa. The obtained sheets of vulcanizates had dimensions of 150×150×2 mm.

Test methods

Determination of the quantitative composition of hydrocarbons in the used wax mixtures according to ASTM D 5442. The quantitative method was used to determine the content of hydrocarbons with a chain length from C17 to C44 included in the composition of the macro- and microcrystalline waxes and their mixtures. The method is based on gas chromatographic determination using an internal standard and a flame ionization detector. A gas chromatograph with Agilent 6850 flame ionization detector and specialized Clarity software for electronic data processing was implemented.

Determination of vulcanization characteristics. The vulcanization characteristics of the investigated rubber compounds were determined on an oscillating disk vulcameter MDR 2000 (Alpha Technologies Inc.), according to the standard of ISO 3417: 2010.

Determination of the physicomechanical parameters of the studied vulcanizates

Determination of Shore A hardness. The Shore A hardness of the test bodies was determined 24 hours after vulcanization using a portable Mitotoyo hardness tester of the company according to ISO 7619-1: 2012. The forced penetration into the material of a special nozzle under certain conditions was measured.

Determination of strength-elastic properties in the course of tensile deformation. 24 hours after vulcanization, double-sided blades (dumbbells) were cut from the test specimens on a punch press with a standard-shaped knife. A micrometer with an accuracy of 0.01 mm was used to set the dimensions of the blades. The stresses at 100 and 300% elongation, tensile strength and elongation at break was determined on a dynamometer at a movable jaw speed of 500 mm/min, according to ISO 37: 2008.

Determination of the residual elongation at tensile deformation. The measurement of the residual elongation in the working area of the samples was performed 1 min after rupture. The two parts of the torn dumbbells were joined and the length of the working section was measured. The residual elongation is calculated from the experimental results by the equation:

$$E_{res.} = \{(\ell_2 - \ell_0) / \ell_0\}.100, \% \quad (1)$$

where: $\varepsilon_{res.}$ - residual elongation, %; ℓ_0 - length of the working section before deformation, cm; ℓ_2 - length of the working section one min after the rupture, cm.

Determination of tear resistance according to ISO 34-1:2012

Determination of resistance to accelerated thermal aging. The resistance to thermal aging was determined in a thermal cabinet with forced air circulation according to ISO 188: 2009. The samples were heated at 70 °C for 72 hours. The "minus" sign in front of the aging coefficient (%) indicated the decrease of the respective mechanical parameters in percent.

The aging coefficients are calculated by the formula:

$$K = [(B-A) / A] .100, \% \quad (2)$$

where: B - value of the studied indicator after aging; A - value of the studied indicator before aging.

Determination of resistance to light aging

Artificial aging was performed in an ILKA Feutron 3001 climate chamber (Germany) with illumination of ultraviolet light for 320 h at 30 °C.

Determination of the abrasion of the studied vulcanizates

Determination of abrasion was performed by means of a device with a rotating cylindrical drum. The method consists in determining the reduction of the volume of a test vulcanizate body under the influence of friction with a certain type of sandpaper (abrasive).

A cylindrical vulcanizate test body with a diameter of 16 mm and a height of 8 mm was exposed to abrasive fabric (sandpaper) with a certain degree of abrasiveness (sandpaper coefficient) at a certain contact pressure on a certain area. The mass loss of the test piece was determined and the reduction in volume was calculated by the density of the material using the equation:

$$\Delta V = \frac{m_0 - m}{\rho.b}.1000 \text{ , mm}^3 \quad (3)$$

where: ΔV - reduction of the volume (erasability) of the working body, mm^3; m - mass of the working body after erasing, g; m_0 - mass of the working body before erasing, g; b - coefficient of sandpaper; ρ-density of the test specimen.

The density of the test specimens was determined by the formula:

$$\rho = \frac{G}{G - (G_1 - G_2)}.\rho_0 \text{ , g/cm}^3 \quad (4)$$

where: G - mass of the test body, g; G_1 - mass of the test piece attached to a needle in water, g; G_2 - the mass of the needle immersed in water; ρ_0 - density of the liquid in which the test body is immersed (in this case water), g/cm^3.

RESULTS AND DISCUSSION

Gas chromatographic determination of the composition of hydrocarbons in the studied wax blends

The composition of hydrocarbons in the tested wax blends is presented in Table 5.

Table 5. Quantitative composition of hydrocarbons in the used wax blends according to data from gas chromatographic analysis.

Sample	N[1] %	ISO[2] %	Max N[3]	Max ISO[4]
1	76	24	27-28	37-38
2	66	34	31-32	34-35
3	63	37	32-33	36-37
4	83	17	26-27	30-31
5	78	22	29-30	31-32

Notes: [1] Quantity of normal hydrocarbons, %; [2] Quantity of iso-hydrocarbons, %; [3] Number of atoms in normal hydrocarbons contained in the largest quantities; [4] Number of atoms in iso-hydrocarbons contained in the largest quantities.

Vulcanization characteristics of elastomeric composites containing wax blends

As seen from Fig. 2, as the amount of normal hydrocarbons in the wax blend increases, the minimum torque gradually decreases. The minimum

torque is related to the effective viscosity of the mixtures. It is obvious that the greater the amount of normal hydrocarbons, the fewer are the branched iso-structures that can cause an increase in viscosity because they hinder the flow of mixtures. As the number of atoms in the normal and iso-hydrocarbons present at maximum amounts in the wax blends increases, the viscosity gradually increases, what can be explained by the increase in the molecular weight of the wax blends, also causing a slower flow. In the case of iso-hydrocarbons, the effects are somewhat more pronounced because the number of atoms in the chains, their molecular weights, respectively, are higher than normal hydrocarbon chains (30-38 *vs*. 26-33). Rubber viscosity is influenced by various factors such as mixing time [9], mixing temperature [10], filler type, filler loading [11, 12] and chemical curatives [13]. This study showed that the addition of small amounts (1 phr) of wax blends into the natural rubber composites has also a noticeable effect on the viscosity depending on their composition, in particular on the ratio between normal and iso-hydrocarbons, and the number of carbon atoms present in them in the largest quantities.

As Fig. 3 shows, the higher amounts of normal hydrocarbons lead to a shorter optimal vulcanization time, i. e. vulcanization is accelerated and proceeds at a higher rate. As the number of atoms in the hydrocarbon chains of both normal and iso-carbons present at maximum amounts increases, the optimal vulcanization time is prolonged. The observed effects may be related to the effect that wax blends have on the access of vulcanizing agents and accelerators to the elastomeric macromolecules. Increasing the number of branched structures and the number of carbon atoms, obviously makes this access difficult, and hampers the migration, which in turn slows down vulcanization. The effect of waxes on the optimal time of vulcanization has been confirmed also by other authors [7].

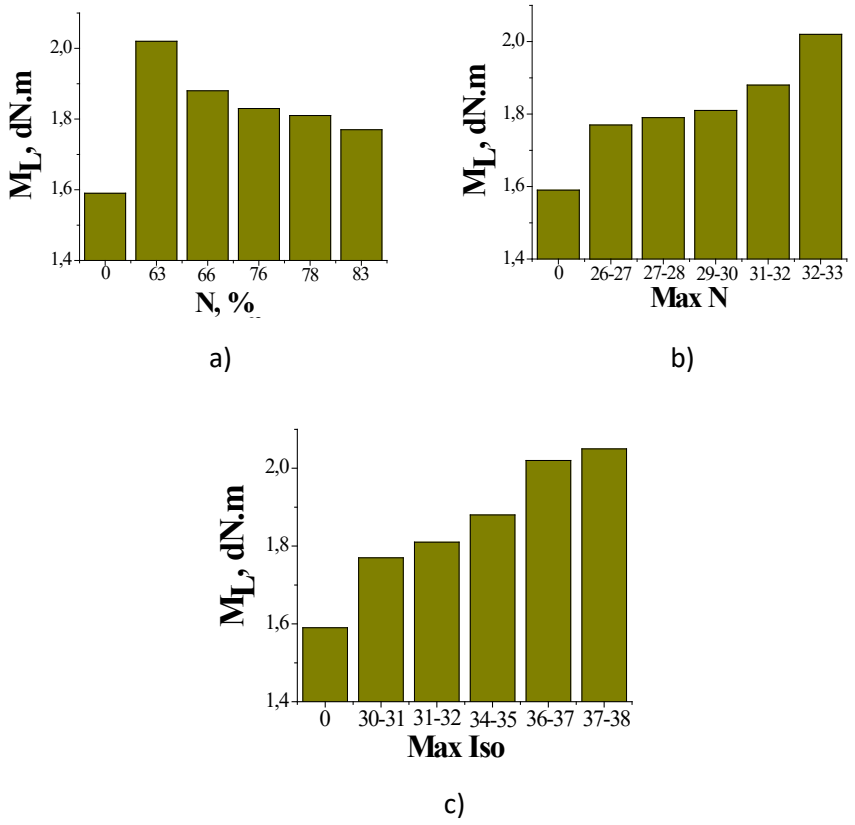

Fig. 2. Dependence of the minimum torque of the tested rubber compounds on: a) the amount of normal hydrocarbons in the composition of the wax blends (N); b) the number of atoms in the normal hydrocarbons contained at maximum amounts in the wax blends; c) the number of atoms in the iso-hydrocarbons contained at maximum amounts in the wax blends.

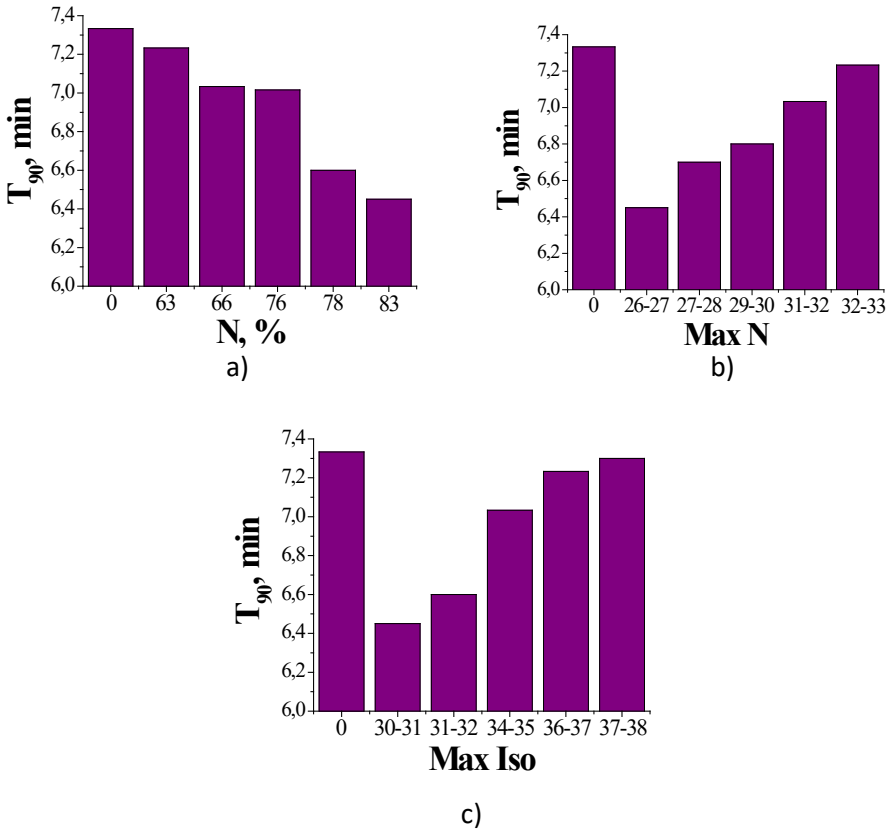

Fig. 3. Dependence of the optimal time of vulcanization of the studied rubber mixtures on: a) the amount of normal hydrocarbons in the composition of the wax blends (N); b) the number of atoms in the normal hydrocarbons contained at maximum amounts in the wax blends; c) the number of atoms in the iso-hydrocarbons contained in maximum amounts in the wax blends.

Physicomechanical parameters of the studied composites

The results presented in Fig. 4 demonstrate that, as expected, the wax blends at the amounts of 1 phr used do not have a noticeable effect on the studied physicomechanical parameters. The values are comparable, the differences being less than 10%.

Tear resistance of the studied composites containing various wax blends

The influence of the wax blends on the tear resistance of the studied composites is shown in Fig. 5. As seen from the figure, with increasing the amount of normal hydrocarbons, the tear resistance decreases, and with increasing the number of atoms in the carbon chains, both normal and iso-, there is a tendency to increase. A crossing through a slightly pronounced optimum is observed in the latter cases. In our opinion, this is due to the different ability of different wax blends to migrate. In general, the presence of wax blends in the elastomeric matrix probably has a certain plasticizing effect, which provides some possibility for mobility of the elastomeric macromolecules relative to each other under the conditions of applied external tear force. The faster migration of normal hydrocarbons to the surface complicates the manifestation of this effect and therefore, with increasing their amount the tear resistance decreases, as the composite depletes the plasticizing agent. As the number of atoms in the hydrocarbon chains present at the maximum amount in the wax blends increases, the migration is hampered due to the increase in their molecular weight, which creates greater opportunities for manifestation of their plasticizing effect. That leads to an increase in the resistance of tearing.

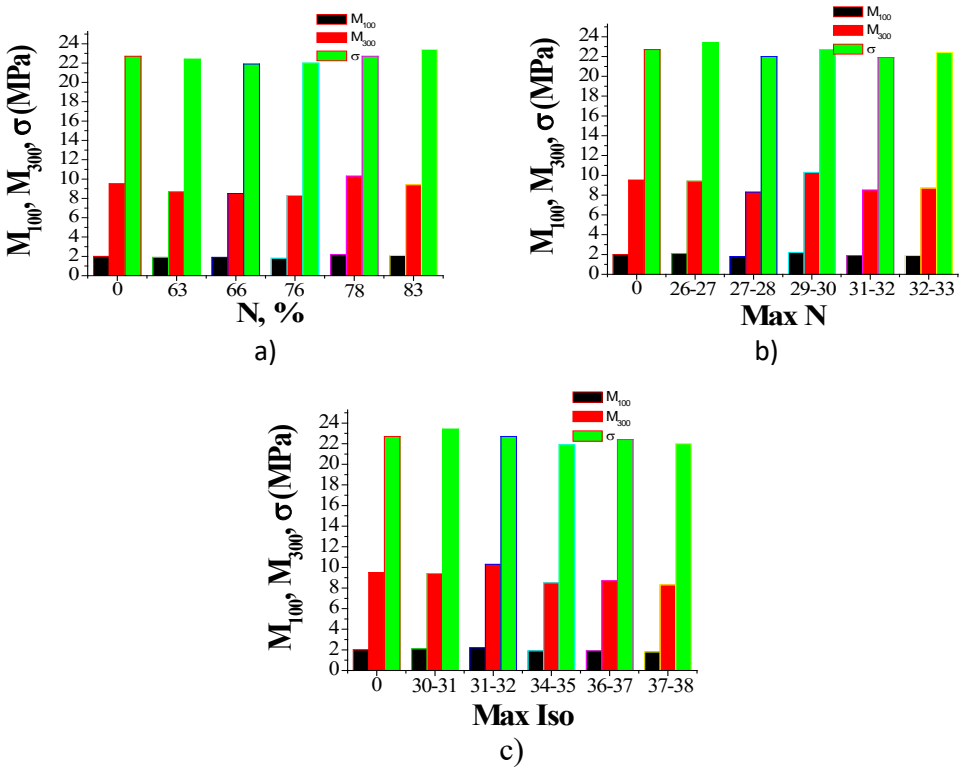

Fig. 4. Dependence of physicomechanical parameters (M100-module at 100% deformation, MPa; M300-module at 300% deformation, MPa; σ-tensile strength, MPa) of the studied vulcanizates on: a) the amount of normal hydrocarbons in the composition of the wax blends (N); b) the number of atoms in the normal hydrocarbons contained at maximum amounts in the wax blends; c) the number of atoms in the iso-hydrocarbons contained at maximum amounts in the wax blends.

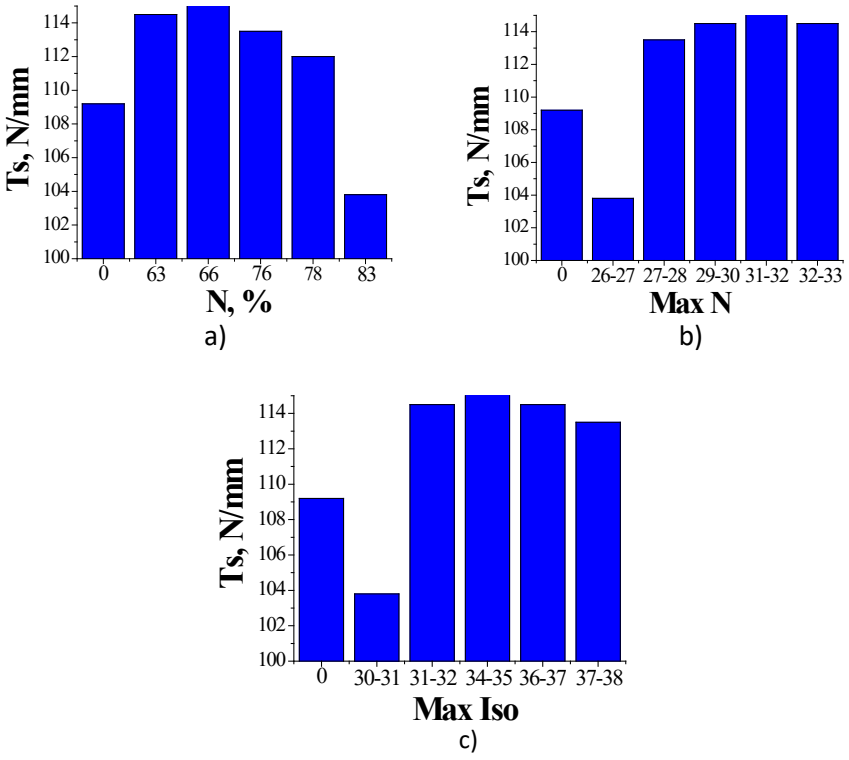

Fig. 5. Dependence of the tear resistance of the studied vulcanizates on: a) the amount of normal hydrocarbons in the composition of the wax blends (N); b) the number of atoms in the normal hydrocarbons contained in maximum amounts in the wax blends; c) the number of atoms in the iso-hydrocarbons contained in maximum amounts in the wax blends.

Abrasion resistance of the studied composites containing different wax blends

The influence of the wax blends on the abrasion resistance of the studied composites is shown in Fig. 6. Here again, the observed effects can be explained by the migration of the wax blends, though in the opposite way to the tear resistance described. The rapid release of waxes to the surface has a lubricating effect, which reduces abrasion and it becomes much lower for normal hydrocarbons, especially with increasing their amounts. The slower migration process and the release of the wax mixtures on the surface with the increase of the molecular weight, and the amount of branched hydrocarbons reduces the lubrication effect during abrasion, hence the abrasion is greater. This statement is proved by the fact that the highest abrasion in all cases undergo composites in which there are no wax blends.

It is well known that the heterocyclic nitrogen-containing stabilizer TMQ is a classical antioxidant of high efficiency. In all the vulcanizates studied, it is present at the same amount, being combined with different wax mixtures, except for the control sample. Therefore, we believe that the different results for the parameters studied are mainly due to the synergetic effect of TMQ and the combination of waxes of different composition and structure, and not to the antioxidant itself.

Aging resistance of the studied composites containing different wax blends

Tables 6 and 7 summarize the results of thermal and light aging of the studied elastomeric composites.

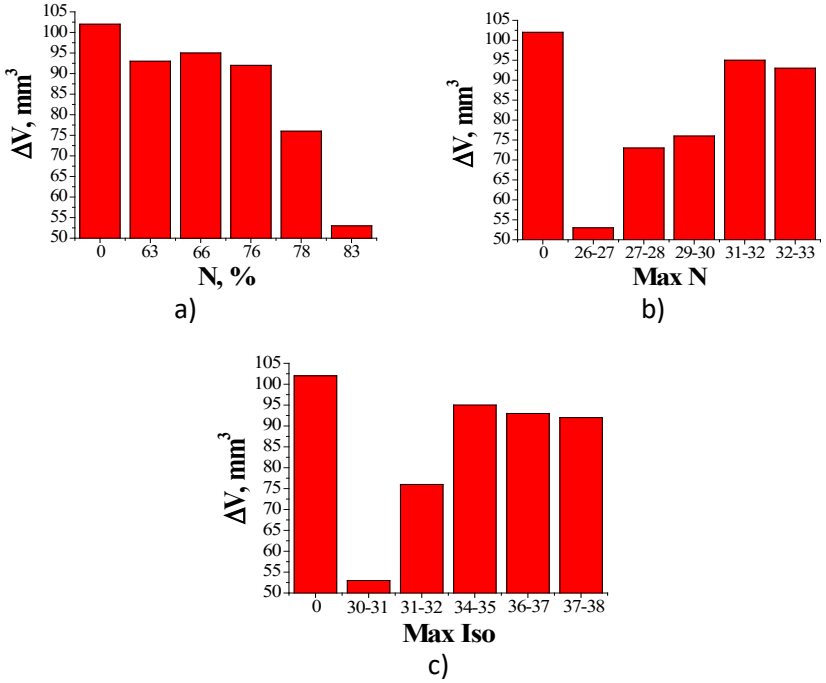

Fig. 6. Dependence of the abrasion resistance of the studied composites on: a) the amount of normal hydrocarbons in the composition of the wax blends (N); b) the number of atoms in the normal hydrocarbons contained at maximum amounts in the wax blends; c) the number of atoms in the iso-hydrocarbons contained at maximum amounts in the wax blends.

Table 6. Change in thermal aging coefficients (K_ε, %) with respect to elongation (70 °C, 72 h) depending on the amount of normal hydrocarbons in the composition of the wax blends N (a); depending on the number of atoms in the normal hydrocarbons present at maximum amounts in the wax blends (b); and depending on the number of atoms in the iso-hydrocarbons present at maximum amounts in the wax blends (c).

a) N	Kε, %	b) Max N	Kε, %	c) Max Iso	Kε, %
0	-15.6	0	-15.6	0	-15.6
63	-4.8	26-27	-9.1	30-31	-9.1
66	-5.4	27-28	-6.5	31-32	-6.5
76	-6.3	29-30	-6.3	34-35	-4.8
78	-6.5	31-32	-5.4	36-37	-5.4
83	-9.1	32-33	-4.8	37-38	-6.3

Table 7. Change in light aging coefficients with respect to elongation (320 hours) depending on the amount of normal hydrocarbons in the composition of the wax blends N (a); depending on the number of atoms in the normal hydrocarbons present at maximum amounts in the wax blends (b); and depending on the number of atoms in the iso-hydrocarbons present at maximum amounts in the wax blends (c).

a) N	Kε, %	b) Max N	Kε, %	c) Max Iso	Kε, %
0	-3.5	0	-3.5	0	-3.5
63	3.7	26-27	-2.2	30-31	-2.2
66	6.0	27-28	-2.9	31-32	3.2
76	3.2	29-30	3.2	34-35	6.0
78	-2.2	31-32	3.7	36-37	3.7
83	-2.9	32-33	6.0	37-38	-2.9

Table 6a shows that with increasing the amount of normal hydrocarbons in the wax mixtures, aging accelerates. That may be due to an increase in the migration of waxes to the surface, which is also accelerated, but the resulting protective film is increasingly ineffective due to the declining amount of iso-hydrocarbons in it. With increasing the molecular weight of normal hydrocarbons as a result of the increasing the number of atoms, their migration to the surface is lessened, the presence of waxes in the volume of the composite hinders oxygen access to the elastomeric macromolecules and aging processes take longer (Table 6b). It is also obvious that there is an optimum in the molecular weight and the number of atoms in the carbon chains of the iso-hydrocarbons, as well as an optimal ratio between normal and iso-hydrocarbons, respectively, between their molecular masses and the number of atoms in them. That ensures maximum protective effectiveness of the film formed as a result of their migration to the surface of the vulcanizate (Table 6c).

The explanation of the observed effects is analogous to that of the effects of thermal aging with the peculiarity that here the effects of aging are much less pronounced, mainly due to the presence of furnace carbon black in the composites. The filler is known to be an effective absorber of ultraviolet light and to increase the resistance to light aging. Another feature that makes a strong impression is that the highest protective efficiency in light aging was observed at the same ratio between normal and iso-hydrocarbons, respectively, the number of atoms in their chains, which is also observed in thermal aging.

The interpretation of the obtained results can be summarized as follows:

- The greater the number of atoms in the hydrocarbon chain, the higher the molecular weight, the higher is the melting point and the higher is the ambient temperature required for the migration and so called blooming of the wax blends on the surface of the rubber product. It should be kept in mind that while paraffin waxes can be said to have a relatively clearly defined melting point, microcrystalline waxes do not have such a clearly defined melting point due to their wider molecular weight distribution. That is why the so-called drop point temperature is often used for their characterization [3].

- The movement (migration) of the waxes to the surface of the rubber product depends on the following factors:

• Molecular weight or the number of carbon atoms in the wax, respectively. The higher they are, the higher is the ambient temperature needed to ensure sufficient mobility for migration [3].

• Branched waxes migrate and bloom slower [3].

•The concentration of wax in the rubber product. After crossing the solubility threshold, the more wax present in the composite, the greater is the concentration gradient to the surface, which will stimulate migration to a higher degree [7].

•Higher ambient temperatures increase the solubility of waxes and increase migration, especially of higher molecular weight waxes.

The waxes that migrate and bloom the most are paraffin waxes. Microcrystalline waxes are too bulky to bloom and to create an effective protective film. However, studies have shown [3, 7] that microcrystalline waxes play another extremely important role in wax mixtures: when paraffin waxes reach the surface, they create a highly crystalline and inelastic film with poor adhesion. In this large-crystal structure, "holes" are formed, which allow air to penetrate freely through them and reach the rubber products. Adding a small but optimal amount of branched (microcrystalline) waxes to the paraffins creates a more amorphous, much finer crystalline protective film on the surface, which is already impermeable to air. The reduction of the film crystallinity due to the presence of microcrystalline waxes in it also makes it more elastic. This more elastic film is no longer so fragile and does not break down so easily, i.e. it is more durable. In addition, the microcrystalline wax has a higher adhesion to the elastomeric surface than the paraffin wax, which

also contributes to the creation of a longer lasting wax film on it. Therefore, the most commonly used wax blends should contain several paraffin waxes of different molecular weight in combination with a small amount of microcrystalline wax. In order to achieve maximum efficiency and optimal properties, the ratio between paraffin and microcrystalline waxes, as well as the number of carbon atoms in the normal and iso-hydrocarbons present in maximum amounts in them must be optimized.

CONCLUSION

The composition of wax blends containing paraffin and microcrystalline waxes, as well as the number of carbon atoms in the hydrocarbons present in maximum quantities in the blends, affect a number of properties of elastomeric composites, as follows:

1. As the amount of normal hydrocarbons in wax mixtures increases, vulcanization is accelerated, and as the number of atoms in the hydrocarbon chains of both normal and iso-carbons present at maximum amounts increases, vulcanization is retarded.

2. The wax blends at the used amounts of 1 phr do not have a noticeable effect on the studied physicomechanical parameters and the values are comparable, the differences being less than 10%.

3. With increasing the amount of normal hydrocarbons in the wax blends, the tear resistance decreases, and with increasing the number of atoms in the hydrocarbon chains, both normal and iso-, there is a tendency of increasing the values of this parameter.

4. All tested vulcanizates containing waxes and TMQ exhibit better resistance to thermal aging compared to the control sample which contains only TMQ as an antioxidant. As the amount of normal hydrocarbons in wax blends increases, aging accelerates. With the inclusion in molecular weight of normal and iso-hydrocarbons the aging process is prolonged.

5. The observed effects of light aging are similar to the effects of thermal aging, but here they are much less pronounced.

By varying the composition of the wax blends with respect to the amount of paraffin waxes with normal hydrocarbons and microcrystalline waxes with iso-hydrocarbons and the number of atoms in the two types of chains present in maximum amounts, a number of properties of the composites containing them can be controlled in the desired direction, including rheological, vulcanizing, mechanical (such as abrasion and tear resistance), resistance to heat and light aging, etc.

The combination of TMQ and an optimized mixture of paraffin and microcrystalline waxes has a synergetic impact and can be successfully used in the production of rubber products for various purposes, as it guarantees good performance and better protection compared to the use of TMQ solely.

Acknowledgement: *The authors thank Evricom Company for providing the wax blends used in the study, as well as Ms. Reneta Doseva who performed their gas chromatographic characterization.*

REFERENCES

1. S. K. Bhatnagar, *The Rubber Inter. Magazine*, **1**, 59 (2009).
2. J. Menough, *Rubber World*, **200,** 14 (1989).
3. Akrochem Corporation, Use of waxes for ozone protection, 2020, https://www.akrochem.com/pdf/technical_papers/waxes_for_ozone_solutions.pdf
4. S. L. Agrawal, S. Mandot, S. Bandyopadhyay, R. Mukhopadhyay, *Progress in Rubber, Plastics and Recycling Technology*, **21**, 139 (2005).
5. N. Ikeda, M. Tajima, *US Pat.* 5 296 129 (1994).
6. N. Dishovsky, G. Tsenkov, Handbook of Rubber, Es Print, Sofia, 2006.
7. A. N. Kamaruddin, A. Ansarifar, F. Saeed, Y. Haile-Meskel, R. J. Ellis, *J. Rubb. Res.*, **15** (2012).
8. Budiarto, *AIP Conference Proceedings,* 1823, 020068 (2017).
9. H. Fries, R. R. Pandit, *Rubb. Chem. Technol*., **55**, 309 (1982).
10. M. Pike, W. F. Watson, *J. Polym. Sci*., **9**, 229 (1952).
11. A. Ansarifar, S. P. Holmes, *J Rubb. Res.*, **8**, 191 (2005).
12. J. T. Byers, *Rubb. Chem. Technol.*, **75**, 527 (2002).
13. S. Ostad-Movahed, K. Ansar Yasin, A. Ansarifar, M. Song, S. Hameed, *J. Appl. Polym. Sci.*, **109**, 869 (2008).

Bulgarian Chemical Communications, Volume 53, Issue 3 (pp. 365 - 370) 2021 *DOI: 10.34049/bcc.53.3.5404*

Antimicrobial activity of colloidal nanosilver 24 ppm *in vitro*

T. P. Popova[1], I. Ignatov[2]*, F. Huether[3], T. Petrova[1]

[1]*University of Forestry, Faculty of Veterinary Medicine, 10 Kl. Ohridski Blvd., Sofia 1756, Bulgaria*
[2]*Scientific Research Center of Medical Biophysics, Sofia, Bulgaria*
[3]*EVODROP AG, Zürich, Switzerland*

Received: April 28, 2021, Revised: May 30, 2021

The antimicrobial effect of colloidal nanosilver (AgNPs) at a concentration of 24 ppm against reference strains of *Escherichia coli*, *Salmonella enterica*, *Staphylococcus aureus*, *Clostridium perfringens*, *Candida albicans* and two clinical isolates (*Pseudominas aeruginosa* and *Streptococcus pyogenes*) was examined. The agar diffusion method, determination of the minimum inhibitory concentrations (MIC) and the time of antimicrobial action of AgNPs were used. In the studies performed by the disc-diffusion method, a very good inhibitory effect of AgNPs 24 ppm was reported in all tested microorganisms. The examined Gram-negative bacteria showed higher sensitivity to colloidal nanosilver in comparison with the Gram-positive microorganisms. In the Gram-positive bacteria, the MIC values of the studied AgNPs were higher than in Gram-negative ones. *C. perfringens* with MIC_{50} 0.5 μg/ml showed the highest sensitivity to AgNPs 24 ppm, and *S. aureus* (MIC_{50} 2 μg/ml) - the lowest. AgNPs 30 ppm inactivated all tested Gram-negative bacterial strains within 1 min. In a suspension with a density of 10^6 cells/ml *C. perfringens* died within 24 min. However, individual cells of *S. aureus* remained viable for more than 60 min, and of *S. pyogenes* and *C. albicans* - for more than 120 min. In a suspension with a density of 10^4 cells/ml Gram-positive microorganisms survived for twice as short time - *C. perfringens* up to 15 min, *S. aureus* over 30 min, and *S. pyogenes* and *C. albicans* - for at least 60 min. These results provide hope for the successful use of AgNPs as disinfectant and antiseptic, as well as for topical therapy of infections involving these microbial species.

Keywords: colloidal nanosilver AgNPs, antimicrobial activity

INTRODUCTION

Silver is known as a broad-spectrum antimicrobial agent. Silver ions have long been known to possess a strong and broad spectrum of activities against different bacterial and fungal species. Today, at a time of growing multi-resistance of microorganisms to antimicrobial drugs, interest in silver as an agent with such properties is growing and studies are being conducted in this direction. In this respect, nanotechnologies today are a rapidly growing promising field for development of compounds and materials with antimicrobial properties including such with nanosilver. Colloidal silver consists of nanosized clusters of silver atoms in an aqueous solution. They are of neutral polarity, but their suspension in the water causes a highly negative (interfacial) electrostatic charge (Zeta potential) that causes a mutual repelling action resulting in an almost permanent suspension [1]. Advanced technology also provides electro-colloidal solutions that produce even better results [2]. In the study nanosized Ag colloids were obtained with the addition of urea which produced intermediates AgOCN and Ag_2CO_3 before the formation of silver and obtained silver colloids of average size of 22 nm [3].

Colloidal silver nanoparticles were synthesized using silver nitrate solubilized in the water core of a microemulsion as a source of silver ions, hydrazine hydrate solubilized in the water core of another microemulsion as the reducing agent, dodecane as the oil phase and sodium bis(2-ethylhexyl) sulfosuccinate (AOT) as the surfactant [4]. This nanosilver colloid has low toxicity and high stability, so the colloidal nanoparticles need not be separated from the solution and the silver sol can be directly used as antibacterial agent. Four 1-butyl-3-methylimidazolium halide ionic liquids were synthesized *via* metathesis and anion exchange reactions [5].

By the method of Mosin and Ignatov, colloidal silver can be obtained *via* electrolysis [6]. The synthesis method uses tetra-n-butylammonium bromide in acetonitrile as a liquid medium for electrolysis. The method of Mosin-Ignatov yields colloidal silver with sizes of 2–7 nm in a solution of tetra-n-butylammonium bromide in acetonitrile. The anode is silver, and the cathode is graphite.

The antimicrobial activity of colloidal nanosilver is tested against Gram-positive and Gram-negative microorganisms [5, 7]. According to Liu and Hurt [8], ion release is a cooperative oxidation process requiring both dissolved

* To whom all correspondence should be sent:
E-mail: mbioph@abv.bg

© 2021 Bulgarian Academy of Sciences, Union of Chemists in Bulgaria

dioxygen and protons. It produces peroxide intermediates. The antibacterial potency, eukaryotic toxicity and environmental release of nanosilver are influenced by the ionic activity associated with the particle suspension. There are studies that support ionic colloidal silver as a broad-spectrum antimicrobial agent against aerobic and anaerobic bacteria, while having a limited and specific spectrum of activity against fungi [9]. Synthesis of stable silver colloids has been successfully achieved by a number of research teams [10-12]. The study has shown a high bactericidal activity of colloidal solutions of nanosilver against strains of *Staphylococcus aureus, Escherichia coli* and *Pseudomonas aeruginosa*, as well as fungicidal activity against *Candida albicans* [13].

The purpose of the present work was devoted to testing and evaluation of the antimicrobial action of colloidal nanosilver against Gram-negative and Gram-positive microorganisms from different groups, one of the most common causes of difficult-to-treat infections in humans and animals.

MATERIALS AND METHODS

Device for colloidal nanosilver. Patent Application: PCT/EP2021/054691 [14] 25.02.2021. Title: Control device and method for driving electrodes of at least one electrolysis device for electrochemical production of nanoparticles. Description: The invention relates to the technical field of water treatment. The object of the invention is a control device and a method for driving electrodes of at least one electrolysis device for the electrochemical production of nanoparticles in water according to the generic terms of claims 1 and 10.

Antimicrobial agent. The antimicrobial effect of colloidal silver nanoparticles (AgNPs) at concentrations of 24 ppm was tested.

Control. As a positive control, the broad-spectrum antibiotic thiamphenicol (Nikovet - Sofia) was used, to which the tested microorganisms did not show resistance.

Microorganisms. Pure cultures of 7 pathogenic strains were tested. Five of them were reference: *Esherichia coli* ATCC - 8739, *Salmonella enterica* subsp. *enterica* ATCC 1304, *Staphylococcus aureus* subsp. *aureus* ATCC - 6538, *Clostridium perfringens* ATCC 13124 and *Candida albicans* ATCC 10231. The other two (*Pseudominas aeruginosa* and *Streptococcus pyogenes*) were isolated from cutaneous inflammatory secretions from dogs in the Laboratory of microbiology at the University Clinic at the University of Forestry, Faculty of Veterinary Medicine in Sofia.

Nutrient media. Mueller-Hinton agar and broth (BUL BIO NCIPD - Sofia), Columbia blood agar (Biolab Zrt. H-1141, Budapest Ov. Utra 43) were used, as well as selective media: Endo agar (Antisel - Scharlau Chemie SA, Spain) for *E. coli* and *S. enterica*, Cetrimide agar (Biolab Zrt. H-1141, Budapest Ov. Utr.) for *P. aeruginosa*, Perfringens TSC agar (MkB Test as, Slovak Republic), as well as Zeissler agar (BUL BIO NCIPD - Sofia) for *C. perfringens* and Sabouraud dextrose agar with chloramphenicol (Antisel - Sharlau Chemie SA, Spain) for *C. albicans.*

The cultivation of the microorganisms was carried out at 35-37° C for 18-24 and 72 hours in an anaerobic environment for *C. perfringens* and under aerobic conditions for the other microbial species. The system Anaerob Pack with palladium catalyst - H_2 + CO_2 (BUL BIO NCIPD - Sofia) in Jar was used to create anaerobic conditions. Indic Strip indicator (BUL BIO NCIPD - Sofia) was used to prove the achievement of anaerobiosis.

Preliminary studies of the substance were performed by the *classical agar diffusion method* of Bauer *et al.* [15] and according to Weinstein [16]. Suspensions of 24 h cultures of the test microorganisms were inoculated at a dose of 2×10^6 cells/ml in a volume of 0.1 ml in 9 cm-diameter Petri dishes on Zeissler agar for *C. perfringens* and Mueller-Hinton agar for the other microorganisms, with pH 7.2 - 7.4 and layer thickness of 4 mm. AgNPs 24 ppm and the control antibiotic were administered by instillation of 0.1 ml in 9-mm wells in the agar at concentrations of active substances per well of 30 μg for AgNPs 24 ppm and 30 μg for thiamphenicol. After incubation for 3-4 hours at room temperature for diffusion, the cultures were incubated at 35-37° C for 18-24 and 72 hours. The results were read by measuring the diameters of the inhibitory zones in millimeters, including the diameter of the well to the nearest 1 mm, with a transparent ruler on the outside of the bottom of the plates. According to the three-stage Bauer-Kirby system, an inhibitory effect of AgNPs 30 ppm was observed in areas > 12 mm, and of thiamphenicol – at > 17 mm. The susceptibility of the tested microorganisms to AgNPs 24 ppm was determined as for non-antibiotic preparations such as sulfonamides, namely: resistant (R) - in areas with diameters $\leq$ 12 mm, moderately sensitive - intermediate (I) - in areas in a range of 13 - 16 mm and sensitive (S) at $\geq$ 17 mm. For thiamphenicol the corresponding limits are as follows: R $\leq$ 12 mm, I - 13 - 17 mm and S - $\geq$ 18 mm [17, 18].

Minimum inhibitory concentrations (MICs) were determined by the method of two-fold serial

dilutions in Zeissler agar for *C. perfringens* and Mueller-Hinton agar for the other microorganisms, described by Ericsson and Sherris [19] and NCCLS [17, 18]. Bacterial suspensions were applied at a dose of 10^6 cells/ml. The test preparations of colloidal silver and the control antibiotic were administered in double increasing final concentrations from 1 to 64 μg/ml agar. After incubation at 35-37° C for 18-24 hours, the number of developed colonies was determined. MIC_{50} and MIC_{90} were calculated mathematically based on the number of inhibited colonies on the agar with the respective dilution of the tested compound compared to the colonies on the media with controls without colloidal silver or antibiotic. The range of growth inhibition (D) was defined as the concentration without visible growth.

Determination of the time of antimicrobial action of AgNPs 24 ppm

• A suspension of each of the tested microbial strains at a concentration of 10^5 cells/ml in an amount of 1 ml was added to 9 ml of AgNPs 24 ppm, reaching a final concentration of 10^4 cells/ml.

• A suspension of each of the tested microbial strains at a concentration of 10^7 cells/ml in an amount of 1 ml was added to 9 ml of AgNPs 24 ppm, reaching a final concentration of 10^6 cells/ml.

• The following controls were applied - sterile distilled water (without AgNPs) with the same content of each of the tested microbial strains, as well as 100% AgNPs 24 ppm without microorganisms.

After homogenization for 1 min on a vortex apparatus (Heidolph - Labimex, Bulgaria) and different time intervals for exposure to AgNPs 24 ppm (1 min, 5 min, 15 min, 30 min, 60 min, 120 min and 24 h) cultures were made from each of the samples on Zeissler agar for *C. perfringens* and Mueller-Hinton agar for the other microorganisms, which were cultured at 37° C for 24 - 48 hours under aerobic and anaerobic conditions. After cultivation, the growth of the tested bacteria was reported. The number of colonies developed and the colony forming units (CFU) in 1 ml of the initial suspensions were determined.

All experiments were performed in triplicate.

The statistical processing of the results was performed according to the classical method of Student and Fisher.

RESULTS

In the studies performed by the disc-diffusion method, a very good inhibitory effect of AgNPs 24 ppm (diameters of the inhibitory zones between 20.0 ± 4.7 and 28.7 ± 2.6 mm) was reported in all studied microorganisms. The results are summarized in Table 1. These values were close to those of the control antibiotic, although lower than them. Slightly higher sensitivity to the colloidal nanosilver was shown by the studied Gram-negative bacteria compared to Gram-positive microorganisms ($P>0.05$).

Table 1. Antimicrobial effect of AgNPs 24 ppm against Gram-positive and Gram-negative microorganisms in the agar-gel diffusion method

Microorganisms	Inhibitory zones in mm	
	AgNPs	Thiamphenicol
E. coli	26.7 ± 3.9	36.0 ± 0.8
S. enterica	28.7 ± 2.6	35.3 ± 0.8
P. aeruginosa	25.0 ± 2.4	34.8 ± 0.8
S. aureus	21.7 ± 4.3	25.7 ± 3.3
S. pyogenes	20.0 ± 4.7	26.0 ± 4.5
C. perfringens	22.0 ± 4.0	21.3 ± 0.5
C. albicans	22.7 ± 4.6	28.7 ± 3.7
Total Gram-negative bacteria	25.9 ± 2.0	35.4 ± 0.5
Total Gram-positive bacteria	20.8 ± 2.0	24.3 ± 2.1
Total bacteria	23.3 ± 3.3	29.9 ± 5.7
Total (all microorganisms)	23.1 ± 3.1	29.7 ± 5.3

The highest sensitivity by this method was reported in *S. enterica*, and the lowest - in *S. pyogenes* and *S. aureus*. All tested microorganisms showed high sensitivity to thiamphenicol used as a positive control. The differences in the diameters of the inhibitory zones of the antibiotic and the tested preparation with colloidal silver were statistically significant ($P<0.05$) in the studied Gram-negative bacteria, but not in the Gram-positive ones ($P> 0.05$). The results obtained in determining the minimum inhibitory concentrations are shown in Table 2. They correspond to those obtained in the agar-gel diffusion method. The highest sensitivity to AgNPs showed *C. perfringens* with MIC_{50} of 0.5 μg/ml, and the lowest - *S. aureus* with MIC_{50} 2 μg/ml. For the other microorganisms tested, the MIC_{50} of AgNPs 24 ppm was 1 μg/ml. In Gram-positive bacteria, the values of MIC were higher than those in Gram-negative, but the differences were not significant ($P>0.05$, t-criterion of Student). The values of the control antibiotic were significantly higher - MIC_{50} 4 - 32 μg/ml. As can be seen from the summary data, the bacterial strains tested in this method showed significantly higher sensitivity to AgNPs 24 ppm compared to the control antibiotic ($P<0.01$, t-test of Student).

The results of the experiments performed to determine the sensitivity of the examined Gram-positive and Gram-negative microorganisms to AgNPs 24 ppm, tested at a final concentration of 10^6 cells/ml by the suspension method, are presented in Table 3.

The data showed that AgNPs 24 ppm inactivated all Gram-negative bacterial strains tested within 1 min. Of the Gram-positive microorganisms, the highest sensitivity to colloidal nanosilver is shown by the strict anaerobe *C. perfringens*, which dies within 30 min. However, individual cells of *S. aureus* remain viable for more than 60 min. *S. pyogenes* and *C. albicans* survived longer in the presence of AgNPs 30 ppm. Single cells of these microorganisms remained viable for a minimum of 120 min.

Data from studies performed by the same method, but with a hundred times lower concentration of microbial suspensions (10^4 cells/ml), can be seen in Table 4. All tested Gram-negative bacterial strains died in 1 min. Gram-positive microorganisms at this suspension concentration survived for twice as short a time. *C. perfringens* died within 15 min. However, individual cells of *S. aureus* remained viable for more than 30 min, and *S. pyogenes* and *C. albicans* - for a minimum of 60 min.

Table 2. Minimum inhibitory concentrations of AgNPs 24 ppm against Gram-positive and Gram-negative microorganisms

Microorganisms	AgNPs			Thiamphenicol		
	MIC_{50}	MIC_{90}	D	MIC_{50}	MIC_{50}	D
Escherichia coli	1	2	4	8	16	64
Salmonella enterica	1	2	4	16	32	64
Pseudominas aeruginosa	1	2	4	8	32	64
Staphylococcus aureus	2	4	8	16	32	64
Streptococcus pyogenes	1	2	4	32	64	128
Clostridium perfringens	0.5	1	2	4	8	16
Candida albicans	1	2	4	32	64	128
Total Gram-negative	1.00 ±0.00	2.00 ±0.00	4.00 ±0.00	10.67 ±3.77	26.67 ±7.54	64.00 ±0.00
Total Gram- positive	1.12 ±0.54	2.25 ±1.09	4.50 ±2.18	21.00 ±11.79	42.00 ±2.36	42.00 ±2.36
Total (all microorganisms)	1.07 ±0.42	2.14 ±0.83	4.28 ±1.66	16.57 ±10.57	35.43 ±19.99	84.00 ±47.16

MIC_{50} -50% growth inhibition; MIC_{90} -90% growth inhibition; D – range of full growth inhibition.

Table 3. Antimicrobial effect of AgNPs 24 ppm against Gram-positive and Gram-negative microorganisms in suspensions with a density of 10^6 cells/ml

Microorganisms	Growth of the strains (percent of colony number in comparison with the untreated controls) after different intervals of exposure						
	1 min	5 min	15 min	30 min	60 min	120 min	24 h
E. coli	0	0	0	0	0	0	0
S. enterica	0	0	0	0	0	0	0
P. aeruginosa	0	0	0	0	0	0	0
S. aureus	50	30	20	10	10	0	0
S. pyogenes	65	50	40	25	25	10	0
C. perfringens	35	10	7	0	0	0	0
C. albicans	40	35	22	15	10	6	0
Untreated controls	100	100	100	100	100	100	100

Table 4. Antimicrobial effect of AgNPs 24 ppm against Gram-positive and Gram-negative microorganisms in suspensions with a density of 10^4 cells/ml

Microorganisms	Growth of the strains (percent of colony number in comparison with the untreated controls) after different intervals of exposure						
	1 min	5 min	15 min	30 min	60 min	120 min	24 h
E. coli	0	0	0	0	0	0	0
S. enterica	0	0	0	0	0	0	0
P. aeruginosa	0	0	0	0	0	0	0
S. aureus	25	15	10	5	0	0	0
S. pyogenes	30	25	20	10	5	0	0
C. perfringens	20	5	0	0	0	0	0
C. albicans	35	20	15	10	5	0	0
Untreated control	100	100	100	100	100	100	100

DISCUSSION

The results of the present studies correspond to those of other authors. Petica *et al.* [10] determined a high antibacterial and antifungal activity of some stable colloidal solutions containing up to 35 ppm of Ag. By determination of minimal inhibitorial concentration they found a significant inhibitory effect against Gram-positive and Gram-negative microorganisms such as *S. aureus, E. coli, P. aeruginosa, Acinetobacter* spp. and a fungi mix of *Aspergillus*, *Penicillium* and *Trichoderma* species. Lkhagvajav *et al.* [11] found antimicrobial activity of colloidal silver nanoparticles prepared by the sol-gel method. High inhibitory effect is observed against *E. coli, P. aeruginosa, Salmonella typhimurium, Klebsiella pneumoniae, Bacillus subtilis, S. aureus,* and the fungus *C. albicans* at a very low concentration of 2-4 μg/ml of nanosilver. The authors explained this very high activity with the advantages induced through the sol-gel method since very small nanoparticles can be obtained, which makes them very active against microorganisms. Pokhrel *et al*. [20] also reported antibacterial effect of citrate - functionalized nanosilver on *E. coli.* The results obtained by Petrus *et al.* [2] suggested that colloidal nanosilver exhibits a good bacteriostatic effect but poor bactericidal effect towards food-borne pathogens such as *E. coli*, *Listeria monocytogenes, Salmonella Typhi, Vibrio cholerae, Vibrio parahaemolyticus, Bacillus cereus* and *S. aureus.* However, the research of Batista *et al.* [12] proved the bactericidal effect of colloidal nanosilver and found that the required time to promote the biocide effect is linked to the time-dependent release of Ag^+. Also, this effect is greatly dependent on the presence of Ag^+ rather than the nanoparticles themselves.

The results of Petrus *et al.* [2] support the notion that the antibacterial activity of AgNPs might be due to their adsorption on the bacterial surface, as well as the inhibition of intracellular enzyme activity. Therefore, the remaining Ag ions in the AgNPs solution or dissolved Ag ions are capable of causing a bacteriostatic or even a bactericidal impact. Also, silver antimicrobial property is very high due to their extremely large surface area, which provides better contact with microorganisms.

Mukha *et al.* [13] studied the mechanism of action of nanosilver on microbial cells by a laser scanning confocal microscope using fluorescent label. They found that the first step of the antimicrobial effect on microorganisms is membrane damage and penetration of silver nanoparticles into the cell.

The results of the present study provide hope for the successful use of AgNPs 24 ppm for topical therapy of infections involving the examined bacterial species, as well as for disinfection.

CONCLUSIONS

In the studies performed by the disc-diffusion method, a very good inhibitory effect of AgNPs 24 ppm was reported in all studied microorganisms. The values of the diameters of the inhibitor zones were close to those reported for the control antibiotic, although lower than them. The studied Gram-negative bacteria showed higher sensitivity to colloidal nanosilver in comparison with the Gram-positive microorganisms.

In the Gram-positive bacteria, the MIC values of the studied AgNPs were higher than in Gram-negative ones. *C. perfringens* with MIC_{50} 0.5 μg/ml showed the highest sensitivity to AgNPs 24 ppm, and *S. aureus* (MIC_{50} 2 μg/ml) - the lowest.

The high sensitivity of the obligate anaerobe *C. perfringens* to AgNPs 24 ppm, established by all methods used, is impressive. Higher susceptibility of the studied Gram-negative bacteria, including *P. aeruginosa* - a species that rapidly builds resistance to chemical factors, was found. These results provide hope for the successful use of AgNPs for disinfection, as well as for topical therapy of infections involving these bacterial species. The lowest sensitivity was shown by *C. albicans*, and of the bacteria - by *S. pyogenes*.

The experimental data show that the examined AgNPs 24 ppm possesses well expressed antimicrobial activity and could be successfully used as an antiseptic and for treatment of infections in animals and humans, caused by Gram-positive and Gram-negative bacteria including obligate anaerobes, as well as fungal diseases caused by *Candida albicans*.

REFERENCES

1. H. Laroo, *Journal of Physical Chemistry & Biophysics,* **3**(5), 130 (2013).
2. E. M. Petrus, S. Tinakumari, L. C. Chai, A. Ubong, R. Tunung, N. Elexson, L. F. Chai, R. Son, *International Food Research Journal,* **18,** 55 (2011).
3. Yu-C. Lu, K.-S. Chou, *Journal of the Chinese Institute of Chemical Engineers*. **39**(6), 673 (2008).
4. W. Zhang, X. Qiao, J. Chen, *Colloids and Surfaces A: Physicochemical and Engineering Aspects*, **299** (1–3), 22 (2007).
5. V. S. Patil, M. Mahajan, K. Kulkarni, C. Patil, A. Rode, A. Coronas, Gi-Ra Yi, *Chemosphere,* **243,** 125302 (2020).
6. O. V. Mosin, I. Ignatov, *Nanotechnology Research and Practice,* **8**(4), 23 (2015).
7. T. Popova, I. Ignatov, *Bulgarian Journal of Veterinary Medicine,* (2021), in press.
8. J. Liu, R. H. Hurt. *Environ. Sci. Technol*., **44** (6), 2169 (2010).
9. K. Morrill, D. May, N. Leek, L. D. Langland, J. Jeane, C. Ventura, S. Skubisz, E. Scherer, E. Lopez, Crocker, R. Peters, J. Oertle, K. Nguyen, S. Just, M. Orian, M. Humphrey, D. Payne, B. Jacobs, R. Waters, J. Langland, *J. Alter. Complement. Med.,* **19**(3), 224 (2013).
10. A. Petica, S. Gavriliu, M. V. Lungu, N. Buruntea, C. Panzaru, *Mater. Sci. Eng. B,* **152**, 22 (2008).
11. N. Lkhagvajav, I. Yasa, E. Celik, M. Kaygusuz, O. Sari, *Digest Journal of Nanomaterials and Biostructures,* **6**(1), 149 (2011).
12. C. C. S. Batista, L. J. C. Albuquerque, I. de Araujo, B. L. Albuquerque, F. D. da Silva, F. C. Giacomelli, *RSC Advances,* **8**, 10873 (2018).
13. I. P. Mukha, A. M. Eremenko, N. P. Smirnova, A. I. Mikhienkova, G. I. Korchak, V. F. Gorchev et al., *Appl. Biochem. Microbiol.,* **49**, 199 (2013).
14. Patent PCT/EP2021/054691. 25.02.2021. Control device and method for driving electrodes of at least one electrolysis device for electrochemical production of nanoparticles. Fabio and Markus Colloidal Engineering GMBH, Switzerland, 2021.
15. A. W. Bauer, W. M. Kirby, J. C. Cherris, M. Truck, *The Am. J. Clin. Pathol.*, **45** (4) 493 (1996).
16. M. P. Weinstein, Performance Standards for Antimicrobial Susceptibility Testing, 30th edn., 2020, p. 332.
17. National Committee for Clinical Laboratory Standards: Performance Standards for Antimicrobial Disc Susceptibility Tests, 6th edn., Approved Standard. NCCLS Document M2 – A6, **17**(1), 1997.
18. National Committee for Clinical Laboratory Standards: Performance Standards for Antimicrobial Susceptibility Testing: Ninth Informational Supplement. NCCLS Document M100 – S9, **18**(1), 1999.
19. H. M. Ericsson, J. S. Sherris, *Acta Path. Microb. Scand. Suppl.,* **217**, 3 (1971).
20. L Pokhrel, R. B. Dubey, P. R. Scheuerman. *Environmental Science: Nano*, **1**, 45 (2014).

Bulgarian Chemical Communications, Volume 53, Issue 3 (pp. 371 - 379) 2021 *DOI: 10.34049/bcc.53.3.5412*

Multivariate statistical assessment of Bulgarian bottled mineral and spring waters

V. V. Mihaylova*, V. V. Lyubomirova, R. G. Djingova

Trace Analysis Laboratory, Department of Analytical Chemistry, Faculty of Chemistry and Pharmacy, Sofia University "St Kliment Ohridski", 1 J. Bourchier Blvd., 1164 Sofia, Bulgaria

Received: May 27, 2021; Revised: July 02, 2021

Water is essential to human life. Our bodies need a certain amount of water intake on a daily basis to function appropriately. Several health benefits have been attributed to the mineral and trace element content of mineral and spring waters. Although the quality of drinking water depends to a large extent on its microelement composition, only limited data are available about trace element content in Bulgarian bottled spring waters. In this study, using ICP-MS a simultaneous determination of 69 chemical elements in bottled spring waters has been performed and the results were compared to the previous analysis obtained for bottled mineral waters sold on the Bulgarian market. The data for both types of water (mineral and spring) prove that all determined elements are below Bulgarian Regulation No 9 of maximum admissible levels. Only Fe in one brand of spring water is slightly higher than Bulgarian health-based value but lower than EPA. Multivariate statistics (cluster, discriminant and factor analysis) were used to reveal groups of similarity among the investigated mineral and spring waters. For everyday use, along with the alternation of different brands of mineral water also change of the water type might be recommended.

Keywords: Spring waters, Mineral waters, Element composition, ICP-MS, Multivariate statistics.

INTRODUCTION

Water makes up 60-75% of human body weight and is the most consumed natural product. It is the only zero-calorie, zero-sugar and additive-free beverage that will ensure a healthy form of hydration. Most people in the EU have good access to high quality drinking water. According to the European Federation of Bottled Waters, the consumption of bottled water in 2019 in Bulgaria was 100 liters *per capita* for drinking purposes [1]. It is also worth mentioning that within the EU, the consumption of bottled mineral water surpasses more than five times that of spring waters [2].

The market of bottled waters is expanding worldwide thanks to health concerns and/or successful marketing [3]. According to the European Federation of Bottled Waters (EFBW) the three types of bottled water: natural mineral, spring and table water differ in respect to origin and applied legislation rules [4]. Both mineral and spring waters originate from recognized underground water sources. They are microbiologically safe. The main difference is that stable mineral balance is typical for natural mineral waters but is not required for spring waters and mineral composition is not demanded on the label of spring water bottles.

Investigations of the element concentrations in bottled waters are mainly directed to natural mineral waters and the number of publications is growing, covering all continents and countries [5−7]. The reason obviously is that mineral waters are mainly recommended for health reasons and the concentrations of major and some trace elements are object of national standards. Although also of natural origin spring waters are rarely investigated or not mentioned explicitly in the study. Many papers report results for bottled waters without description of the type of waters or separate discussion, using other types of classification of bottled waters [7]. In some cases, spring, mineral and table waters are analyzed and discussed together disregarding their different origin and pretreatment [8, 9].

Bulgaria is one of the richest countries in mineral water resources and the bottled mineral waters are certified and controlled [10]. Not so the spring waters although usually they are recommended for daily use because the mineral content is considered to be lower. On the bottle labels concentrations of major elements are given but information for trace elements concentrations is nowhere to be found [11, 12].

Detcheva *et al*. [13] compared the concentrations of 13 elements in a random selection of 7 mineral, 2 spring and 1 table waters. The results indicted stability in the composition with the time of bottling and certain similarity in the composition of some of the samples.

The aim of the present paper is to perform a comparison of the chemical composition of eight spring waters with previously published data for mineral waters [14] available on the Bulgarian market for a maximum number of elements and

*To whom all correspondence should be sent:
E-mail: ahvm@chem.uni-sofia.bg

© 2021 Bulgarian Academy of Sciences, Union of Chemists in Bulgaria

provide basis for the correct choice of suitable drinking water, both for daily needs and after medical recommendation.

EXPERIMENTAL

Bottled mineral and spring water samples

Fig. 1 presents a map of Bulgaria with the mineral and spring water deposits where production of bottled water is allowed. Seventeen brands of mineral waters were subjected to analysis and the results are discussed in details in Lyubomirova *et al*. [14]. Additionally, eight brands of spring water available in the commercial network were purchased: three brands (Devin, Baldaran and Billa) are originating from the same spring (spring Baldaran, village Fotinovo, Rhodope mountains), Bachkovo (spring "Badjova cheshma", village Bachkovo, Rhodope mountain), Rilana (drilling Rilana No 962, Stob village, Rila mountain), H_2O pure (source Puknatinni vodi – Peshtera-Dospat, Bratsigovo village, Rhodope mountains), Mihalkovo (Natural source Peshtera – Chiflika, Rhodope mountains) and Zeolite water (spring Balkan mountains, filtered through natural zeolites).

Fig. 1. Simplified map of Bulgaria with the locations of the registered mineral (in blue) and spring (in pink) water deposits.

ICP-MS analysis

The spring waters were analyzed using ICP-MS (Perkin-Elmer SCIEX Elan DRC-e) with cross-flow nebulizer. The concentration of 69 elements (Ag, Al, As, Au, B, Ba, Be, Bi, Ca, Cd, Ce, Co, Cr, Cs, Cu, Dy, Er, Eu, Fe, Ga, Gd, Ge, Hf, Hg, Ho, In, Ir, K, La, Li, Lu, Mg, Mn, Mo, Na, Nb, Nd, Ni, Os, P, Pb, Pd, Pr, Pt, Rb, Re, Rh, Ru, Sb, Sc, Se, Si, Sm, Sn, Sr, Ta, Tb, Te, Th, Ti, Tl, Tm, U, V, W, Y, Yb, Zn, Zr) were determined as described in Lyubomirova *et al.* [14]. The macroelement (Na, Mg, Si, K and Ca) concentrations were determined by the application of a Dynamic Bandpass Tuning parameter – RPa as described in Lyubomirova *et al.* [15]. The concentrations of arsenic and selenium were determined in a DRC mode [16] for the elimination of Ar-based polyatomic interferences.

Analytical characteristics of the method

The accuracy of the method was checked by analysis of two water SRMs: SPS-SW2 (Reference Material for Measurement of Elements in Surface Waters, Spectrapure Standards, Norway) and NWTM-23.5 (Environmental matrix reference material, a trace element-fortified sample, Environment and Climate Change, Canada). The experimental results were in very good agreement with the certified values. The average recovery for each element concentration was calculated based on the obtained results and the certified values. The results showed that the current method had good recovery (from 98.9 % to 101.6 % for macroelements, from 99.6 % to 100.4 % for microelements and from 99.5 % to 101.3 % for trace elements).

All samples were analyzed in triplicate to assess the precision of the analysis, which is in the interval 1-9 %.

Statistical analysis

The statistical analyses were performed by STATISTICA 7.0 software package. The analytical data were subjected to cluster, discriminant and factor analysis. Although 69 elements were determined, not all of them were used in the statistical analysis. The concentrations of Ag, Au, Be, Cd, Dy, Er, Eu, Gd, Ho, In, Ir, La, Lu, Nb, Nd, Os, Pb, Pd, Pr, Pt, Re, Rh, Ru, Se, Sm, Sn, Ta, Tb,

Tm and Yb which exhibited values usually lower than the limit of detection (LOD) of the method were excluded. A data matrix with 17 mineral water and 8 spring water samples and 39 variables was formed. The data were treated by hierarchical cluster analysis, based on the Ward's method algorithm and the squared Euclidean distance. To verify the correct classification of the mineral and spring samples obtained by cluster analysis, a discriminant analysis with the same 39 variables was performed. The posterior probability for the samples to belong to each group was automatically calculated by the STATISTICA 7.0 statistical software programme.

Factor analysis was also used in the current investigation as a multivariate exploratory technique, which can be used to uncover the latent structure of a set of variables. The Kaiser criterion [17] was applied to determine the total number of factors for each dataset in this analysis. Under this criterion, only factors with eigenvalues greater than or equal to 1 are accepted as possible sources of variance in the data, with the highest priority ascribed to the factor that has the highest eigenvector sum. The rationale for choosing 1 is that a factor must have a variance at least as large as that of a single standardized original variable to be acceptable.

RESULTS AND DISCUSSION

Element concentrations

The concentrations of 55 elements in the spring waters are presented in Table 1 and the mineral water content is presented in [14].

The data for both types of water (mineral and spring) prove that all determined elements are below Bulgarian Regulation No 9, 2001 [18], WHO, 2017 [19] and EPA, 2018 [20] maximum admissible levels. Only Fe in Bachkovo (see Table 1) spring water is slightly higher than Bulgarian health based value but lower than EPA. The concentrations of Dy, Er, Gd, Ir, Lu, Pb, Pd, Pt, Re, Ru, Sm, Ta, Tm, Os, were below the LODs in all the samples of the spring waters and are not presented in the table. The experimentally determined LODs for Dy, Er, Gd, Ir were 0.001 μg/L, for Lu, Os, Pb, Pt, Re and Ru were 0.002 μg/L and for Sm, Ta, Tm were 0.003 μg/L.

Table 1. Element concentrations (μg/L) in Bulgarian spring waters.

Element	Billa	Bach-kovo	Rilana	Devin	Baldaran	H_2O pure	Mihal-kovo	Zeolitna	BG-Reg N9	WHO	EPA
Ag	0.042	0.026	0.011	0.005	<0.003	0.005	0.005	<0.003		100**	
Al	5.18	1.08	0.34	20.2	25.8	2.69	5.89	<0.011	200*	900**	50-200***
As	0.27	1.83	0.20	0.27	0.29	0.89	0.27	0.14	10	10	10
Au	0.02	0.05	0.02	0.02	0.03	0.01	<0.001	<0.001			
B	1.08	41.3	1.31	1.94	2.62	16.1	2.62	0.68	1000	2400	
Ba	0.53	19.2	23.3	1.29	1.08	16.5	5.53	2.71		1300	2000
Be	<0.008	0.066	<0.008	<0.008	<0.008	<0.008	<0.008	<0.008			4
Bi	1.66	1.76	0.19	0.37	0.29	0.36	0.078	0.047			
Ca mg/L	5.83	74.5	18.4	6.02	5.97	51.5	20.7	0.70	150*		
Cd	0.003	0.010	<0.001	<0.001	0.024	<0.001	<0.001	<0.001	5	3	5
Ce	0.004	<0.001	<0.001	0.043	0.032	<0.001	<0.001	<0.001			
Co	0.014	0.15	0.055	0.007	0.010	0.058	0.027	<0.001			
Cr	1.24	2.49	1.47	0.39	0.46	1.73	1.42	1.41	50	50	100
Cs	<0.001	10.6	0.002	<0.001	0.005	0.019	<0.001	0.048			
Cu	<0.011	<0.011	0.36	<0.011	<0.011	0.40	0.038	0.049	2000	2000	1300
Eu	<0.001	0.005	0.007	<0.001	<0.001	0.002	<0.001	<0.001			
Fe	23.1	258	72.0	27.9	37.3	119	65.9	<0.014	200*		300***

Ga	0.060	0.078	0.018	0.014	<0.003	0.051	0.028	0.058			
Ge	<0.001	0.67	<0.001	<0.001	<0.001	<0.001	<0.001	<0.001			
Hf	0.14	0.35	0.035	0.079	0.053	0.52	0.011	0.93			
Hg	0.02	0.05	0.02	0.02	0.03	0.01	0.03	0.05	1	6	2
Ho	0.002	0.003	<0.001	0.003	<0.001	0.002	0.002	<0.001			
In	0.002	0.005	<0.001	<0.001	<0.001	<0.001	<0.001	0.026			
K mg/L	0.84	3.73	2.99	0.93	0.95	3.63	1.67	13.8			
La	<0.001	0.002	0.008	0.007	0.004	0.004	0.008	<0.001			
Li	3.37	61.6	0.83	2.73	2.82	4.71	0.53	0.024			
Mg mg/L	0.32	8.50	2.69	0.29	0.34	6.56	0.64	0.099	80*		
Mn	<0.007	<0.007	<0.007	0.039	<0.007	<0.007	0.86	0.025	50*	400**	50***
Mo	0.23	0.42	0.10	0.045	0.055	0.096	0.036	0.26		70**	
Na mg/L	5.26	25.4	3.96	5.78	5.75	28.9	3.59	0.87	200*	50	
Nb	0.01	0.03	0.01	0.02	<0.001	0.03	<0.001	<0.001			
Nd	0.012	<0.003	0.024	0.009	0.004	<0.003	<0.003	<0.003			
Ni	<0.008	5.79	0.21	<0.008	0.10	1.34	0.62	<0.008	20	70	
P	73.8	1.50	80.2	73.3	96.5	34.4	68.1	20.6			
Pr	0.003	0.003	<0.002	0.004	0.003	<0.002	<0.002	<0.002			
Rb	0.60	11.4	0.27	0.65	0.71	3.56	1.33	2.42			
Rh	<0.001	0.01	<0.001	<0.001	<0.001	0.02	0.01	<0.001			
Sb	1.29	1.68	0.93	0.94	0.52	0.82	0.50	1.37	5	20	6
Sc	13.34	5.11	4.83	12.93	13.26	18.8	9.93	0.24			
Se	1.57	1.56	0.44	0.68	<0.012	0.45	<0.012	0.87	10	40	50
Si mg/L	13.4	5.52	4.94	13.3	14.1	23.4	11.8	0.15			
Sn	0.11	0.15	<0.007	0.07	<0.007	0.11	<0.007	0.16			
Sr	27.6	243	89.9	30.5	29.3	229	47.5	5.84			
Tb	0.002	0.002	<0.001	<0.001	<0.001	<0.001	0.003	<0.001			
Te	0.23	0.64	0.19	0.045	0.14	0.23	0.23	0.70			
Th	0.14	0.098	0.012	0.050	0.043	0.038	0.012	0.73			
Ti	1.20	352	87.4	2.78	9.85	184	73.6	1.07			
Tl	0.009	0.030	<0.006	<0.006	0.009	<0.006	0.013	0.050			2
U	0.19	5.29	0.025	0.20	0.24	1.56	0.17	0.006	30	30	30
V	0.57	0.57	0.47	0.53	0.64	0.39	0.60	0.11			
W	9.44	21.1	1.79	3.03	1.98	2.85	1.39	22.1			
Y	<0.001	<0.001	0.007	0.003	0.003	<0.001	0.006	<0.001			
Yb	<0.003	<0.003	<0.003	0.006	<0.003	0.004	<0.003	0.004			
Zn	0.17	1.90	0.66	<0.002	<0.002	1.20	<0.002	<0.002	4000*		5000***
Zr	0.18	0.65	0.012	0.10	0.042	0.22	0.018	1.12			

*- Indicator value, **- Health-based value, *** - Secondary Drinking Water Regulation

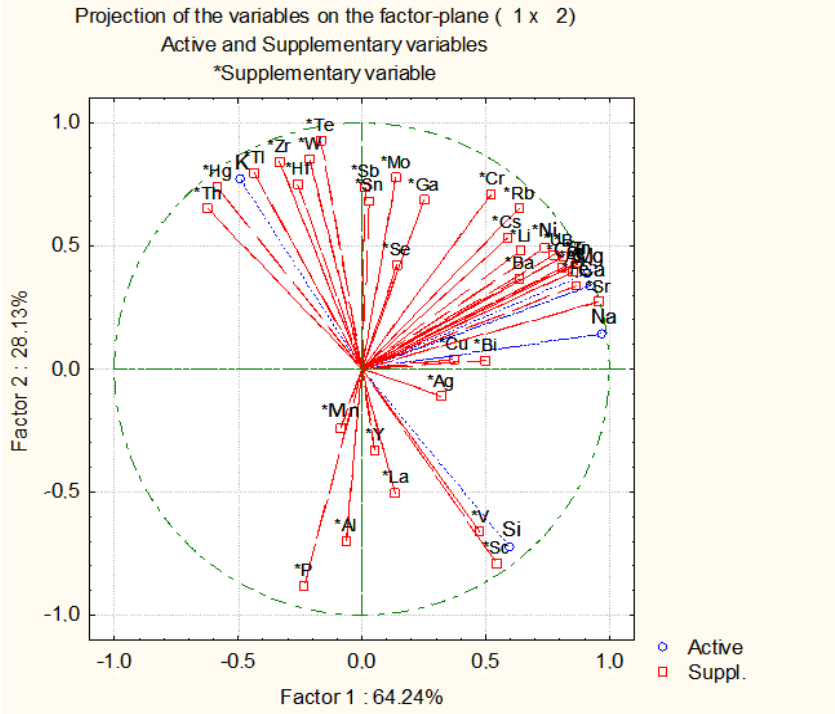

Fig. 2. Two-dimensional plot of projection of the elements on the factor plane

Statistical assessment of the data

Factor analysis was applied to investigate interelement and geochemical correlations among the determined elements in all investigated water samples. The performed factor analysis of the data set revealed three latent factors, explaining 92.37% variance. Figure 2 presents two-dimensional plot projections on the factor plane.

Highest factor loadings in Factor 1 have alkali (without K) and alkaline earth elements, Ti, Fe, Cr, Co, Ni, Zn, As, U and B. Factor 2 includes K, Si, P, V, Zr, Hf, W, Tl, Th, Sc, Sn. Members of Factor 3 are Ag, Cu, Bi, Se. Factor 1 reflects the presence of elements in Fe-Ti oxide minerals and sedimentary carbonate rocks which are widespread in Northern Bulgaria [21]. The Moesian Platform of Northern Bulgaria originates from Hercynian deformation and is mantled by shelf-type Mesozoic and Tertiary carbonate rocks. The elements in Factor 2 are usually present in different combinations in potassium silicates distinctive for the Rhodope massif of southern Bulgaria, which is a mountainous terrain of Precambrian and Paleozoic crystalline rocks [21, 22]. The combination in Factor 3 indicates polymetallic veins [23, 24].

To establish groups of similarity in the chemical composition of the analyzed samples cluster analysis was performed and the respective dendrogram is presented on Fig. 3. A data matrix with 17 mineral water and 8 spring water samples and 39 variables was formed, as described in the experimental part. The samples were combined in two groups and one outlier. The statistical validity of the classification was confirmed by discriminant analysis and the result is presented on Fig. 4.

Cluster 1 includes all mineral waters with the exception of Voditsa and Dragoynovo which join cluster 2 where all spring waters are grouped. The Zeolite water is an outlier. The two-dimensional plot after discriminant analysis (Fig. 4) confirmed the results from the cluster analysis.

The elements responsible for this grouping of the samples are the macroelements - Na, Ca, K, Si and Mg. This result indicates that the major difference between mineral and spring water is the concentration of major elements. Fig. 5 presents the ratio of the average concentrations in the obtained clusters. Na and Si are substantially higher in cluster 1 where the majority of mineral waters are grouped while K, Ca and Mg are higher in cluster 2 including all spring waters and two mineral waters. It is worth noting the differences between Na and Ca, whose average concentrations differ significantly not only in the obtained clusters, but also in the average concentrations of the mineral [14] and spring waters. The average concentrations of K and Mg are also higher in the spring waters compared to the majority of the mineral waters. The only exception is the mineral water Mihalkovo with acidic pH and higher mineral content. The higher average K, Ca and Mg concentration in the group of the spring waters contradicts to a certain extent the accepted opinion that spring waters are much more suitable for everyday use compared to mineral waters due to lower mineral content.

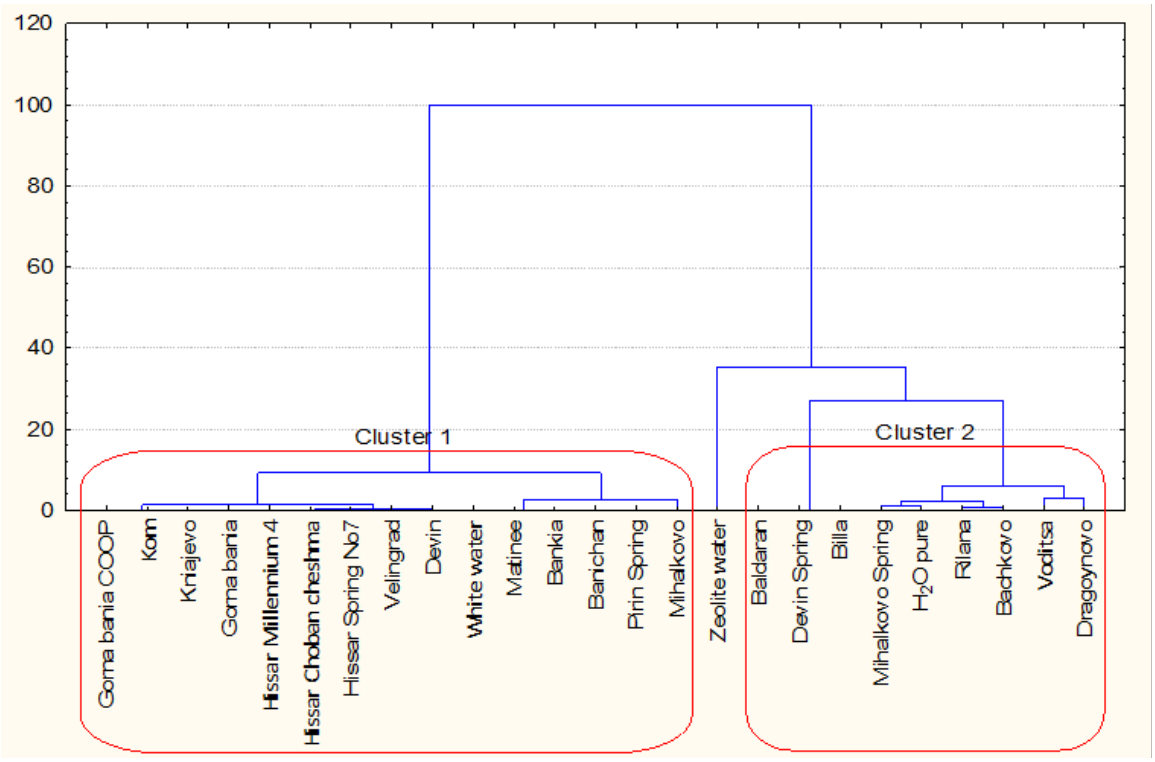

Fig. 3. Dendrogram from the cluster analysis of Bulgarian mineral and spring waters.

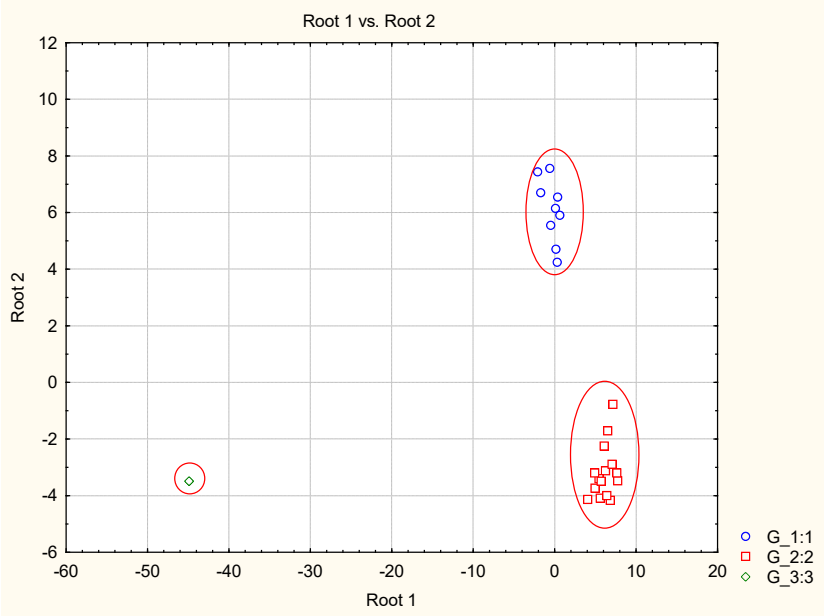

Fig. 4. Two-dimensional plot after discriminant analysis of Bulgarian mineral and spring waters.

Higher mineral content however does not mean that the water has more harmful effects because the concentrations are lower than the maximum permissible level [14], moreover, the effect on an organism depends on their form. For instance, Na in bicarbonate form is considered to have a beneficial effect on blood pressure and metabolic activity [24, 25] while NaCl might show some negative effect. Bulgarian mineral waters are mainly of the $NaHCO_3$ type and may be considered having positive influence on the organisms [14].

The finding about the difference in the concentrations of spring to mineral waters is justified specifically for Bulgarian waters. The lack of information for European bottled spring waters hinders the possibility to conclude whether such tendencies in the element concentrations exist in other regions as well.

However, it is not the total mineral concentration that is important but there is a specific tendency in the element distribution. The microelements' contents are an important part of healthy human diet. Their concentrations in mineral waters are controlled in respect to toxicity while in spring waters the content of microelements is not officially under control.

To compare the concentration of microelements in the analyzed waters and look for similarity groups cluster analysis of the samples was performed. The resulting dendrogram is shown on Fig. 6.

The result from the cluster analysis of microelements showed the formation of four clusters. Cluster 1 includes the mineral waters Kniajevo, Gorna Bania COOP, Gorna Bania - all three samples are from Sofia region where host rocks contain up to 1.1 % Ti, 11.6% Al, 10.5 % Fe, 0.52% P, 0.5 % Sr, 160 μg/g Zn, 70 μg/g Li, which were the elements corresponding to the clustering results [26]. Cluster 2 includes Banichan, Pirin Spring, Kom, Devin, Hissar Choban cheshma, Hissar Millennium 4, Hissar Spring № 7, White water, Velingrad, Mihalkovo. The mineral water deposits are located in the Rhodope, Rila and Pirin mountain regions in Southern Bulgaria region where the host metabasic rocks contain up to 10.3 % Al, 6.7 % Fe, 0.46 % Ti and 0.052 % P [27]. Cluster 3 includes 3 spring waters (Baldaran, Devin Spring and Billa) all of them originating from the same source but bottled by different suppliers and the outlier Zeolite water. Cluster 4 combines 4 mineral (Matinee, Bankia, Voditsa and Dragoynovo) and 4 spring waters (Mihalkovo, Rilana, H_2O pure and Bachkovo) in one group indicating significant similarity in the chemical composition irrespective of the difference in their type and origin.

The spring waters in cluster 4 originate from the Rhodope - Rila mountain region and have similar geochemical background [27]. Obviously, they have different microelement concentrations from the mineral waters from the same region members of the second cluster. The mineral waters in cluster 4 originate from different regions which are not geologically similar. The elements responsible for the grouping are Al, P, Li, Sr, Ti, W and Fe.

There is direct connection between Al, Fe and P during the process of their release from soils and sediments to water depending on acidification and redox processes. It is considered that P may be liberated by reductive dissolution of $Fe(OH)_3$ but remains absorbed on $Al(OH)_3$ [28, 29]. Thus the established similarity in the microelement concentrations of the mineral and spring waters in cluster 4 might be attributed to local redox processes influencing the release of microelements.

CONCLUSION

The results from the present investigation indicate quantitative and qualitative difference in the macroelement concentrations of spring and the majority of mineral waters in spite of the similarity established between certain mineral brands and spring waters. The comparison of microelements also established mixed similarity groups mineral/spring waters. Thus for daily use except the change between types of water (mineral/spring), a change of the water brands may be recommended. Additionally, attention should be paid to the water source since a single source is used by several producers for bottling different brands of water.

The results however confirm that the element concentrations in Bulgarian bottled waters meet all national and international safety standards.

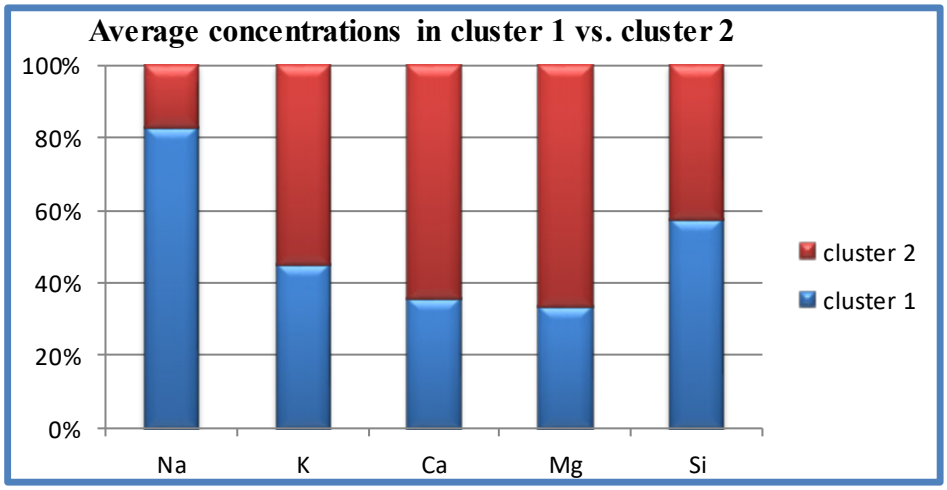

Fig. 5. Ratio of the average concentrations in the clusters.

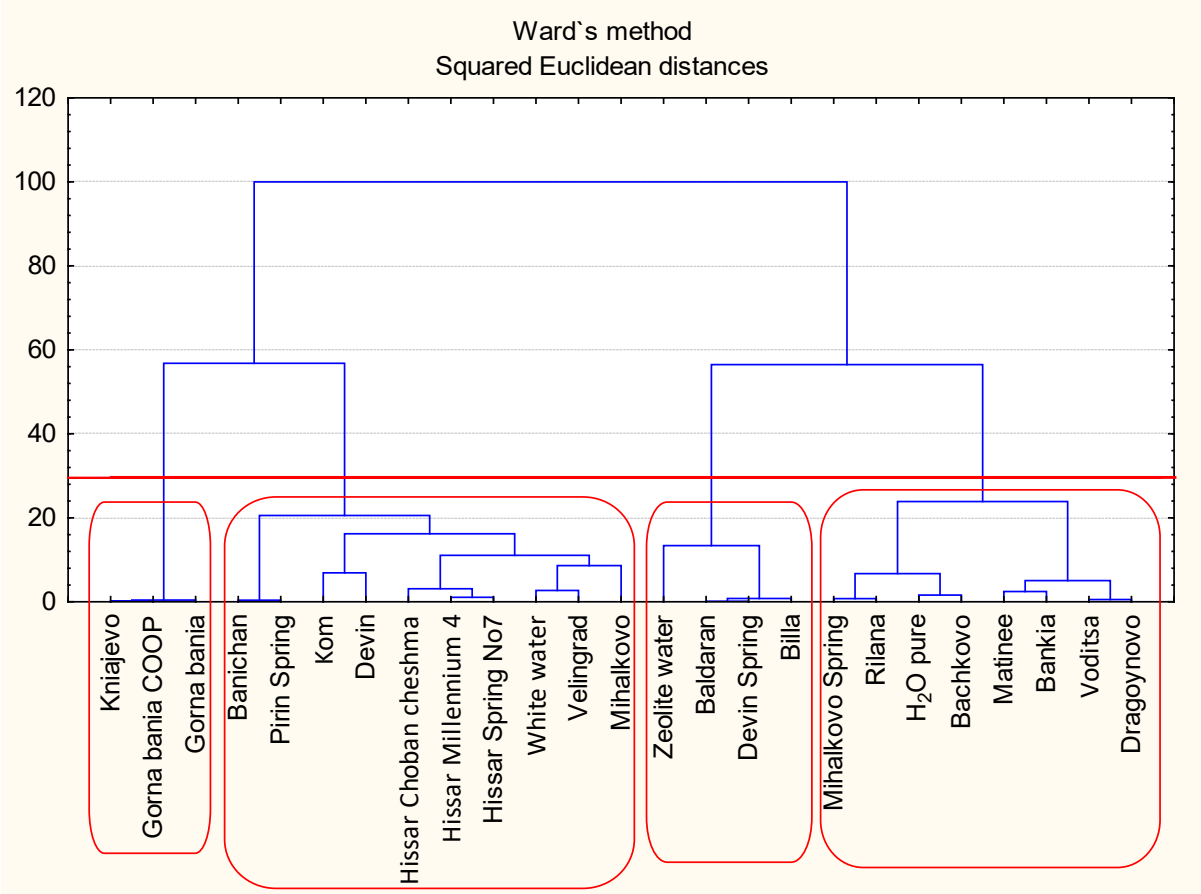

Fig. 6. Similarity groups based on microelement composition of the water samples

Acknowledgement: *This work is part of project BG05M2OP001-1.002-0019: „Clean technologies for sustainable environment – water, waste, energy for circular economy“ (Clean&Circle) 2018 – 2023, for development of a Centre of Competence, financed by the Operational programme "Science and Education for Smart Growth" 2014-2020, co-funded by the European Union through the European structural and investment funds.*

Research equipment of Distributed Research Infrastructure INFRAMAT, part of Bulgarian National Roadmap for Research Infrastructures, supported by the Bulgarian Ministry of Education and Science was used in this investigation.

REFERENCES

1. J. Conway, 2020, https://www.statista.com/statistics/455422/bottled-water-consumption-in-europe-per-capita/.
2. https://naturalmineralwatereurope.org/statistics/.

3. M. Diduch, Z. Polkowska, J. Namieśnik, *J. Expo. Sci. Env. Epid.,* **23***,* 111 (2013).
4. EEFBW, 2020, https://ec.europa.eu/food/safety/labelling_nutrition/mineral_waters_en.
5. T. Zuliani, T. Kanduč, R. Novak, P. Vréc, *Water*, **12**, 2454 (2020).
6. D. Bertoldi, L. Bontempo, R. Larcher, G. Nicolini, S. Voerkelius, G. D. Lorenz, H. Ueckermann, H. Froeschl, M. J. Baxter, J. Hoogewerff, P. Brereton, *J. Food Compost. Anal.,* **24**, 376 (2011).
7. M. Diduch, Z. Polkowska, J. Namiesnik, *J. Food Sci.*, **76**, 178 (2011).
8. V. Roje, P. Šutalo, *J. Geochem. Explor.*, **201**, 79 (2019).
9. C. Lourenço, L. Ribeiro, J. Cruz, *J. Geochem. Explor.,* **107 (3)**, 362 (2010).
10. List of natural mineral waters recognized by Member States, 2011/C 97/01, https://eur-lex.europa.eu/LexUriServ/LexUriServ.do?uri=OJ:C:2011:097:0001:0072:EN:PDF.
11. https://www.moew.government.bg/bg/vodi/registri/mineralni-vodi/ (in Bulgarian).
12. https://www.lex.bg/laws/ldoc/2135488818 (in Bulgarian).
13. A. Detcheva, V. Simeonov, E. Ivanova, *Bulg. Chem. Commun*., **48 (4)**, 684 (2016).
14. V. Lyubomirova, V. Mihaylova, R. Djingova, *J. Food Compost. Anal*., **93**, 103595 (2020a).
15. V. Lyubomirova, V. Mihaylova, R. Djingova, *Spectrosc. Eur.***, 32 (5),** 18 (2020b).
16. V. Lyubomirova, R. Djingova, *C. R. Acad. Bulg. Sci.*, **68 (7),** 847 (2015).
17. H. F. Kaiser, *Educ. Psychol. Meas*., **20**, 141 (1960).
18. Regulation No. 9 on the quality of water intended for drinking and household purposes, 2011 (in Bulgarian).
19. WHO (2017). Guidelines for Drinking Water Quality. Fourth Edition. World Health Organization, Geneva.
20. EPA (2018). Edition of the drinking water standards and health advisories tables. US Environmental Protection Agency, Washington.
21. R. M. Foose, F. T. Manheim, *AAPG Bulletin,* **59 (2)**, 303 (1975).
22. I. Zagorchev, *Bulg. Chem. Commun*., **62 (8)**, 981 (2009).
23. S. McLennan, *Geochemistry, Geophys. Geosystems*, **2 (4)**, 1 (2001).
24. R. Baumgartner, L. Fontboté, T. Vennemann, *Econ. Geol*., **103 (3)**, 493 (2008).
25. U. Schorr, A. Distler, A. M. Sharma, *J. Hypertens*, **14(1)**, 131 (1996).
26. A. Hikov, *Geol. Balcanica*, **32 (2-4)**, 89 (2002).
27. L.-A. Daieva, I. Haydoutov, S. Pristavova, *Geochem., Mineral. and Petr.*, **45**, 109 (2007).
28. F. C. Luft, M. B. Zemel, J. A. Sowers, N. S. Fineberg, M. H. Weinberger, *J. Hypertens.*, **8 (7)**, 663 (1990).
29. T. Wilson, S. Norton, B. Lake, A. Amirbahman, *Sci. Total Environ.*, **404**, 269 (2008).

Bulgarian Chemical Communications, Volume 53, Issue 3 (pp. 380 - 384) 2021 *DOI: 10.34049/bcc.53.3.5427*

Monitoring of mycotoxins produced by *Fusarium* and *Aspergillus* spp. in feed materials in Bulgaria (2017−2019)

M. M. Ignatova, N. M. Sertova*

Agricultural Academy, Institute of Animal Science, 1 Pochivka Str., 2232 Kostinbrod, Bulgaria

Received: July 11, 2021; Revised: July 27, 2021

Toxins produced by *Fusarium* and *Aspergillus* spp. have been recognized as major contaminants of feed materials. Their detection is very important for feed safety and animal nutrition into the conccept of global health. A complex study in Bulgaria for the presence of these toxins was performed on 221 representative samples. They were collected in the 2017-2019 period, including wheat (85 samples), barley (68 samples), maize (32 samples), and sunflower (36 samples). As diagnostic tool the biochemistry assay − Enzyme Linked Immunisorbent Assay method, was used. The contamination with fumonisins was determined in all of the analyzed samples. The highest fumonisin concentration of 4.82 mg/kg was detected in maize, followed by wheat of 4.67 mg/kg, barley -2.89 mg/kg and the lowest of 2.07 mg/kg was detected in sunflower samples. Our survey revealed that mycotoxins produced by *Fusarium* spp. are frequent contaminants of feed grains in Bulgaria. The highest detected concentration of aflatoxins was 14.49 μg/kg in sunflower samples, 11.55 μg/kg in barley, 10.40 μg/kg in wheat and 9.90 μg/kg in maize. The reported pollution levels of both toxins are lower than those referenced in the European regulations. Despite the low levels, the results show the need for more comprehensive research on these two mycotoxins in the feed chain, which is important for animal and human health. We examined for the first time the presence of the two toxins in a wide range of feed grains, in view of feed safety in Bulgaria for a period of three years.

Keywords: barley, ELISA, maize, mycotoxins, sunflower, wheat

INTRODUCTION

Molds produce secondary metabolites such as mycotoxins, pigments, plant regulators, which do not always have an obvious biological function [1]. Although over 300 different mycotoxins have been identified so far, those of most concern based on their toxicity and occurrence are the aflatoxins, ochratoxin A, zearalenone, deoxynivalenol, fumonisins and T-2 toxin, which cause significant health implications, mainly through food and feed contamination [2]. The presence of aflatoxins and fumonisins in feed materials depends on many factors some of which are weather and storage conditions. Aflatoxins are produced by *Aspergillus flavus* and *Aspergillus parasiticus*. They occur mainly after harvest during the grains storage.

Rabbits, turkeys, chickens, pigs, cows and goats are susceptible to aflatoxins contamination [3], and horses, pigs and rats are the most sensitive animals to fumonisins [4, 5]. Animals fed with food contaminated with aflatoxins can transmit the products of transformation of aflatoxins into eggs, milk, dairy products and meat [6]. Iqbal *et al.* [7] in their study demonstrated that contaminated poultry feed with aflatoxins has a high rate of contamination in chicken and eggs in Pakistan. Most of the cereal grains, oilseeds, tree nuts, and dehydrated fruits are susceptible to fungus contamination and mycotoxin formation.

The most important mycotoxigenic fungus associated with maize and other crops, which produces fumonisins is *Fusarium verticillioides* [8, 9]. In 1988, its chemical structure and biological activity were elucidated in South Africa [10]. Fumonisins are found to be relatively heat-stable [11] and they are also water-soluble.

Toxicological investigations on the fumonisins have focused mainly on fumonisin B1(FB1), the major fumonisin produced in nature. The occurrence of fumonisins in grains and grain products has been a world-wide problem. In wheat plants *Fusarium* infections can lead to diseases such as rot. In view of the difficulty in removing the mycotoxins, monitoring of grains during planting to harvest is important for the control of exposure to these toxins.

Fusarium spp. have an impact on the economy by causing lower grain yields and economic losses [12, 13].

Bulgaria is a country with a temperate-continental climate, which favors the formation of mycotoxins of *Fusarium* spp. and after harvesting under the storage conditions aflatoxins are very likely to be produced. The small number of monitoring programs was the reason to monitor the level of contamination of a wide range representative samples from all regions. It is very important to

*To whom all correspondence should be sent:
E-mail: sertova@hotmail.com

© 2021 Bulgarian Academy of Sciences, Union of Chemists in Bulgaria

recommend the bussiness operators to carry out constant monitoring in protection of animal and human health.

EXPERIMENTAL

Materials and methods

Feed samples: Freshly harvested 221 representative corn samples collected from different regions of Bulgaria were analyzed: wheat (85 samples), barley (68 samples), maize (32 samples) and sunflower (36 samples).

Samples analyses: 5 g of ground samples were mixed and processed using 70% methanol (Valerus Ltd, Bulgaria) as solvent for extraction. The filtered (Whatman No 1, Merck) samples were screened for fumonisins and aflatoxins by the Enzyme-Linked Immunosorbent Assay (ELISA) method. A commerccial kit (R-Biopharm, Germany) was used and the samples were prepared according to the instructions of the manufacturer. The measurement was made at 450 nm. The absorbance was inversely proportional to the fumonisins and aflatoxins concentrations in the sample. The values calculated for the standards were entered into the Ridawin program, Computer Systems (ELx800 Universal Microplate Reader, BIOTEK® Instruments, Inc., USA).

RESULTS AND DISCUSSION

The mycotoxins contamination became a more and more important segment of food chain safety. The research conducted for the period of tree years (2017-2019) allowed us to establish the mycotoxicological status of the evaluated feed materials against aflatoxins and fumonisins. Figure 1 sumarises the results for all samples and their contamination with fumonisins during the study period. The difference in mycotoxins contamination of collected crop samples per year is presented (Table 1).

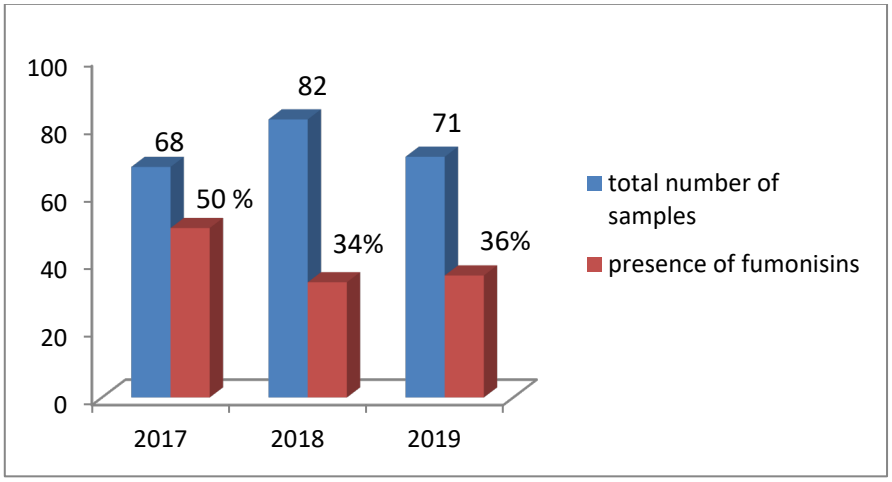

Fig. 1. Number of samples with detected presence of fumonisins in the period 2017-2019

Table 1. Estimated fumonisins contamination of feed materials in the period 2017-2019

Sample	Year	No	% of positive samples	Range (min-max) (mg/kg)	Mean (mg/kg)
Wheat	2017	26	38.5	0.283 - 3.49	1.94±1.19
	2018	34	38.2	0.233 - 4.67	2.1±1.34
	2019	25	28	0.285 - 0.971	0.5±0.21
Barley	2017	22	-	-	-
	2018	24	46	0.300 - 2.89	0.98±0.71
	2019	22	45	0.351-0.738	0.49±0.12
Maize	2017	10	60	1.06 - 4.82	2.60±1.2
	2018	12	33	1.70 - 2.06	1.76±0.25
	2019	10	40	0.380 - 0.520	0.44±0.05
Sunflower	2017	10	50	1.06 - 2.07	1.41±0.36
	2018	12	17	0.782 - 1.86	1.32±0.55
	2019	14	29	0.245 - 0.642	0.38±0.21

Fumonisins were found in all studied materials except of barley samples for 2017 crop and their quantity did not vary widely. This may be caused by the fact that contamination occurred after harvesting, so the *Fusarium* fungi did not have enough time or appropriate conditions to produce detectable

amounts of toxins. Higher concentrations of fumonisins in maize were proved to be 4.82 mg/kg for 2017 crop, (Table 1). The maize sample with the found highest concentration of 4.82 mg/kg originates from the Northwestern region of Bulgaria. This is the highest quantity value of this mycotoxin for all investigated feed materials in the studied period. In another study performed by Rubert *et al.* [14] the highest value of fumonisins obtained in Spanish maize samples was 1.20 mg/kg, which is quite lower than this found by us. It could be because the climatic conditions and latitude are important factors for producing fumonisins in cereal grains.

The lowest mean fumonisin level in maize samples found by us was 0.44 mg/kg (Table 1). This value is close to the levels of 0.55 mg/kg reported by Solovey *et al.* [15] and higher than the 0.01 mg/kg found by Scudamore and Patel [16]. On the other side, the main values for maize samples (2017-2018) determined by us are similar to those reported by Vrabcheva *et al.* [17]. They performed the experiment with Bulgarian maize analysed by the ELISA method and found the presence of fumonisins with a mean value of 1.5 mg/kg, 1.8 mg/kg and 2.1 mg/kg while in the collected sunflower samples values close and in the range of 1.06-2.07 mg/kg for 2017 crop were shown (Table 1). Our results show that for the 2018 crop the highest fumonisins concentration is detected in wheat samples (4.67 mg/kg) while in other studied samples the values are lower. It should be mentioned that this trend was also observed in 2019 harvest.

It can be mentioned that for all studied feed materials the content of fumonisins is lower in the 2019 crop. The lowest concentration was found in maize samples (0.380-0.520 mg/kg), followed by sunflower (0.245-0.642 mg/kg), in barley samples (0.351-0.738 mg/kg) and in wheat samples (0.285-0.971 mg/kg) (Table 1).

Similar percent values for positive samples show maize 60% and sunflower 50%, 2017 harvest. The lowest numbers of 17% and 28% positive samples for the study period (2018-2019) were found in sunflower and wheat samples, respectively (Table 1). Mycotoxins produced by *Fusarium* spp. are a serious problem for feed grains and maize.

In another study conducted by Manova and Mladenova [18] on fumonisins contamination in maize in Bulgaria, a wide prevalence (94.7%) was found in the tested samples and only in one of the samples the contamination was found to exceed the maximum limits for untreated corn. In our survey we found that only one maize sample has fumonisins content of 4.82 mg/kg (Table 1). This value is very low compared to the maximum permitted level (60 mg/kg) as referred in EC Recommendation 576/2006 [19]. The presence of fumonisins in almost all of the tested samples could be attributed to the warmer and raining period during the harvest in the studied period. *Fusarium* toxins have been associated with the temperature at which the cultivation, harvest, and storage of cereals occur. As it is known, molds produced by *Fusarium* spp. are so-called "field" mycotoxins and they are formed during growth and harvest. These findings confirm the special importance of *Fusarium* spp. as major contaminants of cereals in areas with temperate continental climates, where our country falls. Our results confirm the opinion that *Fusarium* contamination is high, especially in the northern part of the country (Fig. 3).

Aflatoxins and fumonisins produced by the genera *Fusarium verticillioides* spp. and *Aspergillus flavus* spp. have the ability to infect fodder crops including maize, wheat and barley [20]. This was the reason why feed materials were tested for fumonisins and aflatoxins. Compared to fumonisins the presence of aflatoxins was not registered in all of the studied feed materials. It is evident from the results in Table 2. The highest concentrations are 14.49 μg/kg and 12.45 μg/kg and the highest mean levels are 10 μg/kg and 10.54 μg/kg, respectively. These values were detected in sunflower samples from 2017 and 2018 crops. And the lowest values were found mainly in 2017 crop for maize and wheat samples (1.10-2.73 μg/kg and 2.76-5.65 μg/kg, respectively) with mean levels of 2 μg/kg and 3.9 μg/kg (Table 2).

We found the presence of aflatoxins in all of the studied samples for 2019 crop. It has to be noted that it varies by regions and dominates in the South central part, (Fig. 3). Concerning aflatoxins contamination it should be mentioned that maize, sunflower and feed grains are favorable substrates for the development of aflatoxins. The maximum level of aflatoxins – 14.49 μg/kg found in sunflower samples is below 20 μg/kg as referred to in Ordinance № 10 of 3.04.2009 [21] for the maximum eligible concentrations of unused substances and products feed.

This sample originates from the northwest of the country, while the minimum level of 5.60 μg/kg is for a sample originating from the northeast. It should be mentioned that the mean values of fumonisins for the studied period are considerably lower than these of aflatoxins, which is not in correlation with the established high percent of molds contamination. In Figure 2 are shown the total number of representative samples and their contamination with aflatoxins in percent during the study period. Taking

into account the warmer climate in Europe the role of molds of genus *Aspergillus* should not be underestimated which are potential producers of mycotoxins with acute toxic effects.

Figure 3 shows the distribution of both mycotoxins by regions.

Table 2. Estimated aflatoxins contamination of feed materials in the period 2017-2019

Sample	Year	No	% of positive samples	Range (min-max) (µg/kg)	Mean (µg/kg)
Wheat	2017	26	19	2.76-5.65	3.9±1.1
	2018	34	-	-	-
	2019	25	20	8.29-10.40	9.3±0.83
Barley	2017	22	-	-	-
	2018	24	-	-	-
	2019	22	18	2.18-11.55	7.23±3.38
Maize	2017	10	30	1.10-2.73	2±0.68
	2018	12			
	2019	10	20	7.94-9.90	8.92±1.11
Sunflower	2017	10	20	5.60-14.49	10±4.4
	2018	12	16.7	8.63-12.45	10.54±1.65
	2019	14	14.3	7.23-9.23	8.23±1.01

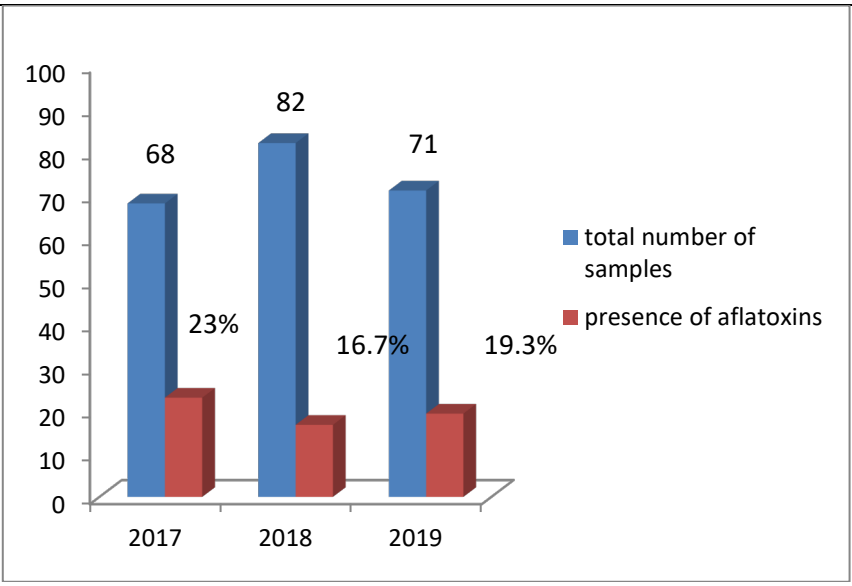

Fig. 2. Number of samples with detected presence of aflatoxins in the period 2017-2019

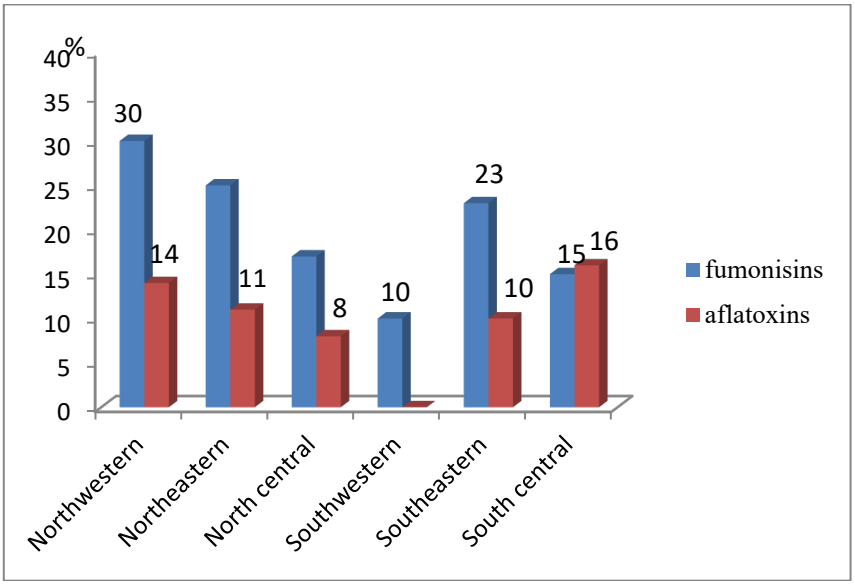

Fig. 3. Fumonisins and aflatoxins occurrence in feed materials and its distribution by regions during 2017-2019

As can be seen, fumonisins predominate. This observation can be explained by latitude and the climatic conditions. If the latitude of the location decreased, the fumonisin content could be increased. Keep in mind that fumonisins are field mycotoxins, climatic conditions could have an important influence in determining the prevalence of the *Fusarium* species.

CONCLUSION

Fumonisins and aflatoxins were found as natural contaminants for wheat, barley, maize and sunflower for the period 2017-2019 while in barley samples their presence was not found in 2017 crop. Maize produced in Northern Bulgaria is more contaminated with fumonisins than that in Southern Bulgaria. Aflatoxin contamination is twice less than that of fumonisins. The presence of fumonisins in feed materials is more widespread than that of aflatoxins in the country. No aflatoxins were detected in the studied representative samples in the south-western region.

Taking into account our results and the values referred in the EC regulation it could be mentioned that the analyzed range of feed grains can be used for animal nutrition because of low levels of contamination.

The contents of mycotoxins measured during the present study did not exceed the permissible levels recommended by the European Commission for animal feed. Analyzing the results according to European regulations, it can be concluded that contamination with aflatoxins and fumonisins does not pose a potential risk to the health and productivity of farm animals. Nonetheless, it is recommended that seeds be monitored continuously to protect against the risk of mycotoxin contamination for safer food and feed.

REFERENCES

1. N. Aiat, *JASR*, **11**, 874 (2006).
2. S. K. Chhonker, D. Rawat, R. A. Naik, R. K. Koiri, *Clin. Oncol*., **3**, 1 (2018).
3. E. G. Lizárraga-Paulín, E. Moreno-Martínez, S. P. Miranda-Castro, in: Aflatoxins - biochemistry and molecular biology, R. Guevara-González (ed.), InTech Janeza Trdine Rijeka, Croatia, 2011, p. 255.
4. K. A. Voss, W. J. Chamberlain, C. W. Bacon, R. A. Herbert, D. B. Walters, W. P. Norred, *Toxicol*. Sci., **24**(1), 102 (1995).
5. M. Šegvić, S. Pepeljnjak, *Vet. Arh*., **71**(5), 299 (2001).
6. P. M. Fratamico, A. K. Bhunia, J. L. Smith, *Emerg. Infect. Dis*., **12**, 2003 (2006).
7. S. Z. Iqbal, S. Nisar, M. R. Asi, S. Jinap, *Food Control*, **43**, 98 (2014).
8. S. A. Okoth, M. A. Kola, *Afr. J. Health Sci*., **20** (1–2), 56 (2012).
9. F. Nyinawabali, A survey of fungi and mycotoxins in selected food commodities from Rwanda. Thesis for MSc degree, University of Johannesburg, Johannesburg, South Africa, 2013.
10. W. F. O. Marasas, J. D. Miller, R. T. Riley, A. Visconti, in: Fusarium. Paul E. Nelson Memorial Symposium, B. A. Summerell, J. F. Leslie, D. Backhouse, W. L. Bryden, L. W. Burgess (eds.), APS Press, The American Phytopathological Society, St. Paul, Minnesota, 2001, p. 332.
11. P. C. Howard, M. I. Churchwell, L. H. Cough, M. M. Marques, D. R. Doerge, *J. Agric. Food Chem*., **46**, 3546 (1998).
12. B. Scherm, V. Balmas, F. Spanu, G. Pani, G. Delogu, M. Pasquali, Q. Migheli, *Mol. Plant Pathol*., **14**, 323 (2013).
13. B. Teli, A. Chattopadhyay, S. C. Meen, G. P. Gangwar, S. K. Pandey, in: Diseases of wheat and their management, S. Vaish (ed.), New Delhi, Astral International, India, 2016, p. 79.
14. J. Rubert, J. M. Soriano, J. Mañes, C. Soler, *Food and Chemical Toxicology*, **56,** 387 (2013).
15. M. M. S. Solovey, C. Somoz, G. Cano, A. Pacin, S. Resnik, *Food Addit. Contam.*, **16** (8), 325 (1999).
16. K. A. Scudamore, S. Patel. *Food Addit. Contam*., **17** (5), 407 (2000).
17. T. Vrabcheva, J. Stroka, E. Anklam, *Mycotoxin Res*., **18**, 46 (2002).
18. R. Manova, R. Mladenova, *Food Control,* **20**, 362 (2009).
19. Commission Recommendation (EC) No 576/2006 of 17 August 2006 on the presence of deoxynivalenol, zearalenone, ochratoxin A, T-2 and HT-2 and fumonisins in products intended for animal feeding.
20. Ch. P. Woloshuk, S. Won-Bo, *Microbiol. Rev.*, **37** (1), 94 (2013).
21. Ordinance no 10 of April 2009 for the maximum permitted concentrations of adverse substances products in feed, issued by the Ministry of Agriculture and Food.

Instructions about Preparation of Manuscripts

General remarks: Manuscripts are submitted in English by e-mail The text must be typed on A4 format paper using Times New Roman font size 11, normal character spacing. The manuscript should not exceed 15 pages (about 3500 words), including photographs, tables, drawings, formulae, etc. Authors are requested to use margins of 2 cm on all sides

Manuscripts should be subdivided into labelled sections, e.g. **Introduction, Experimental, Results and Discussion**, *etc*. **The title page** comprises headline, author's names and affiliations, abstract and key words. Attention is drawn to the following:

a) **The title** of the manuscript should reflect concisely the purpose and findings of the work. Abbreviations, symbols, chemical formulas, references and footnotes should be avoided. If indispensable, abbreviations and formulas should be givenin parentheses immediately after the respective full form.

b) **The author**'s first and middle name initials and family name in full should be given, followedby the address (or addresses) of the contributing laboratory (laboratories). **The affiliation** of the author(s) should be listed in detail by numers (no abbreviations!). The author to whom correspondence and/or inquiries should be sent should be indicated by asterisk (*) with e-mail address.

The abstract should be self-explanatory and intelligible without any references to the text andcontaining not more than 250 words. It should be followed by key words (not more than six).

References should be numbered sequentially in the order, in which they are cited in the text. The numbers in the text should be enclosed in brackets [2], [5, 6], [9–12], etc., set on the text line. References are to be listed in numerical order on a separate sheet. All references are to be given in Latin letters. The names of the authors are given without inversion. Titles of journals must be abbreviated according to Chemical Abstracts and given in italics, the volume is typed in bold, the initial page is given and the year in parentheses. Attention is drawn to the following conventions:a) The names of all authors of a certainpublications should be given. The use of "*et al*." inthe list of references is not acceptable.b) Only the initials of the first and middle names should be given. In the manuscripts, the reference to author(s) of cited works should be made without giving initials, e.g. "Bush and Smith [7] pioneered...". If the reference carries the names of three or more authors it should be quoted as "Bush *et al*. [7]", if Bush is the first author, or as "Bush and co-workers [7]", if Bush is the senior author.

Footnotes should be reduced to a minimum. Each footnote should be typed double-spaced at thebottom of the page, on which its subject is first mentioned.**Tables** are numbered with Arabic numerals on the left-hand top. Each table should be referred to inthe text. Column headings should be as short as possible but they must define units unambiguously.The units are to be separated from the preceding symbols by a comma or brackets. Note: The following format should be used when figures, equations, *etc*. are referred to the text (followed by the respective numbers): Fig., Eqns., Table, Scheme.

Schemes and figures. Each manuscript should contain or be accompanied by the respective illustrative material as well as by the respective figure captions in a separate file (sheet).As far as presentation of units is concerned, SI units are to be used. However, some non-SI units are also acceptable, such as °C, ml, l, etc.The author(s) name(s), the title of the manuscript, the number of drawings, photographs, diagrams, etc., should be written in black pencil on the back of the illustrative material (hard copies) inaccordance with the list enclosed. Avoid using more than 6 (12 for reviews, respectively) figures in the manuscript. Since most of the illustrative materials are to be presented as 8-cm wide pictures, attention should be paid that all axis titles, numerals, legend(s) and texts are legible.

The authors are required to submit the text with a list of three individuals and their e-mail addresses that can be considered by the Editors as potential reviewers. Please, note that the reviewers should be outside the authors' own institution or organization. The Editorial Board of the journal is not obliged to accept these proposals.

The authors are asked to submit **the final text** (after the manuscript has been accepted for publication) in electronic form by e-mail. The main text, list of references, tables and figure captions should be saved in separate files (as *.rtf or *.doc) with clearly identifiable file names. It is essential that the name and version of the word-processing program and the format of the text files is clearly indicated. It is recommended that the pictures are presented in *.tif, *.jpg, *.cdr or *.bmp format.

The equations are written using “Equation Editor” and chemical reaction schemes are written using ISIS Draw or ChemDraw programme.

EXAMPLES FOR PRESENTATION OF REFERENCES

REFERENCES

1. D. S. Newsome, *Catal. Rev.–Sci. Eng*., **21**, 275 (1980).
2. C.-H. Lin, C.-Y. Hsu, *J. Chem. Soc. Chem. Commun*., 1479 (1992).
3. R. G. Parr, W. Yang, Density Functional Theory of Atoms and Molecules, Oxford Univ. Press, New York, 1989.
4. V. Ponec, G. C. Bond, Catalysis by Metals and Alloys (Stud. Surf. Sci. Catal., vol. 95), Elsevier, Amsterdam, 1995.
5. G. Kadinov, S. Todorova, A. Palazov, in: New Frontiers in Catalysis (Proc. 10th Int. Congr. Catal., Budapest,(1992), L. Guczi, F. Solymosi, P. Tetenyi (eds.), Akademiai Kiado, Budapest, 1993, Part C, p. 2817.
6. G. L. C. Maire, F. Garin, in: Catalysis. Science and Technology, J. R. Anderson, M. Boudart (eds), vol. 6, SpringerVerlag, Berlin, 1984, p. 161.
7. D. Pocknell, *GB Patent* 2 207 355 (1949).
8. G. Angelov, PhD Thesis, UCTM, Sofia, 2001, pp. 121-126.
9 JCPDS International Center for Diffraction Data, Power Diffraction File, Swarthmore, PA, 1991.
10. CA **127**, 184 762q (1998).
11. P. Hou, H. Wise, *J. Catal.*, in press.
12. M. Sinev, private communication.
13. http://www.chemweb.com/alchem/articles/1051611477211.html.

Texts with references which do not match these requirements will not be considered for publication!!!

CONTENTS